THE USE OF SCALE MODELS FOR INVESTIGATING THE DYNAMIC BEHAVIOUR OF ROPE-GUIDE MINE SHAFT INSTALLATIONS

by

WILLEM JACOB VAN DER ELST

Submitted in Partial Fulfilment of the Requirements
for the Degree of

Doctor of Science in Engineering

in the

Faculty of Engineering
University of Pretoria
PRETORIA

November 1965

SUMMARY

In order to establish the rules and criteria to be satisfied in order to develop a scale model, which may be employed to predict the dynamic behaviour of a fullscale rope-guide mineshaft installation, the theory of the dynamic behaviour of rope-guides is considered. In order to establish to what degree a scale model rope-guide system may be expected to simulate the dynamic behaviour of its fullscale prototype a series of correlation tests on an existing rope-guide installation and its dynamic scale model are described.

A further series of model investigations into the aerodynamic scale effects which may occur in rope-guide installations, are also described. These investigations demonstrate certain limitations in the use of dynamic scale models of rope-guides and also explain the mechanism of air flow in shafts containing bluff bodies.

On the strength of the experience gained in this research recommendations are made for the execution of efficient experimental investigations into the dynamic behaviour of various rope-guide mineshaft installations. Some information is also provided on the actual design of fullscale rope-guide systems.

I N D E X

1. INTRODUCTION

1.1 The use of guide ropes in mineshafts.

Although rigid rails are most commonly employed for guiding mineshaft conveyances in general mining practice, the use of rope-guides has proved to be very successful in many instances. In such a mineshaft installation the guide rails are replaced by steel ropes, freely suspended in the shaft and suitably tensioned by means of tensioning weights or some springloaded tensioning device situated at the shaft bottom. Conveyances are provided with sliding bearings or guide rope shoes which allow the conveyances to slide freely along the greased guide ropes during hoisting operations. The guide rope inertias and guide rope tensions are solely responsible for steadying conveyances while travelling up and down the shaft and such shafts are therefore entirely devoid of buntons or supporting structures which are normally encountered in shafts with conventional rail guides.

Rope guide mineshaft installations are by no means a modern development. In the United Kingdom such installations have been applied to shafts of moderate depths for very many years. Rope-guides were introduced to the Witwatersrand Gold Mines in 1909 by the New Modderfontein Gold Mining Company. A few installations in shafts of moderate depths in the Witwatersrand area have been operating successfully for some thirty to forty years. In these older installations the guide ropes have not exceeded 3000 feet in depth and some authorities considered this to be close to the limit of safe operation. In recent years, however, several deep shafts in South Africa have been fitted with rope-guides. For example, the Hartebeesfontein Gold Mining Company, the Buffelsfontein Gold Mine as well as the Saaiplaas Gold Mine are all utilising rope-guide installations in shafts of depths slightly in excess of 5000 feet.

Rope-guide installations have some distinct advantages over the conventional rail guided systems. The absence of buntons and internal structures substantially increases the ventilating

capacity of a mineshaft equipped with rope-guides and thus contributes towards economy in ventilation costs.

When rope-guides are to be used, the sinking and equipping of such a shaft is simplified considerably. It is no longer necessary to ensure that the shaft lining is accurately set as is required for the proper alignment of buntons in a shaft with rail guides. Furthermore the installation of rope-guides in deep shafts is not so time consuming as in the case of a rail guide system with its intricate supporting structure. The spacing and alignment of a rope-guide installation can also be effected with superior accuracy.

Higher winding speeds and smoother operation are possible with rope-guides, and the shock loads, so common with slightly misaligned rail guides, are completely avoided. Maintenance of a rope-guide installation is reduced considerably and in general it is found that the conveyances and hoist ropes on such an installation have extended working lives.

In spite of its various advantages, the rope-guide system does not enjoy the whole-hearted approval of all mineshaft authorities. Many engineers are reluctant to employ rope-guides because at present there is a lack of knowledge regarding the exact dynamic behaviour of rope-guide mineshaft installations under various operating conditions. For example, various authorities have widely divergent views regarding the provision of clearances between conveyances running in a shaft, and between conveyances and shaft walls. Some guide rope installations in England operate satisfactorily with as little as 3 inches clearance between conveyances. Rubbing ropes, installed between such conveyances, are regarded as a sufficient safeguard against possible collision. In South African rope-guide installations, clearances of 3 feet between conveyances are common, although clearances have been reduced to as little as 11 inches. Widely divergent views are also held regarding the number and disposition of guide ropes and rubbing ropes, the sizes and weights of such ropes and the rope tensions required.

1.2 Problems encountered in South African mineshafts.

In South African gold mines the problems and uncertainties regarding the design of safe rope-guide installations are greatly enhanced by the fact that such installations are invariably required for shafts exceeding 3000 feet in depth. Modern developments in gold mining practice on the Witwatersrand require rope-guide installations in shafts which may even exceed 8000 feet in depth. Design codes developed in Great Britain over the years apply only to relatively shallow shafts (less than 3000 feet) and become impracticable when applied to deeper shafts.

One of the main problems peculiar to rope-guides of great length is the fact that the considerable weights of such ropes reduce the allowable tensioning at their lower extremities. Guide rope tension therefore varies considerably along the length of a rope and the effect this might have on the lateral swaying motion of conveyances is by no means readily predictable.

Due to the very high initial costs involved in sinking and equipping a deep mineshaft, it becomes necessary, from considerations of economy, to utilise the shaft as a passage for ventilation air while at the same time accomodating as many conveyances as possible in the shaft. For example[1x], such a deep shaft should accomodate, say, one pair of large cages, two pairs of bridles with inter-changable skips and cages and also one service cage.

No such layout employing rope-guides has as yet been attempted and the following major problems[1] arise:

(a) What minimum clearances are necessary to avoid collisions?

(b) What number and what disposition of guide ropes and rubbing ropes is necessary for optimum operating conditions, commensurate with lowest cost?

(c) Will one conveyance, travelling ahead of another, create turbulent air conditions which will cause buffeting and consequent dangerous swaying of the following conveyance?

(d) Should the shaft be widened at the meetings to avoid mutual interference?

..... 4

x Number indices refer to References.

(e) What will be the effect on a conveyance travelling at high hoisting speed past shaft insets where ventilation air enters or leaves?

With due cognizance of these devious problems encountered by engineers concerned with development of rope-guide installations in South African gold mines, the National Mechanical Engineering Research Institute of the S.A. Council for Scientific and Industrial Research was requested by a mining group to conduct a research programme on rope-guides. Subsequently the sponsorship of this research project was taken over by the Transvaal and Orange Free State Chamber of Mines.

1.3 Investigations at the C.S.I.R.

Soon after commencing with the project on rope-guides the investigators decided that dynamic scale model testing would provide by far the most expedient method for solving the great variety of problems encountered in rope-guide engineering practice. It was argued that a scale model, proved to be dynamically similar in all significant aspects to a particular fullscale rope-guide installation, could be efficiently used to predict the behaviour of its fullscale counterpart under any given set of operating conditions.

It was also realised that a mathematical analysis of the rope-guide problem, as far as it is possible with a problem of so complex a nature, was essential in order to form a clear concept of the principles involved, and for serving as a basis for the design and operation of dynamic scale models of rope-guide installations. The theoretical principles, governing the exact simulation of dynamic behaviour of rope-guide systems with a scale model, have been studied by way of dimensional analysis using the laws of similitude, and also by establishing the differential equations of motion of such systems. Solutions to the equations of motion[2] were also found for certain simplified conditions of operation.

Initial dynamic scale model investigations were concerned with the probable behaviour of rope-guided conveyances in a proposed installation for the Buffelsfontein Gold Mining Company. Although being of a rather superficial nature, these investigations

indicated that such dynamic model testing of rope-guide systems might indeed prove very effective. At the conclusion of these investigations it was decided to establish the validity and also the possible limitations of dynamic scale model testing of rope-guide systems, by means of correlation tests. This decision gave rise to the instigation of a basic research project aimed solely at establishing the degree of similarity that could be obtained between the dynamic behaviour of a given rope-guide installation and its dynamic scale model. For the purposes of this research a suitable mineshaft, equipped with rope-guides (Durban Roodepoort Deep Circular Shaft) was selected and used for investigating the dynamic behaviour of fullscale conveyances. A dynamic scale model of this installation was developed at the laboratories of the National Mechanical Engineering Research Institute and extensive correlation tests ultimately indicated the degree of similarity in behaviour existing between such a model and its fullscale prototype. The limitations on the use of such dynamic scale models of rope-guide systems were established and it was possible to evaluate the practicability of this method of investigation.

1.4 The Scope and purpose of this work.

This work is concerned with investigations into the feasibility of utilising results of dynamic scale model experiments to predict the behaviour of fullscale rope-guide mineshaft installations. The inherent limitations as well as the conditions for satisfactory execution of dynamic scale model testing of rope-guide systems are established.

The research work dealt with in this report was therefore not aimed at establishing a design code for the development of rope-guide mineshaft installations. The ultimate aim of this work has been to establish a general code to be followed when conducting research into problems concerned with the design and operation of rope-guide mineshaft installations.

While conducting these investigations considerable knowledge was

..... 6

gathered on the general behaviour of fullscale rope-guide installations. In the final chapter of this report some information on the general design of such installations are presented.

2. THEORETICAL CONSIDERATIONS.

2.1 General.

In developing a scale model of some physical system (such as a rope-guide mineshaft installation) it is necessary to establish certain criteria which will ensure that the two systems are dynamically similar in all significant aspects. Furthermore when using a scale model of a physical system to predict the dynamic behaviour of its fullscale counterpart it becomes necessary to establish certain rules which will ensure the correct interpretation of the behaviour of the model. Such criteria and rules are established by analysing the behaviour of the physical systems theoretically.

This theoretical analysis may be conducted by two different methods; firstly by utilising differential equations of motion and secondly by way of the basic laws of dynamic similitude and dimensional analysis. These two methods of theoretical approach to the study of dynamic scale models will now be considered separately and each method will be applied to the rope-guide problem.

2.2 The use of differential equations of motion.

2.2.1 General significance of differential equations.

It is possible to express the dynamic behaviour of any physical system symbolically by means of differential equations of motion. In the case of complicated physical systems it is very often extremely difficult or even impossible to obtain complete solutions for these governing differential equations. However, if it is desired to establish criteria which will ensure dynamic similarity between a physical system and a geometric scale model of such a system, this may readily be achieved by using the governing equations of motion in their differential form. After

..... 7

obtaining the differential equations of motion for, say, the full-scale prototype of some physical system under consideration, it will be necessary to establish these equations in a non-dimensional form. If it is ensured that all the non-dimensional terms in these equations are numerically equal to corresponding terms applicable to a scale model of the physical system under consideration, the differential equations will then be equally valid for both the model and the fullscale prototype. The dimensionless terms in these differential equations of motion will provide the necessary criteria to ensure dynamic similarity between model and fullscale prototype and will also provide rules required for the correct interpretation of model behaviour.

2.2.2 Differential equations of motion for rope-guide mineshaft installations. Figure 1 depicts a typical mine-shaft conveyance suspended by means of a single hoist rope and guided by means of a number of guide ropes, (usually four). For the purpose of determining dynamic similarity criteria the motion of this conveyance and ropes will be considered two-dimensionally in the vertical pitching plane as indicated in Figure 1. Analysis of motion in the vertical yawing plane and in the horizontal rolling plane may be executed along similar lines and will not be considered in the present analysis since no new similarity criteria will be introduced. (The nomenclature and the general form of the equations used in this analysis are similar to those used in Reference 2).

X and Y are the co-ordinates specifying the position of the centre of gravity of the conveyance. Any convenient fixed point in the shaft may be arbitrarily chosen as the origin for these co-ordinates. The hoist rope and the portions of each guide rope running upwards away from the conveyance and downwards away from the conveyance are considered separately, each with its own system of co-ordinates x and y designated by suitable suffixes. x represents the rope co-ordinate vertically away from the conveyance and y the co-ordinate rotated 90° clockwise from x. The origin of x and y may again be chosen arbitrarily. For example, if a conveyance commences a hoisting run from some position in the

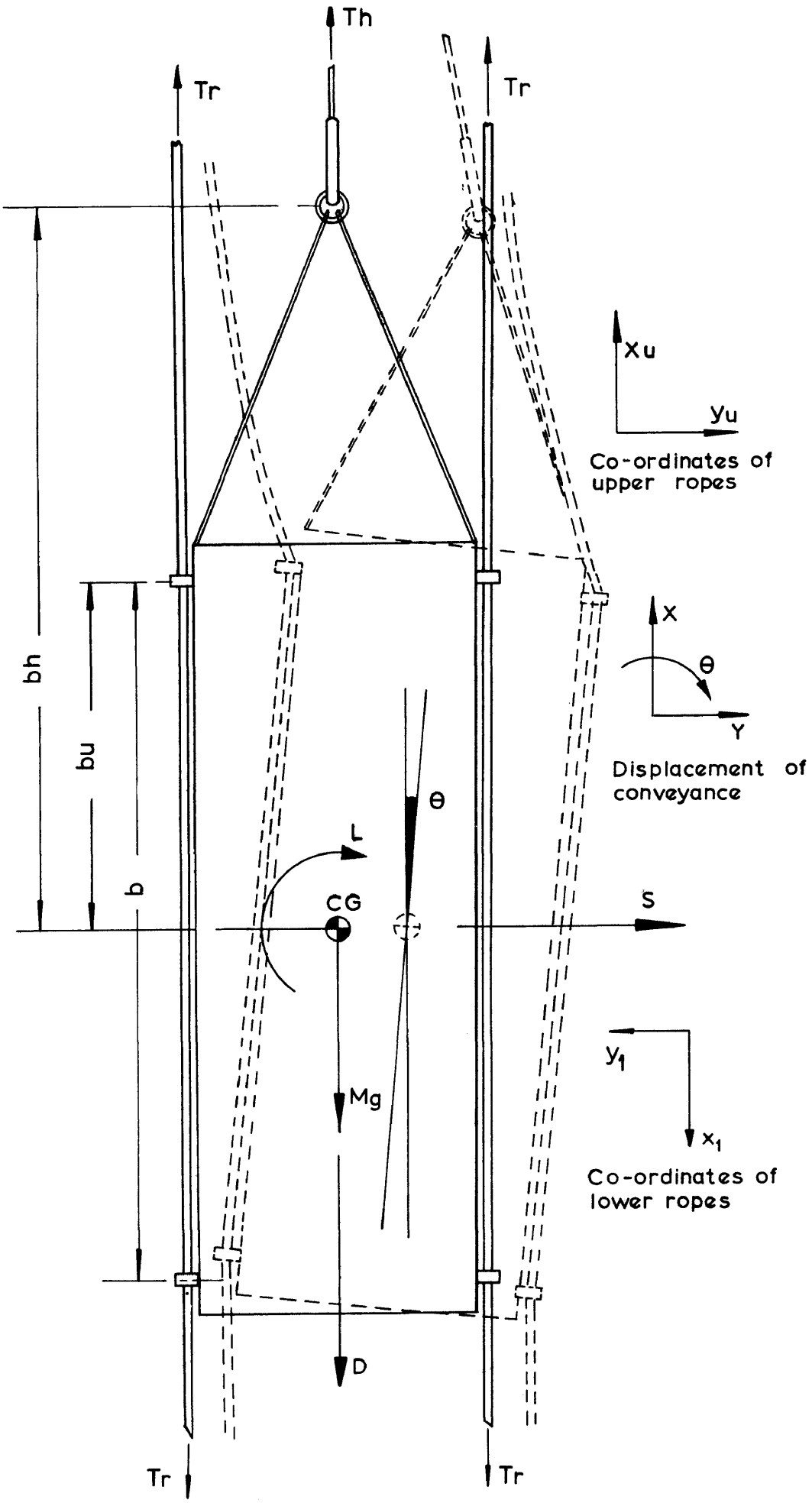

FIGURE 1

Forces and displacements on a rope-guided conveyance

shaft the origins for the co-ordinate systems of the guide ropes may be taken as the points of contact of the ropes with the conveyance in its stationary position. The origin of the hoist rope co-ordinate system may be regarded as moving with the conveyance and remaining at the point where the hoist rope is fixed to the conveyance.

Suffix h refers to the hoist rope, suffixes r = 1, 2, 3, ... n refer to n guide ropes and suffixes u and l refer to the upper and lower portions of a guide rope respectively. Suffix s refers to the point of contact of a rope with the conveyance.

R = a steady aerodynamic drag force acting on the conveyance in the vertical direction.

S = a steady aerodynamic side force acting on the conveyance.

L = a steady aerodynamic moment acting on the conveyance.

M = mass of conveyance.

I = moment of inertia of conveyance in the pitching plane.

T = tension in a rope at the point of contact with the conveyance.

b_h = vertical distance between point of contact of hoist rope and the centre of gravity of the conveyance.

b_u = vertical distance between the upper points of contact of guide ropes and centre of gravity of conveyance.

b = vertical distance between upper and lower points of contact between guide ropes and conveyance.

θ = angle of pitch of conveyance.

m = mass per unit length of a rope.

v = velocity of the conveyance.

H = depth of shaft.

s = non-dimensional time.

w = velocity of ventilation air in the shaft.

z = linear scale factor.

In this analysis it is assumed that the motion of the conveyance does not appreciably affect the tensions in the ropes and that in general all slopes of ropes, expressed by $\frac{dy}{dx}$, remain small.

It is further assumed that all elastic forces and couples in the ropes as well as internal rope friction forces are negligibly small compared with rope tension forces and couples resulting from these rope tension forces (refer to section 2.4).

The differential equation of motion governing translational motion of the conveyance in the vertical pitching plane may be written as follows:

$$M \frac{d^2Y}{dt^2} = S + T_h \left(\frac{dy}{dx}\right)_{hs} + \sum_{r=1}^{n} T_r \left\{\left(\frac{dy}{dx}\right)_{rus} - \left(\frac{dy}{dx}\right)_{rls}\right\} \quad \ldots\ldots (1)$$

The differential equation governing rotational motion of the conveyance in the vertical pitching plane becomes:

$$I \frac{d^2\theta}{dt^2} = L + b_h T_h \left(\frac{dy}{dx}\right)_{hs} + \sum_{r=1}^{n} T_r \left\{ b_u \left(\frac{dy}{dx}\right)_{rus} + (b - b_u) \left(\frac{dy}{dx}\right)_{rls} \right\} - \left(b_h T_h + \sum_{r=1}^{n} T_r b\right) \theta \quad \ldots\ldots\ldots\ldots (2)$$

When neglecting friction forces exerted by the guide ropes on the conveyance the equation for vertical hoisting motion becomes:

$$M \frac{d^2X}{dt^2} = T_h - R - Mg \quad \ldots\ldots\ldots\ldots\ldots\ldots\ldots\ldots\ldots\ldots\ldots\ldots (3)$$

When the guide ropes are or the hoist rope is disturbed in any way such a disturbance will be propagated along the ropes in the form of a wave. In order to determine the dynamic behaviour of a rope-guide mineshaft installation completely, it will also be necessary to establish the differential equation for the motion of a tensioned rope hanging vertically and executing oscillations in the horizontal direction.

Figure 2 depicts an element dx of a rope, the upper extremity of which is at a distance x from the origin, and experiencing a tension force

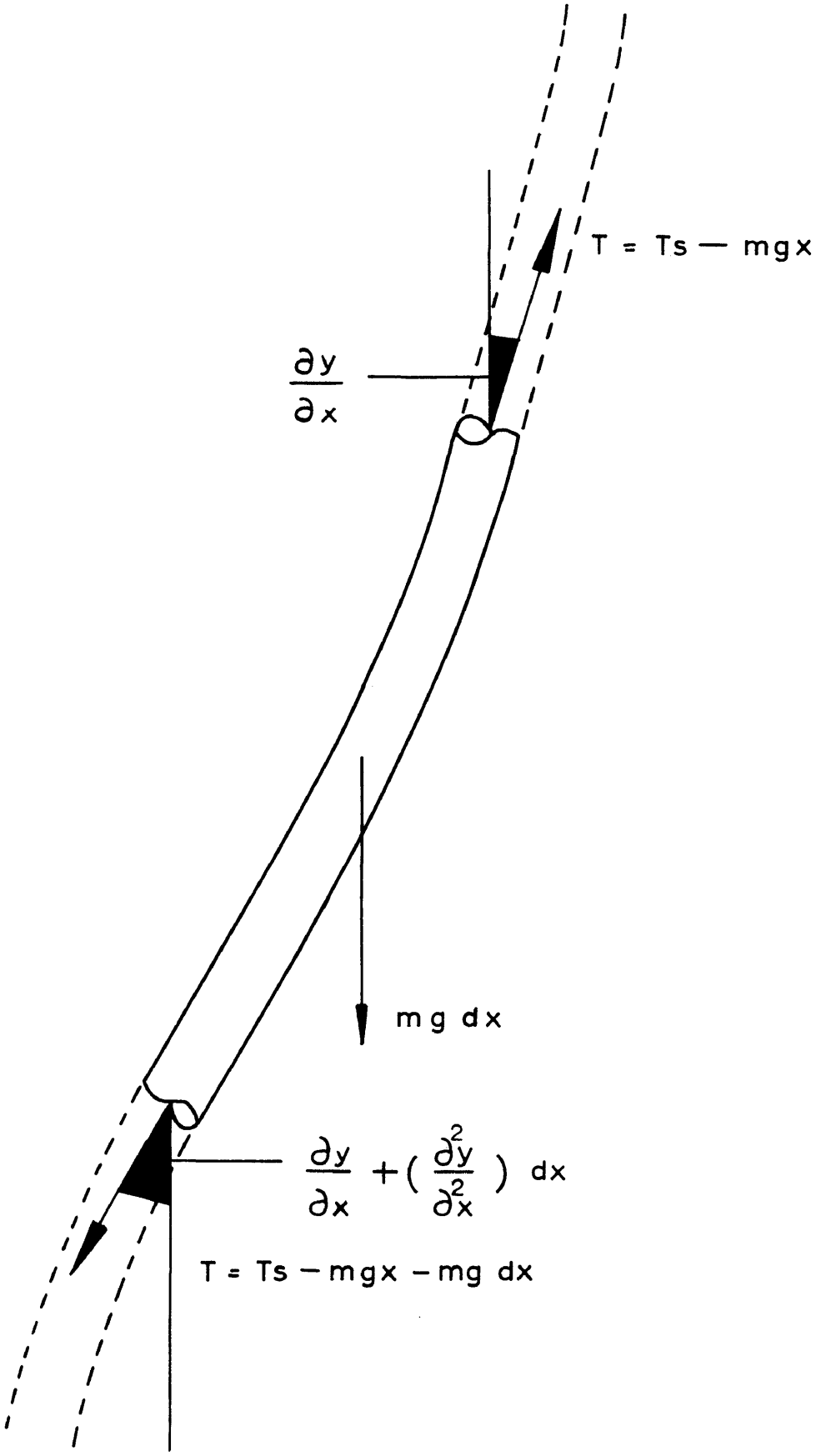

FIGURE 2

Forces and displacements in a rope

$$T_x = T_s \pm mg\,x$$

where the plus and minus signs refer to the portions of the ropes above and below the conveyance.

At the lower extremity of the element the tension is

$$T_{x+dx} = T_s \pm mgx \pm mg\,dx.$$

Considering the balance of the lateral force components,

$$T_x + dx\left\{\frac{\partial y}{\partial x} + \frac{\partial^2 y}{\partial x^2}\,dx\right\} - T_x\frac{\partial y}{\partial x} = m\,\frac{\partial^2 y}{\partial t^2}\,dx.$$

By substituting for T_x and T_{x+dx} and neglecting squares of small quantities, the differential equation of motion for the rope becomes

$$\left(\frac{T_s}{m} \pm gx\right)\frac{\partial^2 y}{\partial x^2} \pm g\frac{\partial y}{\partial x} - \frac{\partial^2 y}{\partial t^2} = 0 \quad \ldots\ldots\ldots\ldots\ldots\ldots\ldots \quad (4)$$

This is a form of the universal wave equation for which it is necessary to establish the appropriate end conditions, given in this case by the motion of the conveyance at one end and the rope fixture at the other end. If the conveyance is moving up with a velocity v from an initial depth H_o in a shaft of depth H the end conditions after a time lapse t become:

For the upper portions of the guide ropes:

at the top of the shaft

$$y = o \text{ at } x = H - H_o - b_u$$

at the conveyance

$$y = Y + b_u\,\Theta \text{ at } x = + vt$$

For the lower portions of the guide ropes:

at the bottom of the shaft

$$y = 0 \text{ at } x = H_o - (b-b_u)$$

at the conveyance

$$y = -Y + (b-b_u)\,\Theta \text{ at } x = -vt$$

$\ldots\ldots\ldots$ (5)

For the hoist rope:

at the top of the shaft

$$y = o \text{ at } x = H - H_o - b_h - vt$$

at the conveyance

$$y = Y + b_h \theta \text{ at } x = o$$

} ..... (5)

Differential equations of motion (1) to (4) together with the end conditions (5) completely determine the motion of the system in the vertical pitching plane. The aerodynamic forces S and R and the couple L acting on the conveyance deserve further attention. It is assumed that the conveyance has a bluff shape for which aerodynamic viscous forces are negligibly small (refer to section 2.4). These quantities may then be expressed by the following equations:

$$S = C_S \tfrac{1}{2} \rho (w + v)^2 b^2 \quad \text{.....} \quad (6)$$

$$R = C_R \tfrac{1}{2} \rho (w + v)^2 b^2 \quad \text{.....} \quad (7)$$

$$L = C_L \tfrac{1}{2} \rho (w + v)^2 b^3 \quad \text{.....} \quad (8)$$

w and v are respectively the velocity of the ventilation air flowing in the shaft, and the conveyance hoisting velocity. C_S, C_R and C_L are non-dimensional aerodynamic force and couple coefficients, referred to a typical linear dimension b of the conveyance.

2.2.3 Non-dimensional rendering of equations.

Equations (1) to (8) are rendered non-dimensional by dividing each equation by a convenient quantity having the same dimensions as the terms in the equation. Thus equation (1) may be made non-dimensional by dividing by Mg:

$$\frac{1}{g}\frac{d^2Y}{dt^2} = \frac{S}{Mg} + \frac{T_h}{Mg}\left(\frac{dy}{dx}\right)_{hs} + \sum_{r=1}^{n} \frac{T_r}{Mg}\left\{\left(\frac{dy}{dx}\right)_{rus} - \left(\frac{dy}{dx}\right)_{rls}\right\}$$

Linear displacement may be made non-dimensional by dividing such displacements by the shaft diameter D, while the time t may be rendered non-dimensional by defining a non-dimensional time $s = t\sqrt{\frac{g}{D}}$

The acceleration $\frac{d^2Y}{dt^2}$ may now be written in the form

$$\frac{d^2Y}{dt^2} = \frac{d}{dt}\left(\frac{dY}{dt}\right) = \frac{d}{ds}\left(\frac{dY}{ds} \cdot \frac{ds}{dt}\right)\frac{ds}{dt}$$

But $\frac{ds}{dt} = \sqrt{\frac{g}{D}}$

Therefore $$\frac{d^2Y}{dt^2} = \frac{d^2Y}{ds^2} \cdot \frac{g}{D} = \frac{d^2\frac{Y}{D}}{ds^2}\, g$$

The complete non-dimensional form of equation (1) then becomes:

$$\frac{d^2\frac{Y}{D}}{ds^2} = \frac{S}{Mg} + \frac{T_h}{Mg}\left(\frac{d\frac{Y}{D}}{d\frac{x}{D}}\right)_{hs} + \sum_{r=1}^{n} \frac{T_r}{Mg}\left\{\left(\frac{d\frac{Y}{D}}{d\frac{x}{D}}\right)_{rus} - \left(\frac{d\frac{Y}{D}}{d\frac{x}{D}}\right)_{rls}\right\} \quad \ldots\ldots\ldots \quad (9)$$

Equations (2), (3), (4) and (5) may be treated in a similar fashion, yielding the following non-dimensional versions: Equation (2) becomes

$$\frac{I}{MD^2}\frac{d^2\theta}{ds^2} = \frac{L}{MgD} + \frac{b_h T_h}{Mg\ D}\left(\frac{d\frac{Y}{D}}{d\frac{x}{D}}\right)_{hs} +$$

$$\sum_{r=1}^{n} \frac{T_r}{Mg}\left\{\frac{b_u}{D}\left(\frac{d\frac{Y}{D}}{d\frac{x}{D}}\right)_{rus} + \frac{b - b_u}{D}\left(\frac{d\frac{Y}{D}}{d\frac{x}{D}}\right)_{rls}\right\}$$

$$- \left(\frac{b_h T_h}{Mg\ D} + \sum_{r=1}^{n} \frac{T_r\, b}{Mg\ D}\right)\theta \quad \ldots\ldots\ldots\ldots\ldots\ldots\ldots\ldots\ldots\ldots \quad (10)$$

Equation (3) becomes

$$\frac{d^2\frac{X}{D}}{ds^2} = \frac{T_h}{Mg} - \frac{R}{Mg} - 1 \quad \ldots\ldots\ldots\ldots\ldots\ldots\ldots\ldots\ldots\ldots\ldots\ldots\ldots\ldots \quad (11)$$

Equation (4) becomes

$$\left(\frac{T_s}{mg\,D} \pm \frac{x}{D}\right) \frac{\partial^2 \frac{Y}{D}}{\partial^2 \left(\frac{x}{D}\right)^2} \pm \frac{\partial \frac{Y}{D}}{\partial \frac{x}{D}} - \frac{\partial^2 \frac{Y}{D}}{\partial s^2} = 0 \qquad \ldots\ldots\ldots\ldots\ldots\ldots (12)$$

After a time lapse expressed non-dimensionally by s the end conditions given by equation (5) become:

For the upper portions of the guide ropes:

at the top of the shaft

$$\frac{Y}{D} = o \text{ at } \frac{x}{D} = \frac{H}{D} - \frac{H_o}{D} - \frac{b_u}{D}$$

at the conveyance

$$\frac{Y}{D} = \frac{Y}{D} + \frac{b_u}{D}\,\theta \text{ at } \frac{x}{D} = + \frac{v\,s}{\sqrt{gD}}$$

For the lower portions of the guide ropes:

at the bottom of the shaft

$$\frac{Y}{D} = o \text{ at } \frac{x}{D} = \frac{H_o}{D} - \left(\frac{b}{D} - \frac{b_u}{D}\right) \qquad \ldots\ldots\ldots\ldots\ldots\ldots (13)$$

at the conveyance

$$\frac{Y}{D} = - \frac{Y}{D} + \left(\frac{b}{D} - \frac{b_u}{D}\right)\theta \text{ at } \frac{x}{D} = - \frac{v\,s}{\sqrt{gD}}$$

For the hoist rope:

at the top of the shaft

$$\frac{Y}{D} = o \text{ at } \frac{x}{D} = \frac{H}{D} - \frac{H_o}{D} - \frac{b_h}{D} - \frac{v\,s}{\sqrt{gD}}$$

at the conveyance

$$\frac{Y}{D} = \frac{Y}{D} + \frac{b_h}{D}\,\theta \text{ at } \frac{x}{D} = o$$

Equations (6), (7) and (8) may be written in the following non-dimensional form:

$$\frac{S}{\frac{1}{2}\rho(w+v)^2 b^2} = C_S \qquad \ldots\ldots\ldots\ldots\ldots\ldots\ldots\ldots\ldots\ldots\ldots\ldots\ldots\ldots\ldots\ldots\ldots\ldots\ldots\ldots\ldots\ldots (14)$$

$$\frac{R}{\frac{1}{2}\rho(w+v)^2 b^2} = C_R \qquad \ldots\ldots\ldots\ldots\ldots\ldots\ldots\ldots\ldots\ldots\ldots\ldots\ldots\ldots\ldots\ldots\ldots\ldots\ldots\ldots\ldots\ldots (15)$$

$$\frac{L}{\frac{1}{2}\rho(w+v)^2 b^3} = C_L \qquad \ldots\ldots\ldots\ldots\ldots\ldots\ldots\ldots\ldots\ldots\ldots\ldots\ldots\ldots\ldots\ldots\ldots\ldots\ldots\ldots\ldots\ldots (16)$$

Equations (9) to (16) now represent the complete non-dimensional equations for the motion of the conveyance in the vertical pitching plane.

It is possible to obtain mathematical solutions to these equations for conveyances executing oscillatory motion while suspended in a mineshaft[2]. However, this mathematical treatment of the problem does not fall within the scope of this report These equations will be used in their differential form to establish criteria for dinamic similitude between a model of a rope-guide mineshaft installation and its fullscale prototype.

2.2.4 Criteria for dynamic similitude.

All the non-dimensional terms occurin, in equations (9) to (16) may be listed separately as terms involving ratios of linear dimensions, ratios of forces and moments, ratios of moments of inertia, mass ratios, ratios of time intervals and ratios of velocities.

Ratios of linear dimensions:

$$\frac{Y}{D}, \frac{y}{D}, \frac{x}{D}, \frac{b_h}{D}, \frac{b}{D}, \frac{b_u}{D}, \frac{X}{D}, \frac{H}{D}, \frac{H_o}{D}, \theta.$$

Ratio of moment of inertia:

$$\frac{I}{MD^2}$$

Ratio of time interval:

$$s = \frac{t}{\sqrt{\frac{D}{g}}}$$

Ratios of forces, force coefficients and ratios of moments:

$$\frac{S}{Mg}, \frac{T_h}{Mg}, \frac{T_r}{Mg}, \frac{R}{Mg}, \frac{T_s}{mg\ D}, \frac{L}{Mg\ D}$$

Using equations (6), (7) and (8), $\frac{S}{Mg}$, $\frac{R}{Mg}$ and $\frac{L}{Mg\ D}$ may also be written in the form

$$\frac{S}{Mg} = C_S\ \tfrac{1}{2}\ \frac{\rho b^3}{M}\ \frac{(w+v)^2}{gb}$$

$$\frac{R}{Mg} = C_R\ \tfrac{1}{2}\ \frac{\rho b^3}{M}\ \frac{(w+v)^2}{gb}$$

$$\frac{L}{Mg\ D} = C_L\ \tfrac{1}{2}\ \frac{\rho b^3}{M}\ \frac{(w+v)^2}{g\ D}$$

These expressions incorporate velocity ratios

$$\frac{w+v}{\sqrt{gb}} \text{ and } \frac{w+v}{\sqrt{g\ D}} \text{ as well as the mass ratio } \frac{\rho b^3}{M}$$

Another velocity ratio, $\frac{v}{\sqrt{g\ D}}$, occurs in equation (13)

The force ratio $\frac{T_r}{Mg}$ may be written in the form

$\frac{T_r}{Mg} = \frac{T_s}{Mg} + \frac{mg\ x}{Mg}$ where mx represents the mass of a guide rope of length x feet. This expression yields an additional mass ratio $\frac{mx}{M}$

In order to ensure that a rope-guide system and its model are similar in their dynamic behaviour, the non-dimensional equations must be equally applicable to both the model and its fullscale prototype. All the above terms must therefore be identical for both systems. This implies that all the above linear dimensions,

..... 18

forces, moments, moments of inertias, masses, velocities and time intervals occurring in the fullscale system must be reduced by constant scale factors when applied to a model which is to be dinamically similar to its fullscale prototype. Furthermore there exists an implicit relationship between these various scale factors which may be readily reduced from the above ratios.

In the subsequent analysis the subscript m refers to the model while p refers to the fullscale prototype.

Let the linear scale factor z be defined as

$$z = \frac{\text{a fullscale linear dimension}}{\text{a corresponding model linear dimension}}$$

e.g. $z = \frac{D_p}{D_m}$

Using the time interval ratio $\frac{t}{\sqrt{\frac{D}{g}}}$ it follows from the condition for dynamic similitude that

$\frac{t_p}{\sqrt{\frac{D_p}{g}}} = \frac{t_m}{\sqrt{\frac{D_m}{g}}}$ g being the same for the model and the fullscale prototype.

Hence the time scale factor $\frac{t_p}{t_m} = \sqrt{\frac{D_p}{D_m}} = \sqrt{z}$.

The mass scale factor may be found by using the mass ratio $\frac{\rho b^3}{M}$

Assuming that air of the same density is used in the model and fullscale shafts, it follows that

$$\frac{\rho b_p^3}{M_p} = \frac{\rho b_m^3}{M_m}$$

Hence the mass scale factor $\frac{M_p}{M_m} = \left(\frac{b_p}{b_m}\right)^3 = z^3$

Should it be decided to use air of a different density in the model shaft (i.e. presurised or rarefied air) the mass scale factor will be given by

$$\frac{M_p}{M_m} = \frac{\rho_p}{\rho_m} z^3$$

Similarly, by using, say, the velocity ratio $\frac{v}{\sqrt{g\,D}}$ the velocity scale factor $\frac{v_p}{v_m} = \sqrt{z}$ may be deduced. Regarding mass, length and time as fundamental dimensional units, the scale factors for any other physical quantities such as impulses or momenta may be readily deduced as functions of the linear scale factor z.

2.3 The use of laws of similitude and dimensional analysis.

2.3.1 The basic concept of similitude between two physical systems. The significance of the term "similarity" as applied to physical systems is rather subjective. Various degrees of similarity may exist between two physical systems. If it is desired to use one physical system (a model) to interpret the behaviour of some or other property of another physical system (the prototype), the exact nature of the information required will actually determine the necessary degree of similarity to be attained.

Geometrical similarity between two physical systems exists when all linear dimensions occurring in one of the systems bear a constant ratio to corresponding linear dimensions in the other system. Thus a geometrical scale model of some fullscale physical system is obtained by multiplying all the linear dimensions in the fullscale prototype by a constant linear scale factor.

If it is desired to obtain kinematic similarity[3], i.e. similarity of motion, between two physical systems it is necessary also to observe constant time lapse ratios in addition to constant linear dimensional ratios occurring in the two systems. This implies that corresponding velocities and accelerations in the two systems will always occur in constant ratios.

Suppose that in addition to linear dimensions and time intervals, the corresponding component masses in two physical systems occur in a constant ratio. It then follows that all corresponding forces and other physical quantities which can be expressed in the fundamental units of Mass, Length and Time, will occur in constant ratios in the two physical systems.

Should a further fundamental dimension, occurring in a physical system, be reproduced to scale in another similar system, a higher degree of physical similarity may be attained. For instance if the fundamental dimensions of Mass, Length, Time and Temperature correspond to scale in two systems, thermodynamic similitude may be attained.

In many mechanical systems, a rope-guide mineshaft installation being a typical example, all physical quantities of significance may be expressed in the three fundamental dimensions of Mass, Length and Time. When it is desired to establish the behaviour of such a mechanical system by studying its dynamicallly similar scale model, it is merely necessary to determine the relevant Mass, Length and Time scale factors. All scale factors for other relevant physical parameters may then be readily deduced from these fundamental dimensions. However, it is not essential to select Mass, Length and Time as the three fundamental dimensions[4]. For example Force, Velocity and Density may be chosen as fundamental units and it will again be possible to deduce scale factors for all other significant physical quantities from knowledge of the scale factors for these three fundamental dimensions.

Definite relationships will exist between the scale factors for the fundamental dimensions. Again this relationship will be subjective, i.e. it will depend on the nature of the problem under consideration. It is generally found that all the significant physical quantities pertaining to a particular physical system (e.g. velocities, densities, linear dimensions, etc.) may be grouped together to form one or more non-dimensional parameters. The nature of the problem to be investigated will

..... 21

dictate which of these non-dimensional parameters are important.

It is found that for dynamical systems (i.e. mechanical systems in which all physical quantities are reducible to fundamental units of Mass, Length and Time) the significant non-dimensional parameters can most conveniently be derived from consideration of force ratios. All the forces acting in such a system are expressed in terms of the physical quantities involved in the problem (e.g. velocities, densities, lengths, etc.). Consideration of all possible force ratios will then yield one or more non-dimensional groups of these physical quantities. Such groups then represent the significant non-dimensional parameters pertaining to the system. Although these significant non-dimensional parameters can usually be obtained most readily by considering force ratios, ratios of other physical quantities, as for example momentum ratios, may also be used. It is, however, necessary that any such physical quantity chosen shall contain the three fundamental dimensions Mass, Length and Time.

The law governing dynamic similitude[3] between two physical systems (e.g. a model and its prototype) require that these significant non-dimensional parameters, containing the physical quantities involved in the problem, be the same for both systems. This implies that all the physical quantities pertaining to the one system (model) are related to the corresponding quantities pertaining to the other system (prototype) by constant scale factors and that definite relationships exist between the scale factors for the various quantities. The relationships between the scale factors for the fundamental dimensions (and for all other physical quantities) may be derived readily.

2.3.2 Application of laws of similitude to a rope-guide mineshaft installation and its dynamic scale model. The following are regarded to be the significant physical quantities related to a rope-guide mineshaft installation:

A typical linear dimension D (shaft-diameter in feet).

..... 22

A typical linear velocity v (velocity of conveyance in feet seconds^{-1}).

The density of air ρ (in slug feet^{-3}).

Viscosity of air μ (in slug feet^{-1} seconds^{-1}).

The density σ' of a typical material from which the solid components of the installation is constructed (e.g. the density of steel in slug feet^{-3})

Young's modulus E for steel used in the wire ropes (in pounds feet^{-2})

The friction coefficient of the conveyance guide blocks on guide ropes η .

A typical time interval t (in seconds).

For a given rope-guide installation subjected to given operating conditions, it is sufficient to specify only typical physical quantities.

The significant forces acting in such an installation may be expressed in terms of the significant physical quantities as follows:

Aerodynamic pressure forces $\propto \rho v^2 D^2$

Aerodynamic inertia forces $\propto \rho D^3 \frac{v}{t}$

$$\propto \rho \frac{D^3 v}{\frac{D}{v}} \propto \rho D^2 v^2$$ (Reference 5)

Aerodynamic viscous forces $\propto \mu v D$

Rope tension forces $\propto \sigma' D^3 g$

..... 23

Gravity forces $\propto \sigma D^3 g$

Inertia forces on conveyances and ropes

$$\propto \sigma D^3 \frac{v}{t} \propto \frac{\sigma D^3 v}{\frac{D}{v}} \propto \sigma D^2 v^2$$

Friction forces between conveyance guide blocks and ropes $\propto$

Rope tension forces $\times \eta \propto$

$$\sigma D^3 \eta g$$

Elastic forces due to bending of ropes $\propto eE D^2$

where e is the strain in such a rope.

Internal rope friction forces are not readily expressed in terms of the above physical quantities. These forces will have a dampening effect on lateral oscillatory movements of a conveyance and the logarithmic decrement d of amplitudes of oscillations will serve as a measure of such dampening forces but will naturally also include aerodynamic dampening forces.

On considering all possible ratios of the above forces the following non-dimensional parameters are obtained:

$\frac{\rho v D}{\mu}$ (known as the Reynolds number)

$\frac{v^2}{gD}$ (the Froude number)

$\frac{\sigma' Dg}{E}$ (the elasticity number) alternatively $\frac{\rho v^2}{E}$

η (the friction coefficient for conveyance guide blocks on guide ropes)

d (the logarithmic decrement of lateral amplitudes of oscillation of conveyance)

In order to develop a dynamically similar scale model of such a rope-guide installation all the above non-dimensional parameters

must be identical for both model and prototype. Practically speaking some of these parameters are incompatible. For example the Froude number calls for a reduction in velocity v when decreasing the linear dimension D while the Reynolds number requires an increase in velocity v. Both these numbers may be maintained by operating the model conveyance in a liquid medium instead of in air, the liquid having the appropriate value for $\frac{\rho}{\mu}$. However, since all densities in the model and prototype are related by constant scale factors, a rediculously high density σ will usually be required for the solid components of the model.

It is well established that for turbulent flow past such bluff bodies as mineshaft conveyances, the pressure forces eclipse the viscous forces in magnitude. The Reynolds number may therefore be neglected. (Refer to section 2.4). Assuming that elastic forces due to bending of ropes are small (refer to section 2.4) when compared with aerodynamic pressure forces and rope tension forces, the elasticity number may also be ignored. The friction coefficient will depend on the construction and material of model ropes and the exact simulation of friction forces is not essential since friction forces will be very small compared to the weight of a conveyance. It has also been established experimentally that the logarithmic decrement d will not effect the dynamic behaviour of a conveyance to any significant extent. (Refer to section 4.5).

It follows that the Froude number will be the only significant parameter to be maintained in both the model and the prototype in order to obtain satisfactory dynamic similarity in behaviour and this result may now be used to deduce the scale factors necessary for the design of a dynamic scale model.

Let subscripts m and p refer to model an prototype respectively.

$$\text{Then} \quad \frac{v_m^2}{D_m g} \qquad \frac{v_p^2}{D_p g}$$

Since g remains the same for model and prototype, it follows that

$$\frac{v_p}{v_m} = \sqrt{\frac{D_p}{D_m}} = \sqrt{z}$$

where z is the linear scale factor.

Since the typical velocity v is proportional to $\frac{D}{t}$ it follows that the time scale factor

$$\frac{t_p}{t_m} = \sqrt{z}$$

If it is assumed that the air used in the model has the same density as the air in the fullscale shaft, it follows that the mass scale-factor

$$\frac{M_p}{M_m} = z^3$$

since ρ is proportional to $\frac{M}{D^3}$

All other scale factors necessary for the design of a dynamic scale model may be readily deduced from knowledge of the Mass, Length and Time scale factors.

To facilitate the construction of such a model, it is permissible in certain instances to deviate from the rule of constant scale factors. For example, it is not necessary to maintain the diameters of hoist and guide ropes exactly to scale in a model. Rope diameters will only affect elastic forces due to bending of ropes as well as aerodynamic forces acting on ropes and these forces may be assumed to be insignificant. However, it is important to observe correct scale factors for rope masses which affect tension and inertia forces.

Again, provided the outer aerodynamic shape of a conveyance as well as its mass and moments of inertia is to scale the actual structure of such a conveyance may be simplified to facilitate manufacture.

2.4 Justifications for assumptions.

2.4.1 Elastic forces in ropes. The assumption that elastic forces due to bending of ropes are insignificant has been investigated theoretically[2] for static forces in ropes. It was

..... 26

found that even if typical model ropes were considered as solid steel bars, the elastic forces due to bending were approximately one tenth of the lateral components of tension forces.

If ropes were considered to be perfectly elastic, their points of contact with the sliding blocks on a conveyance could be considered to be pin joints. The effect of elasticity of ropes is to move the effective position of the pin joints outside the two guide blocks on the conveyance by a distance s as illustrated in Figure 3. This distance s is expressed approximately by

$$s = \frac{\frac{2\ EI}{bT}}{1 + \frac{2}{b}\sqrt{\frac{EI}{T}}} \qquad \text{(Reference 2)}$$

where E is the modulus of elasticity of the rope material, I is the sectional moment of inertia of the rope and T is the rope tension. Calculations show that for a typical fullscale installation s is always small. In a model installation where elastic forces are comparatively greater their effect may be cancelled by moving the sliding blocks inwards by this distance s.

For purely translational movement of a model conveyance in the lateral direction, it will be clear that, even if no correction is made for s, the effect of elastic bending of the ropes will still be insignificant. The elasticity of the ropes will, however, have a stabilising effect when pitching motion of the conveyance occur. However, in all subsequent experimental work (refer to section 4.5), it was found that pitching motion of conveyances was negligibly small. It is therefore felt that in general any elastic effects of ropes may be safely ignored.

2.4.2 Aerodynamic Viscous Forces. In experimental work which is concerned with turbulent flow past bluff bodies it is customary practice to ignore the effect of fluid viscosity on the body[6]. In general it is true that the total aerodynamic force on such a body is mainly caused by aerodynamic pressure forces acting on its surfaces. However, if only the lateral component

..... 27

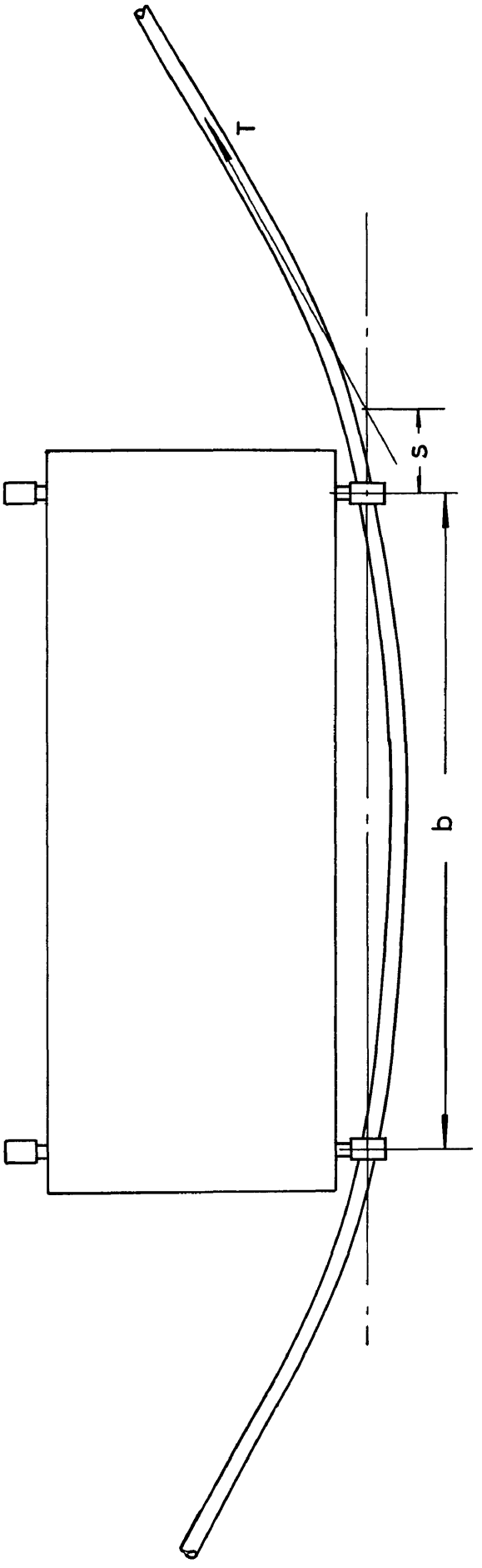

FIGURE 3

The effect of rope elasticity

of the total aerodynamic force acting on a mineshaft conveyance is considered (i.e. the component perpendicular to the direction of hoisting), it is found that viscous forces may not be ignored under all circumstances. At certain low Reynolds numbers which may be encountered in a model mineshaft installation, viscous forces often influence the lateral component of the aerodynamic force to a considerable degree. Since this fact has a very important bearing on the validity of model tests, extensive experimental investigations have been carried out in this connection. (Refer to section 5).

3. THE VERTICAL MINESHAFT WINDTUNNEL AND MINESHAFT MODELS

3.1 General.

As practisised at the CSIR, dynamic scale model testing of rope-guide mineshaft installations generally required mineshaft models to a scale of approximately 1:20 to 1:25, which implied very long models. It was also found most convenient to simulate the shaft in which a rope-guide system operates by means of metal ducting which had to be erected exactly vertically and had to be aligned perfectly. It became necessary to develop a semi-permanent facility which would accommodate such long ducts and which would also include the necessary equipment for hoisting model mineshaft conveyances inside these ducts and for simulating the flow of ventilation air through the ducts. Such a facility was errected at the CSIR in Pretoria and became known as the Vertical Mineshaft Windtunnel since it was essentially a tunnel which caused the flow of air in a model.

3.2 The layout of the Vertical Mineshaft Windtunnel.

In order to obtain a free vertical drop of 160 feet, which was considered sufficient for envisaged mineshaft models, a ten-foot diameter, 80-foot deep pit was sunk and an 80-foot high tower, constructed from three inch steel angle girders, was erected directly over the pit. Figure 4 reflects the general layout

..... 29

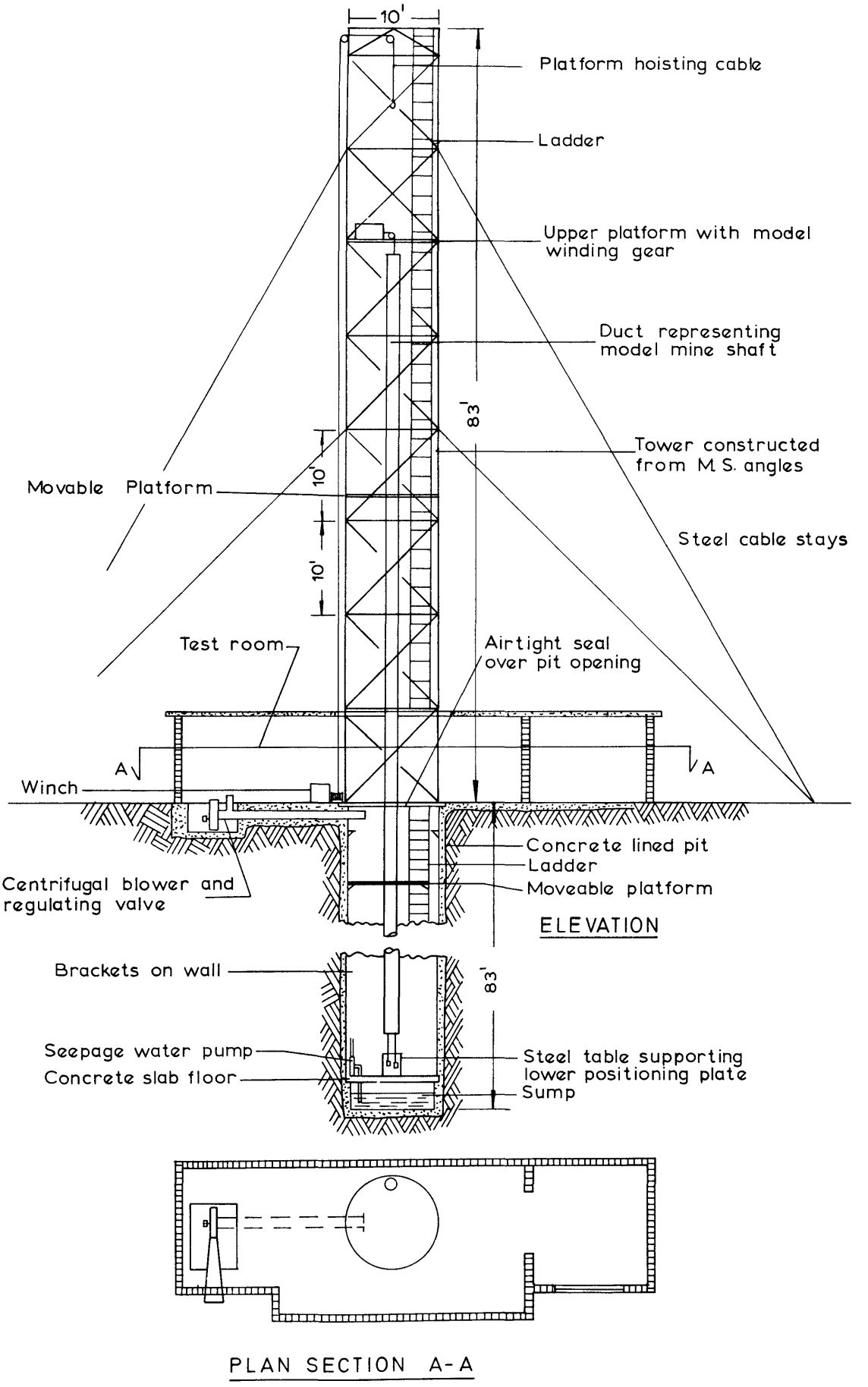

FIGURE 4

General layout of vertical mineshaft windtunnel

of this Vertical Mineshaft Windtunnel. The tower was built up in ten feet cubical bays and could be readily dismantled. The height of the tower could therefore be decreased to reduce the tendency to sway when models shorter than 160 feet were to be accommodated. Steel cable stays, equipped with turnbuckles for tensioning, were also installed at the four corners of the tower to reduce swaying and distortion of the structure. The pit was lined with reinforced concrete, and seepage water, leaking through these walls, collected in a sump situated at the pit bottom and covered with a floor of concrete slabs. This seepage water was removed by a centrifugal pumping unit situated on the floor and operated automatically by a limit switch connected to a float.

In addition to steel ladders up the tower and down the pit, platforms were provided by means of which any level in the tower and pit could be reached. Steel brackets, spaced at six foot intervals down the pit, were installed to support the platform in the pit. The platform in the tower could be supported on any of the steel cross girders. Hoisting of these platforms was effected by a small electric driven winch.

Two carefully aligned parallel steel angles were installed along the length of the tower and pit. These served as anchoring rails for brackets which supported the ducting representing the model mineshaft.

At ground level the base of the tower and the mouth of the pit was enclosed in a concrete roofed building which also accommodated the centrifugal blower installation, winch, switchgear and all the necessary instruments.

The winding gear for hoisting model conveyances was situated on a wooden platform in the top bay of the steel tower.

A battery operated field telephone system was installed to effect communication between research staff stationed on the upper tower platform, in the test room on ground level or at the bottom of the

..... 31

pit.

Figure 5 shows the interior of the pit with a mineshaft model installed. Figure 6 depicts the general appearance of the 80-foot high steel tower and the test room.

3.3 The hoisting mechanism for model conveyances.

A rope-guide mineshaft installation may comprise two or more conveyances which usually travel simultaneously in a mineshaft. Sometimes separate winding systems are employed for different conveyance pairs which will then operate completely independant of each other. In some cases rope-guides and rail guides are both used in the same shaft for two separate hoisting systems. In a mineshaft model it was found possible to simulate all hoisting configurations in the shaft with one single model hoist. It was found more convenient to utilize balanced hoisting systems, i.e. either operating conveyances in pairs or using counter weights, running on rail or rope-guides, to balance the weights of conveyances. Hoisting drums of various diameters, mounted on a single drive shaft, could be used conveniently to cater for various relative hoisting speeds of conveyances. The direction of hoisting of conveyance pairs relative to each other could readily be altered by suitably crossing model winding ropes. Since a single hoisting unit proved sufficient for most model installations, a permanent hoist, mounted on the upper platform in the tower, was developed.

This hoisting unit could be used for operating any model mineshaft installation. It was only necessary to provide a hoisting drum to suit the hoisting requirements of any particular model. Figure 7 depicts the layout of this permanent model hoisting unit. The hoist was driven by a 1.5 H.P. 1750 rpm variable speed d.c. motor operated from a plate rectifier unit. The speed of the hoisting drum shaft was reduced by means of a 5.25:1 worm gear. An emergency band brake, operated automatically in case of accidental overwinding, was also incorporated in the design.

..... 32

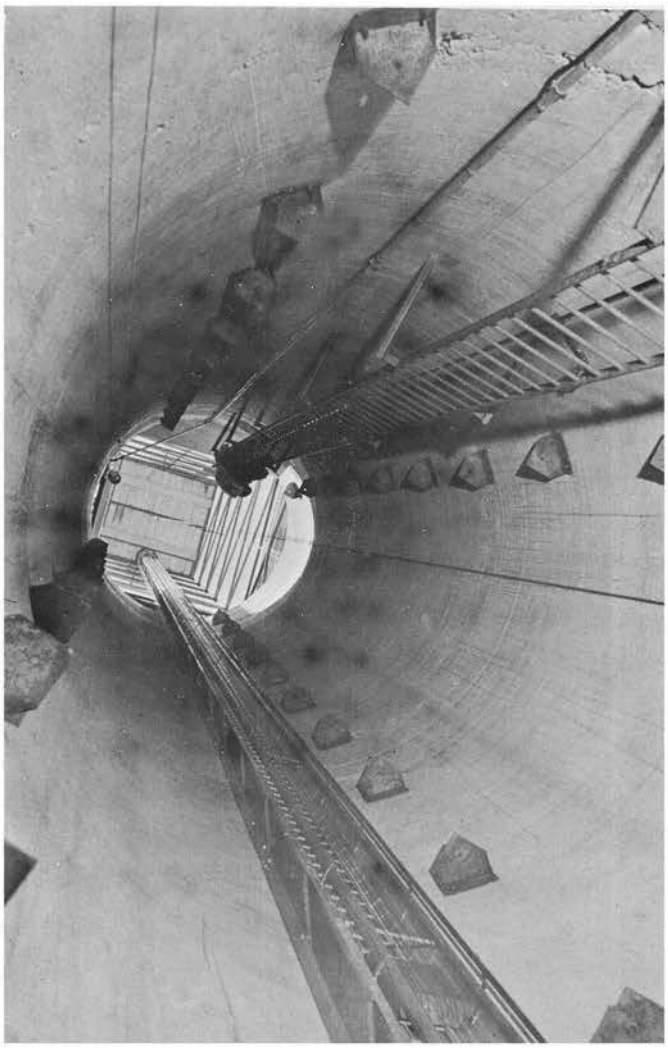

FIGURE 5

The 80 feet deep pit

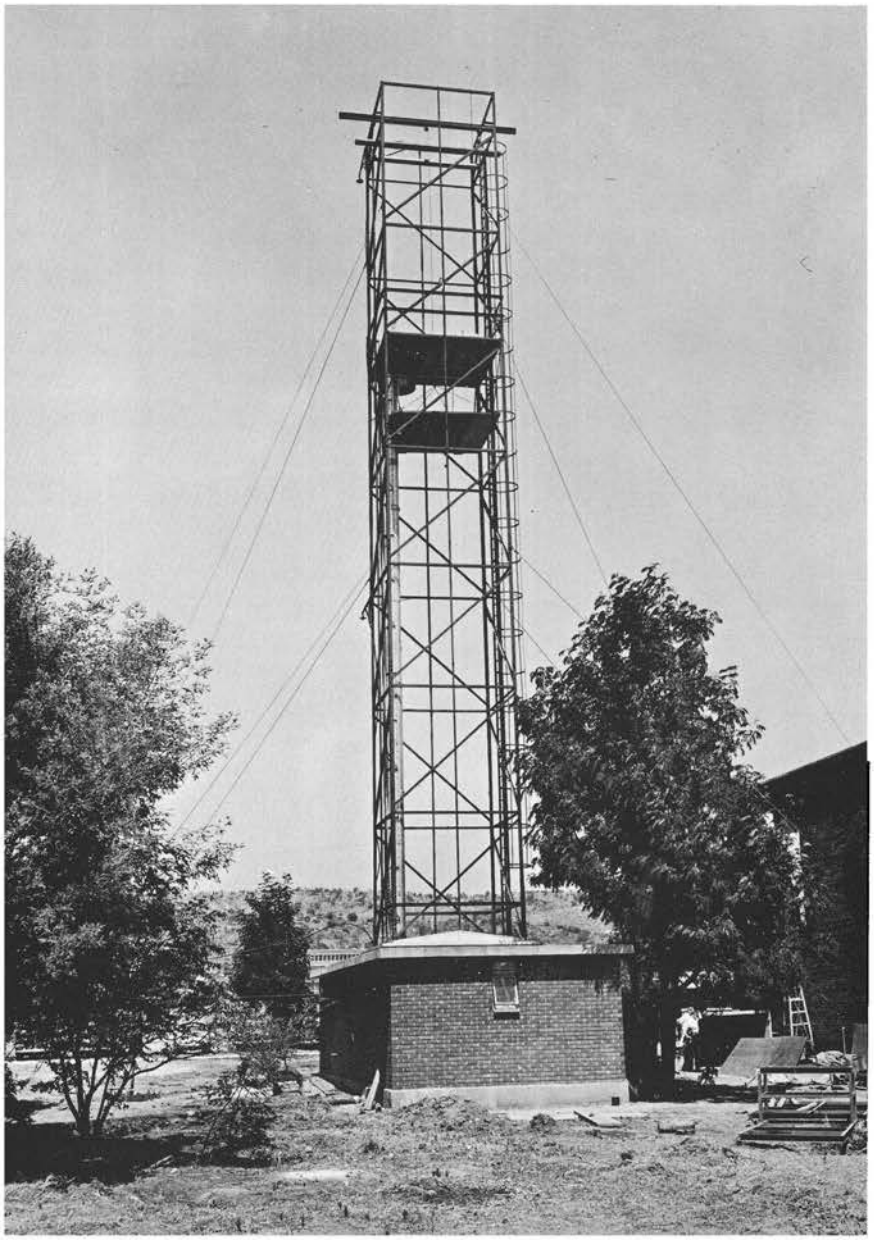

FIGURE 6

The 80 feet high steel tower

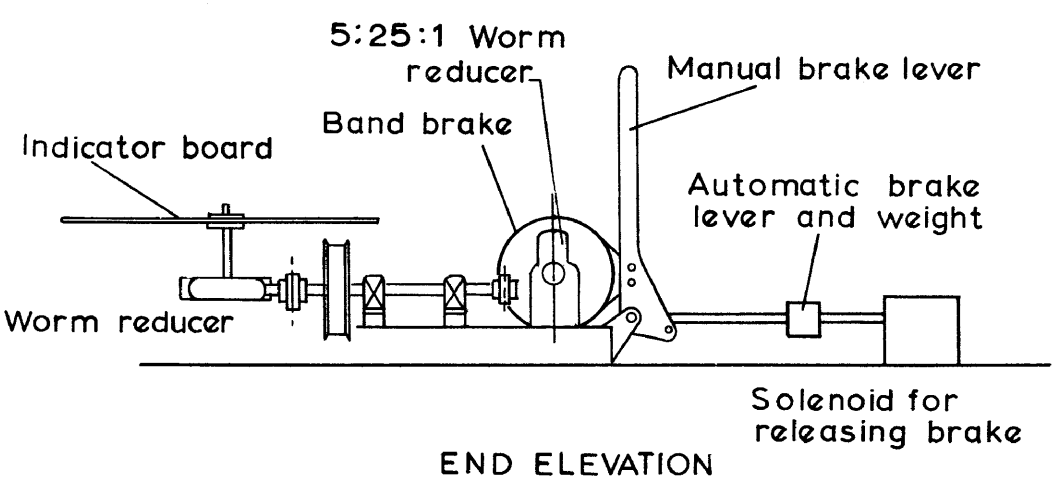

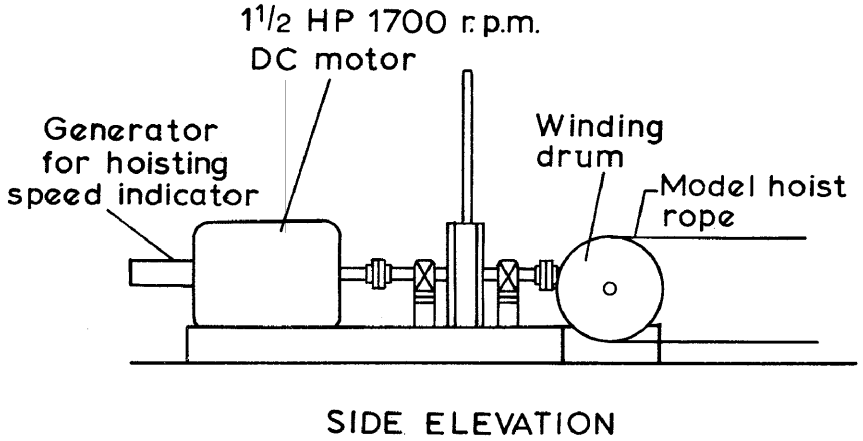

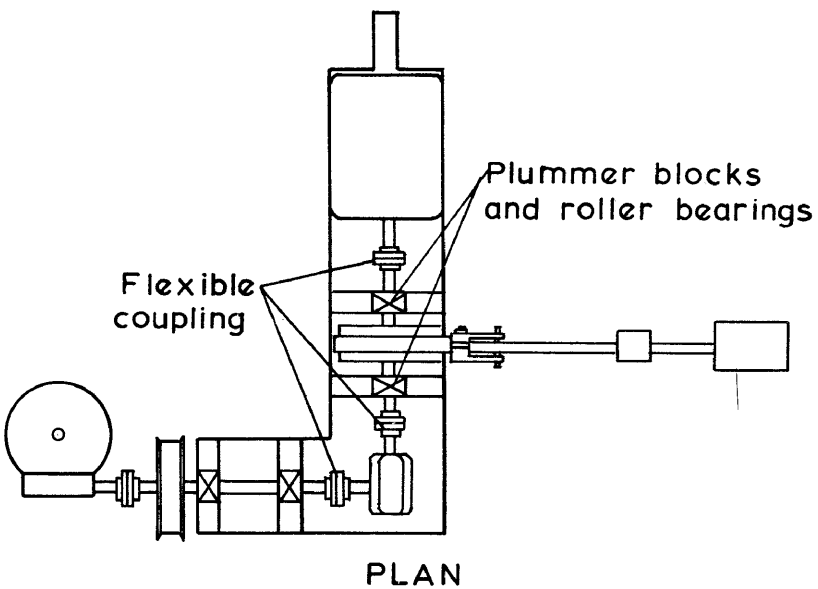

FIGURE 7

Details of model hoisting unit

The automatic brake mechanism consisted of a weighted lever which operated the steel brake band and was released by means of a solenoid actuated by limit switches in the model shaft. These limit switches were actuated by the conveyances themselves when these conveyances were accidentally allowed to pass the safe limit of their travel. In addition to the automatic braking system a brake lever for manual operation was also included as indicated in Figure 7.

The rotational speed of the winding drum shaft was indicated on a calibrated volt meter connected to a small generator which was coupled directly to the motor shaft.

When carrying out a hoisting test it was always necessary to simulate a predetermined hoisting cycle and it was also necessary to know the exact position of a conveyance in the model shaft. A device which fulfilled this function is illustrated in Figure 8. A circular indicator board of approximately two feet in diameter was coupled to the hoisting drum shaft through a reduction worm gear. This reduction ratio ensured that, for the average rope-guide installation model, the indicator board would make approximately one complete revolution when a model conveyance travelled along the entire depth of the model shaft. As indicated in Figure 8, such an indicator board was graduated radially as well as circumferentially, thus enabling a polar diagram of any particular hoisting cycle to be drawn. Circumferential graduations represented hoisting drum revolutions which indicated the exact position of a conveyance in the shaft. The indicator board was graduated radially in hoist drum revolutions per minute. Thus, by suitably converting the required conveyance speed of any particular model installation in terms of hoist drum speed, it was possible to plot a polar hoisting-speed diagram on the indicator board. A pointer which could be moved radially over the indicator board by hand was connected through a suitable pully arrangement to a needle on the hoisting speed indicator as shown diagramatically in Figure 8. The scale to which the hoist drum speed polar diagram was plotted on the indicator board, and the geometry of the pulley

..... 36

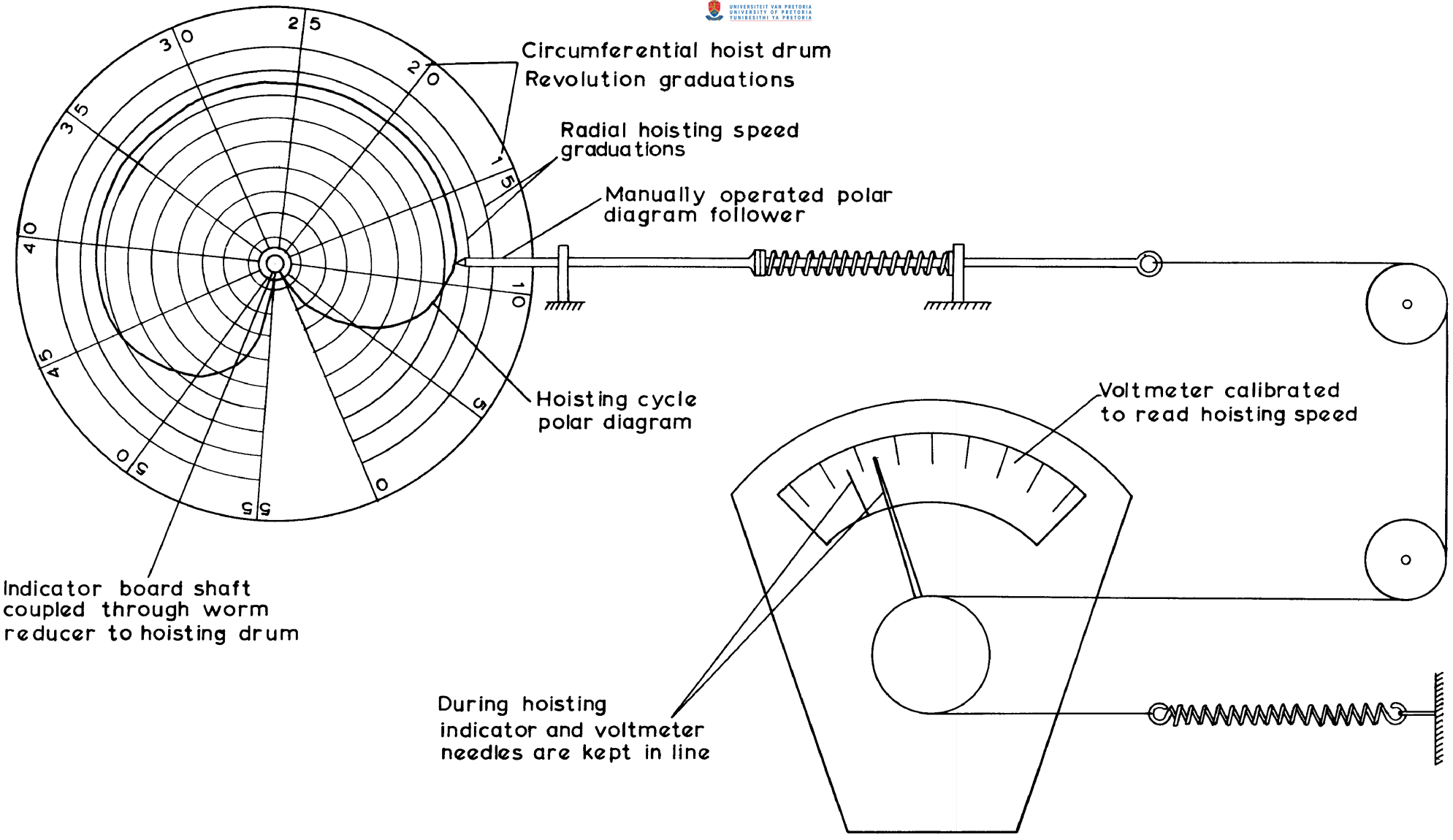

FIGURE 8

Device for simulating hoisting cycles

arrangement was such that the second needle on the hoisting speed dial indicated the exact required hoist motor speed. It was therefore only necessary for the hoist operator to control the motor speed in such a way that the two indicator needles on the dial always remained in line with each other.

This apparently intricate method of simulating fullscale hoisting cycles nevertheless proved to be very satisfactory, as may be judged from the model and fullscale hoisting graphs for the Durban Roodepoort Deep correlation tests. (Refer to Figures 40(a) to 40(j)).

The switch lever for reversing the rotation of the motor, the motor rheostat control and the motor speed indicator dial were all mounted on the front board of a cabinet containing the rectifier unit and other electrical gear and circuits.

Figure 9 shows the general arrangement of the winding gear without the two-foot diameter indicator board. Model hoist ropes were suitably guided by small pulleys and for each particular model it was necessary to design a suitable head gear which also served for fixing model guide ropes. This head gear, all guiding pulleys and the hoist drum fitted to the shaft of the hoist were regarded as forming a part of the model being tested. Such equipment had to be redesigned for each model installed.

3.4 Simulation of ventilation air flow.

The unit employed for producing air flow in the shaft is shown in Figure 10. Air was drawn from the pit by means of a 10 HP centrifugal fan unit, situated in the test room. The air was exhausted through a diffuser to atmosphere outside the test room. The opening of the pit was closed with wooden beams and was sealed off airtight with a polythene sheet cover, thereby ensuring that all the air drawn through the fan passed down the model shaft. The air flow was regulated with a by-pass valve situated on the inlet side of the fan. The rate of air flow in the model shaft

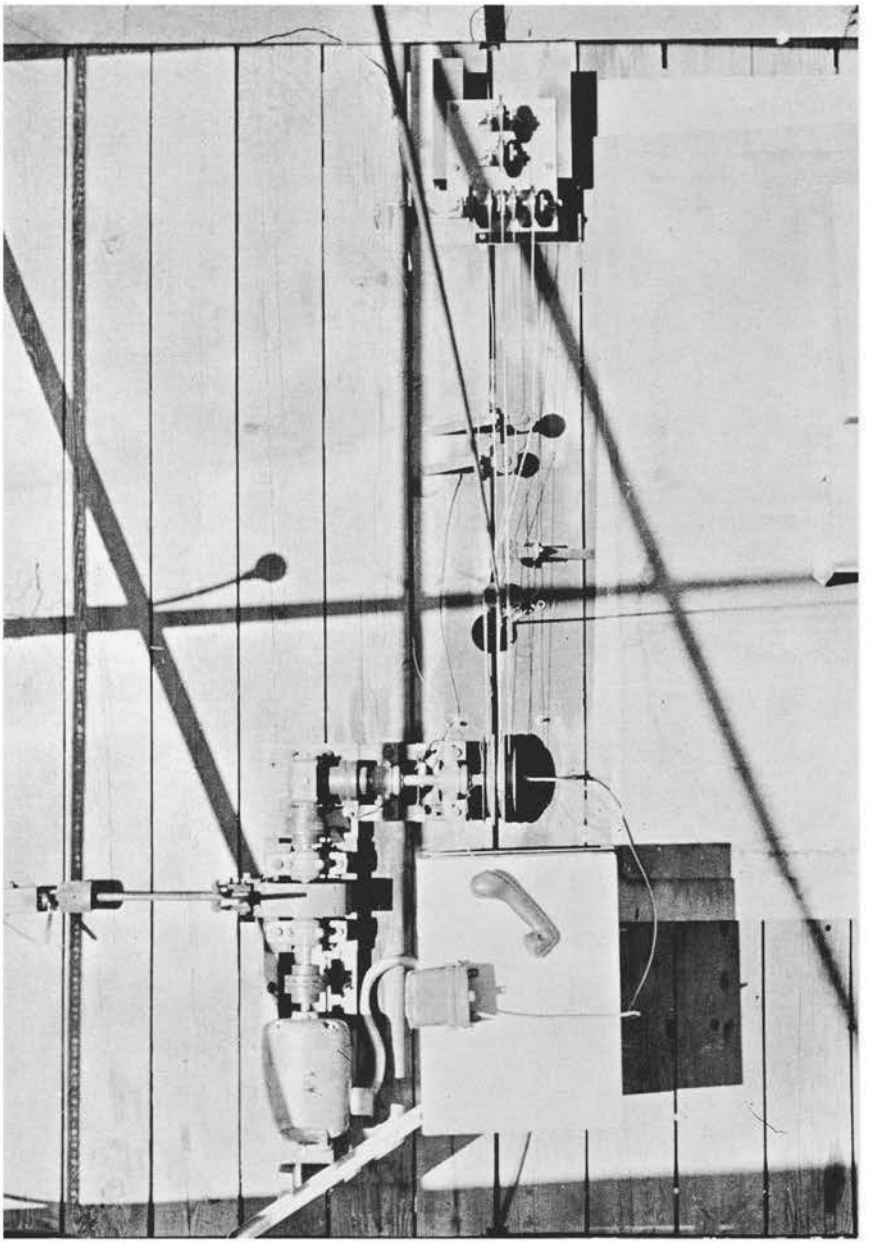

FIGURE 9

The upper platform

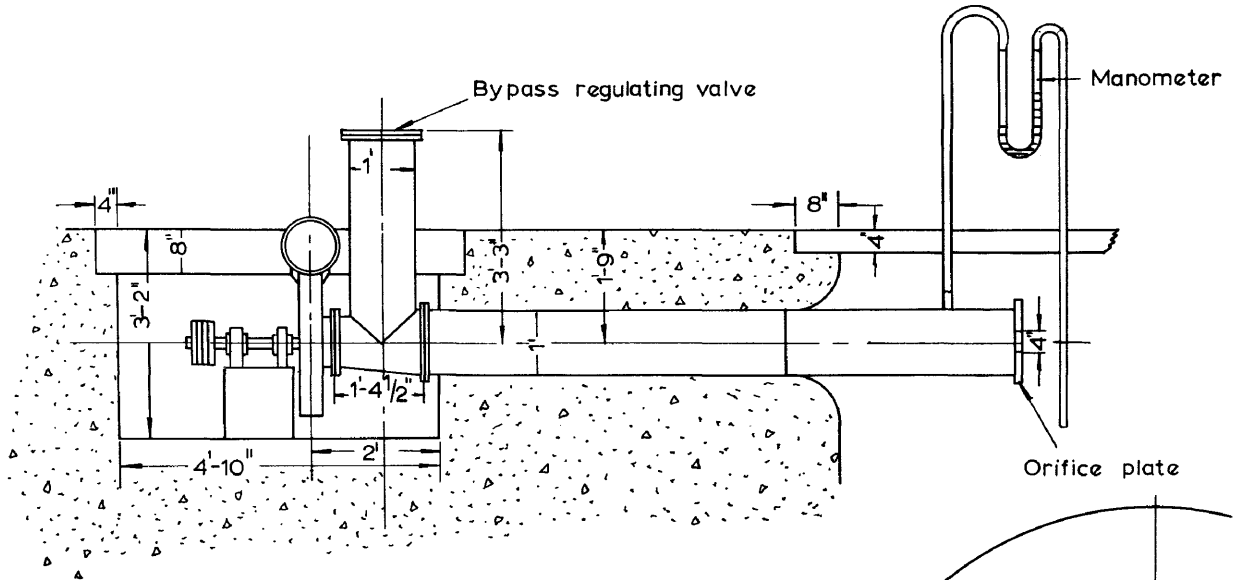

SIDE ELEVATION

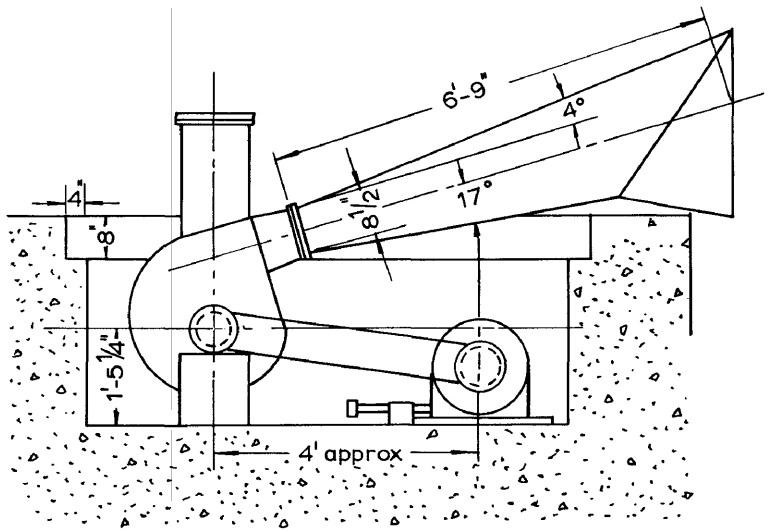

END ELEVATION

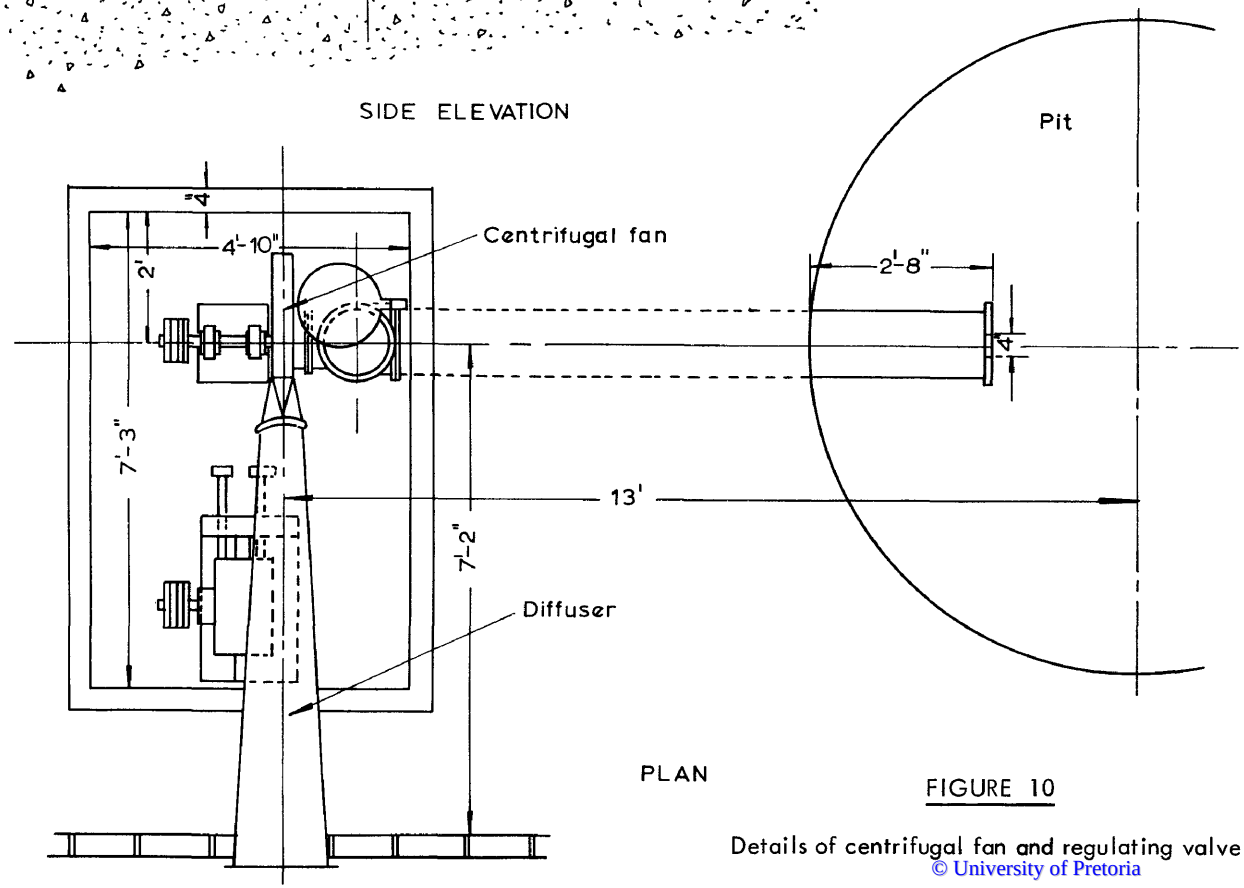

PLAN

FIGURE 10

Details of centrifugal fan and regulating valve

was measured with an orifice plate flowmeter situated at the inlet of the shaft metal duct leading to the fan intake. The pressure drop over the orifice plate was measured with a manometer situated in the test room.

3.5 Models of rope-guided mineshaft installations.

A model mineshaft installation comprised the actual duct which represented the mineshaft together with all guide ropes, hoist ropes and conveyances and also any possible internal structures inside the shaft. As described in Chapter 2, suitable scale factors had to be derived for all significant variables occurring in the shaft. All significant linear dimensions, masses, hoisting velocities etc. had to conform to these derived scale factors.

When designing a model it was also necessary to provide ancilliary equipment such as upper and lower positioning plates for locating guide ropes and hoist ropes and furthermore suitable head gear pulleys, guide pulleys and a suitable hoisting drum.

Of all the components of a mineshaft model, the design of rope-guides and hoist ropes were found to be the most difficult. Since the rope-guides are actually the most important of all components from the point of view of dynamic behaviour, suitable guide ropes were selected and the correct linear scale factor for the model was then deduced from knowledge of the weight of such model ropes. In this way it was ensured that the model guide ropes were exactly to scale. Standard multi-lay thin steel ropes were found to be satisfactory but the natural spiral coiling of such ropes were very difficult to remove. Specially manufactured copper ropes were found to be more suitable. It was usually possible to select a suitable hoist rope from the available range of steel wire ropes. Model conveyances were constructed from brass shimstock and care was taken to obtain the overall mass, as well as the mass distribution to scale. Changes in mass distribution were readily obtained by the application of solder. Loading of conveyances were effected with wooden blocks representing man loads and pebbles and sand representing rock loads. Some

mineshafts utilise both rope-guides and rail guides. It was found that model rail guides could be conveniently readily constructed from curtain rails. The air ducts and water piping, often encountered in mineshafts, could be readily simulated with steel tubing and rods. Figure 11 depicts three model conveyances in a model shaft and shows the ropes as well as the internal structure.

Tensioning of guide ropes were usually affected with tensioning weights at the shaft bottom and Figure 12 illustrates the lower end of a shaft model, showing the lower positioning plate and tensioning weights.

3.6 Measurement and recording of conveyance deflection and lateral movements.

When performing dynamic tests on a model rope-guide conveyance, it is necessary to establish the degree of lateral swaying motion of the conveyance for a given hoisting cycle. In early model investigations use was made of a system of electric sensing wires which indicated the maximum conveyance deflection in any particular direction with reasonable accuracy. However, this method gave no indication of the exact trace followed by the model conveyance. Figure 13 depicts a cross-section of a model shaft with a rope-guide installation and indicates the position of five such sensing wires around the conveyance which was under investigation. These sensing wires were suspended along the length of the model shaft and were suitably tensioned. Each sensing wire could be shifted towards or away from the model conveyance along accurately calibrated scales fixed to both the shaft top and shaft bottom positioning plates. Copper wire contact rails were soldered in suitable positions at the top and bottom of the conveyance as indicated in Figure 13. The sensing wires were electrically insulated from the metal structure of the model and were connected to one terminal of a 4.5 Volt battery, the other terminal being earthed to the metal structure of the model. Contact of the conveyance with any particular sensing wire was indicated by one of the five electric bulbs, each of which were in circuit with

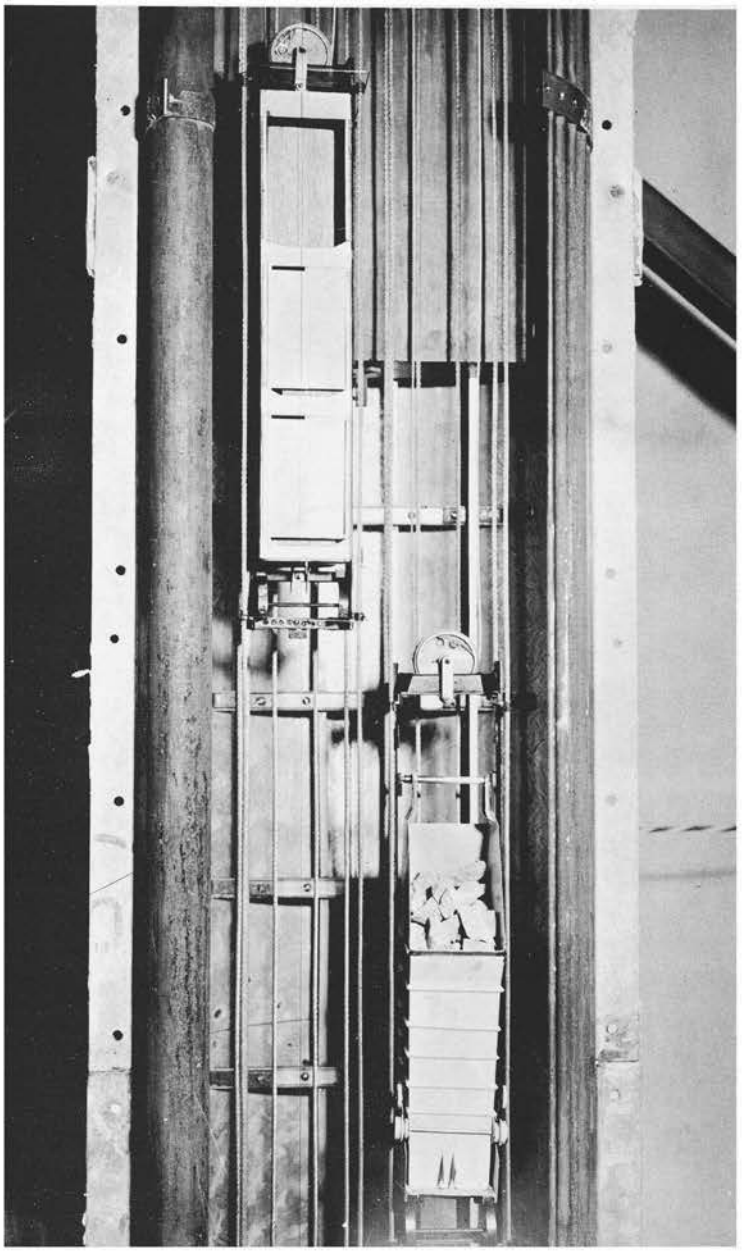

FIGURE 11

A model cage, skip and rail-guided cage in a shaft

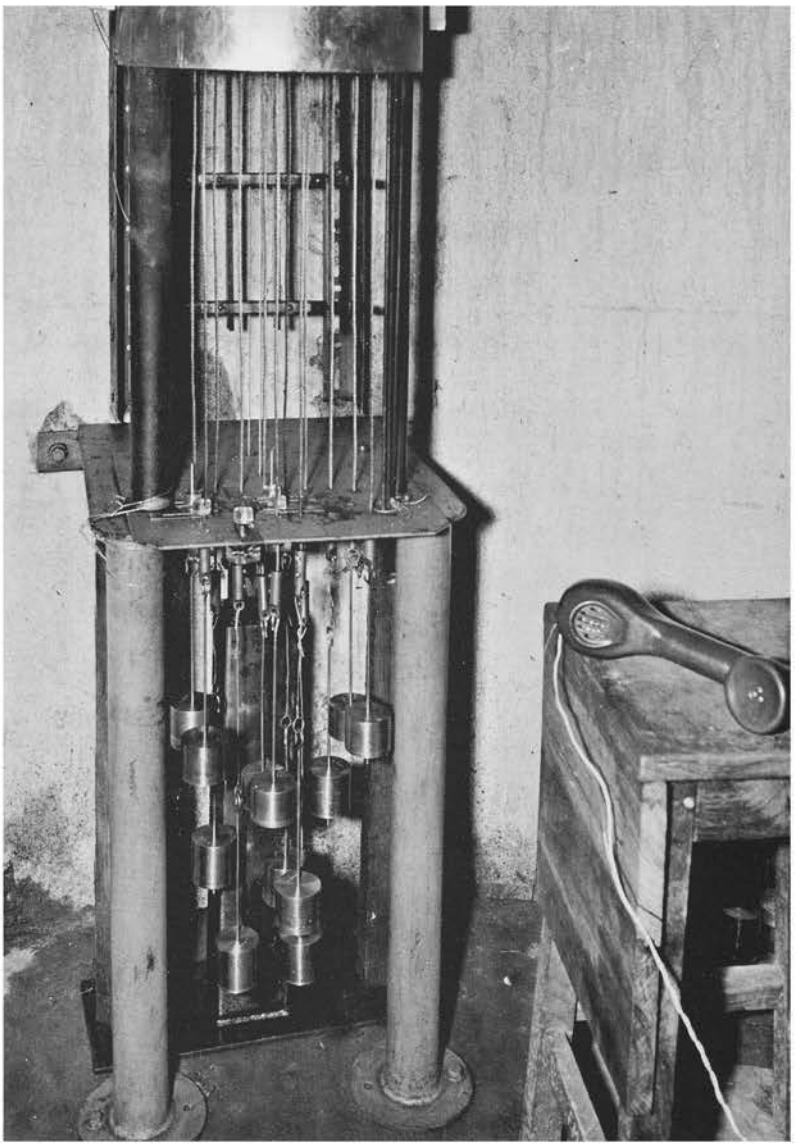

FIGURE 12

The model shatt bottom

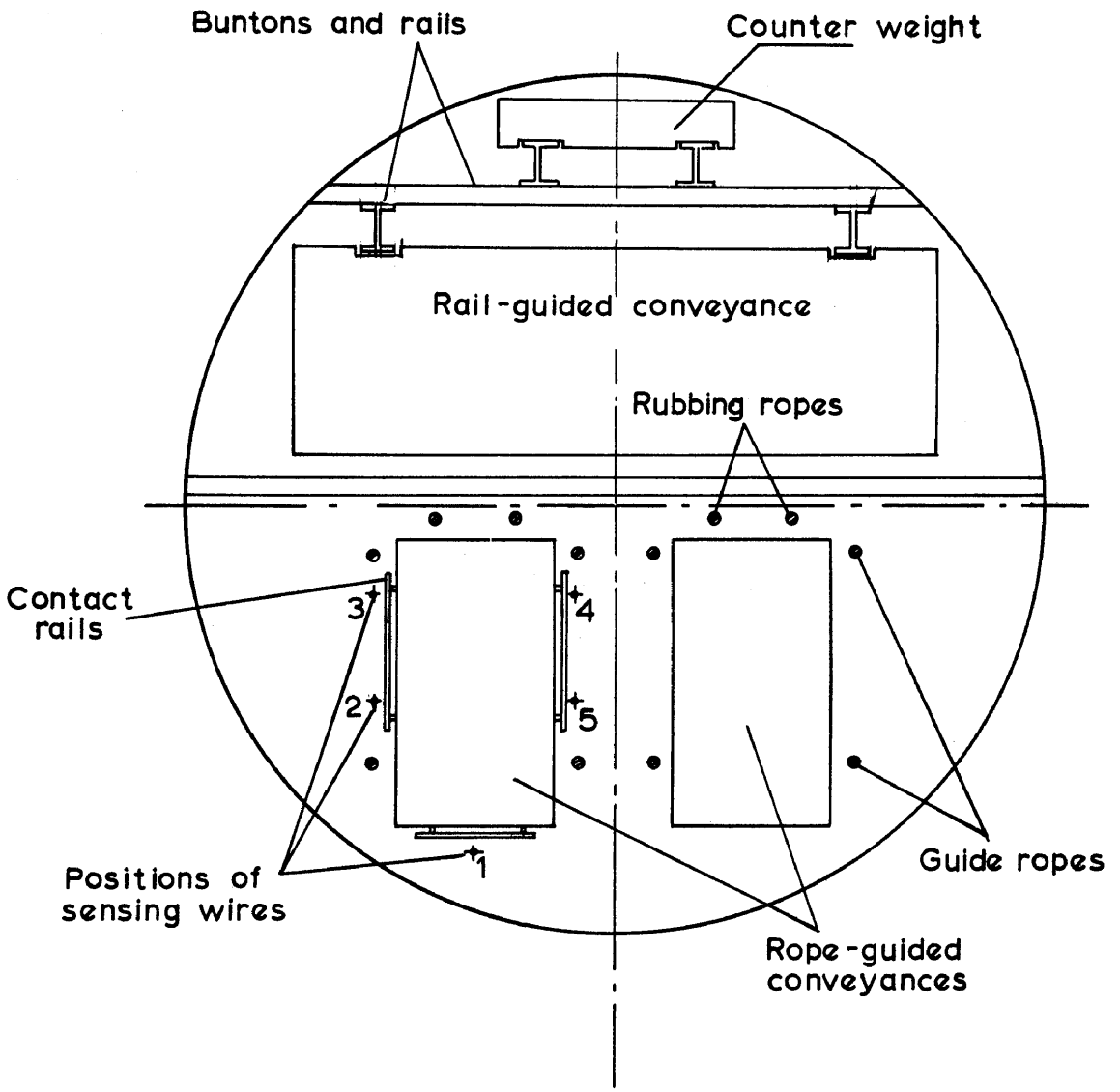

FIGURE 13

Cross-section of a model mineshaft showing positions of sensing wires

one of the five sensing wires. During testing the sensing wires were adjusted outwards until the conveyance just failed to touch any of them. It was found that conveyance deflections could be determined accurately to within 0.02 inches with this method. Difficulty was sometimes experienced with vibrations in the sensing wires during operation of the model. However, it was found that under such circumstances a slight change in the tension of the sensing wire brought it away from its resonant condition.

More detailed studies of the dynamic behaviour of rope-guide installations require graphic recordings of lateral conveyance displacements as well as pitching and yawing motion throughout a hoisting cycle. A system operating on an electro-magnetic induction principle was therefore developed to achieve such graphic recordings.

Induction coils of the type illustrated in Figure 14 were mounted on the conveyance so that their protruding legs flanked a vertical indicator cable tensioned along the entire length of the model shaft, as shown in Figure 15. This indicator cable was earthed to the metal shaft duct at the shaft bottom and insulated from the metal positioning plate at the shaft top.

A high frequency alternating magnetic field was generated between the legs of each coil by passing an electric current from a miniature high frequency transistor oscillator, installed inside the model conveyance, through the coil windings. In this manner an e.m.f. was generated in the loop formed by the indicator cable and the metal structure of the model shaft. The e.m.f. was fed, through amplifying and rectifying equipment, to a three-channel ink-jet recorder which was installed in the test room.

As illustrated in Figure 14 the magnetic lines of force between the legs of the induction coil were found to be reasonably uniform and parallel in the central area where the indicator cable was situated. Any relative displacement between the indicator cable and induction coil (or conveyance) in the direction perpendicular

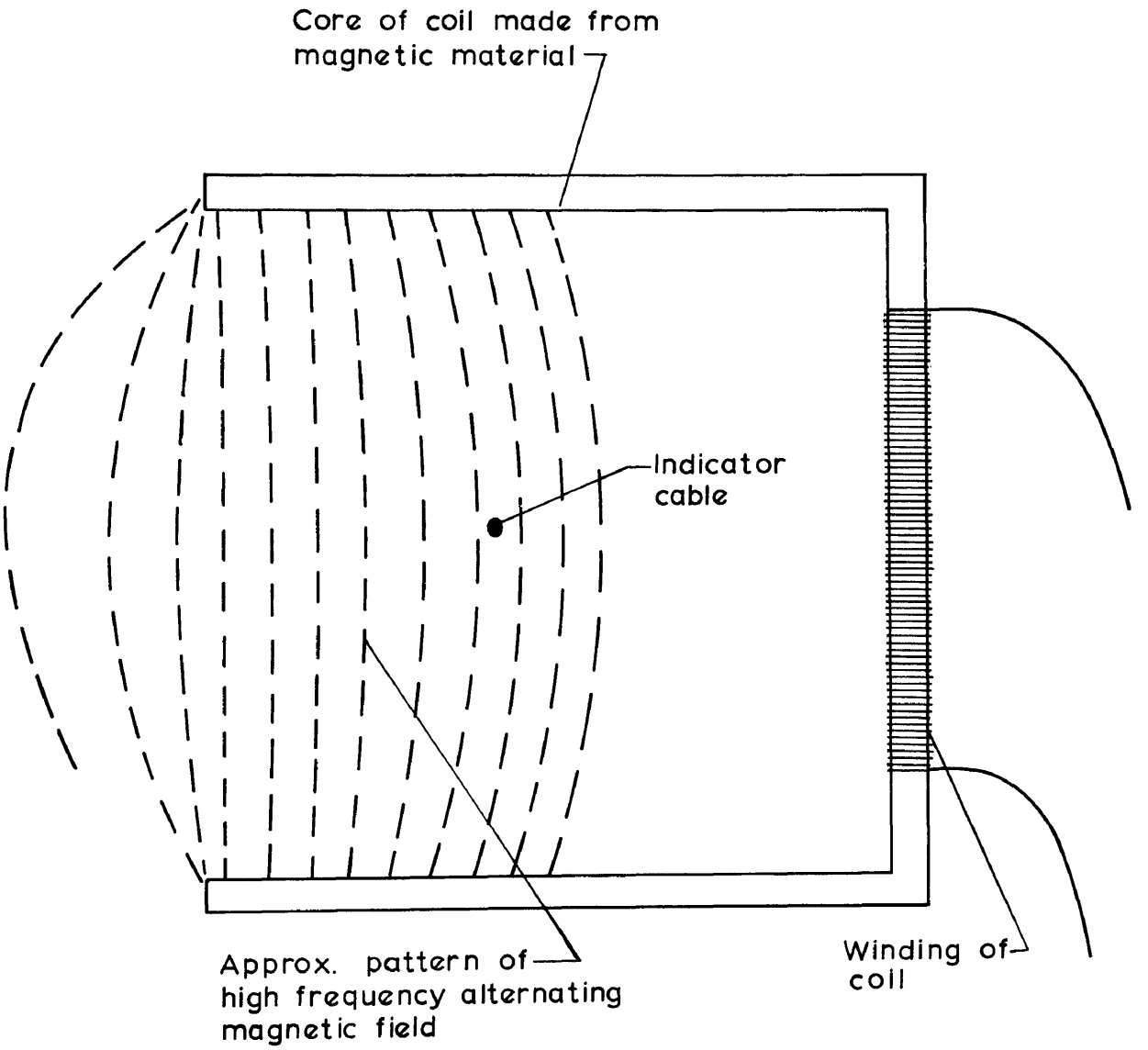

FIGURE 14

The induction coil

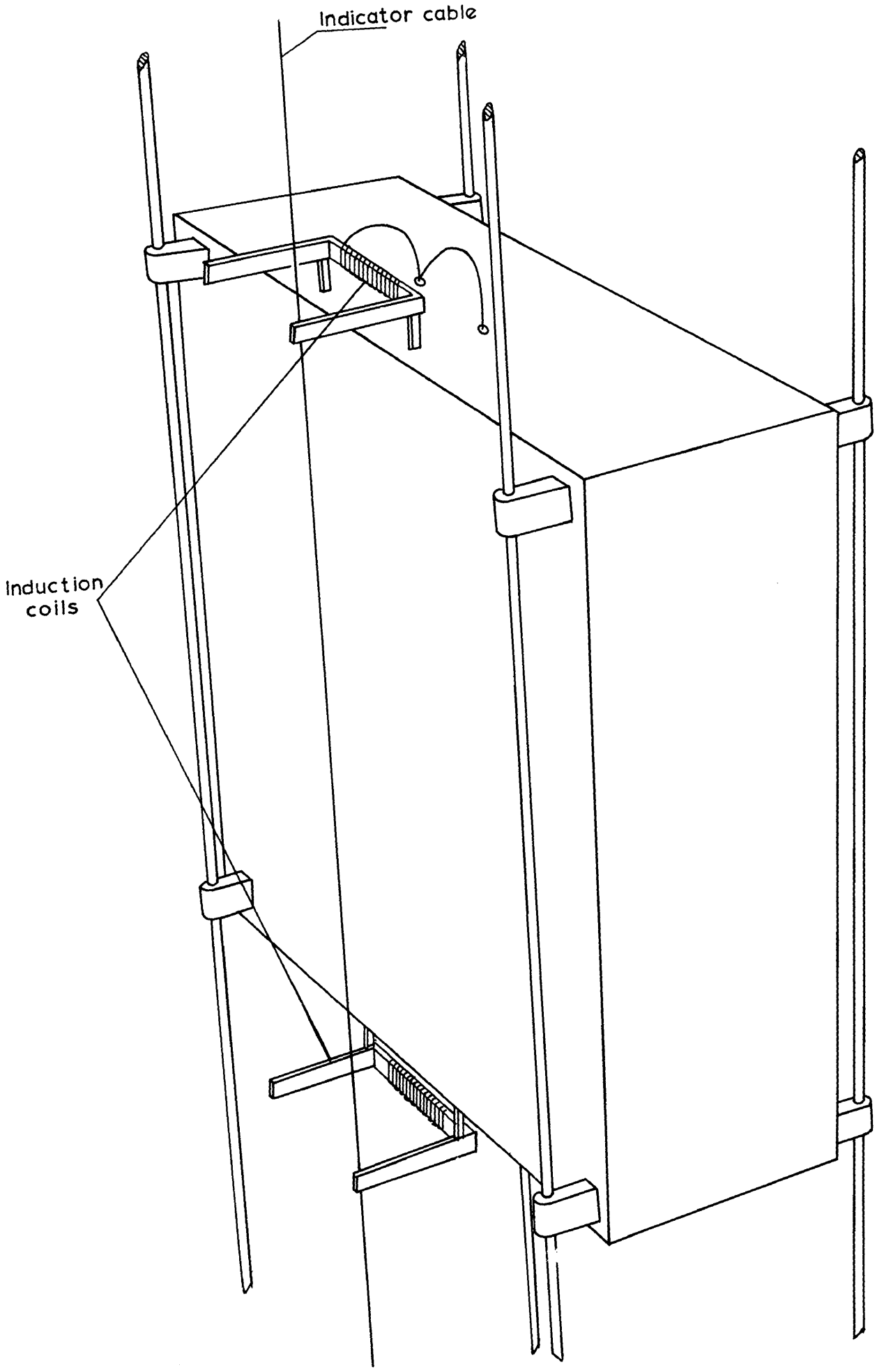

FIGURE 15

Induction coils mounted on a model conveyance

to the magnetic lines caused a change in the e.m.f. induced in the indicator cable, owing to the resulting change in the number of magnetic lines linking the indicator cable. This change in e.m.f. was proportional to the displacement by virtue of the uniformity of the magnetic field in the vicinity of the cable. By suitable calibration it was then possible to interpret linear displacement of the induction coil in terms of the induced e.m.f. recorded.

The equipment was furthermore practically insensitive to small displacements in a direction normal to that just considered because of the parallel pattern of the magnetic lines in the vicinity of the indicator cable.

In order to measure displacements of the conveyance simultaneously in two mutually perpendicular directions, a system of two induction coils and two separate indicator cables was used.

For the study of pitching motion of the conveyance two induction coils were fitted vertically in line with each other, one at the top and the other at the bottom of the conveyance as illustrated in Figure 15. By operating the coils at different frequencies a single indicator cable could thus be used for picking up both signals simultaneously.

The arrangement of the electronic equipment used for such a dual recording system is illustrated schematically in Figure 16. The electronic oscillator units, utilising transistors and powered by small mercury cells, were extremely small and it was found that these units could be readily installed in small model conveyances, forming part of the rock-load or man-load. The e.m.f. signals induced in the indicator cable were fed into a radio frequency transformer and from there into two duplicated parallel net-works. Each net-work consisted of a tuned amplifier, adjusted to pick up only one of the two frequencies and a detector which converted the A.C. signal into a steady D.C. signal and also served to back-off the potential to a suitable level. The two signals were then fed into the two channels of a standard ink-jet recorder.

..... 49

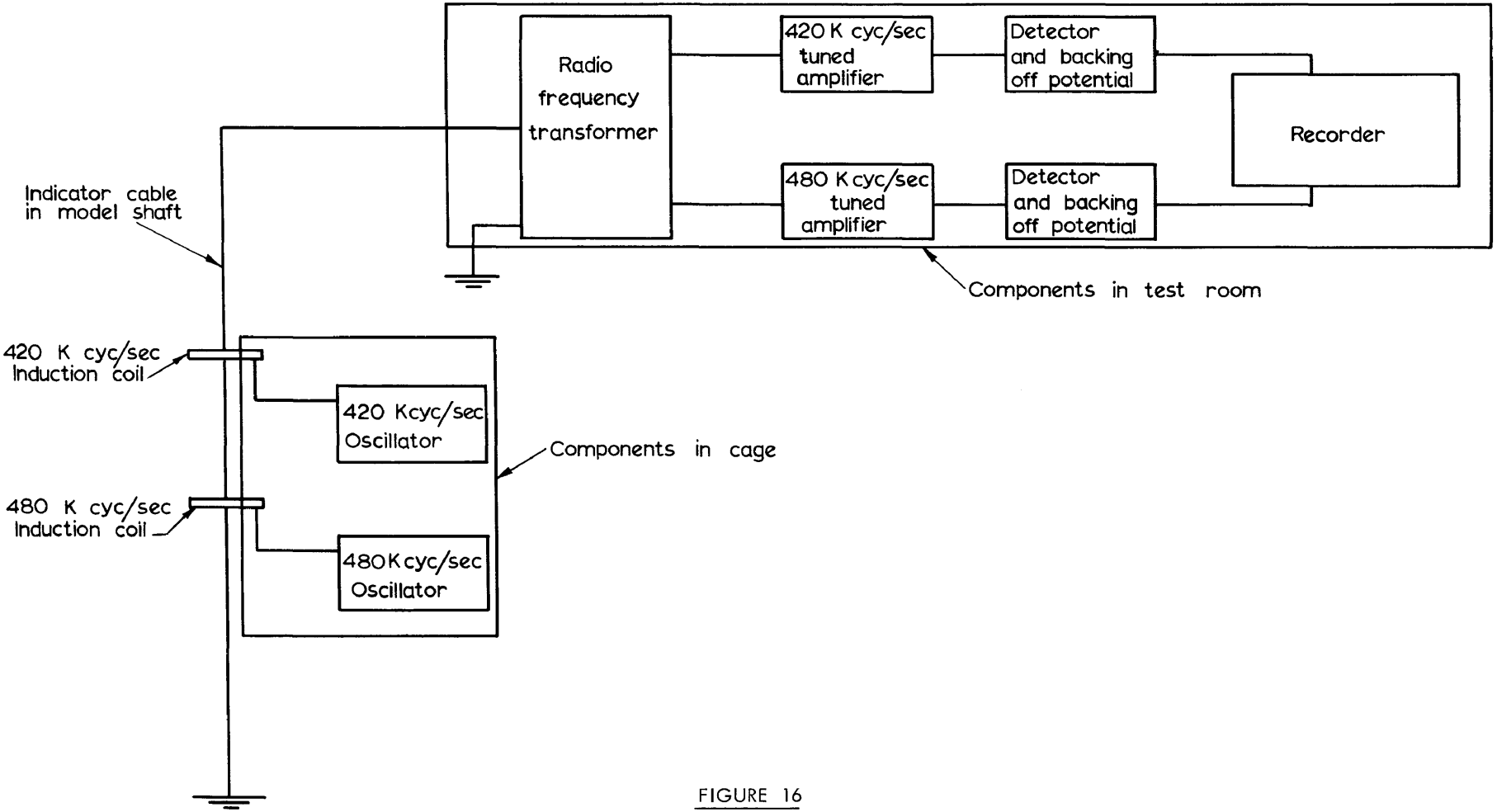

FIGURE 16

Schematic block diagram of electronic equipment used in model tests

Figure 17 gives a circuit diagram for a type of miniature high frequency oscillator which was found suitable for installation in model conveyances.

Since lateral displacements of conveyances were recorded on a time base in the ink-jet recorder, it was necessary to provide distance marks, relating the vertical position of the conveyance in the shaft to the time base on the displacement recordings. To achieve this the third channel of the ink-jet recorder was connected into an electric circuit which included a simple contact switch on the model hoisting drum. In this way it was possible to produce displacement pips, each representing one revolution of the hoist drum, on the recording paper. These distance marks and the time scale on the recording paper provided a convenient means of deducing the instantaneous velocity of the conveyance at any level in the shaft.

The displacement recording system was calibrated by moving the conveyance with its induction coils towards and away from any particular indicating cable in measured steps and recording the induced e.m.f. on the recording paper of the jet recorder at each position. The calibration scale thus produced, enabled displacement of the conveyance to be derived from the traces on the recording paper at any position of the conveyance in the shaft. Figure 18 shows a device which was constructed to effect this calibration. The model conveyance was clamped to a small platform which could be moved by two lead screws in two mutually perpendicular directions. The heads of these lead screws were calibrated to read off the displacement of the conveyance accurately to within 0.002 inches.

4. CORRELATION TESTS.

4.1 General.

As pointed out in section 1.3 it was decided to conduct correlation tests in order to establish with what degree of confidence dynamic scale model investigations may be used to predict the dynamic behaviour of a fullscale rope-guide mineshaft installation.

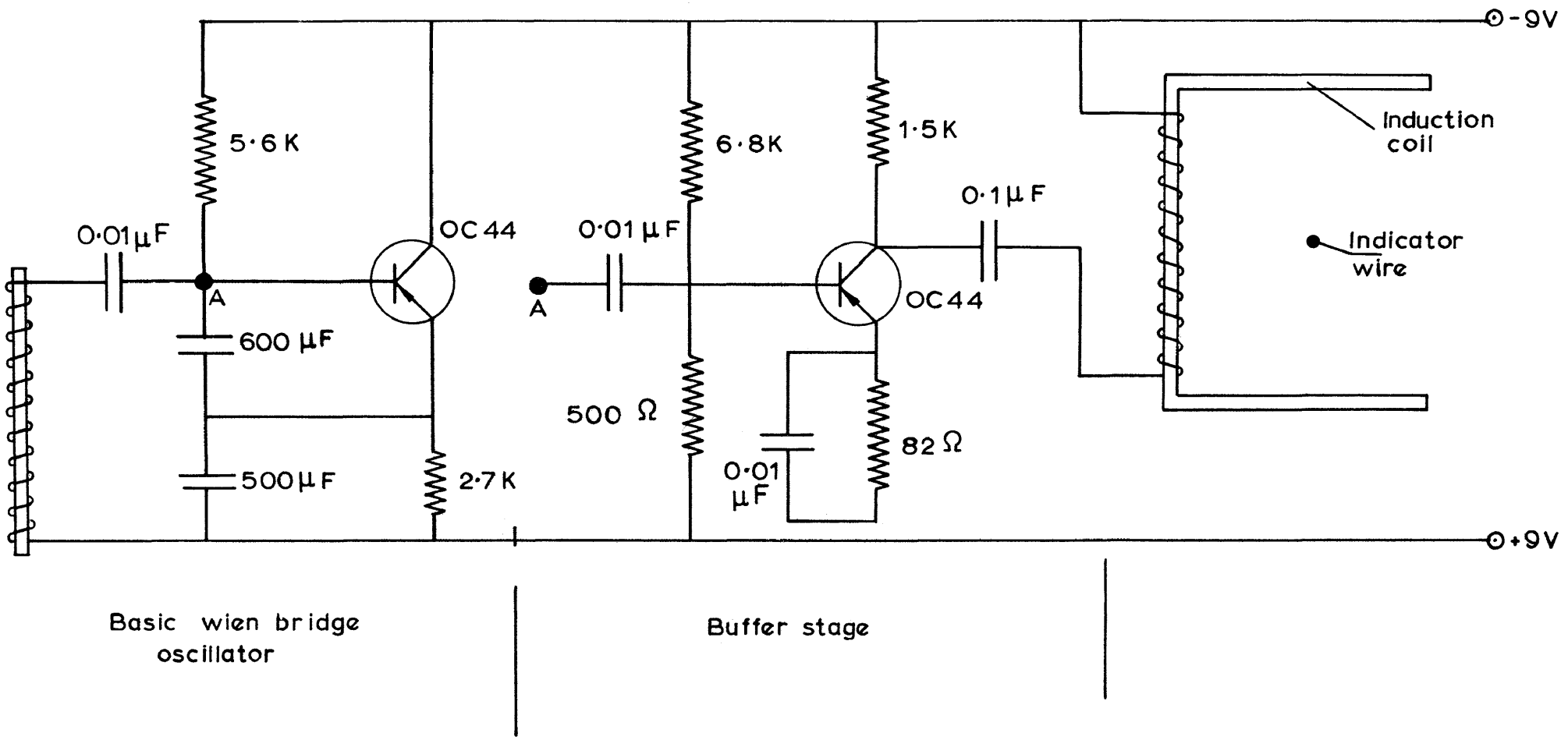

FIGURE 17

450 K. cyc/sec. oscillator and buffer stage used in model instrumentation

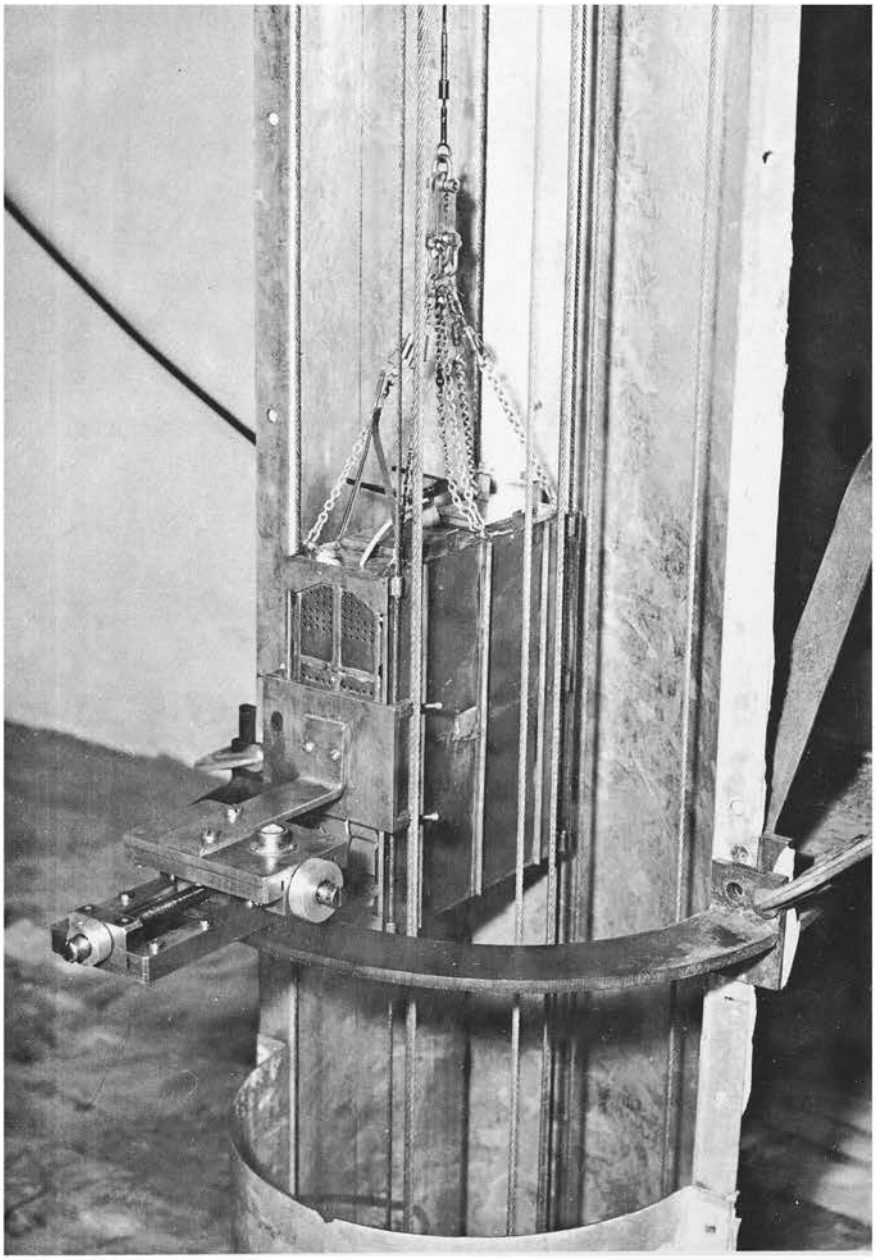

FIGURE 18

Device for calibrating deflection of model conveyance

The rope-guide installation in the Durban Roodepoort Deep Circular Shaft was selected as a suitable fullscale prototype and a dynamic scale model of this installation was developed for the purpose of the correlation tests.

Two types of correlation tests were conducted, namely:

(i) Hoisting tests in which the lateral displacements and the pitching motion of a conveyance were studied during normal hoisting cycles and in which all force effects encountered in practice were prevalent.

(ii) Impact tests, in which the oscillatory motion of the conveyance, initially at rest, was studied after measured impulses were imparted to the conveyance in a lateral direction. In these tests inertia and tension forces were prevalent and aerodynamic forces were relatively insignificant. The impact tests were therefore chiefly aimed at comparing the wave motions in the model and fullscale ropes and at the study of damping forces acting on an oscillating conveyance.

The impact tests were regarded as supplementary to the hoisting tests. Oscillatory motion of the conveyances and wave motion in ropes are of course also prevalent during hoisting tests but it was thought advisable to investigate these oscillatory conditions separately without the added complication of aerodynamic force effects on a moving conveyance. Furthermore the stationary impact tests afforded the opportunity to examine and compare the reaction of model and fullscale conveyances to impulsive forces.

4.2 Experimental Equipment.

4.2.1 Fullscale Equipment.

4.2.1.1 Shaft Data. The Durban Roodepoort

..... 54

Deep Circular Shaft, which was made available for the correlation tests at the request of the Chamber of Mines, is a downcast shaft equipped with two closed-type rope-guided conveyances, operated by a balanced drum winding system.

Figure 19 illustrates the vertical layout of the shaft along its overall depth of 3036 feet, while a plan view of the cage and rope arrangement in the shaft is presented in Figure 20. The two cages in this mineshaft are identical and are arranged symmetrically in the shaft. All tests were performed on the cage in the south compartment.

Ventilation air flows at a rate of approximately 85,000 c.f.m. and is drawn off through station cuttings at 17 and 18 Levels and through an air passage at the bottom of the shaft. No air is drawn off through the station cutting at 12 Level.

The upper extremities of the $1\frac{7}{8}$ inch diameter guide ropes are fixed to the headgear structure 82 feet above ground level. At 18 Level the guide ropes are located by guide eyes and the guide rope tensioning weights are situated just below this level. Figure 31, which is a photograph of a scale model, illustrates the cage design. A man-load of 6000 pounds can be transported on the upper deck while the lower deck supports two trucks each having a rock-load capacity of 6600 pounds. The cage suspension consists of the conventional capple, hook and four chains with two slack safety chains in the centre of the cage. The protective roof attached to the suspension chains is only provided when men are travelling on top of the cage.

The following data relating to the fullscale installation were of importance for the design of a dynamic scale model.

Guide ropes

Weight at date of installation: 8.50 pounds $feet^{-1}$
Present weight (making a correction for wear): 8.33 pounds $feet^{-1}$
Free length measured from upper support to bottom guide eyes: 3082 feet.

..... 55

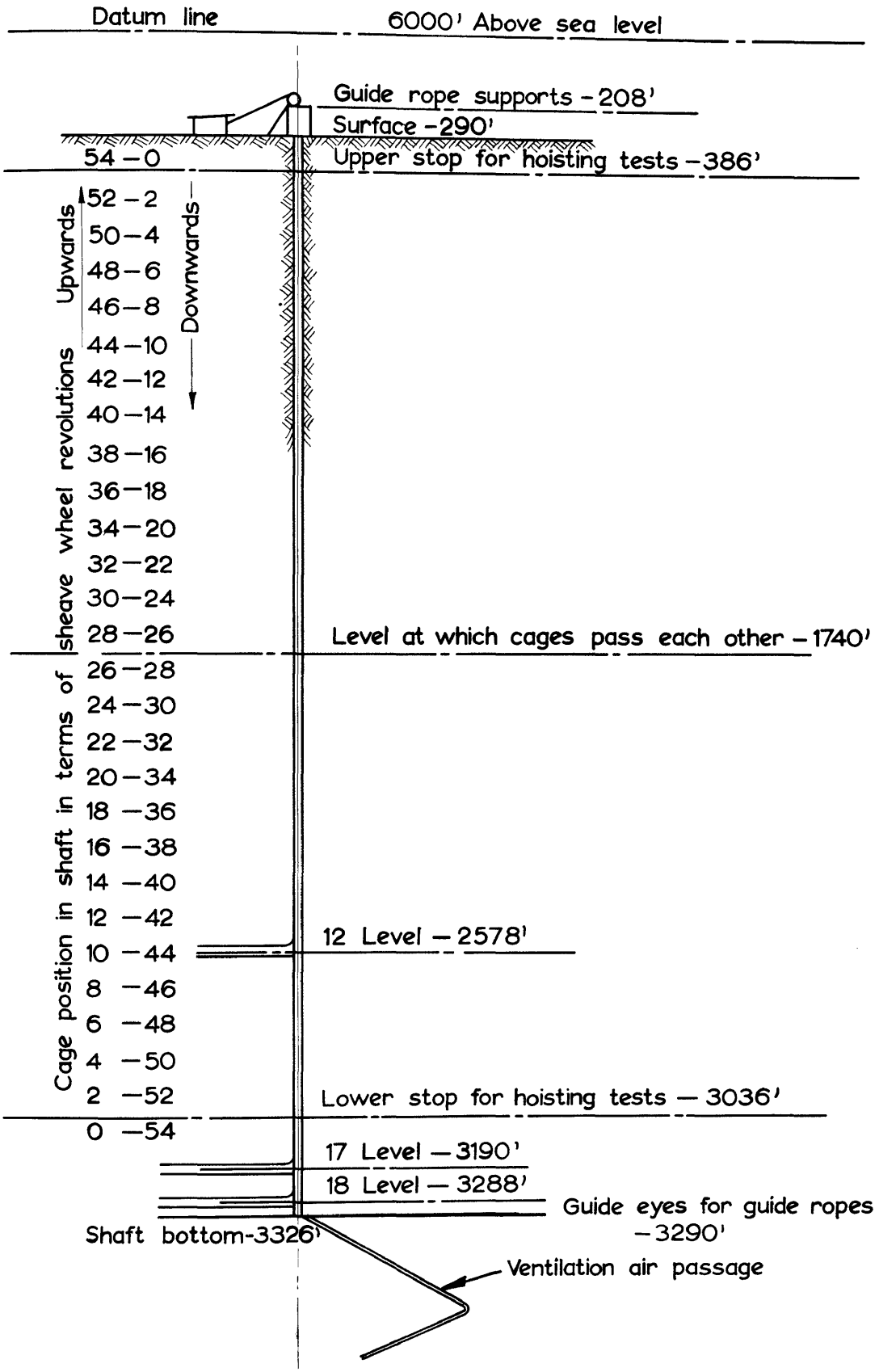

FIGURE 19

Vertical layout of the Durban Roodepoort Deep circular shaft

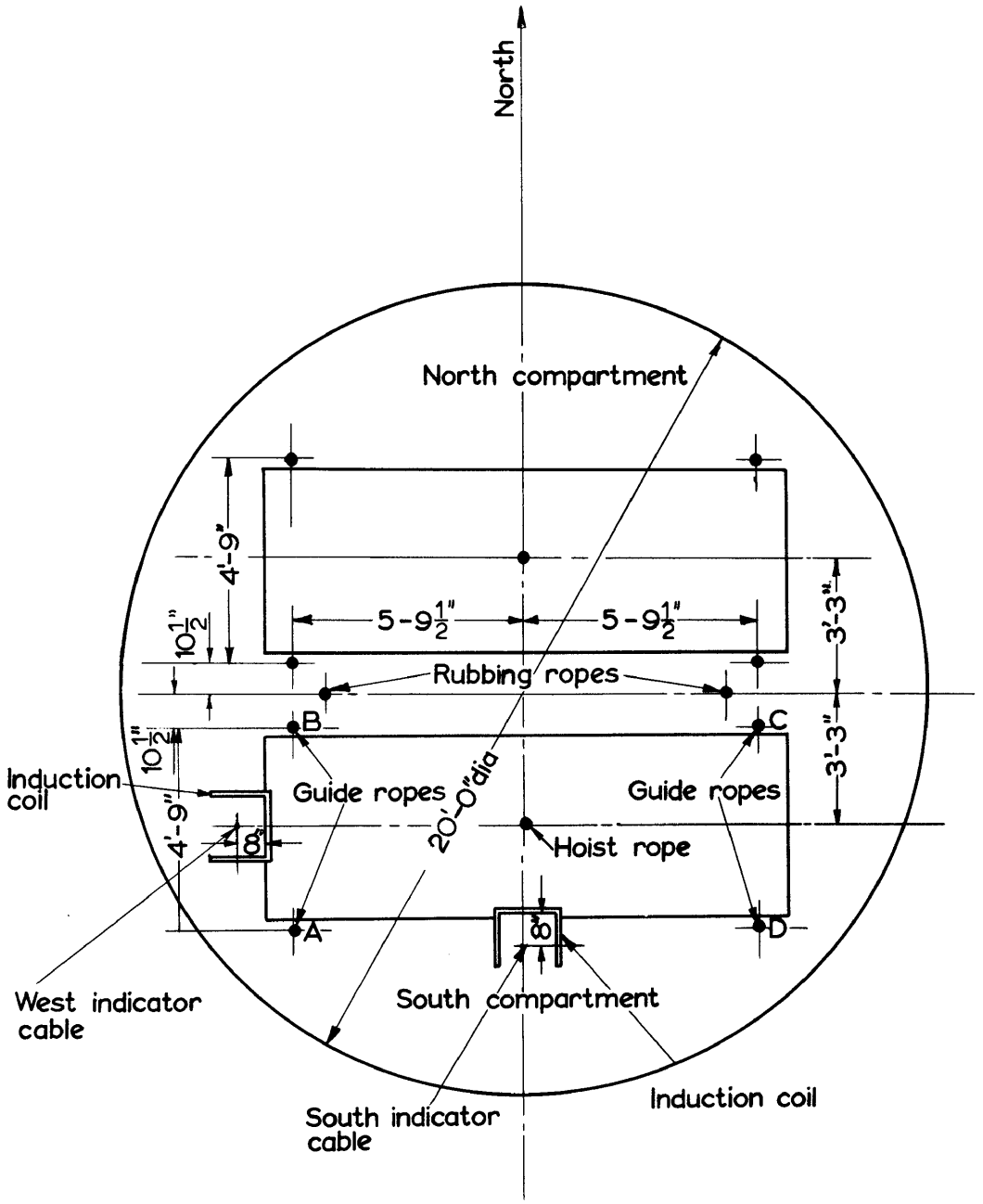

FIGURE 20

Cross-section of Durban Roodepoort Deep circular shaft

Type: Half locked coil.

Guide rope tensioning weights

Referring to Figure 20, tensioning weights on guide ropes A, B, C and D were respectively 10500 pounds, 9450 pounds, 10500 pounds and 11550 pounds.

Hoist rope

Weight: 5.627 pounds $feet^{-1}$
Type: Non-spin.

Cage and loads

Weight of cage and suspension: 14366 pounds.
Weight of railing and protective roof on top of cage: 560 pounds.
Weight of one empty truck: 2000 pounds.
Weight of rock load in one truck: 6600 pounds.

Air and cage velocities

Normal ventilation air flow: approximately 85,000 $feet^{3}$ $minutes^{-1}$.
Maximum hoisting speed: approximately 2,700 feet $minutes^{-1}$.

4.2.1.2 Displacement Recording Equipment.

In order to study the dynamics of this fullscale rope-guide installation, it was necessary to obtain graphic recordings of the lateral displacements as well as pitching motions of a conveyance during hoisting operations. A system operating on an electro-magnetic induction principle, identical to the system described in section 3.6, was therefore developed for this purpose.

Figure 21 illustrates the type of electro-magnetic induction coil with its wooden supporting structure, used on the cage. Figure 22 depicts two such induction coils mounted on the south side of the cage for measuring north-south deflections and pitching in the north-south plane. The oscillators serving these two coils were installed inside the cage together with the two twelve-volt accumulators used as a power source. Figure 23 illustrates a

..... 58

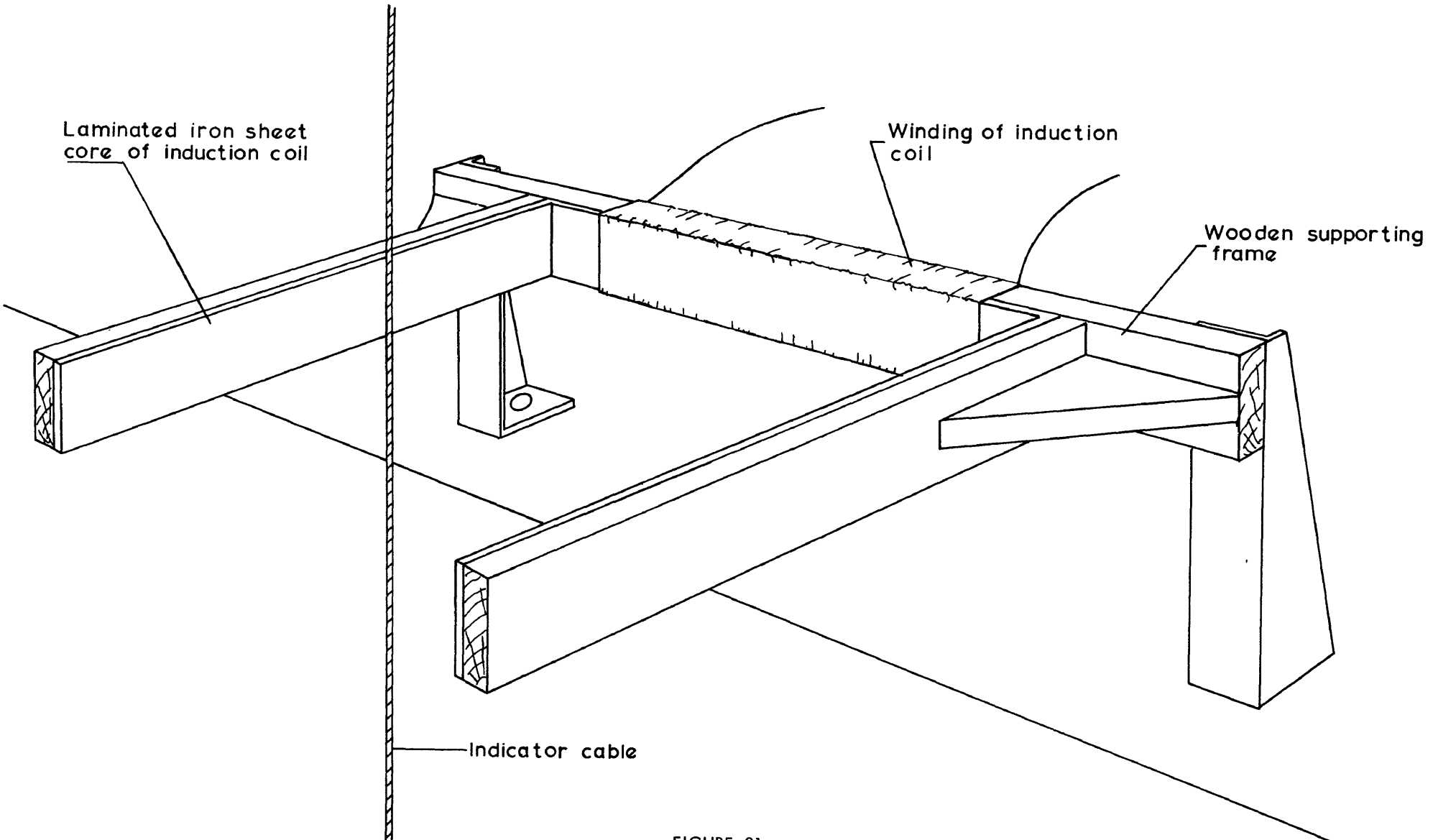

FIGURE 21

An induction coil mounted on a cage root

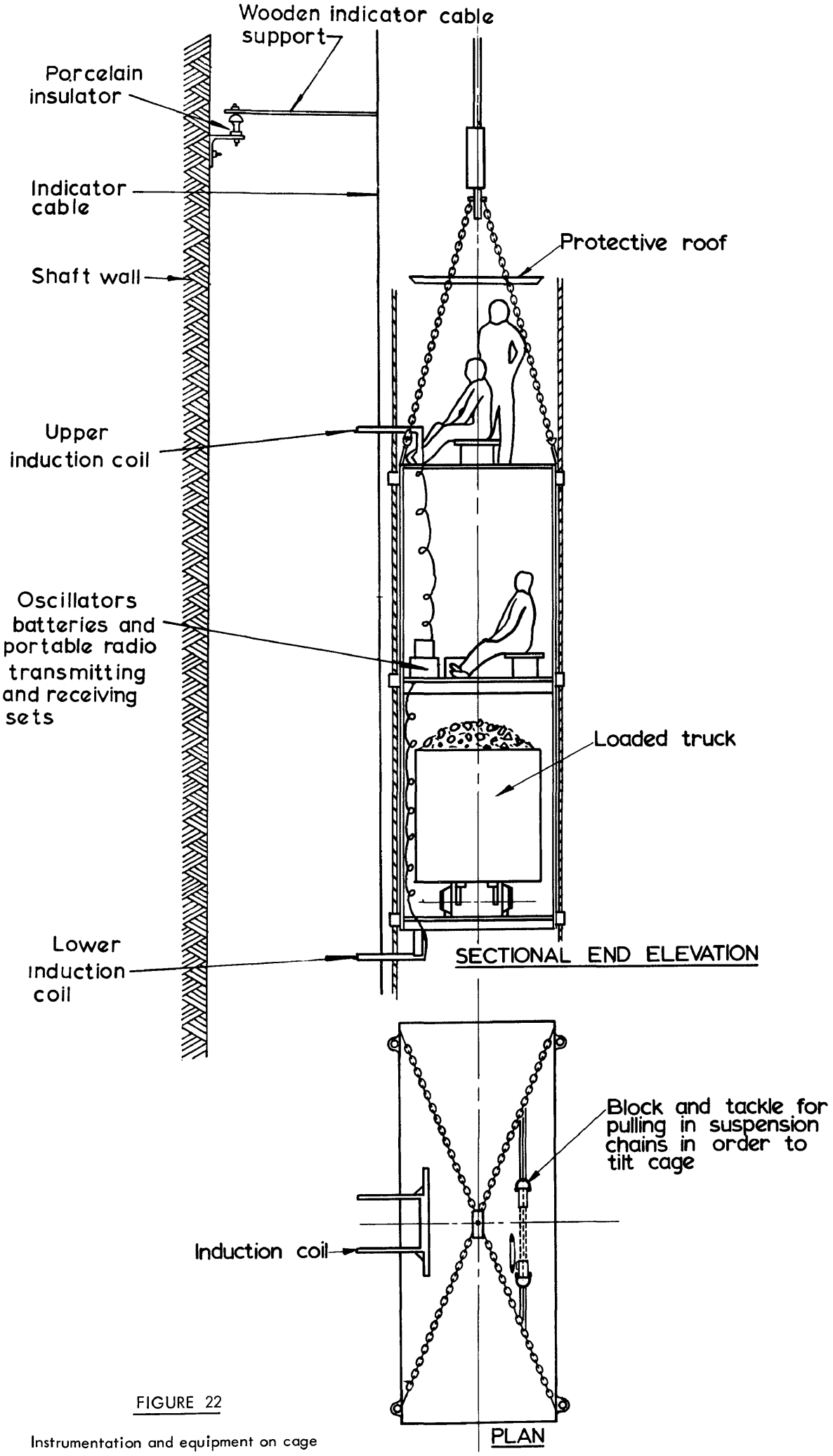

FIGURE 22

Instrumentation and equipment on cage

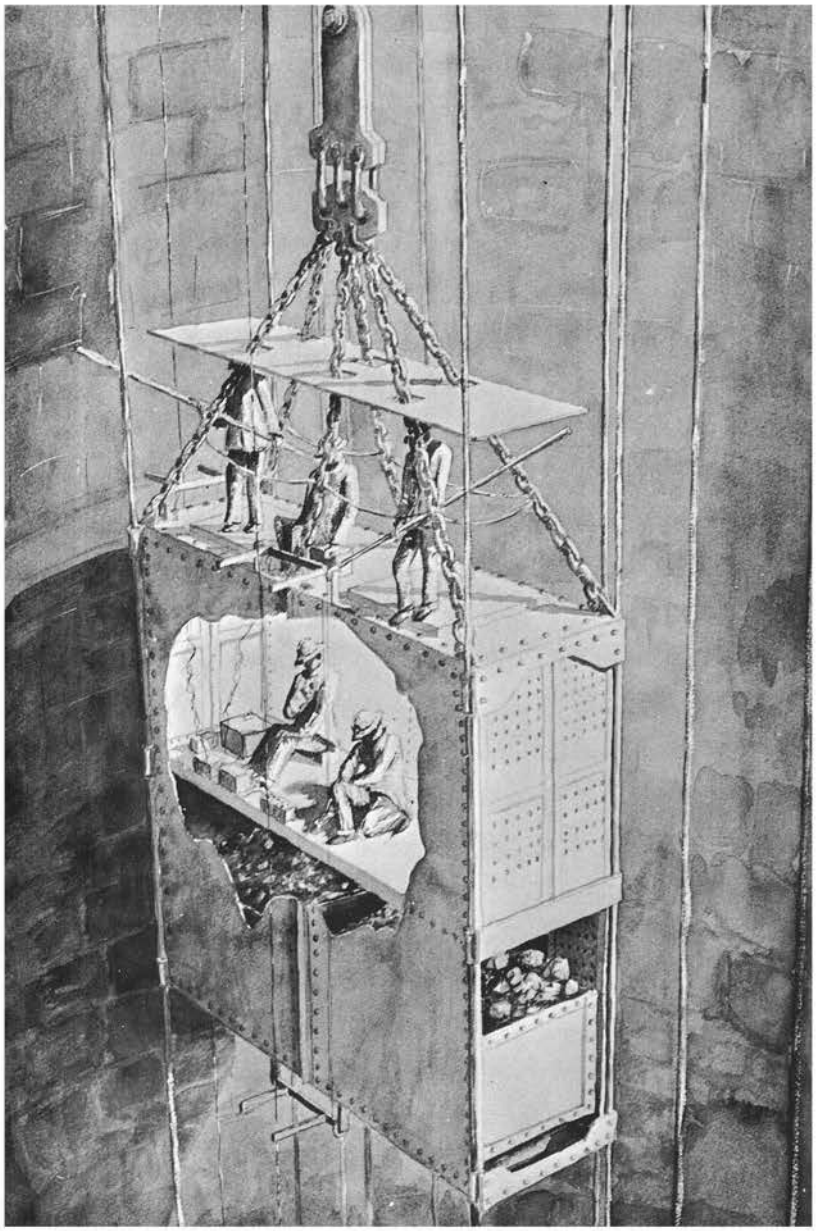

FIGURE 23

Full-scale conveyance equipped for tests

cage in the shaft fully equipped and manned for testing purposes.

Since the indicator cables, rigged up along the entire length of the shaft, represented the reference lines from which cage deflections were measured it was imperative that they remained rigid during hoisting operations. These cables were of steel, $\frac{3}{8}$ inch in diameter, each tensioned by a 200 pound weight and supported at intervals of 200 feet by light wooden brackets illustrated in Figure 22. These brackets were attached to the shaft wall with porcelain insulators to ensure no current leakage and the cable was carefully attached to the wooden struts to ensure that they remained plumb. Observations made with a theodolite at 12 Level indicated that no swaying or vibration of any consequence took place in the cables during hoisting.

At the top of the shaft the indicator cables were lashed to one of the supporting girders of the head gear but was carefully insulated from the steel structure. At the shaft bottom the indicator cables were earthed to one of the steel guide ropes, thus forming circuits for inducing the high frequency signals from the induction coils on the cage. Three leads, two from the indicator cables and one earth lead connected to the steel structure of the head gear, transmitted the signals to the electronic amplifying and filtering equipment and recorder which was housed in a panel van standing next to the head gear tower. The arrangement of all the electronic equipment is illustrated schematically in Figure 24.

Because of the limited power available from the accumulators which had to be used to power the oscillators, it was of course necessary to operate these large oscillators at relatively low frequencies of 1000 and 350 cycles per second. At these frequencies interference effects on the induction system, due to various power sources in and around the mineshaft, is considerably more troublesome than for the high frequencies employed in model induction systems described in section 3.6. As indicated in Figure 24 it was necessary to include 350 cycles per second and 1000 cycles per second filters in the circuits in order to

..... 62

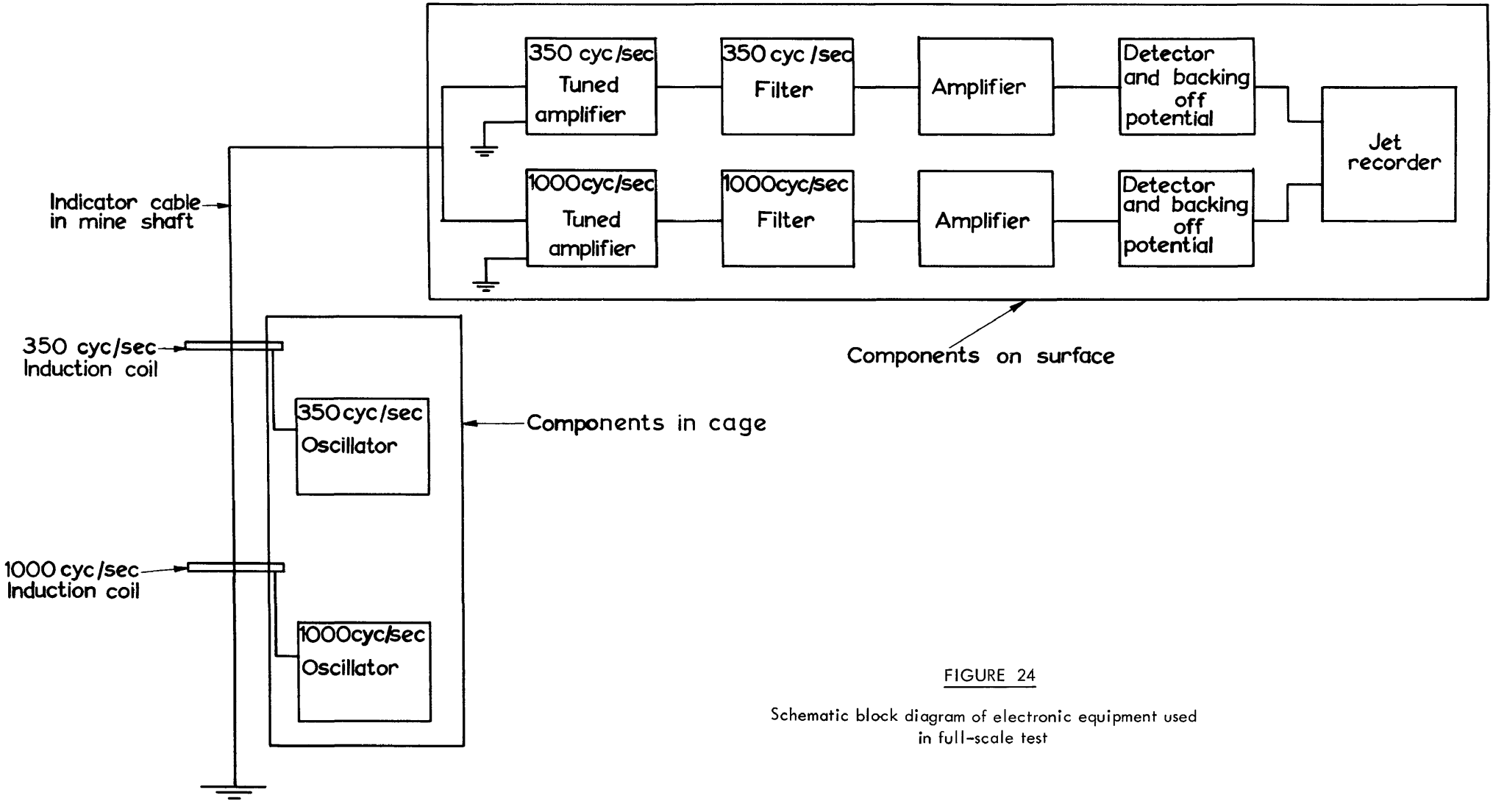

FIGURE 24

Schematic block diagram of electronic equipment used in full-scale test

minimise interference effects.

Figure 25 depicts a circuit diagram for a transistor oscillator and power amplifier which was installed in the cage. A simple spring contact switch operated by a cam on the sheave wheel in the head gear, was used to produce electrical impulses which could be recorded by the ink-jet recorder as displacement pips on the recordings of cage motion. The vertical position of the cage in the shaft was therefore given in terms of sheave wheel revolutions. Figure 19, which represents the vertical layout of the Durban Roodepoort Deep Shaft to scale, indicates cage positions in the shaft in terms of sheave wheel revolutions.

4.2.1.3 The Impulse Machine. In order to examine the effect of impulsive forces acting on a rope-guided conveyance, it was necessary to develop a device which would be capable of imparting a measured impulse to a conveyance suspended at rest in the shaft. For this purpose an apparatus, operating on the principles of an impact hammer, was developed.

Figure 26 depicts the 9 feet 8 inches long pendulum of this impulse machine. This pendulum was pivoted at point O on ball bearings in a steel frame and consisted of a light steel angle structure supporting a steel box filled with lead. The total weight of the pendulum was 740 pounds. A semi-circular steel impact head A which made contact with the cage imparting an impulse to the latter, was bolted to the pendulum. Its location was such that the line of the imparted impulse vector passed through the centre of percussion B of the pendulum, thus ensuring no undue reaction at the pivot bearing O. A calibrated angular scale attached to the frame which supported the pendulum allowed the measurements of the initial angle of elevation of the pendulum as well as the angle of rebound after the impulse had been imparted to the cage. Figure 34 depicts the whole impulse machine showing the pendulum mounted inside its supporting frame.

Figure 27 illustrates the installation of the pendulum and its supporting frame in the station cutting at 12 Level where these

..... 64

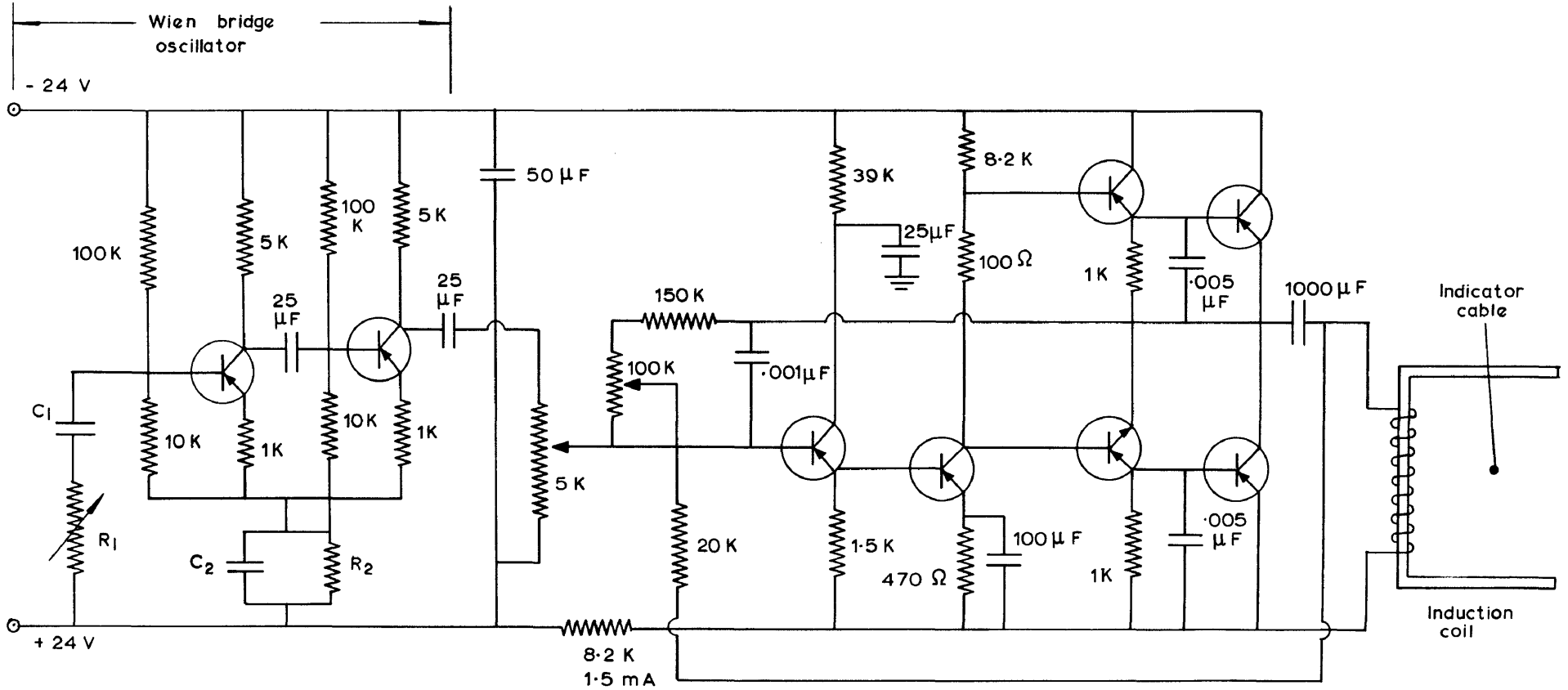

FIGURE 25

Transistor oscillator and power amplifier used in full-scale recording equipment

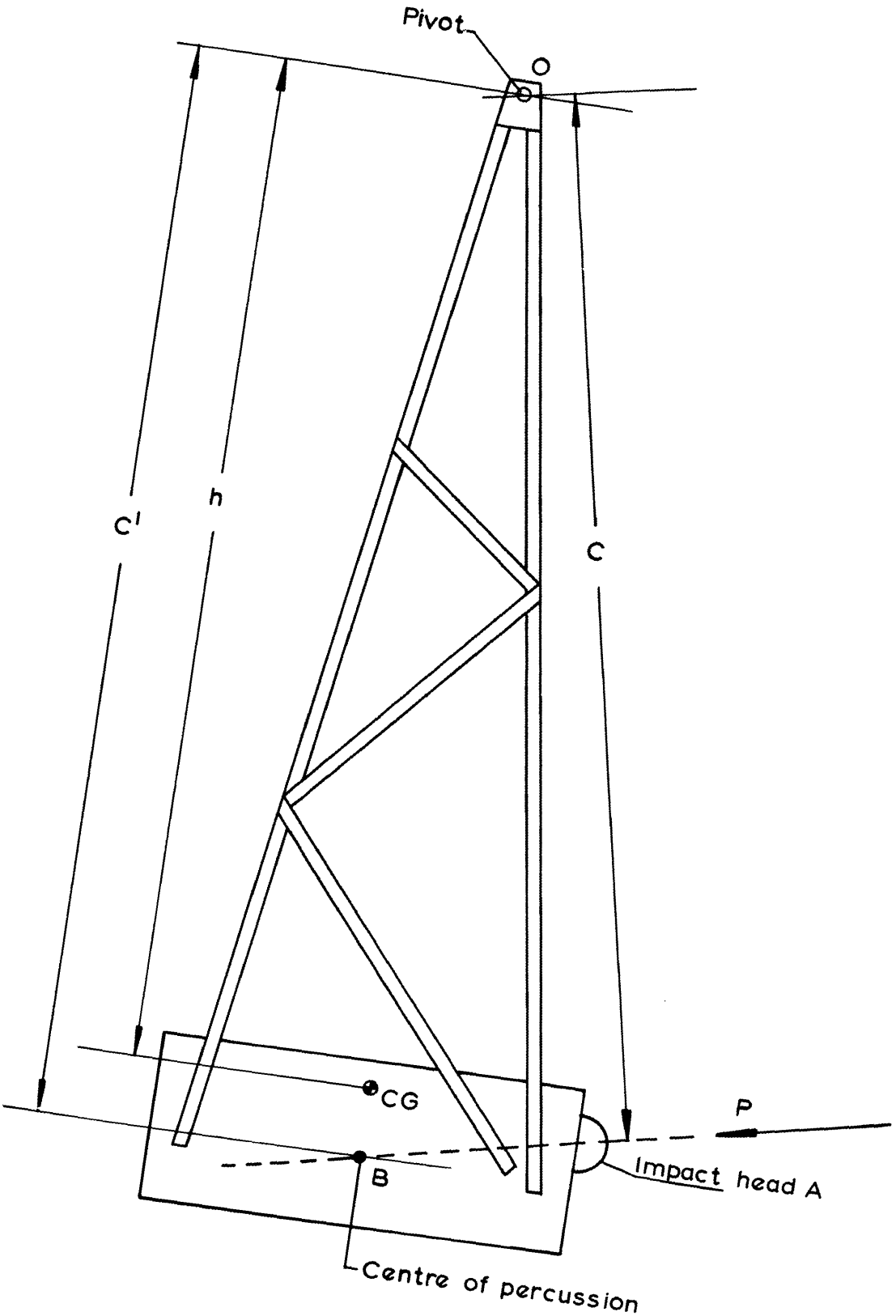

FIGURE 26

The impulse pendulum

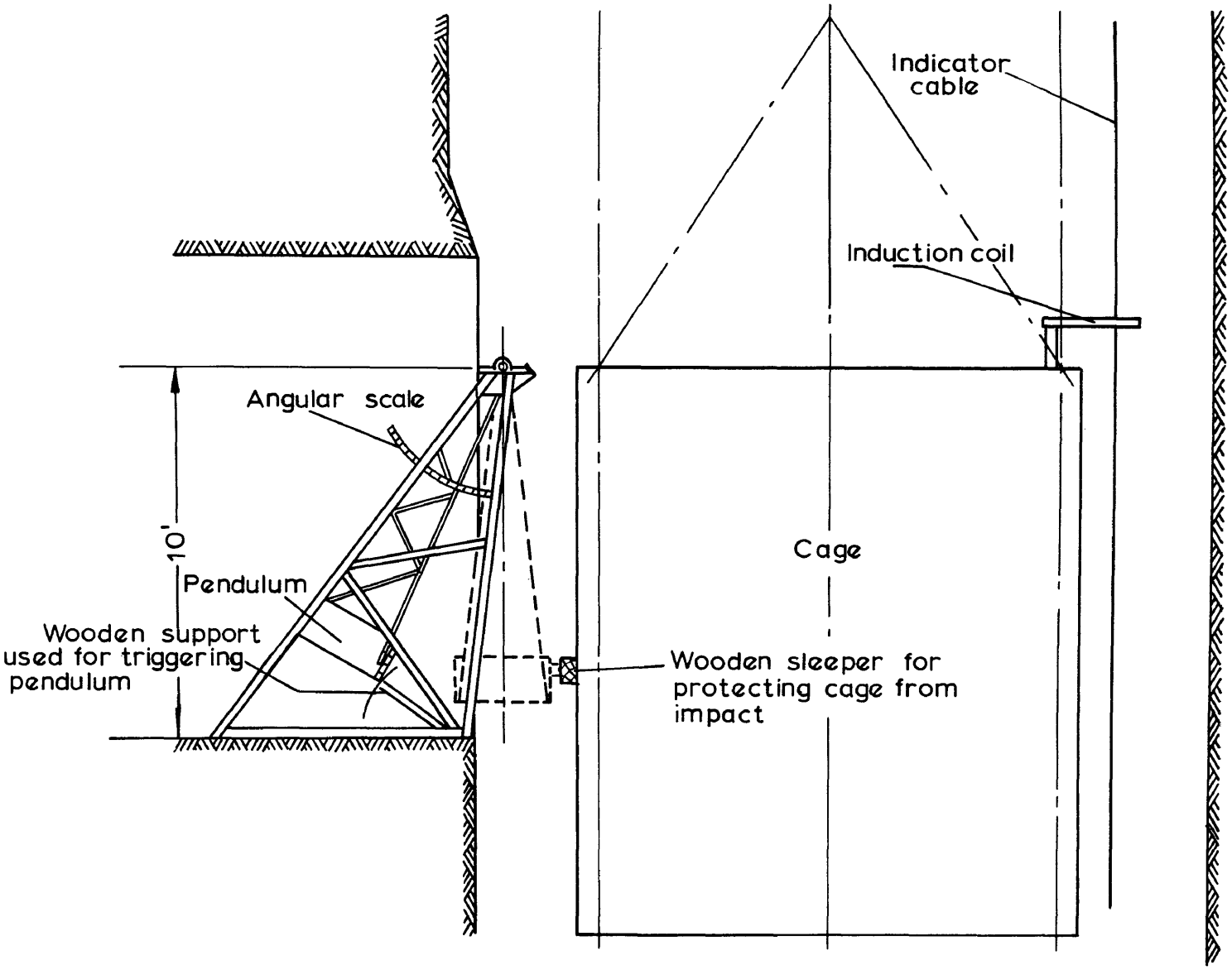

FIGURE 27

The impulse machine installed in the station cutting at 12 level

impact tests were carried out. A wooden sleeper, receiving the impact from the hammer and preventing damage to the cage structure, was bolted to the side of the cage in line with its centre of gravity. The pendulum was suspended so that, when hanging at rest the steel impact head just touched this wooden sleeper. The upper induction coil on the west side of the conveyance, directly opposite the impulse machine was used to record the oscillatory motion of the cage following an impact.

Referring again to Figure 26 let

P = impulse in pound seconds imparted by the pendulum.

M_p = mass of pendulum in slugs.

k = radius of gyration of pendulum about the pivot point O in feet.

h = distance in feet of the centre of gravity of the pendulum from its pivot point.

c = perpendicular distance in feet between the line of action of the impulse P and the pivot point of the pendulum.

C^1 = distance in feet between the centre of percussion and the pivot point of the pendulum.

θ_1 = initial angle of elevation of pendulum before release, measured from its position of rest.

θ_2 = angle of rebound of pendulum after impact, measured from its position of rest.

$\dot{\theta}_1$ = angular velocity of pendulum in radians seconds^{-1} just before impact.

$\dot{\theta}_2$ = angular velocity of rebound of pendulum just after impact.

..... 68

Considering angular momentum of the pendulum about O during the process of the impact.

$$P = \frac{M_p k^2}{c} (\dot{\theta}_1 + \dot{\theta}_2) \qquad \ldots\ldots\ldots\ldots\ldots\ldots\ldots\ldots (1)$$

Potential energy gain when pendulum is raised to its angle of elevation θ_1

$$= g M_p h (1 - \cos \theta_1) \text{ foot pounds}$$

Kinetic energy of pendulum just prior to impact

$$= \tfrac{1}{2} M_p k^2 \dot{\theta}_1^{\,2} \text{ foot pounds}$$

Equating potential and kinetic energy and ignoring the slight friction losses it follows that

$$\dot{\theta}_1 = \sqrt{\frac{2gh}{k^2} (1 - \cos \theta_1)} \qquad \ldots\ldots\ldots\ldots\ldots\ldots\ldots\ldots (2)$$

Potential energy gain when pendulum reaches its angle of rebound θ_2.

$$= g M_p h (1 - \cos \theta_2) \text{ foot pounds.}$$

Kinetic energy immediately after impact

$$= \tfrac{1}{2} M_p k^2 \dot{\theta}_2^{\,2} \text{ foot pounds.}$$

Equating potential and kinetic energy after impact and ignoring small friction losses it follows that

$$\dot{\theta}_2 = \sqrt{\frac{2gh}{k^2} (1 - \cos \theta_2)} \qquad \ldots\ldots\ldots\ldots\ldots\ldots\ldots\ldots (3)$$

Substituting for $\dot{\theta}_1$ and $\dot{\theta}_2$ in equation (1) it follows that

$$P = \frac{M_p k \sqrt{2gh}}{c} \left(\sqrt{1 - \cos \theta_1} + \sqrt{1 - \cos \theta_2} \right) \quad - (4)$$

By measuring the initial elevation angle θ_1 and the angle of rebound θ_2 from the graduated scale on the supporting frame of the pendulum

..... 69

equation (4) may be used to calculate the imparted impulse P.

Before the impulse machine could be used for impact tests it was necessary to determine the constants M_p, k, h and c for the pendulum.

The mass of the pendulum finally used for the impact tests was

$$M_p = 23 \text{ slugs.}$$

Determination of the centre of gravity of the pendulum indicated that

$$h = 7.918 \text{ feet.}$$

The radius of gyration k was determined by measuring the pendulum frequency n which proved to be

$$n = 0.301 \text{ cycles per second.}$$

For a compound pendulum

$$k = \frac{\sqrt{gh}}{2\pi n} \text{ from which it followed that}$$

$$k = 8.45 \text{ feet.}$$

The distance of the centre of percussion from the pivot point of such a pendulum is given by

$$C^1 = \frac{k^2}{h} \text{ from which it followed that}$$

$$C^1 = 9.02 \text{ feet.}$$

The impact head A of the impulse pendulum was then fixed in such a position that the line of action of the impulse P passed through the point of percussion B. From the geometry of the pendulum it was found that

$$C = 8.82 \text{ feet.}$$

In order to express the imparted impulse P non-dimensionally equation (4) may be conveniently divided by the factor $M\sqrt{gD}$ where M is the mass of the cage receiving the impact and D = 20 feet is the shaft diameter.

For a cage containing a rockload

$$M = 998 \text{ slugs.}$$

Therefore

$$\frac{P}{M\sqrt{gD}} = 0.01946\left(\sqrt{1 - \cos\theta_1} + \sqrt{1 - \cos\theta_2}\right) \quad (5)$$

Formula (5) was used for determining the non-dimensional impulses imparted to the fullscale cage during impact tests.

4.2.2 Model Equipment.

4.2.2.1 General layout. The dynamic scale model of the Durban Roodepoort Deep Circular Shaft and its rope-guide installation had to be designed to fit the available accommodation offered by the Vertical Mineshaft Windtunnel described in Chapter 3.

Figure 28 depicts this model installed in the vertical mineshaft windtunnel. Following standard procedure, the model shaft was constructed from galvanised iron sheet ducting specially rolled in two halves so that one half could be removed for installation of model guide ropes. On installation this duct was carefully aligned on its supporting brackets along the steel tower and pit. Figure 29 shows the outside appearance of the steel tower with the Durban Roodepoort Deep model installed and also shows the cabin, constructed on the top of the tower, for the protection of personnel and equipment.

An accurately constructed dynamic scale model of the cage in the south compartment of the fullscale shaft was used as test cage.

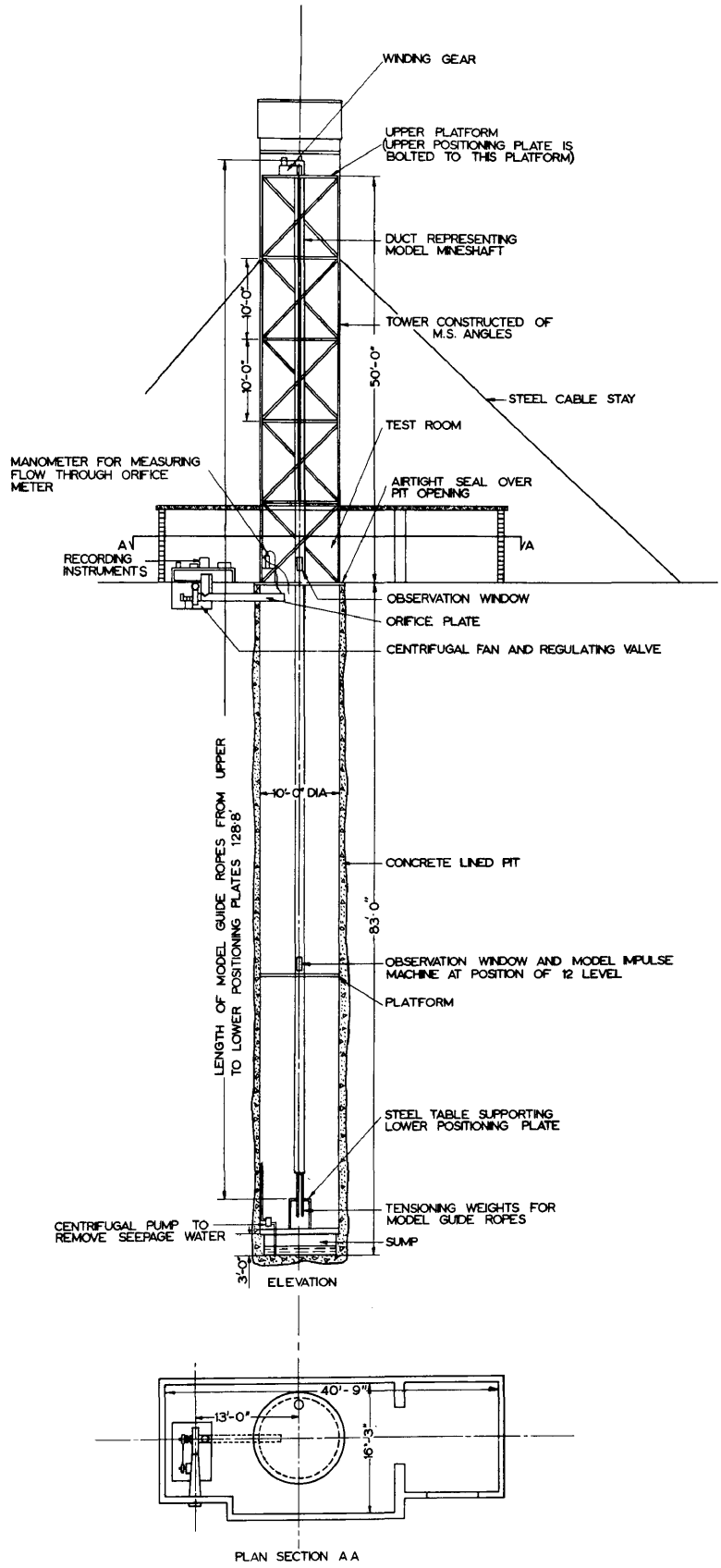

FIGURE 28

General layout of the vertical mineshaft windtunnel with the model of the Durban Roodepoort Deep circular shaft installed

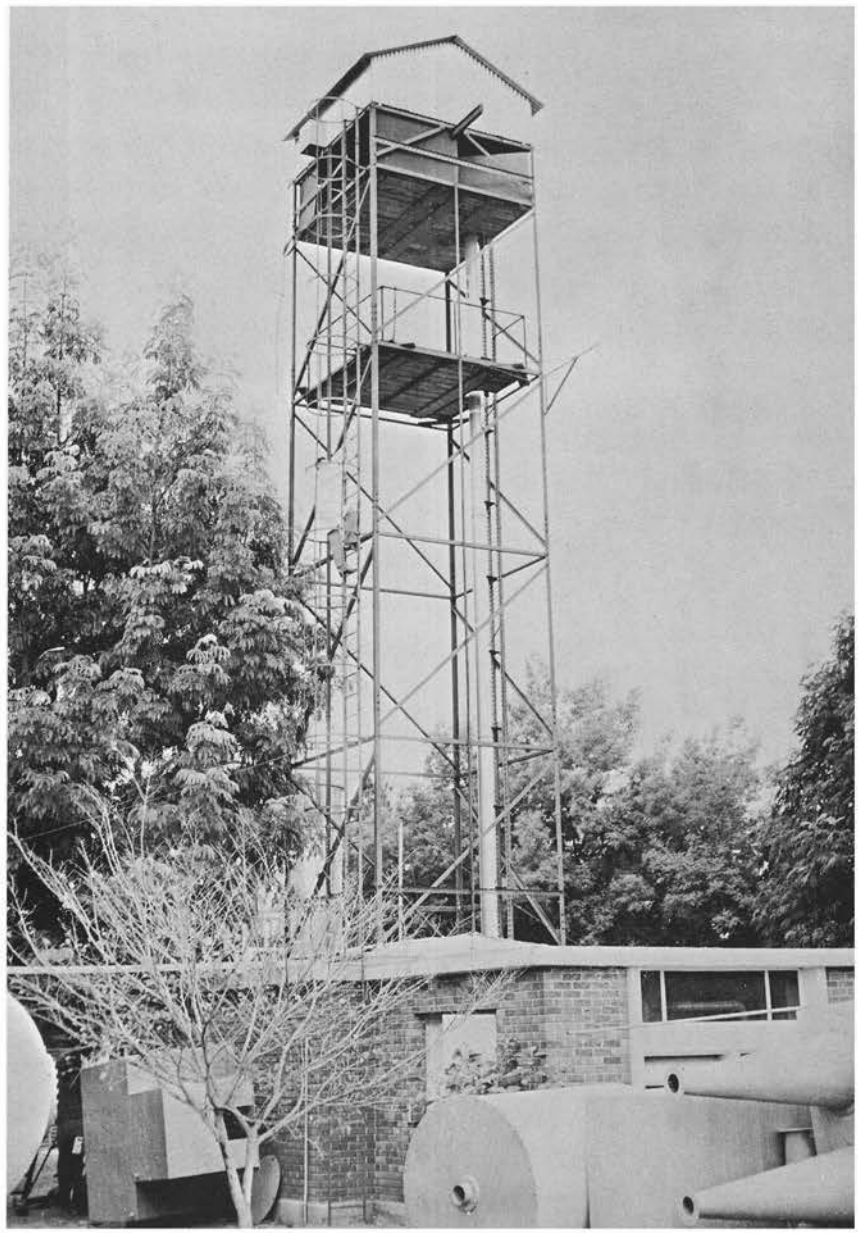

FIGURE 29

The steel tower and test room

The model ropes in this compartment were also made to scale. Since no tests were to be carried out on the installation in the north compartment it was not necessary for the installation in this compartment to be dynamically similar to its fullscale counterpart. A wooden dummy cage, guided by highly-tensioned steel cables was therefore employed, care being taken, however, to obtain the correct shape, so as to ensure that any possible aerodynamic interference between the two conveyances would be correctly simulated.

To ensure the correct spacing of all guide and hoist ropes, the ropes passed through accurately located holes in two positioning plates installed at the top and the bottom of the shaft respectively. The guide rope tensioning weights were situated below the lower positioning plate which was mounted on a small table near the bottom of the pit. The upper positioning plate was mounted on a platform on top of the tower, where the hoisting gear was installed.

All recording instruments were accommodated in the test room of the Vertical Mineshaft Windtunnel at ground level, the interior of which is depicted in Figure 30. The equipment used in the model impact tests was installed on a service platform in the pit at a depth corresponding to the position of 12 Level in the fullscale mineshaft.

Telephones provided a means of communication between personnel stationed on the upper and lower platforms and in the test room.

4.2.2.2 Guide Ropes, Hoist Ropes and Conveyances.

It has been explained in section 2 that, although the laws of dynamic similitude in theory require the use of constant scale factors for determining all physical quantities in a model of a rope-guide installation, in practice certain concessions may be made which will not affect the dynamic behaviour of the model.

The exact simulation of guide ropes in the model was not possible, since available steel cables of suitable size proved to be very unlike the locked-coil type of guide ropes used in the fullscale installation, particularly with regard to flexibility.

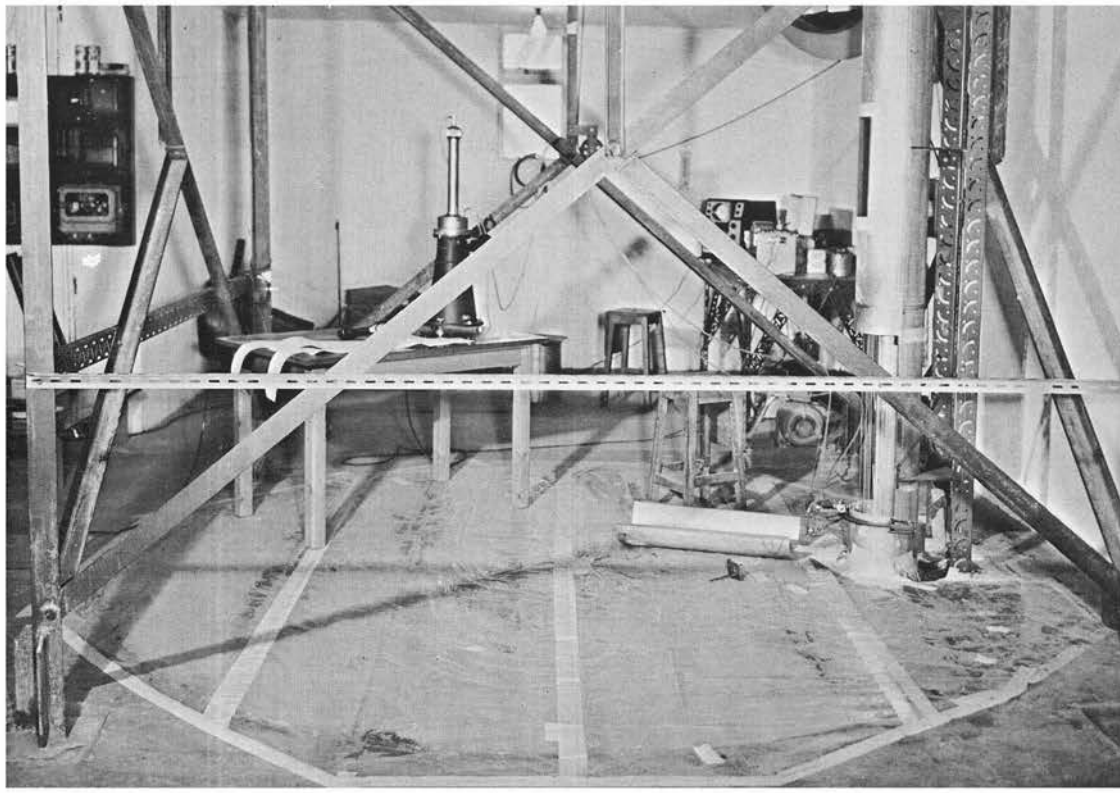

FIGURE 30

Interior of test room

A more supple type of 6 x 19 ordinary lay copper chord specially constructed by a rope manufacturing company for this investigation was therefore selected, and the geometric scale factor between fullscale and model system was calculated on the basis of the weight ratio between the fullscale and model ropes. The copper chord has a weight of 0.0146 pounds $feet^{-1}$ which yielded a mass ratio z^3 = 13,660 and a geometric scale factor of z = 23.9.

This fixed the overall length and diameter of the model shaft at 128.8 feet and 10.03 inches respectively. With reference to Figure 20, the required tensioning weights on the model guide-ropes A, B, C and D amounted to 0.769, 0.692, 0.769 and 0.846 pounds respectively.

Ordinary lay 7 x 7 steel cable weighing 0.00928 pounds $feet^{-1}$ was selected for the model hoist rope. The weight of this rope was about 6% below the weight actually required, but this discrepancy was considered to be acceptable in view of the fact that the hoist rope represented only one of five ropes whose weight would affect the cage motion, the other four being the accurately simulated guide ropes.

In constructing the model test cage of the south compartment, care was taken to obtain the correct dimensions, mass and mass distribution. As it was important that the material of the model should be non-magnetic to prevent interference with the displacement recording instrumentation, brass shimstock was used. The gauge thicknesses of the various components were carefully selected to obtain the correct mass and mass distributions. The rope-guide eyes on the cage were provided with white metal bushes to ensure that the soft copper guide ropes would not be damaged during the extensive hoisting tests that were to follow.

The protective roof on top of the fullscale cage was accurately reproduced in the model, as indicated in Figure 31. Figure 32 shows the model with two lower deck trucks removed. The rock loads in these trucks were represented partly by pebbles and partly by the batteries and oscillators of the recording system.

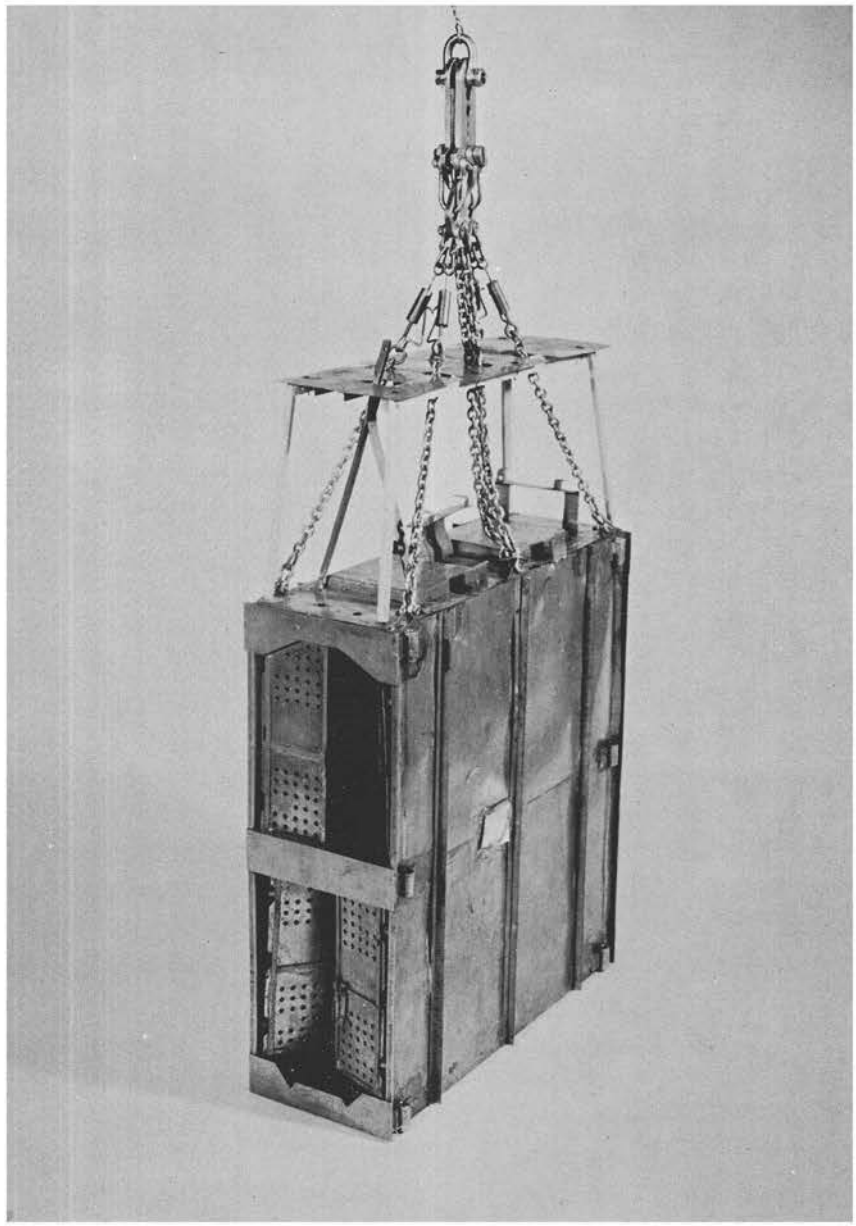

FIGURE 31

Model conveyance with roof

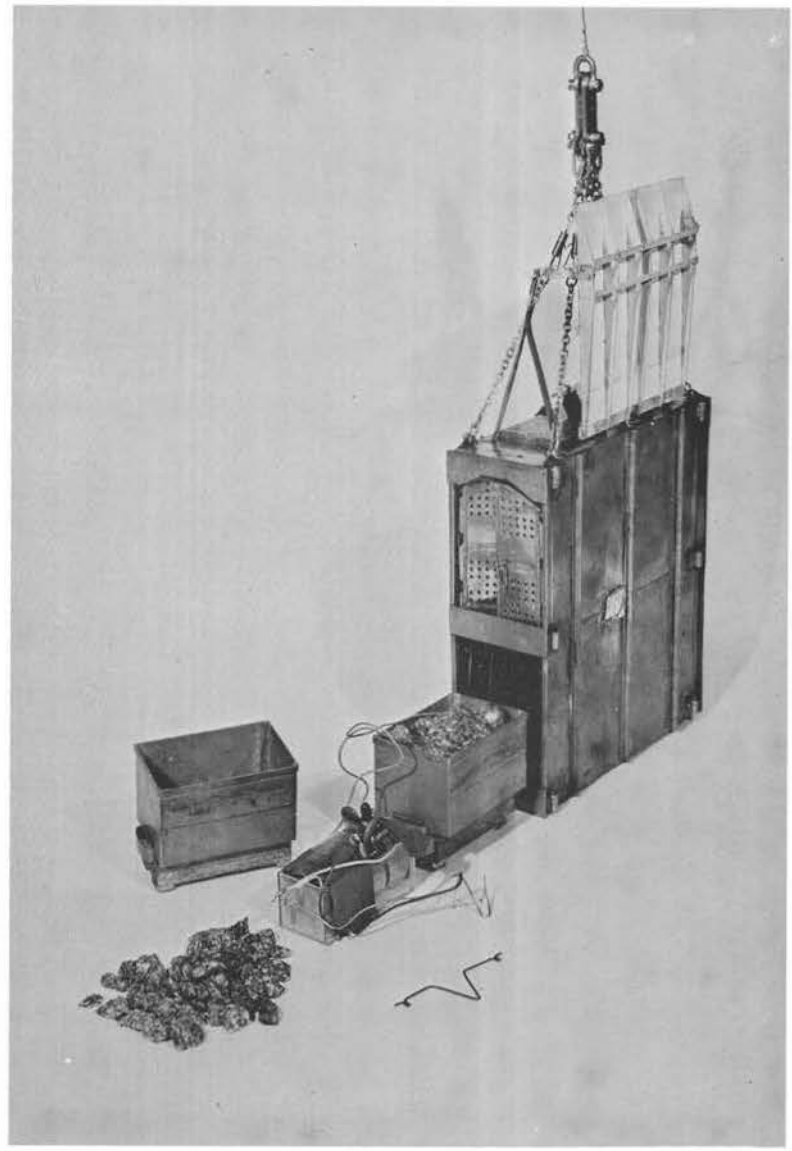

FIGURE 32

Model cage with trucks, rock load, oscillators and batteries

The dummy cage in the north compartment was constructed of wood, weighted with sand and ran on highly-tensioned steel guide ropes. The method of anchoring and tensioning the copper and steel guide ropes of the test and dummy cages is illustrated in Figure 33.

4.2.2.3 The hoisting of model cages and ventilation air flow. The hoisting gear, installed on the upper platform on top of the steel tower as shown in Figure 33 is described in Chapter 3 and forms a part of the permanent equipment belonging to the Vertical Mineshaft Windtunnel. It was only necessary to design a suitable hoisting drum for winding the model hoisting rope, together with a model head gear and suitable pulleys to guide the hoist ropes.

As pointed out in Chapter 3, hoisting drum revolutions may be conveniently reproduced as displacement pips on the ink-jet recording paper, and these pips provide a means of measuring the vertical position of the conveyance in the shaft. Since the sheave wheel revolutions were used for this purpose in the full-scale installation it was decided to scale down the 15.834 feet diameter sheave wheel linearly, giving a hoist drum diameter of $\frac{15.834}{23.9} = 0.663$ feet. Displacement pips, represented on the model recording paper as hoist drum revolutions were therefore directly comparable with the fullscale displacement pips. These sheave wheel revolutions provided a good non-dimensional basis for measuring vertical cage displacement for the model and fullscale installations and were used for all the correlation tests.

The velocity scale factor with which all fullscale velocities were divided to obtain their equivalent values in the model, amounted to $\sqrt{z} = 4.89$ where z denotes the linear scale factor. It was found that by using the above-mentioned 0.663 feet diameter hoisting drum, the maximum hoisting speed of 2700 feet per minute encountered in the fullscale installation could be readily reproduced to scale in the model.

Furthermore it was necessary to prepare indicator boards (refer

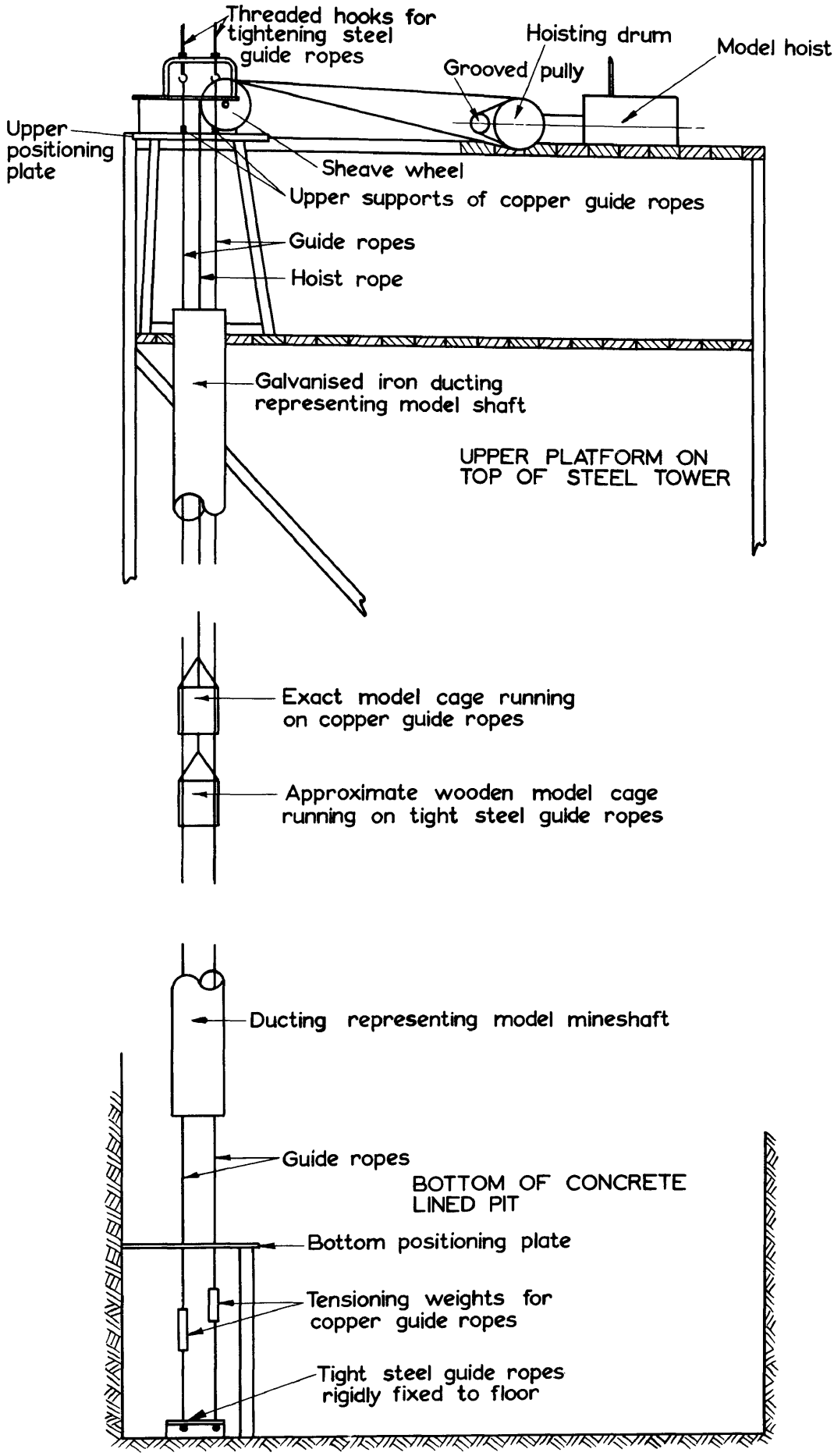

FIGURE 33

General layout of guide-rope and hoist-rope systems

to Figure 8) which could be used for plotting out the hoisting cycles obtained in tests in the fullscale shaft. Such hoisting cycles could then be followed as accurately as possible with this apparatus.

The hoist rope for the two cages was continuous, passing from one cage over a sheave wheel to the hoisting drum and back again over a second sheave wheel to the other cage (refer to Figure 33). Small ball bearing swivels were incorporated in the suspension of the model cages to relieve the inevitable twisting of the rope during hoisting. These swivels prevented couples from acting on the test cage and causing undue rolling motion of the cage.

The scale factor with which the fullscale ventilation air flow rate had to be divided to obtain the model flow rate, amounted to

$\sqrt{z} \cdot z^2 = 2795$ where z denotes the linear scale factor. Dividing the fullscale average flow rate of 85,000 cubic feet per minute by this flow scale factor a flow rate of 30.4 cubic feet per minute was obtained for the model. This air flow rate in the model was measured by means of the standard orifice plate equipment described in section 3.4.

4.2.2.4 Recording of lateral cage deflections.

The induction method of recording and measuring cage deflections, described in section 3.6, was utilised for this model installation. Miniature induction coils were mounted on the model in a fashion similar to that illustrated in Figure 21 and 22. The miniature oscillator and mercury cells used for powering the oscillator were installed in one of the rockload trucks and made out part of the rockload. Figure 32 illustrates the model cage with the two trucks removed and shows the miniature electronic equipment which was installed in one of the trucks.

The radio frequency transformer, tuned amplifiers, etc. which transmitted the signals picked up by the indicator cables were all housed in the test room together with the ink-jet recorder used for producing the traces of model cage movements.

..... 81

4.2.2.5 The model impulse machine. A model impulse machine of similar design as the fullscale apparatus described in section 4.2.1.3 was constructed for the model impact tests. A photograph of the model and fullscale machines is presented in Figure 34.

No attempt was made to construct a dynamic scale model of the full-scale impulse hammer, as this would have required the simulation of the elastic properties of the impact head on the pendulum and of the cage, together with its buffer block which received the impacts. The model was consequently designed with the primary specification that it should have the same non-dimensional impact capacity as the fullscale apparatus. Using equations (4) and (5) given in section 4.2.1.3. and making some experiments with model pendulums it was readily established that a pendulum with the following constants would be suitable (refer to Figure 26).

M_p = 0.002012 slugs (mass of pendulum).

h = 0.872 feet (distance of C.G. from pivot point).

c = 1.55 feet (distance of impact head from pivot point).

k = 1.135 feet (radius of gyration).

From equation (4) it follows that for this model pendulum

$$P = 0.01105 \left(\sqrt{1 - \cos \theta_1} + \sqrt{1 - \cos \theta_2}\right) \text{ pound seconds.}$$

and non-dimensionally

$$\frac{P}{M\sqrt{gD}} = 0.02917 \left(\sqrt{1 - \cos \theta_1} + \sqrt{1 - \cos \theta_2}\right)$$

This formula was used for determinging the non-dimensional impulses imparted to the model cage.

The frame of the model pendulum was constructed from balsa wood and was mounted in an airtight perspex box which was in turn

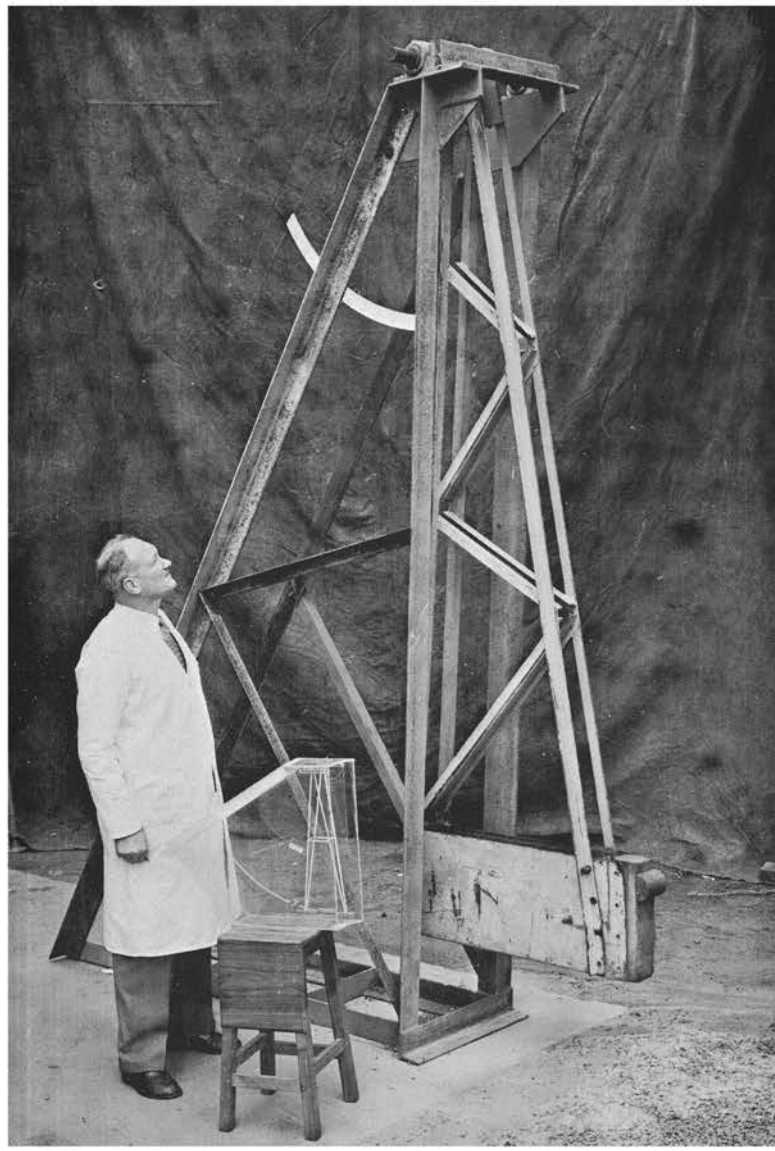

FIGURE 34

The full-scale and model impulse machines

fitted over an aperture in the wall of the model shaft at a position corresponding to 12 Level in the fullscale shaft. This model impulse machine is illustrated in Figure 35. An angular scale for measuring the initial angle of elevation and the angle of rebound was inscribed on one of the panels of the perspex box. A catch with which the pendulum could be released from any desired angle of inclination was provided and the whole perspex box was sealed off so as to prevent any air leakage into the model shaft.

4.3 Main test programme.

4.3.1 Stationary tests.

4.3.1.1 Object and scope. The object of the stationary tests was to correlate the behaviour of the model and fullscale installations when the conveyances were subjected to impulsive forces. In such tests where the conveyance remained suspended at a fixed level in the shaft it was possible to correlate all dynamic effects apparent in such a shaft installation with the exception of steady aerodynamic side forces which only become prevalent during hoisting. It was argued that by conducting tests where severe aerodynamic effects were excluded it would be easier to assess the significance of dissimilar effects in the model due to the incorrect simulation of elastic forces and other possible inaccuracies. The experiments consisted primarily of a series of impact tests (for examining the reaction of a conveyance to impulsive forces and for studying the damping effects on the oscillating conveyance) and also a series of measurements of wave velocities in the guide and hoist ropes.

4.3.1.2 Experimental procedure. Measurements of the velocity of wave propagation in the model and fullscale guide and hoist ropes were executed by giving each rope a sharp blow near its upper end, and measuring the time taken for ten reflections of the wave to appear, using a stopwatch. In this manner the time required by a wave to travel from the top to the

..... 84

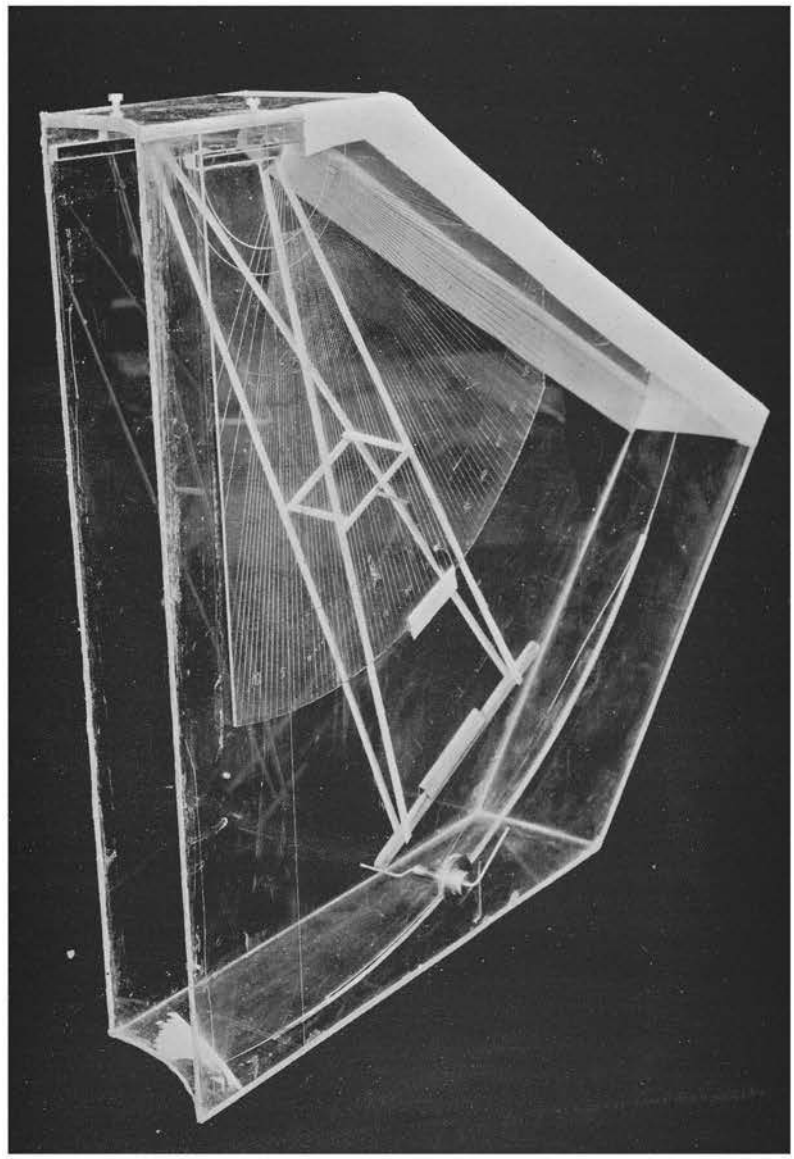

FIGURE 35

The model impulse machine

bottom of the shaft and back again could be accurately derived.

In the fullscale impact tests the induction coils were mounted on the west side of the cage, the impact hammer, situated in the 12 Level Station Cutting, imparting impulses on the eastern face of the cage. Small portable radio transmitting and receiving sets permitted communication between personnel operating the hammer and personnel tending the recording instruments on ground level.

Tests were executed with different magnitudes of impulses. After each impact the test cage was allowed to oscillate freely for some 30 or 40 cycles while a trace of the motion was taken on the recorder at ground level. The magnitudes of the impulses imparted to the model were regulated so as to have the same equivalent range as the fullscale impulses. In all model tests the flow of ventilation air in the model shaft was correctly simulated.

4.3.1.3 Results and discussion. The results of model and fullscale measurements of the rates of wave propagation in the guide and hoist ropes are given in Table 1. The four guide ropes are denoted by A, B, C and D, according to the code in Figure 20. The time intervals taken by waves to travel from the top of the shaft to the bottom and back again are given, the model time intervals being converted to their equivalent fullscale values.

Table 1.

Equivalent fullscale time intervals in seconds for waves to travel down whole length of shaft and back again.

Rope designation	A	B	C	D	Hoist rope
Fullscale	20.63	21.3	21.53	20.2	16.14
Model	20.92	21.5	20.86	20.4	15.9

These results show that the velocities of wave propagation in guide ropes A, B and D and in the hoist rope were simulated accurately to within about 1.5% in the model. The discrepancy exhibited by guide rope C was investigated and it was found that in the fullscale installation the tensioning weight for this guide rope touched the bottom of the shaft floor, thus slightly reducing the rope tension. This fact was not realised initially since the lower portions of all the tensioning weights were immersed in drainage water. The discrepancy in the tension of model guide rope C was rectified by reducing its tensioning weight until its velocity of wave propagation agreed to within 1% with that of the fullscale rope.

In order to correlate the model and fullscale cage oscillations obtained in the impact tests, it was necessary to consider the four essential properties of the wave motions, namely the amplitudes, the periods, the wave shapes and the damping characteristics.

In considering the amplitudes, the maximum amplitude recorded for each model and fullscale impact test was measured directly from the trace on the recording paper from the ink-jet recorder. All amplitudes were divided by the diameter of the shaft thus presenting amplitudes of cage oscillations in a non-dimensional form. The magnitude of non-dimensional impulses were determined from knowledge of the angles of elevation and rebound of the model and fullscale pendulums. The results of the fullscale and model tests are presented in Tables 2 and 3 respectively. Figure 36 gives the relationship between non-dimensional imparted impulses and non-dimensional amplitudes in a graphical form for both the model and the fullscale installation.

It will be noticed that the relationship between maximum amplitude and imparted impulse was approximately linear in the test region, and that, within experimental error, the points for the model and fullscale tests fit a single curve. Correlation between model and fullscale amplitudes of oscillation was therefore considered to be satisfactory.

TABLE 2

Variation of maximum amplitude of cage oscillation with imparted impulses for fullscale tests.

θ_1 = angle of elevation of impulse pendulum in degrees.

θ_2 = angle of rebound of impulse pendulum in degrees.

$$\frac{P}{M\sqrt{gD}} = 0.01946\left(\sqrt{1 - \cos\theta_1} + \sqrt{1 - \cos\theta_2}\right)$$

(Non-dimensional impulse)

M = mass of cage and load = 998 slugs.

D = shaft diameter = 20 feet

Non-dimensional maximum amplitude is defined as:

$$\frac{\text{Maximum amplitude in inches}}{\text{Shaft diameter in inches}}$$

Impact test number	θ_1	θ_2	$\frac{P}{M\sqrt{gD}}$	Non-dimensional maximum amplitude
1	30.75	15.75	0.01108	0.0475
2	30.75	16.25	0.01118	0.04395
3	33.75	17.75	0.01225	0.0525
4	39.75	13.75	0.01265	0.05532
5	46.75	11.75	0.01373	0.0554

..... 88

TABLE 3

Variation of maximum amplitude of cage oscillation with imparted impulses for model tests.

θ_1 = angle of elevation of impulse pendulum in degrees.

θ_2 = angle of rebound of impulse pendulum in degrees.

$$\frac{P}{M\sqrt{gD}} = 0.02917 \left(\sqrt{1 - \cos \theta_1} + \sqrt{1 - \cos \theta_2} \right)$$

(Non-dimensional impulse)

M = mass of cage and load = 0.07305 slugs.

D = shaft diameter = 0.836 feet.

Non-dimensional maximum amplitude is defined as:

$$\frac{\text{Maximum amplitude in inches}}{\text{Shaft diameter in inches}}$$

Impact test number	θ_1	θ_2	$\frac{P}{M\sqrt{gD}}$	Non-dimensional maximum amplitude
1	23.9	10.3	0.01227	0.0496
2	12.5	6.7	0.00692	0.0283
3	12.5	6.5	0.00696	0.0292
4	20.5	10.6	0.01118	0.0467
5	25.5	12.5	0.01363	0.0579
6	25.5	12.0	0.01344	0.0562
7	30.5	10.5	0.01466	0.0600
8	30.5	9.3	0.01418	0.0579
9	30.5	9.3	0.01418	0.0583
10	35.5	7.0	0.01510	0.0621
11	35.5	7.0	0.01510	0.0638
12	40.5	4.5	0.01592	0.0658
13	40.5	4.4	0.01588	0.0638
14	45.5	1.0	0.01628	0.0661

..... 89

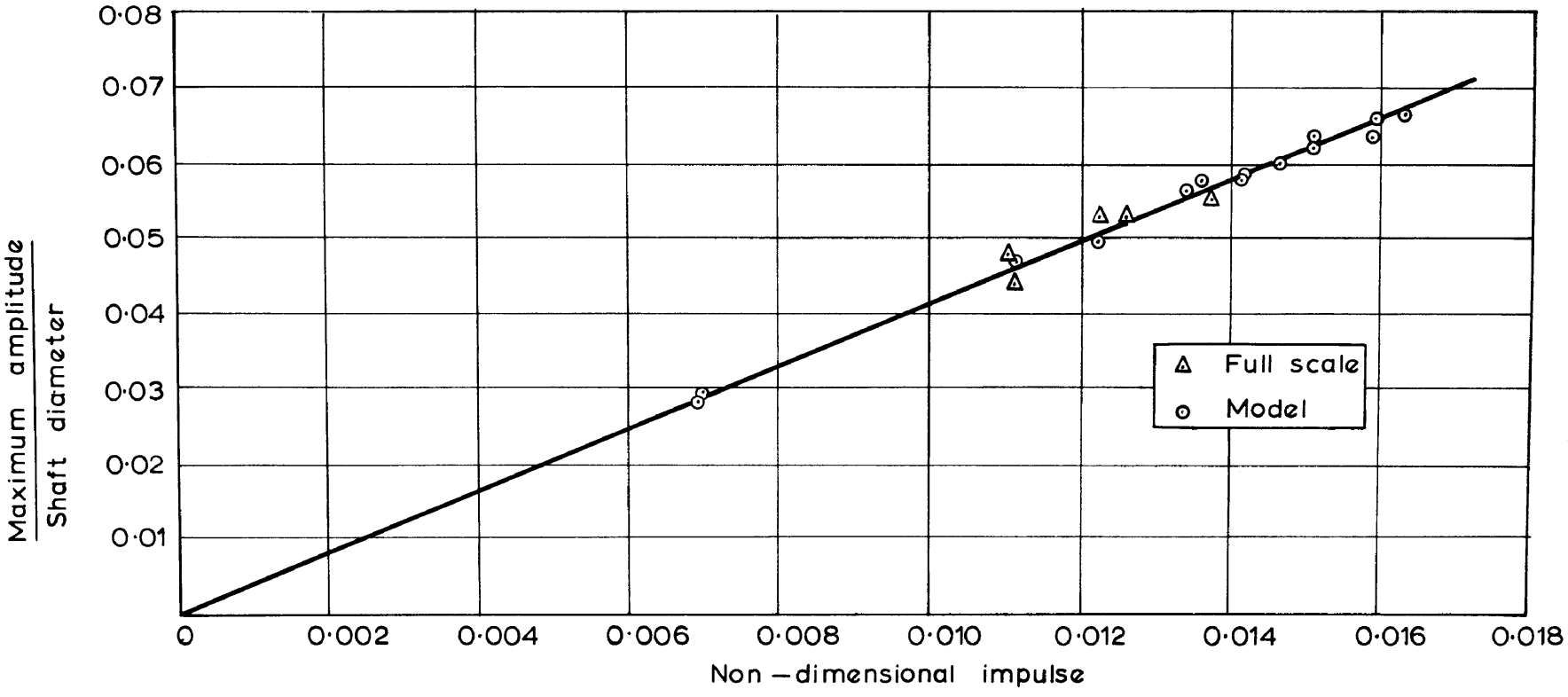

FIGURE 36

Relationship between magnitude of imparted impulse and maximum amplitude of oscillation for model and full-scale cages

Model and fullscale periods of oscillation were determined by measuring, on the recordings made of the cage motion, the total time taken for the cage to execute some 30 oscillations. The period of the fullscale oscillations proved to be 26.3 seconds while the period of the model oscillations was 5.36 seconds. These periods may be conveniently rendered non-dimensional upon division by the factor $\sqrt{\frac{D}{g}}$, D being the diameter of either the fullscale shaft or the model shaft. For the fullscale installation $\sqrt{\frac{D}{g}} = 0.788$ and for the model $\sqrt{\frac{D}{g}} = 0.1611$. Hence the non-dimensional periods for the fullscale installation and the model become 33.35 and 33.25 respectively. The period of cage oscillation was therefore simulated accurately to within 0.3% in the model.

In all the fullscale impact tests the shapes of corresponding waves of the recorded cage oscillations were similar, irrespective of the magnitude of the imparted impulse. This also proved to be the case for the model. In order to compare the wave shapes of the model and fullscale cage oscillations two typical recordings of a fullscale and model impact tests were replotted so that their maximum amplitudes coincided. Figure 37 depicts these comparative wave shapes for one cycle of the cage oscillation, the time lapse being rendered non-dimensional by dividing the actual time lapse in seconds by $\sqrt{\frac{D}{g}}$. It was found that the wave shapes remained similar for the first 5 or 6 cycles after which the wave shape of the model oscillation gradually deviated from that of the fullscale oscillation. This deviation is most probably due to slight inaccuracies in the model which have a cumulative effect on the model wave shape as the oscillations progress. However, for a time interval equal to the duration of a normal hoisting cycle the wave shapes of the model oscillations resemble the fullscale wave shapes very closely.

The model and fullscale damping effects are illustrated in Figure 38 where the amplitudes of cage oscillations, expressed non-dimensionally as a fraction of the shaft diameter are plotted against the number of completed cycles for a typical model

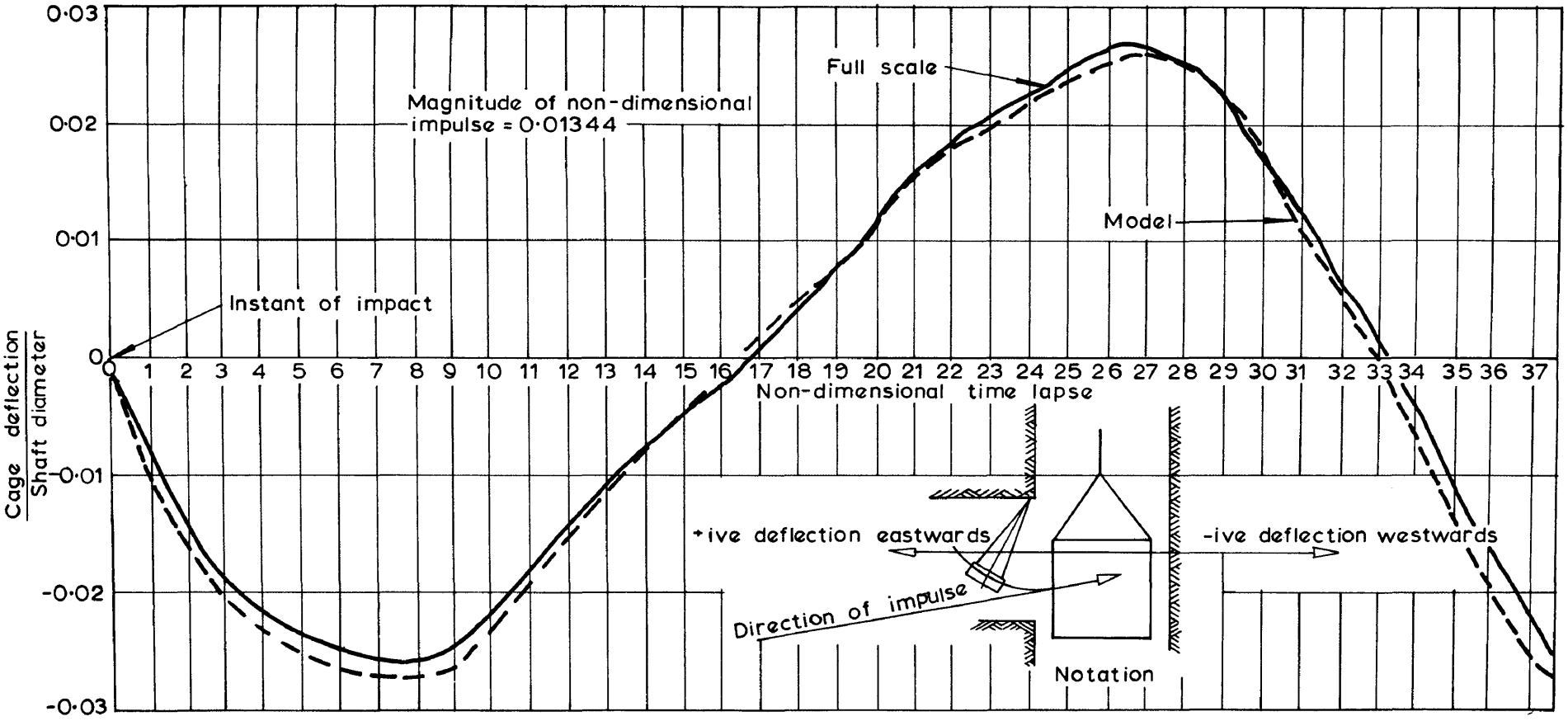

FIGURE 37

Graphical representation of model and full-scale oscillatory motion immediately after imparting an impulse to the cage

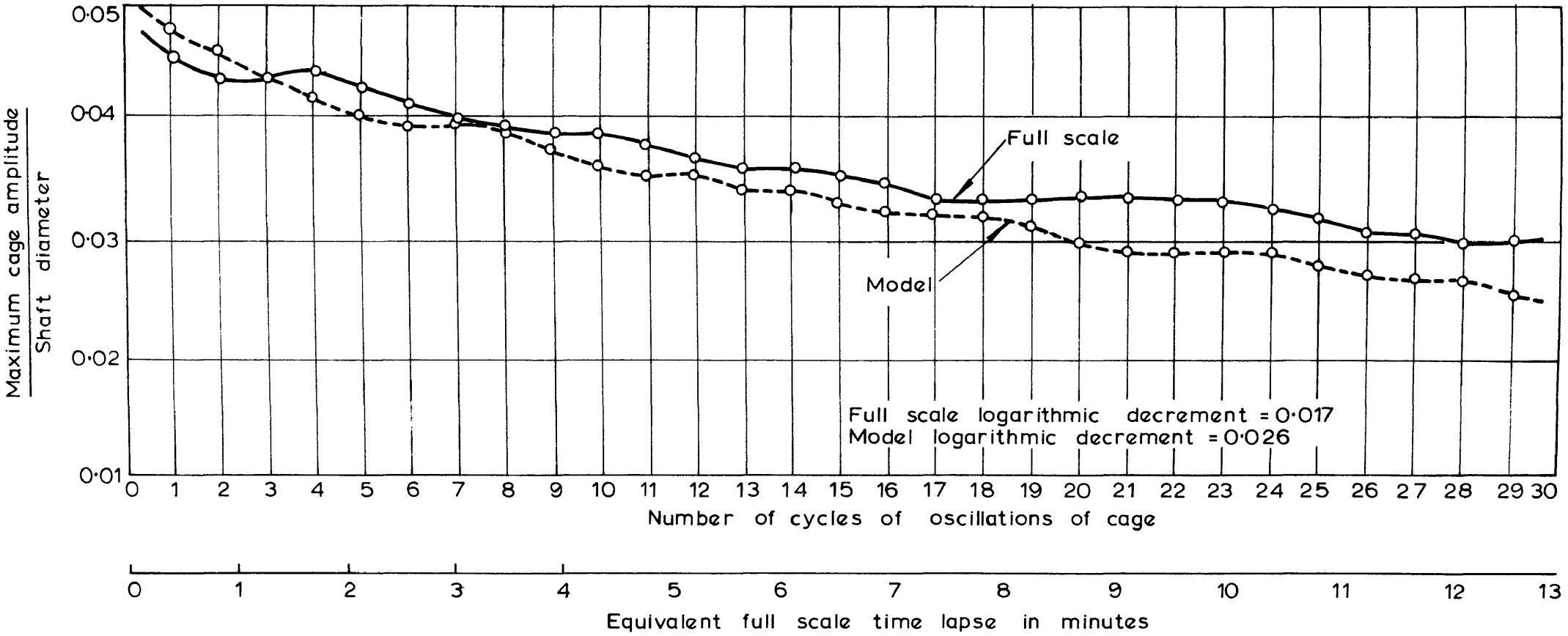

FIGURE 38

Decrease in amplitudes of model and full-scale cage oscillations

and fullscale impact test. These curves show that the equivalent damping forces in the model were larger than the fullscale damping forces, the logarithmic decrements of the model and fullscale oscillations being 0.026 and 0.017 respectively. Damping forces were therefore not accurately simulated in the model, but this could not have been expected since no attempt had been made to obtain the correct damping characteristics when the model was designed. This inaccuracy in the simulation of damping forces will not detract from the value of model tests, however, since damping effects will be small for the short durations of normal hoisting cycles.

4.3.2 Hoisting tests.

4.3.2.1 Object and scope. The object of fullscale and model hoisting tests was to establish to what degree the model simulated the behaviour of the fullscale rope-guide installation under dynamic conditions where all forces, including aerodynamic forces, come into play. To perform these hoisting correlation tests the traces giving the lateral north-south and east-west movements of the center of gravity of both the model and the fullscale cages at various hoisting speeds were recorded. It was also necessary to determine the pitching motion of both the model and the fullscale cages at these hoisting speeds.

4.3.2.2 Experimental procedure. Fullscale upward and downward hoisting test runs were performed between the upper and lower stopping positions indicated in Figure 19. Before commencing a run, the lateral oscillations of the cage were allowed to die down to an amplitude of less than $\frac{1}{2}$ inch.

The induction coils on the cage and the instruments on the surface, described in section 4.2.1.2, were in continuous operation during any test series, thus enabling the personnel at the surface station to take a recording of the cage motion at any instant. In this way it was possible to establish if conditions were suitable for a test run before instructing the hoist operator by telephone to proceed. Communication between personnel manning the cage

and personnel attending the recording instruments on ground level was effected by means of small radio transmitting and receiving sets. The positions occupied by observers in the cage is illustrated in Figure 22.

As described in section 4.2.1.2 a graphic recording of the cage motion on the jet recorder gave a trace of the motion of the cage on a time base while distance marks in terms of sheave wheel revolutions indicated the position of the cage in the shaft. Figure 39 is an example of an actual recording taken in the full-scale shaft. For this particular recording the two induction coils on the cage were mounted to record north-south and east-west deflections simultaneously. The recording shows the non-linear scale to which deflections had to be measured, as well as the zero lines of deflection and the distance marks, which, in conjunction with the time scale, could be used to calculate the hoisting speed of the cage at any position in the shaft.

The tests were performed at different hoisting speeds varying from 2920 feet per minute down to 510 feet per minute. Due to the limited time available for testing in the mineshaft, not more than 5 or 6 test runs could be made at each hoisting speed.

Soon after commencing with the hoisting tests it was discovered that the motion of the cage was only translatory, and that no pitching motion could be detected. This simplified the routine of testing since under these circumstances only one induction coil was required on each of the southern and western faces of the cage. Both the north-south and east-west translatory motions could then be simultaneously obtained on a single recording.

While performing tests it was arranged that all ventilation air was led down the ventilation air passage at the shaft bottom, shown in Figure 19, the passages leading from 17 and 18 levels being closed off. The rate of the ventilation air flow down the shaft was then determined by carrying out velocity traverses with a vane anemometer in this ventilation air passage.

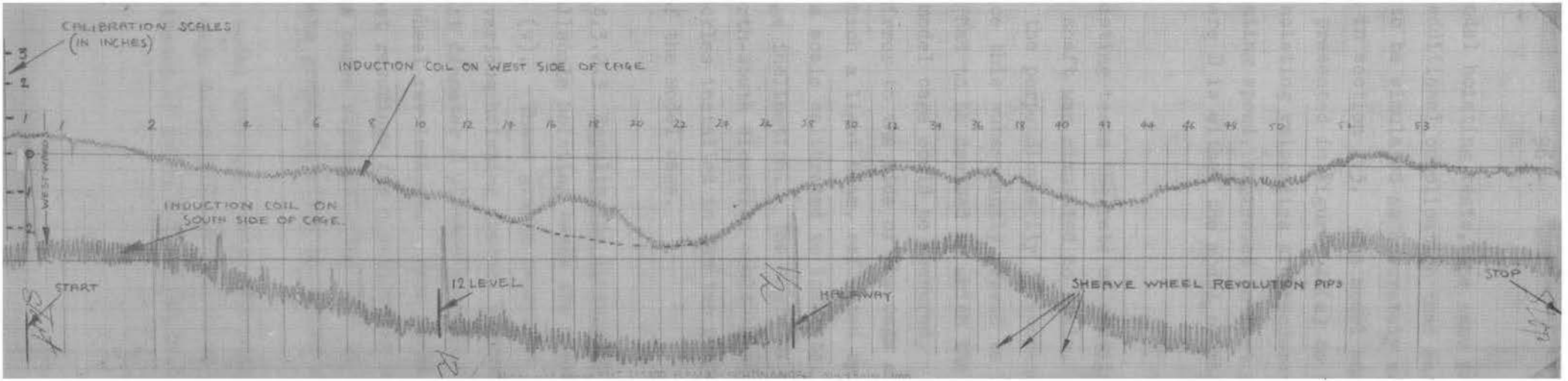

FIGURE 39

Example of actual recording of cage motion taken during full-scale hoisting tests in the mineshaft

In performing the model hoisting tests, the same procedure was followed, with the additional complication that each fullscale hoisting cycle had to be simulated as accurately as possible by the method outlined in section 3.3. The model and fullscale hoisting cycles are presented in Figures 40(a) to (j). In these diagrams the hoisting velocities are rendered non-dimensional by dividing the hoisting speed, expressed in feet per second, by the factor $\sqrt{D\ g}$ where D is either the model or the fullscale shaft diameter.

During all model hoisting tests the rate of ventilation air flow down the model shaft was simulated to scale. As there existed doubt as to the perpendicularity of suspension of the model cage, and since this subsequently proved to be extremely important, a method had to be devised by which the angle of inclination of the model cage could be measured. This was done by fixing a small mirror to the side of the cage and devising an optical system in which a light beam, reflected by the mirror, was projected onto a scale calibrated to indicate, in minutes, small changes in cage inclination. The angle of inclination of the model in the north-south direction could be adjusted by means of two small turnbuckles installed in the two suspension chains on the south side of the model cage.

4.3.2.3 Results and discussion. The results of the model and fullscale hoisting tests are presented graphically in Figures 41(b) to (v). These graphs represent the lateral cage deflection at various hoisting speeds, expressed as a fraction of the shaft diameter D plotted against distance travelled in terms of sheave wheel revolutions. Each model curve represents the mean of ten test recorings for a particular hoisting cycle, while each fullscale curve represents the mean of 5 or 6 recordings. The notation for these graphs is given in Figure 41 (a).

When commencing the model hoisting tests, the correlation between model and fullscale cage deflections proved to be disappointing. Figure 41(b) shows traces of model and fullscale cage movement

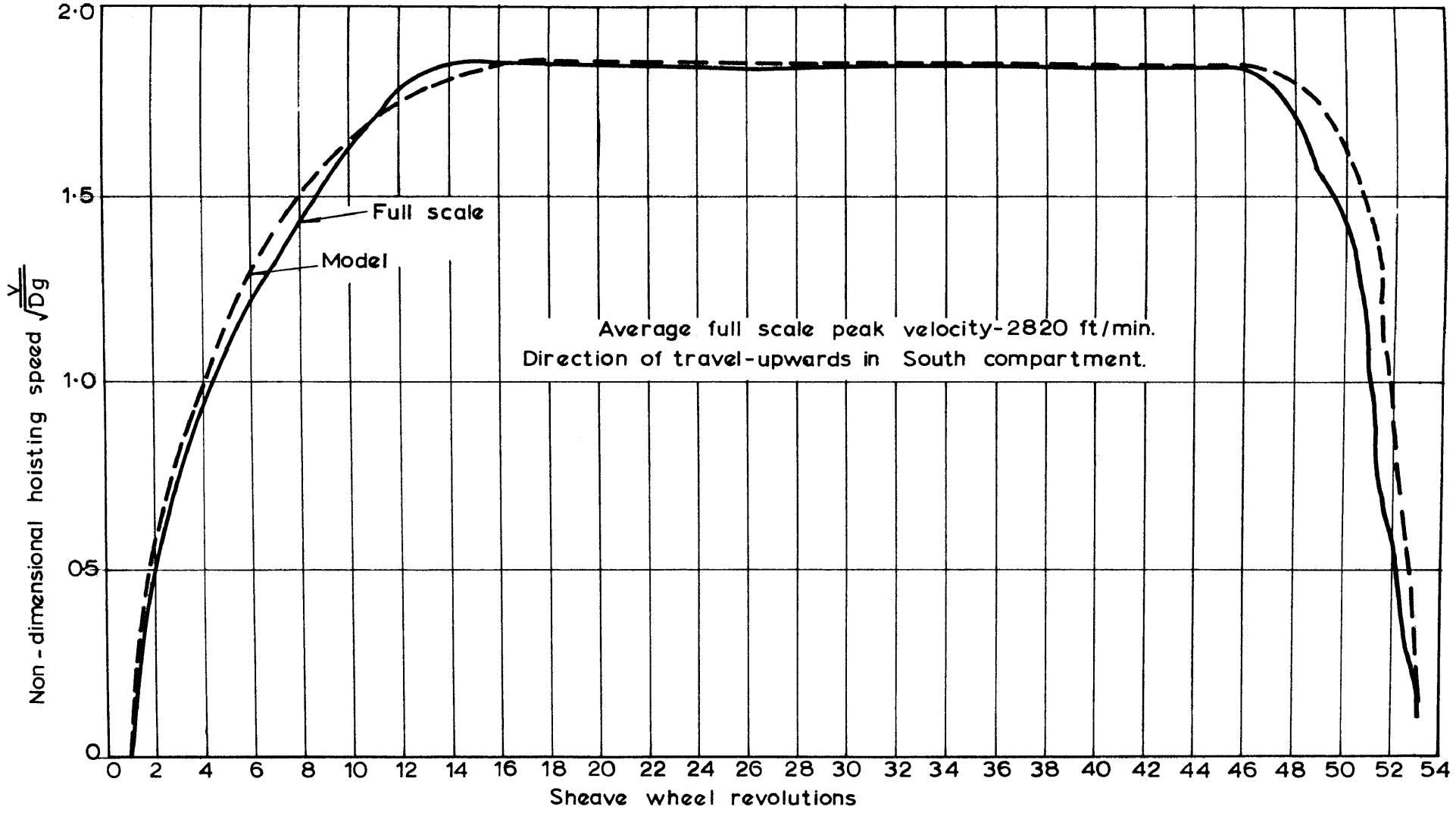

FIGURE 40(a)

Model and full-scale hoisting cycles

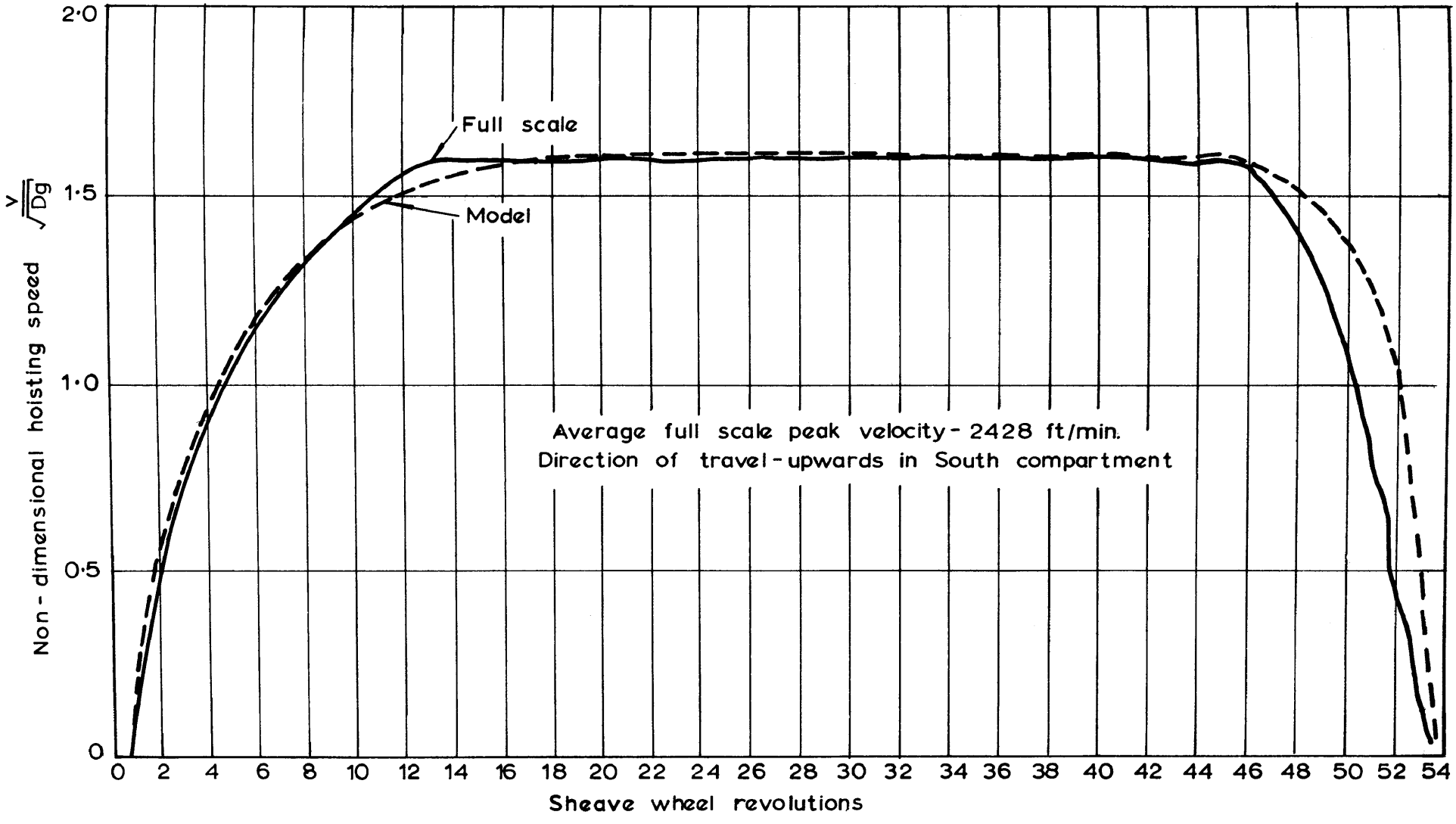

FIGURE 40(b)

Model and full-scale hoisting cycles

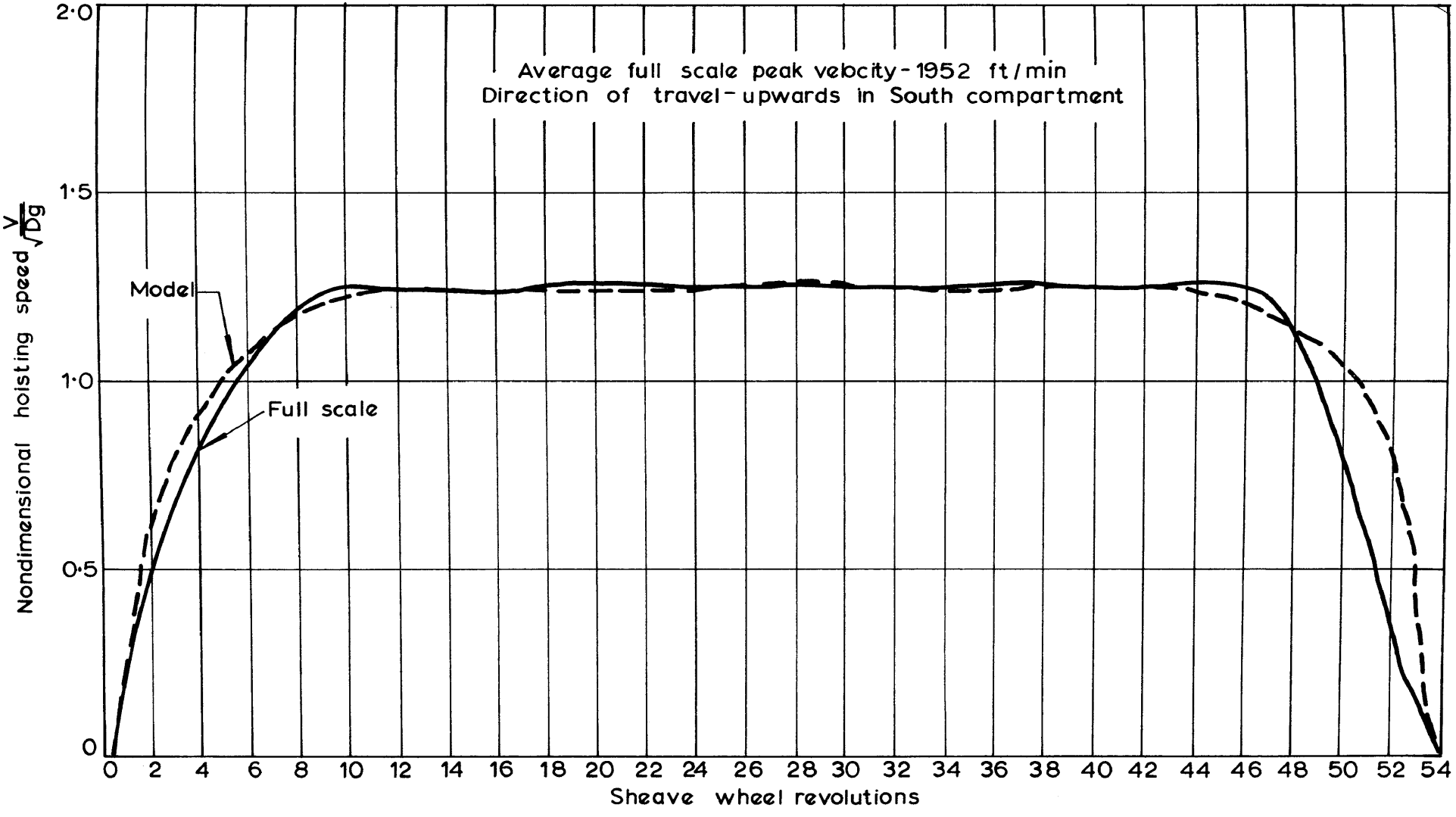

FIGURE 40(c)

Model and full-scale hoisting cycles

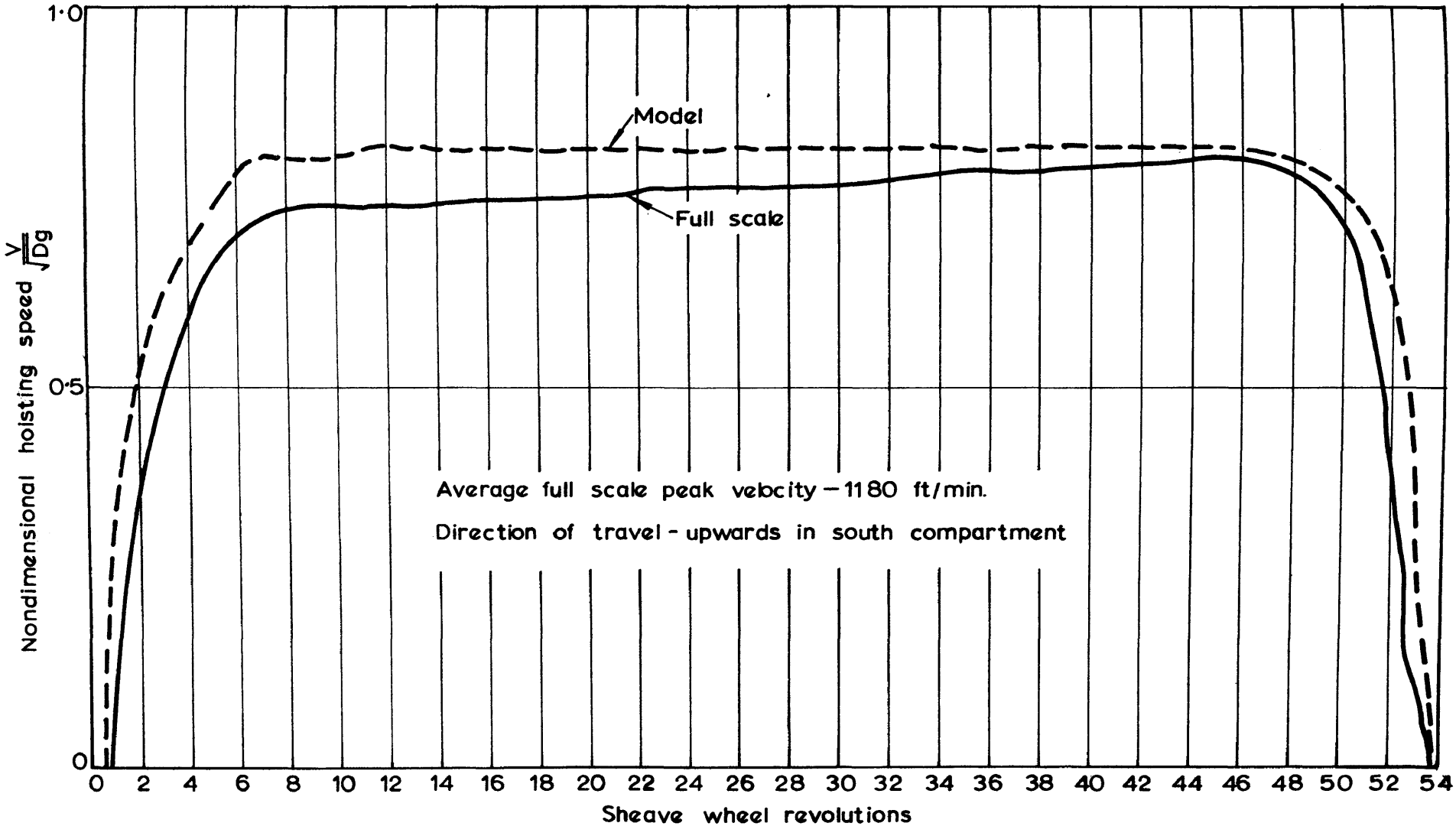

FIGURE 40(d)

Model and full-scale hoisting cycles

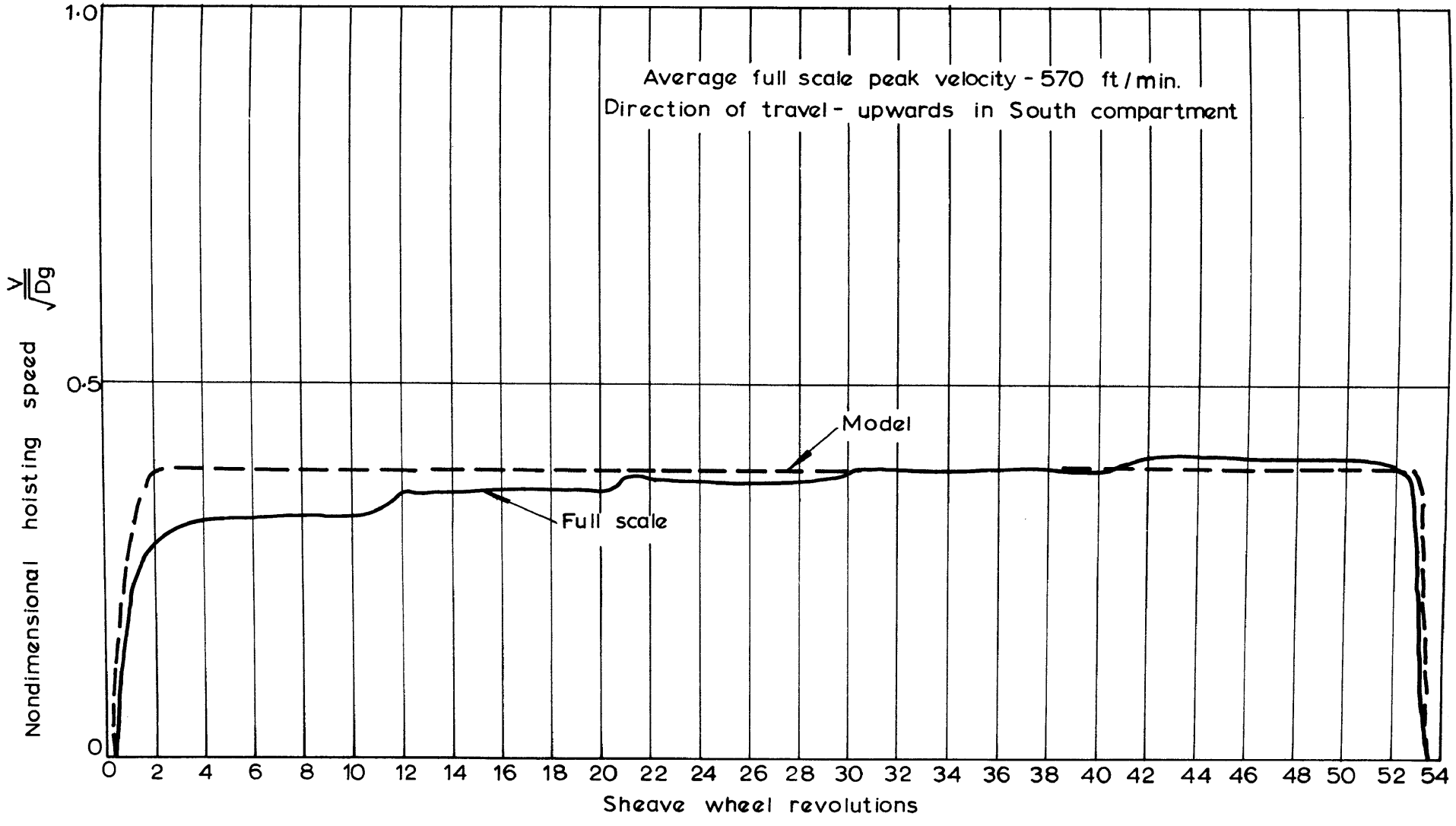

FIGURE 40(e)

Model and full-scale hoisting cycles

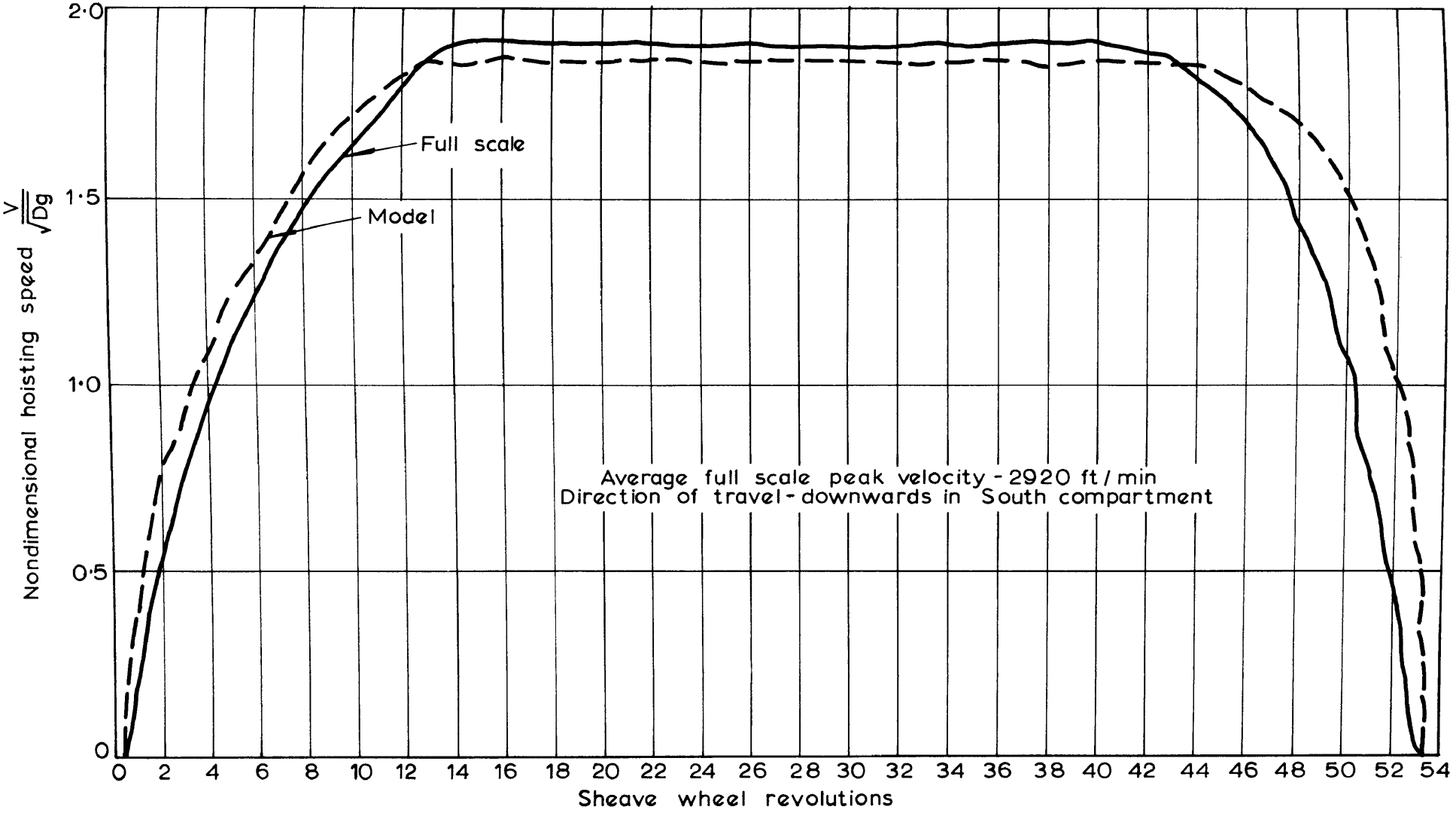

FIGURE 40(f)

Model and full-scale hoisting cycles

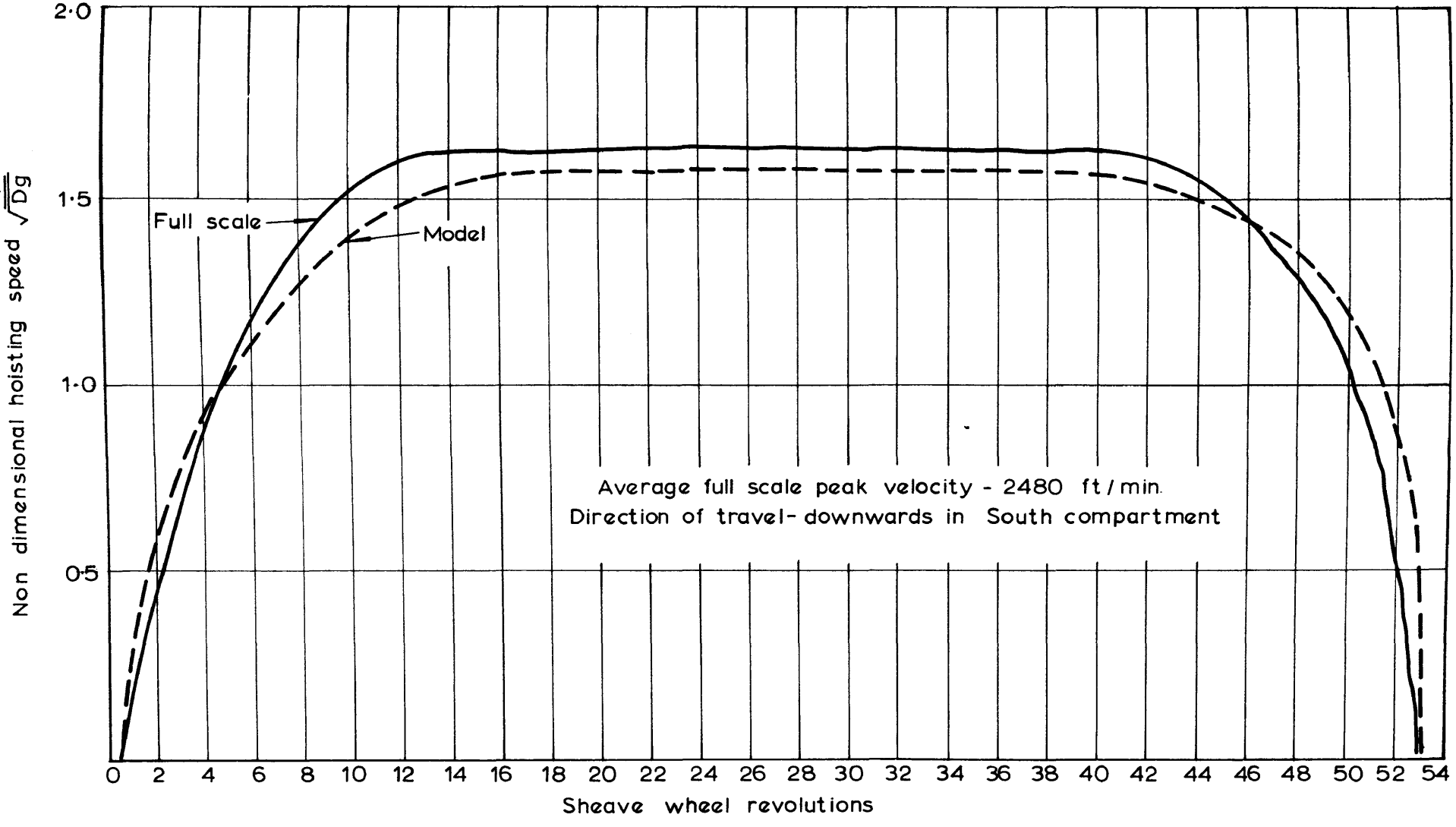

FIGURE 40(g)

Model and full-scale hoisting cycles

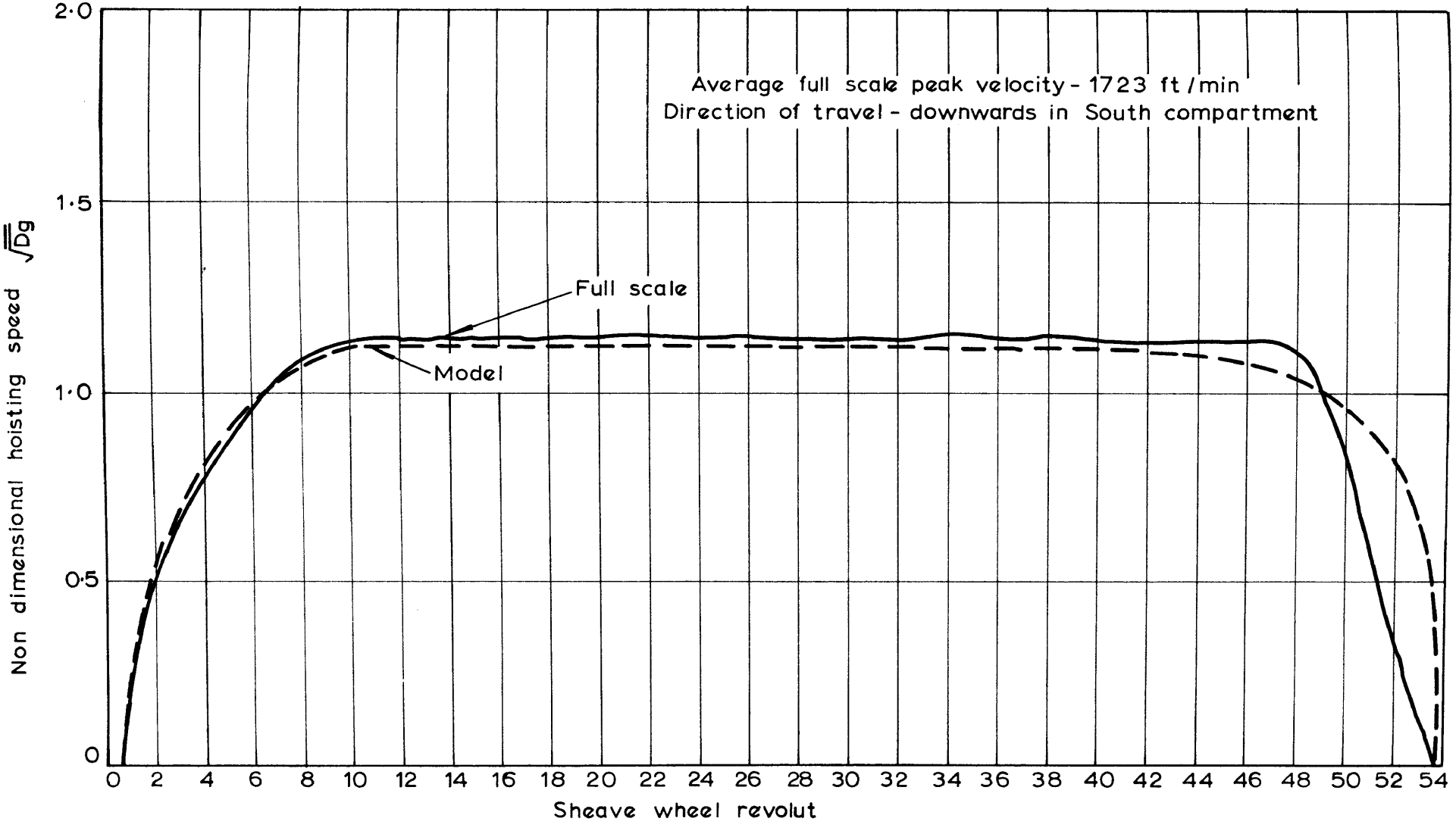

FIGURE 40(h)

Model and full-scale hoisting cycles

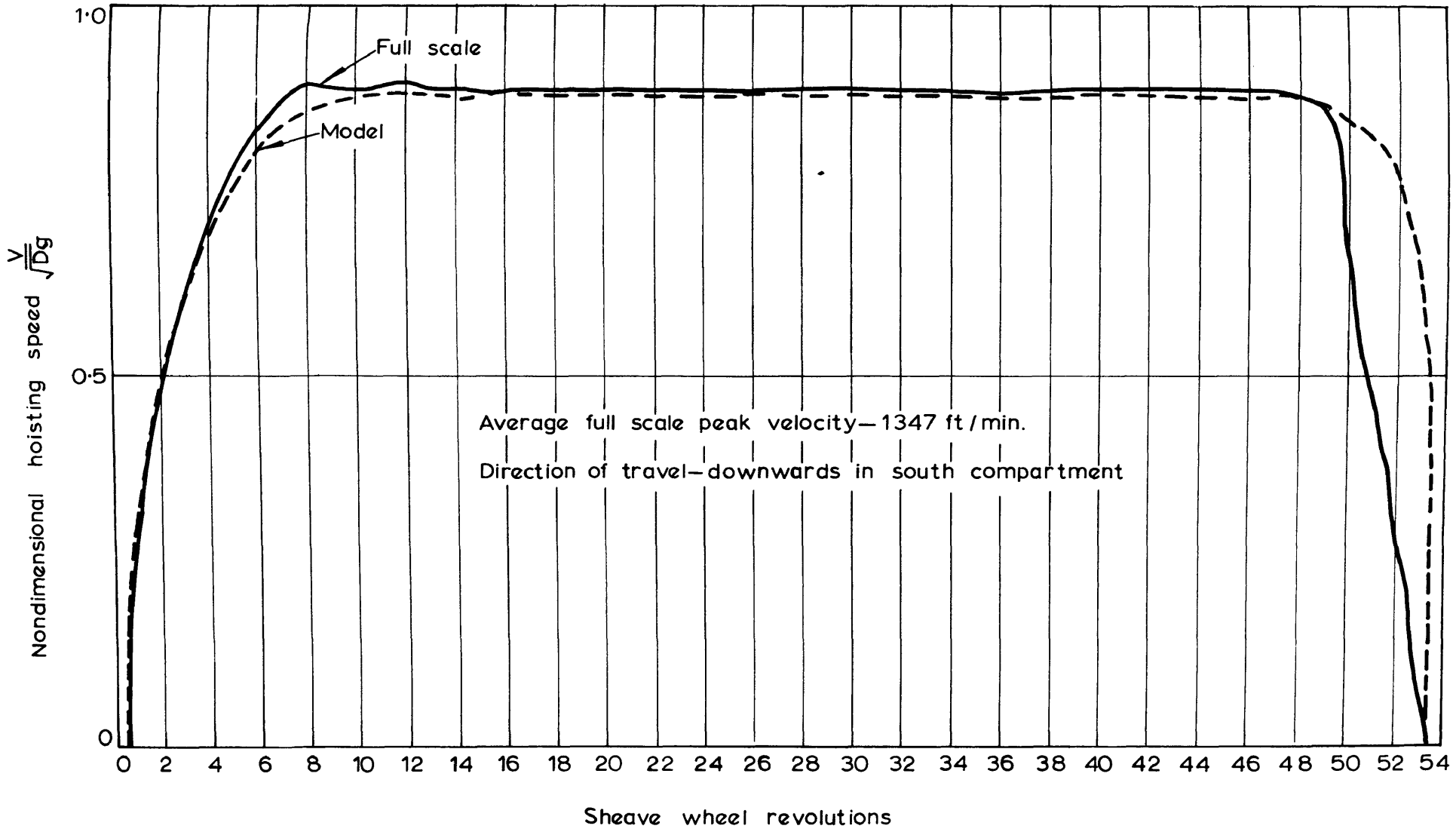

FIGURE 40(i)

Model and full-scale hoisting cycles

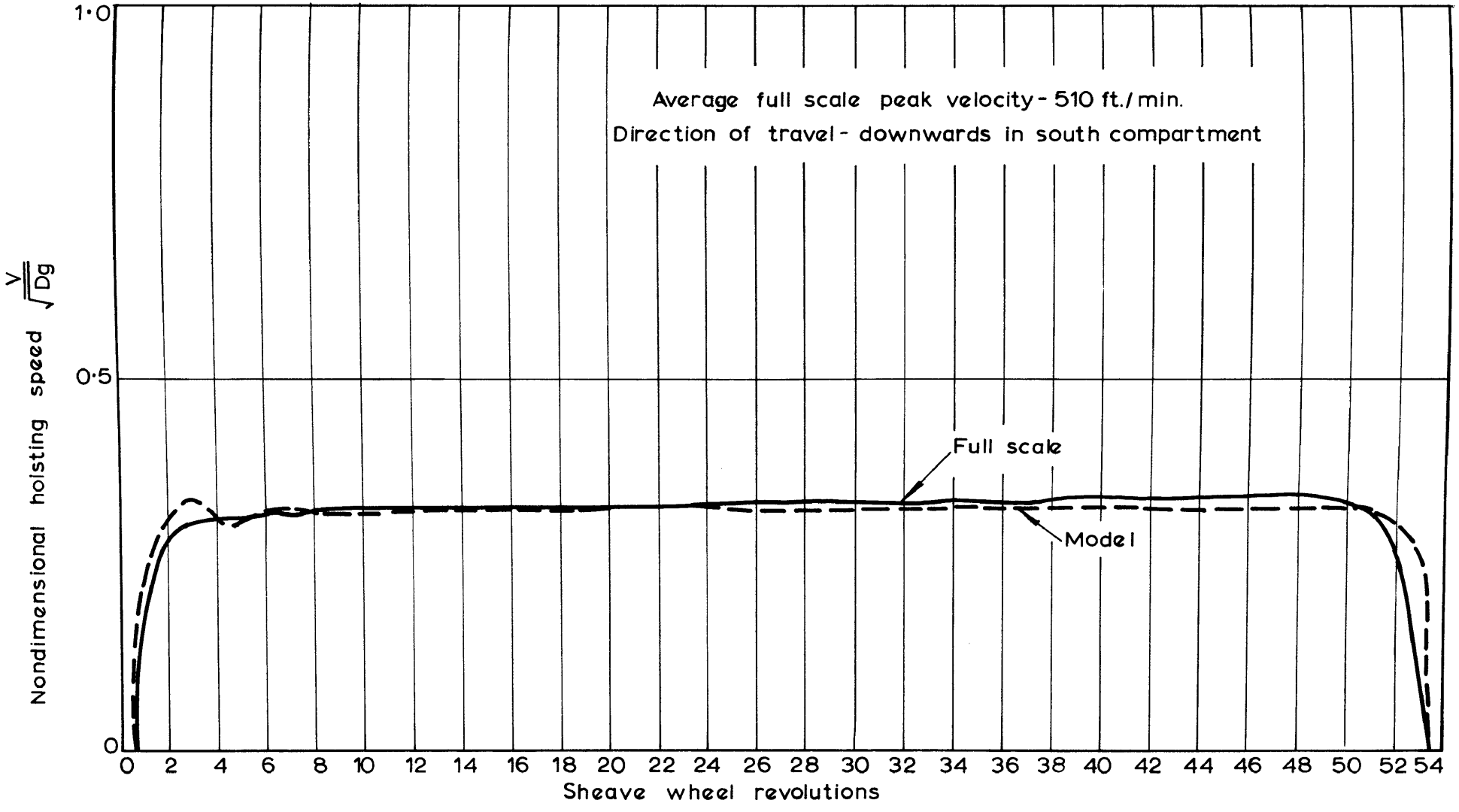

FIGURE 40(j)

Model and full-scale hoisting cycles

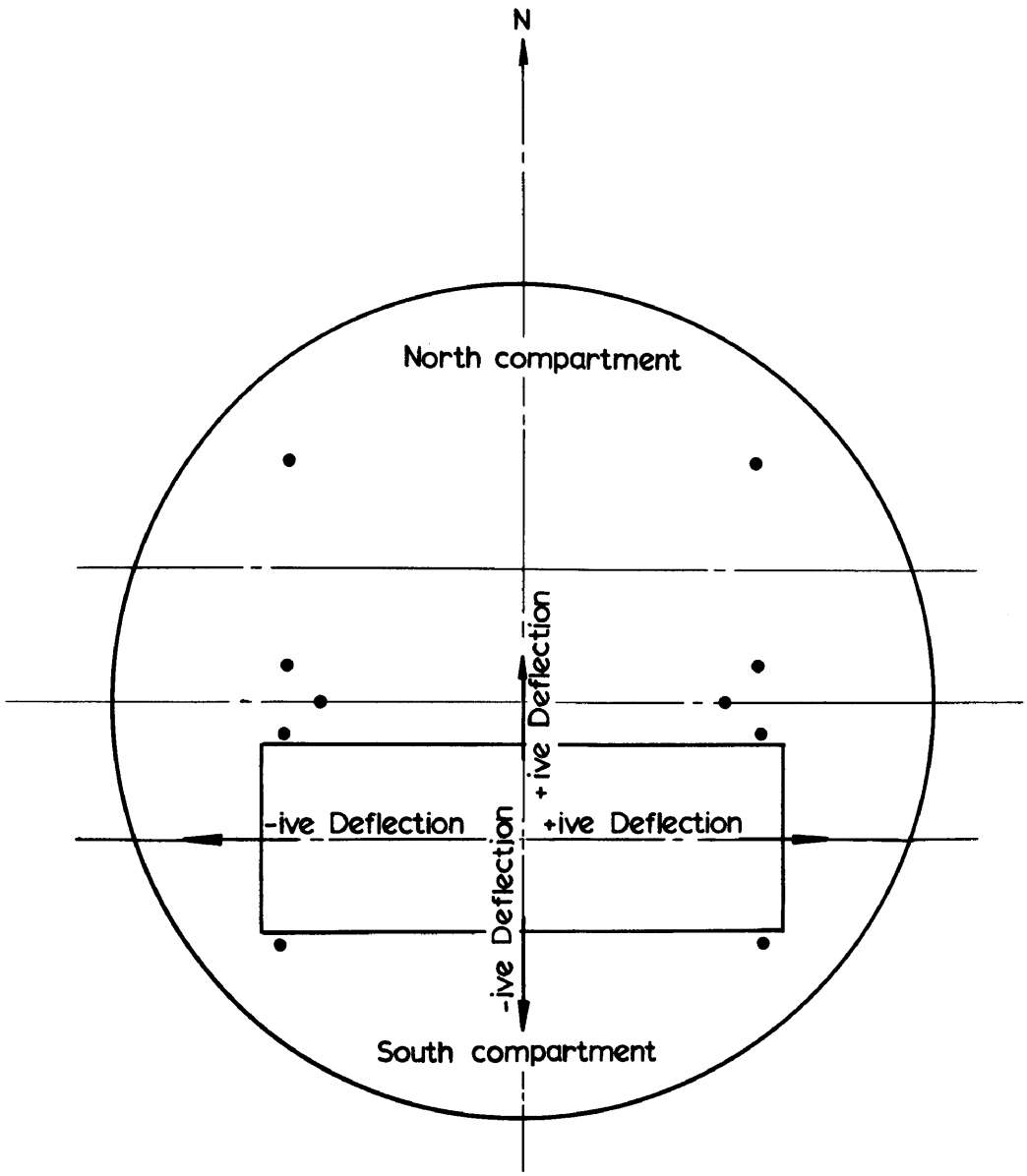

FIGURE 41(a)

Cross-section of shaft indicating the notation used for cage deflection in hoisting test results

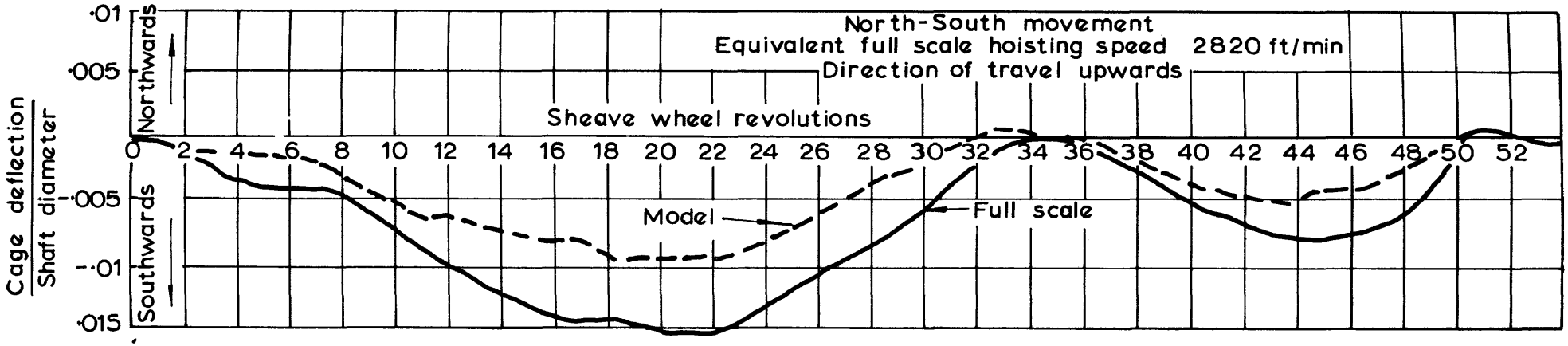

FIGURE 41(b)

Model and full-scale cage deflections with cage at original inclination

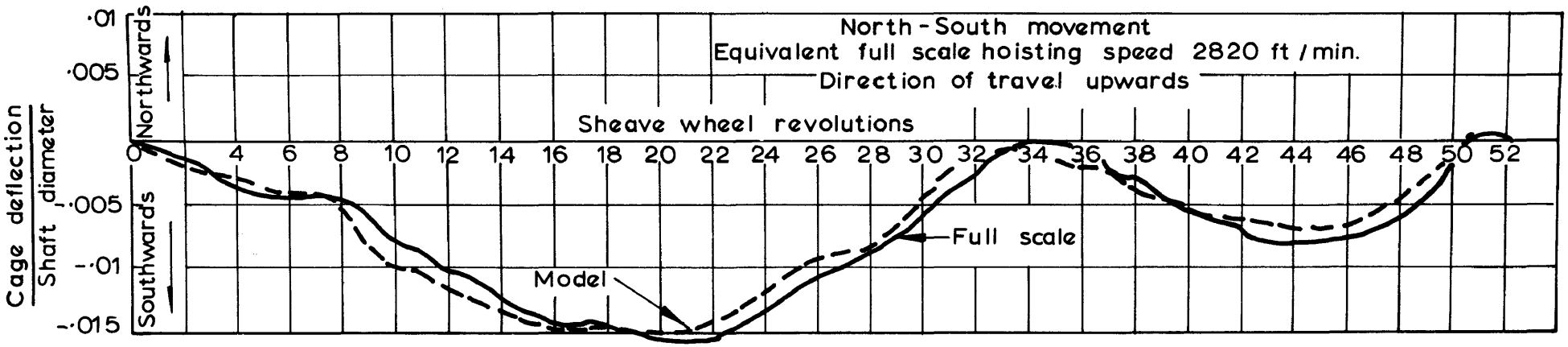

FIGURE 41(c)

Model and full-scale cage deflections with cage inclination increased by 14 minutes

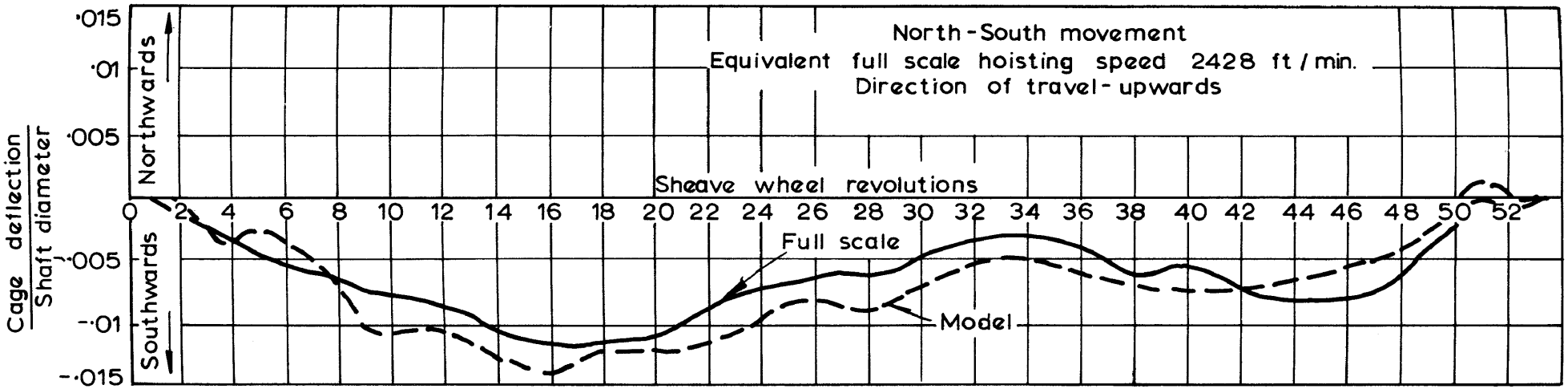

FIGURE 41(d)

Model and full-scale cage deflections

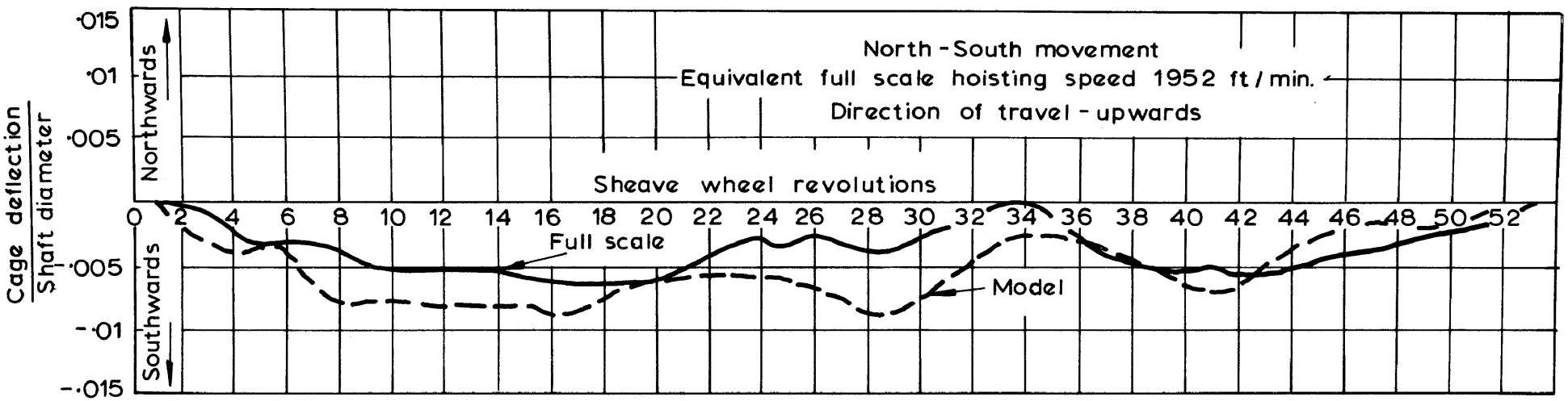

FIGURE 41(e)

Model and full-scale cage deflections

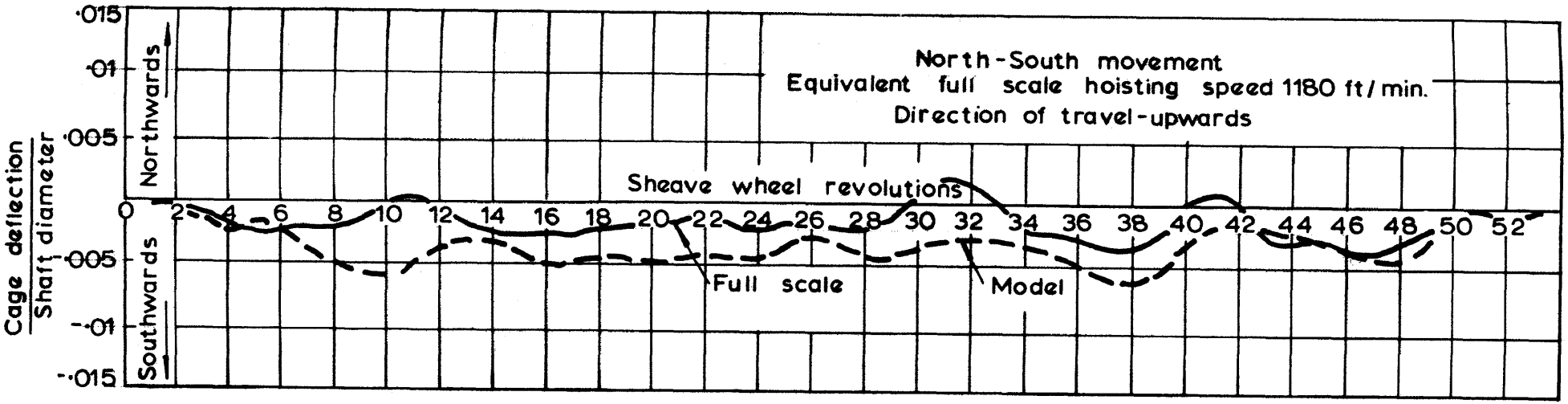

FIGURE 41(f)

Model and full-scale cage deflections

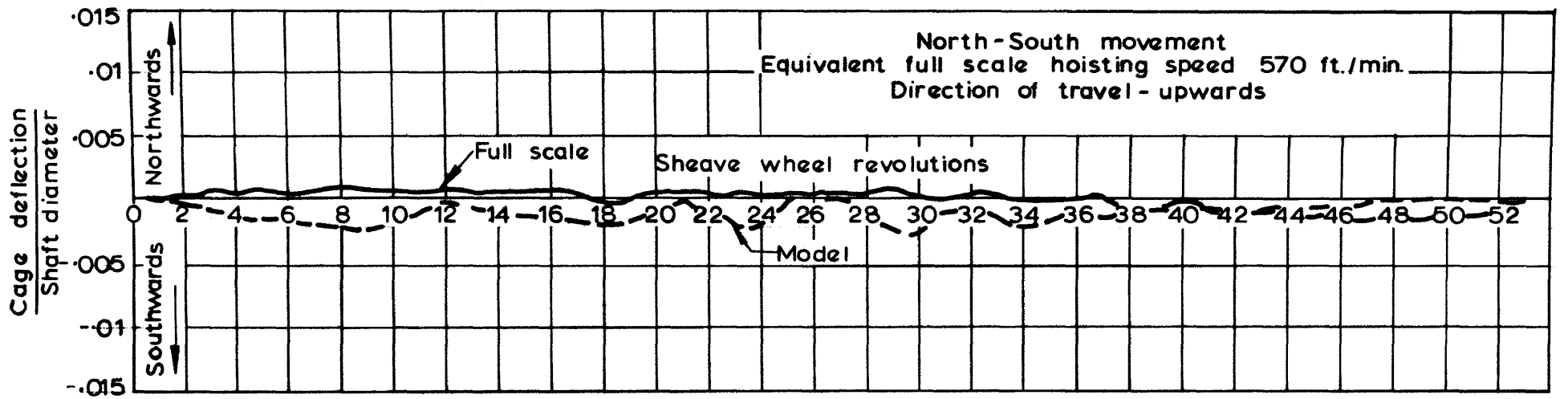

FIGURE 41(g)

Model and full-scale cage deflections

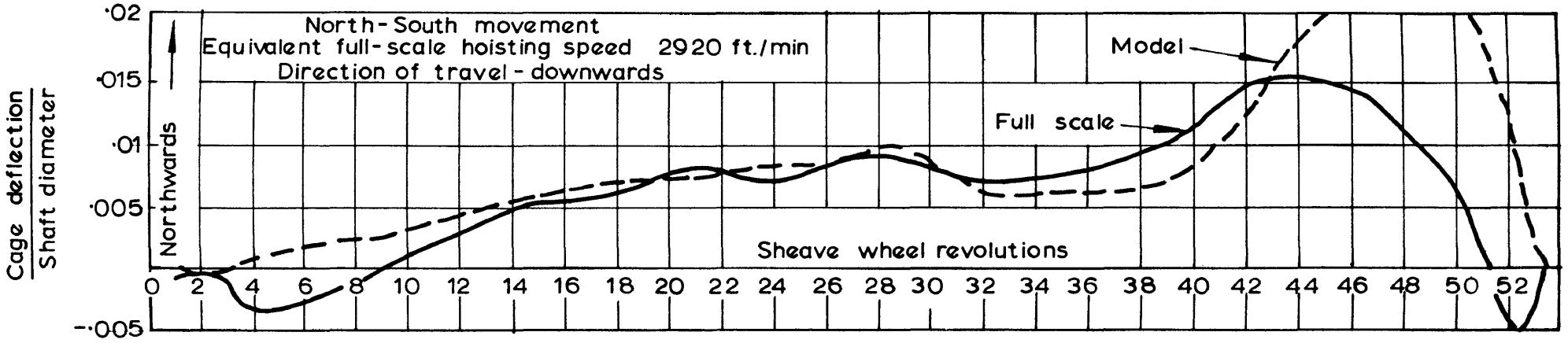

FIGURE 41(h)

Model and full-scale cage deflections

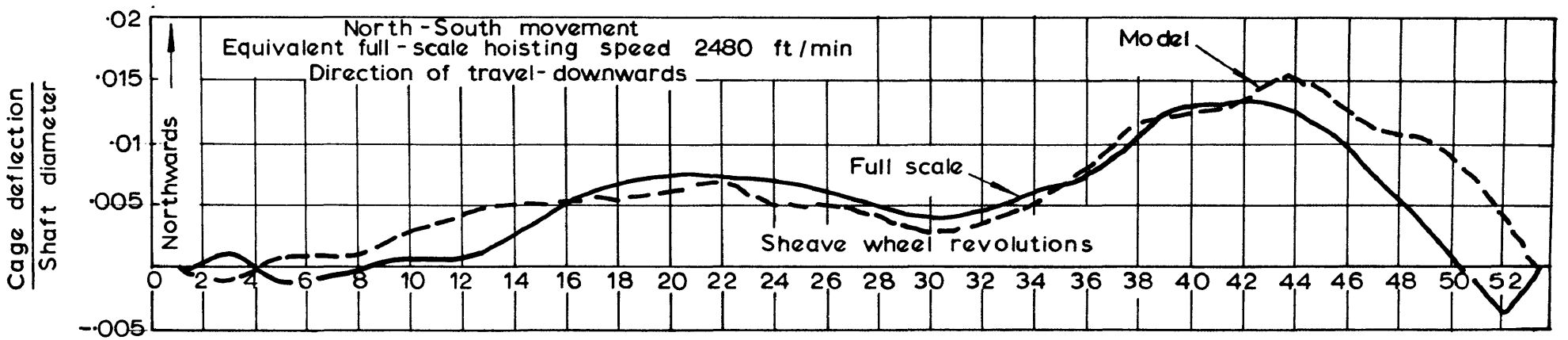

FIGURE 41(i)

Model and full-scale cage deflections

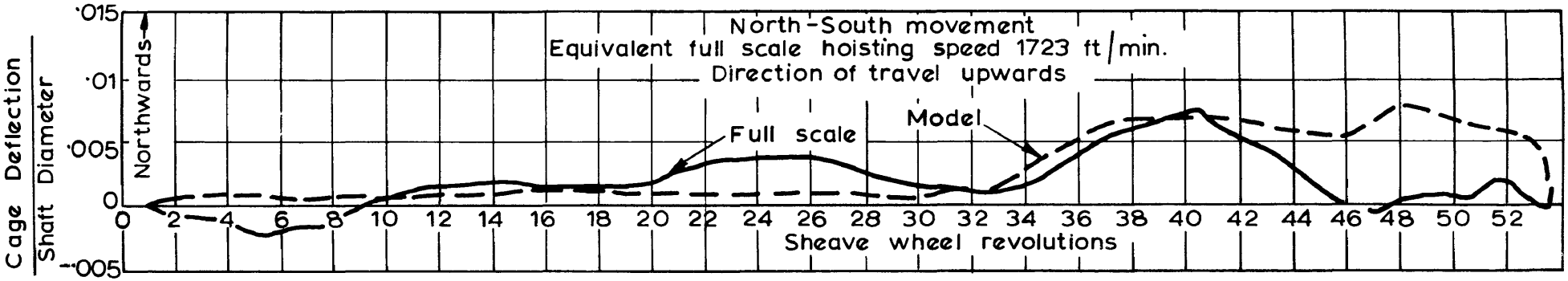

FIGURE 41(j)

Model and full-scale cage deflections

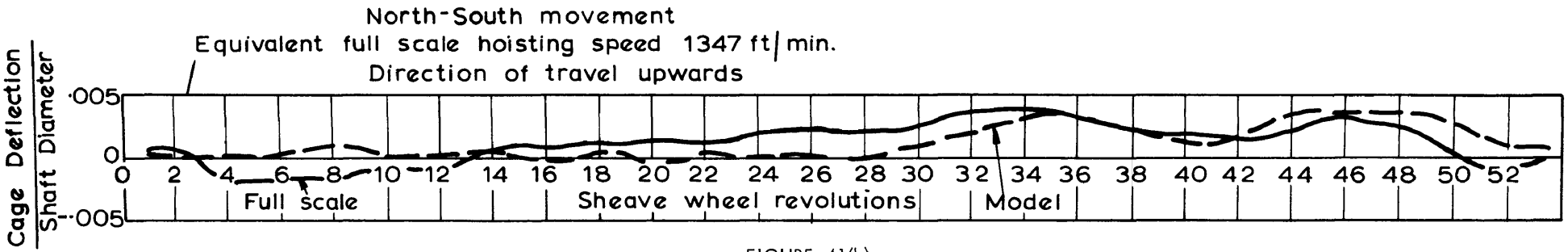

FIGURE 41(k)

Model and full-scale cage deflections

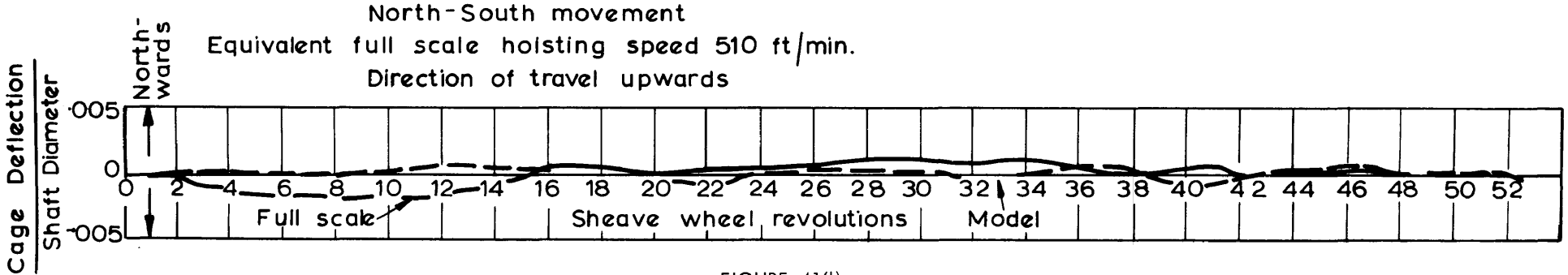

FIGURE 41(l)

Model and full-scale cage deflections

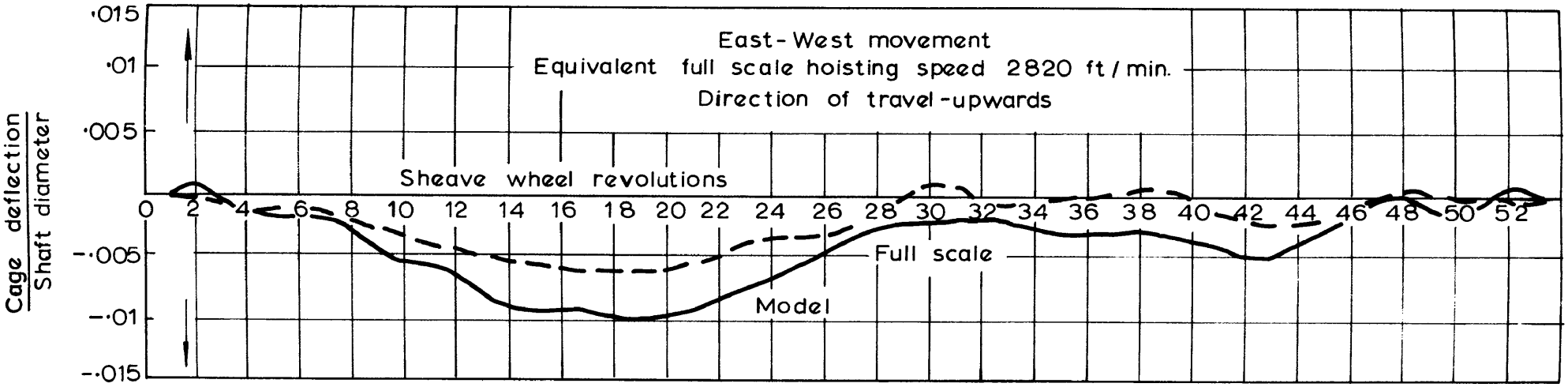

FIGURE 41(m)

Model and full-scale cage deflections

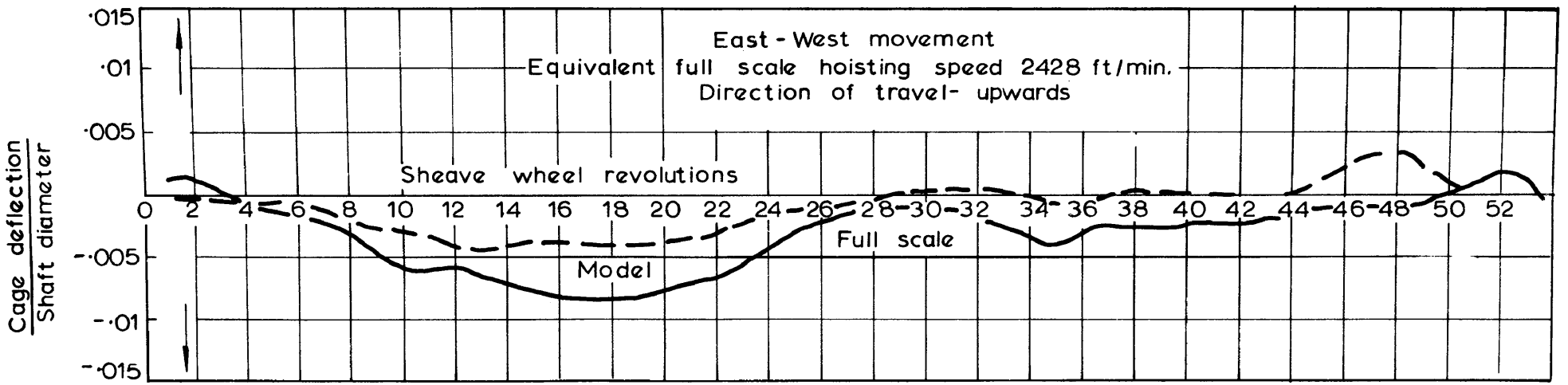

FIGURE 41(n)

Model and full-scale cage deflections

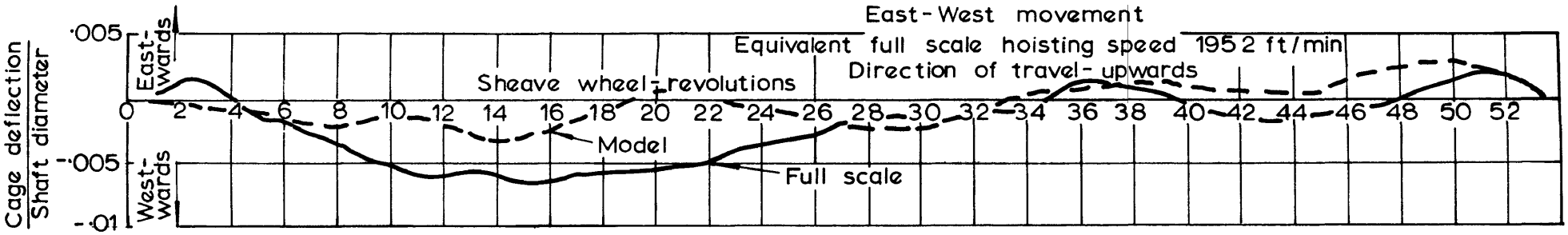

FIGURE 41(o)

Model and full-scale cage deflections

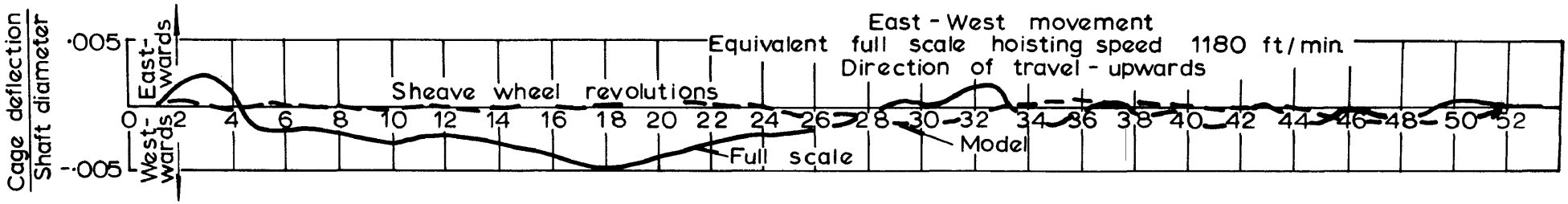

FIGURE 41(p)

Model and full-scale cage deflections

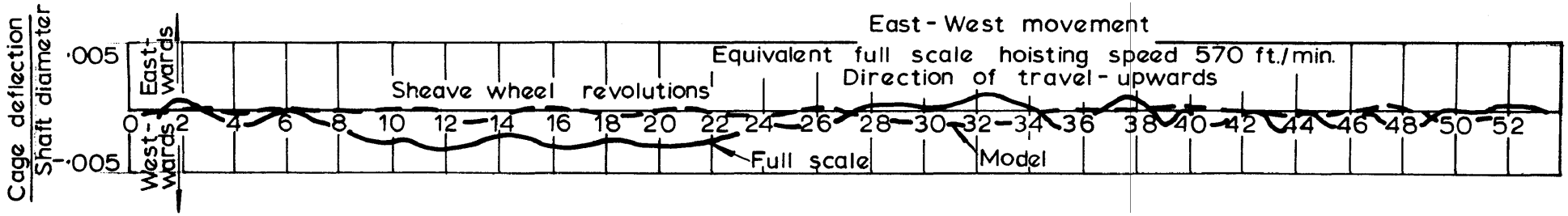

FIGURE 41(q)

Model and full-scale cage deflections

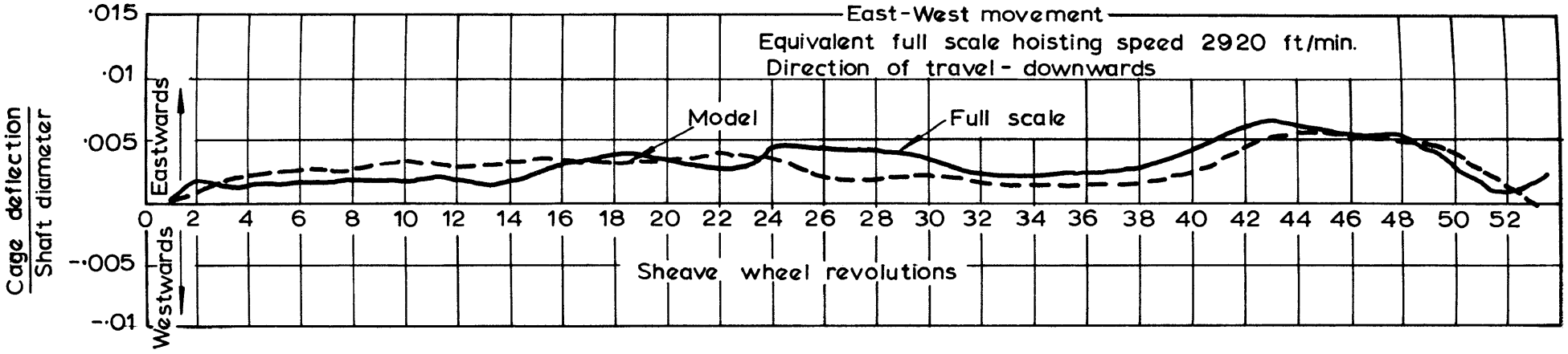

FIGURE 41(r)

Model and full-scale cage deflections

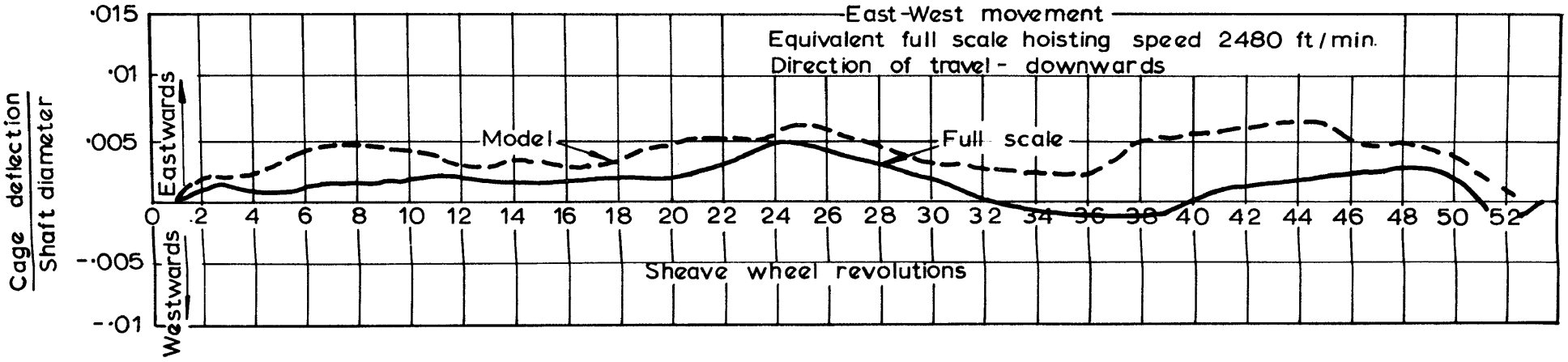

FIGURE 41(s)

Model and full-scale cage deflections

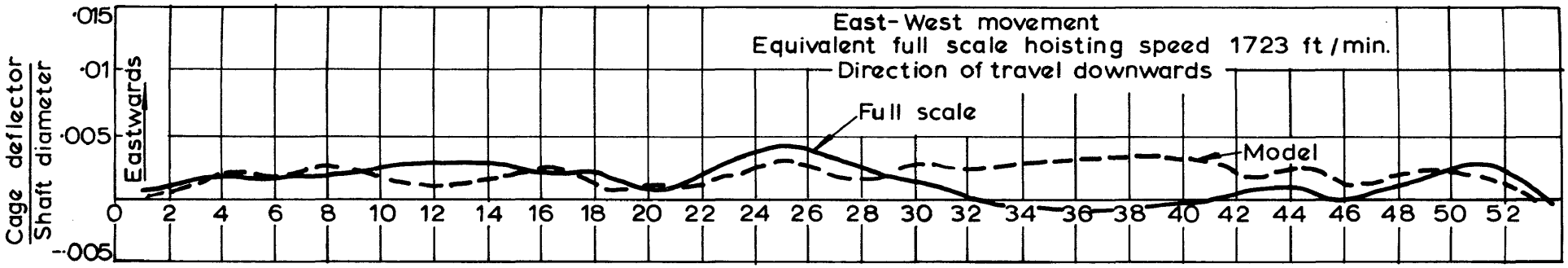

FIGURE 41(t)

Model and full-scale cage deflections

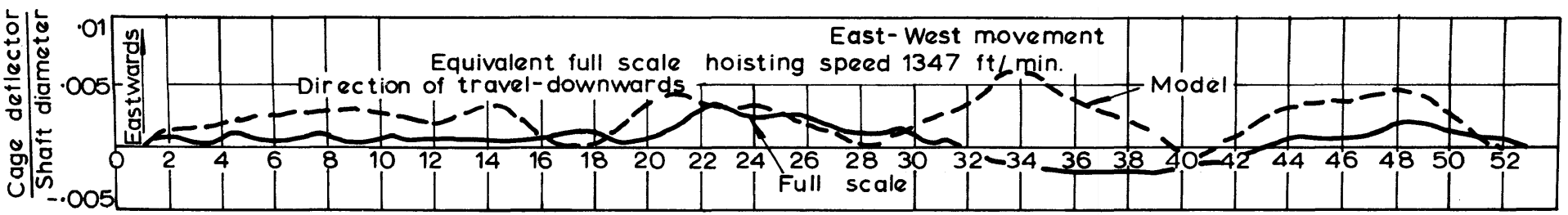

FIGURE 41(u)

Model and full-scale cage deflections

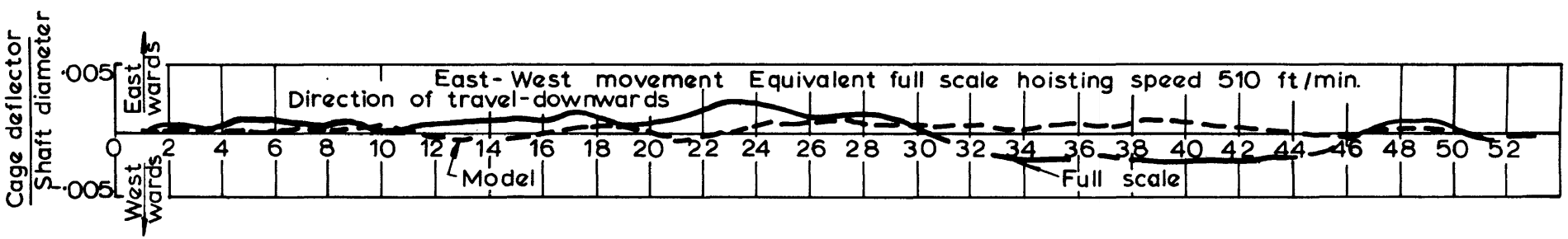

FIGURE 41(v)

Model and full-scale cage deflections

in the north-south direction, indicating that the model exhibited a much smaller lateral deflection than the fullscale cage. It was then discovered that very small changes in the angle of inclination of the model cage had a marked effect on the magnitude of lateral deflection in the north-south direction. Some doubt now arose as to whether the cage was suspended absolutely vertically in the shaft.

When the model was designed and constructed the importance of slight errors in the angle of suspension of the cage was not realised, and no provision was made for installing the cage absolutely vertically in the shaft. Subsequent measurements indicated that the cage was slightly scew, and the problem of how the cage should be suspended in the shaft so as to be vertical relative to the guide ropes had to be solved. Figure 42 shows a calibration curve relating the angle of inclination of the cage to the number of turns applied to the turnbuckles in the suspension chains. This calibration curve exhibits a discontinuity in its slope, a small portion having a greater slope than the rest. This portion of the curve indicates the limits at which the guide ropes were hanging slack in their guide eyes on the cage; its centre corresponded to the attitude of the cage when it was hanging vertically in the shaft. This calibration graph therefore showed that the cage had been hanging approximately 14 minutes out of plumb in the north-south direction.

Hoisting tests were resumed, after making this correction to the angle of suspension. Figure 41(c) shows the results for the same test illustrated in Figure 41(b), after the correction to the angle of suspension had been made, indicating that correlation between model and fullscale systems for this particular test was now much improved.

A study of Figures 41(c) to 41(v), which present the model and fullscale results for all upward and downward hoisting tests, will reveal that in general the behaviour of the model was very similar to its fullscale prototype. However, the magnitudes of lateral deflections of the model did not, in some cases, tally well with the fullscale deflections. Notably in the east-west

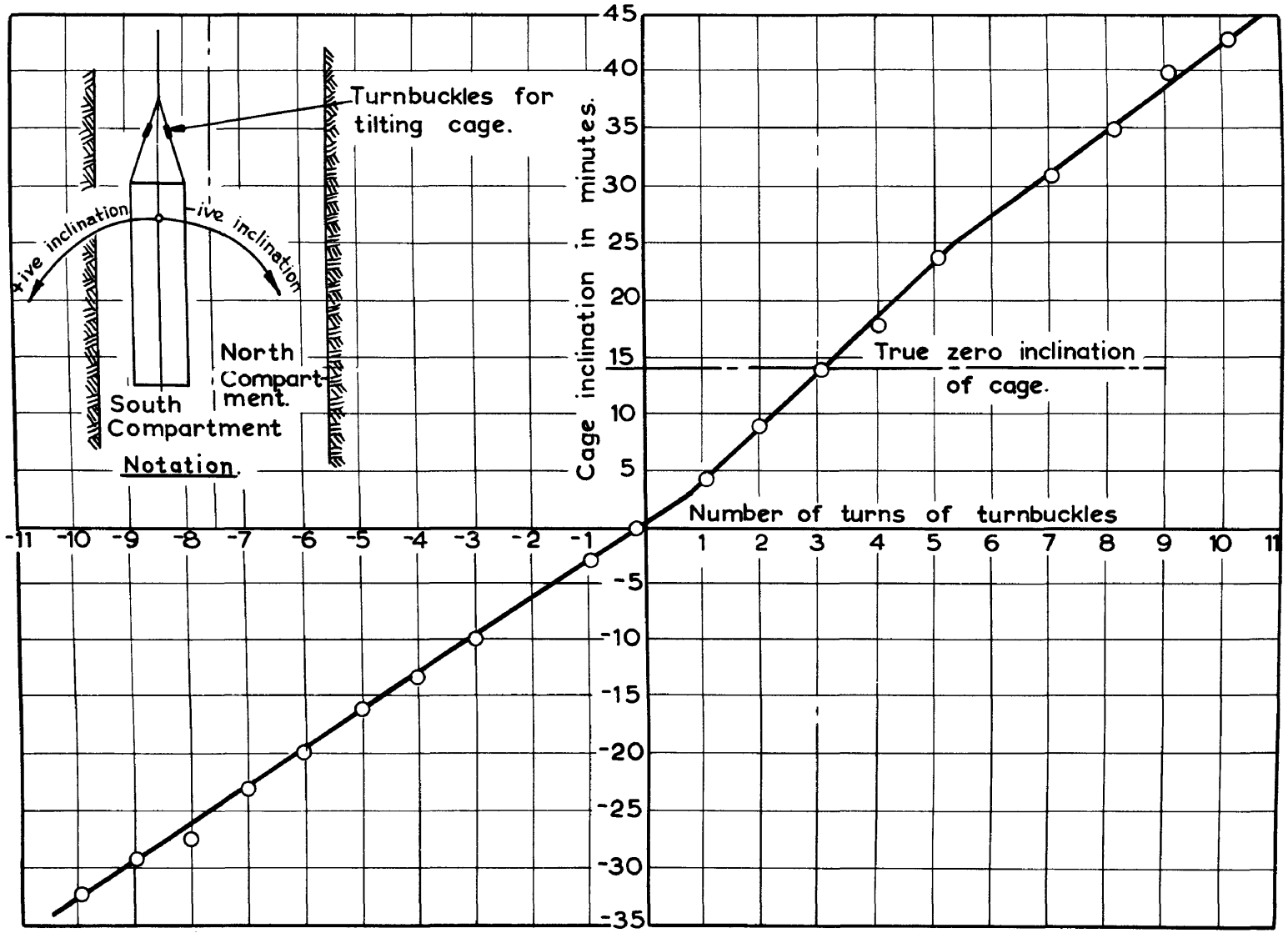

FIG. 42: RELATIONSHIP BETWEEN NUMBER OF TURNS ON TURNBUCKLES AND ANGLE OF INCLINATION OF CAGE.

FIGURE 42

Relationship between number of turns on turn-buckles and angle of inclination of cage

direction, as indicated in Figure 41(m), the model deflection was less than what it should have been for good correlation.

The effect which the tilting of the cage had on the east-west motion was investigated but was found to be of little importance. This was expected since the perforated cage doors were situated on the eastern and western faces of the cage, thus making these surfaces less sensitive to aerodynamic side forces.

It was realised that the model cage was suspended completely symmetrically about the north-south axial plane of the shaft. It is therefore clear that any east-west lateral motion of the cage would have been completely arbitrary as far as aerodynamic forces were concerned. Slight misalignment in the cage suspension may cause such a cage to be deflected either in the eastward or in the westward direction. In actual fact it was found that the model cage was deflected eastwards whereas the fullscale cage moved to the west. In order to facilitate comparison the model and fullscale traces were all plotted as westward deflections in Figures 41(m) to (v).

Apart from aerodynamic forces acting on a moving conveyance it is also necessary to consider the Coriolis force caused by the rotation of the earth. This force is admittedly small but full-scale and model deflection measurements have shown that small sustained lateral forces of only a few pounds cause a noticeable deflection of a conveyance.

Let Ω = 0.0000727 radians second^{-1} be the rotational speed of the earth and v = 47 feet second^{-1} be the upward hoisting speed of the fullscale conveyance.

The Coriolis acceleration for the fullscale conveyance will then be given by $2\Omega v$ = 0.00683 feet second^{-2} and, taking the mass of the conveyance as 730 slugs, the Coriolis force has a magnitude of 730 x 0.00683 = 4.98 pounds westwards for upward hoisting. The order of magnitude of aerodynamic forces which will cause the fullscale conveyance to deviate as depicted in Figure 41(m)

(at a hoisting speed of 2820 feet per minute) will be approximately 12 to 15 pounds. It is therefore doubtful whether the observed east-west deflection in the fullscale installation may be attributed entirely to the Coriolis effect. Nevertheless it is clear that the Coriolis force is of the same order of magnitude as aerodynamic forces and must therefore be taken into consideration.

It is significant that the model exhibited a tendency to deviated eastwards, i.e. in a direction opposite to the fullscale deflection, for upward hoisting. On erecting the model the importance of the Coriolis force was not realised. However, by a fortunate coincidence the north-south axis of the model shaft was orientated approximately along the meridian but the model shaft was actually rotated through 180 degrees, so that the compartment designated as the south compartment in the model actually pointed northwards. The Coriolis force acting on the model cage was therefore in a sense directly opposite to the Coriolis force acting in the fullscale cage.

Unfortunately the Coriolis force given by $2 M \Omega v$ was not simulated to scale in the model. While both M and v were reduced to scale in the model Ω remained unchanged whereas it should have been increased by a factor $z = 4.89$. The magnitude of the Coriolis force was therefore too small by a factor of $\frac{1}{4.89}$ in the model. Figure 41(m) does indicate a smaller deflection for the model but not to such a degree as would be expected with the greatly reduced Coriolis force. This again indicates that additional aerodynamic force effects were present. At very low upward hoisting speeds the model cage showed very little lateral deflection whereas the fullscale deflection was still noticeable (refer to Figures 41(p) and 41(q)). Since the Coriolis force is linearly proportional to the hoisting speed, whereas aerodynamic forces are proportional to the square of the hoisting speed, it is reasonable to expect that the Coriolis effect will overshadow aerodynamic effects at very low hoisting speeds. For a cage travelling downwards at very low speed (Figure 41(v) the model again showed less lateral deviation than its fullscale counterpart.

..... 121

In general, downward runs were not executed very satisfactorily in the model.

In Figure 41(h) it appears that on the downward run the model cage was deflected more than the fullscale prototype in the northward direction near the bottom of the shaft. On decelerating it was not possible to follow the fullscale hoisting cycle accurately, as may be seen in Figures 40(a) to (j). Furthermore, slight movements of the personnel who were operating the hoisting gear on the upper platform, and vibrations of the hoisting gear itself, caused movements in the guide ropes while the model cage was moving downwards. It is therefore reasonable to assume that cage deflections measured in the lower portion of the model shaft included errors due to the above-mentioned causes.

From the results of the hoisting tests it is clear that the conveyance executed a slow swinging motion in the shaft, superimposed on a lateral deflection. The swinging motion is attributed to the reflection of rope waves from the upper and lower extremities of the ropes, these reflected waves causing the conveyance to swing back after an initial deflection, caused by lateral forces. In order to further illustrate the degree of correlation between the model and the fullscale installation, maximum amplitudes of swinging motion have been plotted against hoisting speed for both the model and fullscale tests. (Figures 43(a), 43(b), 43(c) and 43(d)).

The model and fullscale amplitudes for north-south movement correspond reasonably well at various hoisting speeds as illustrated by Figures 43(a) and 43(b). Furthermore the maximum amplitude is seen to vary allmost parabolically with the hoisting speed thus indicating that the maximum amplitude for a travelling conveyance varies approximately linearly with the lateral aerodynamic force.

Figures 43(c) and 43(d), depicting east-west movement, show a difference between model and fullscale amplitudes and, as

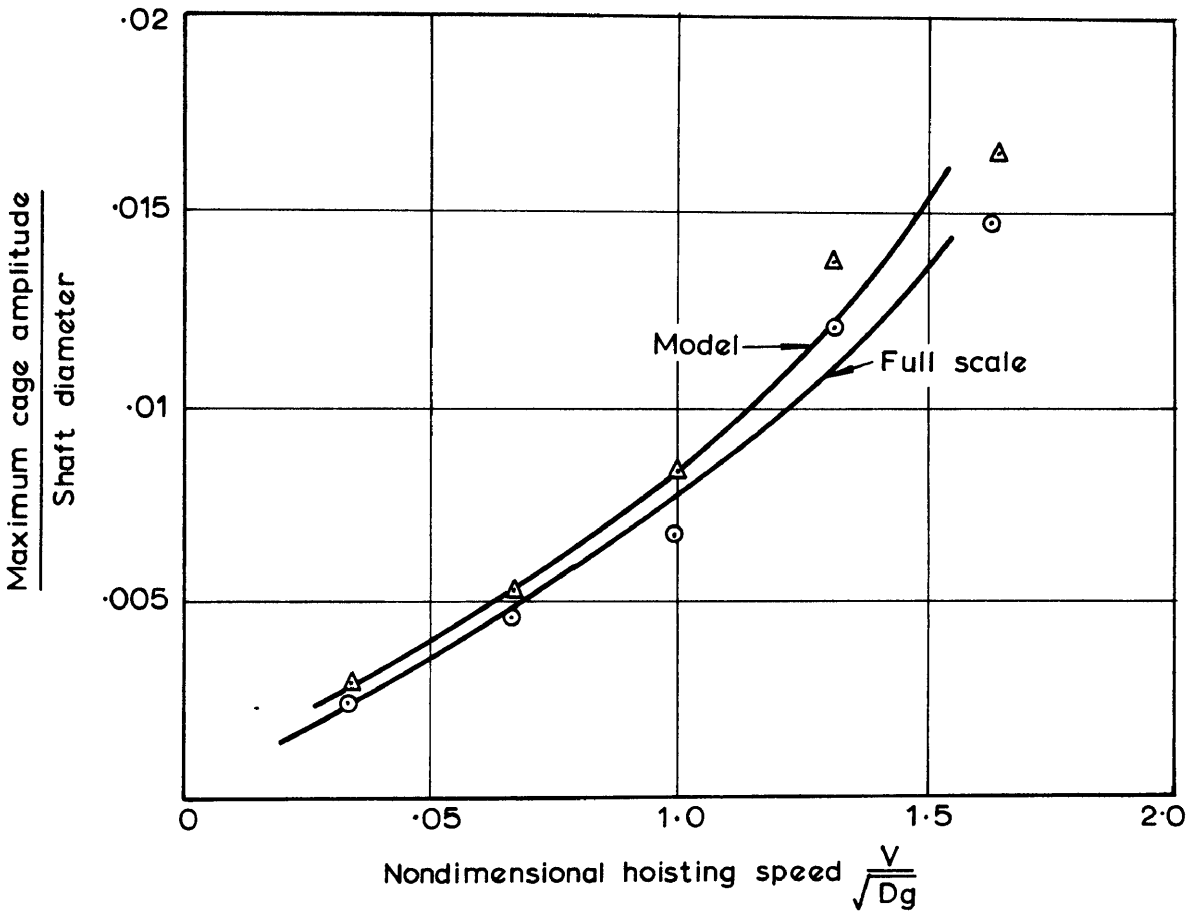

FIGURE 43(a)

Relationship between cage deflection and hoisting speed.
North - South deflection. Upward hoisting

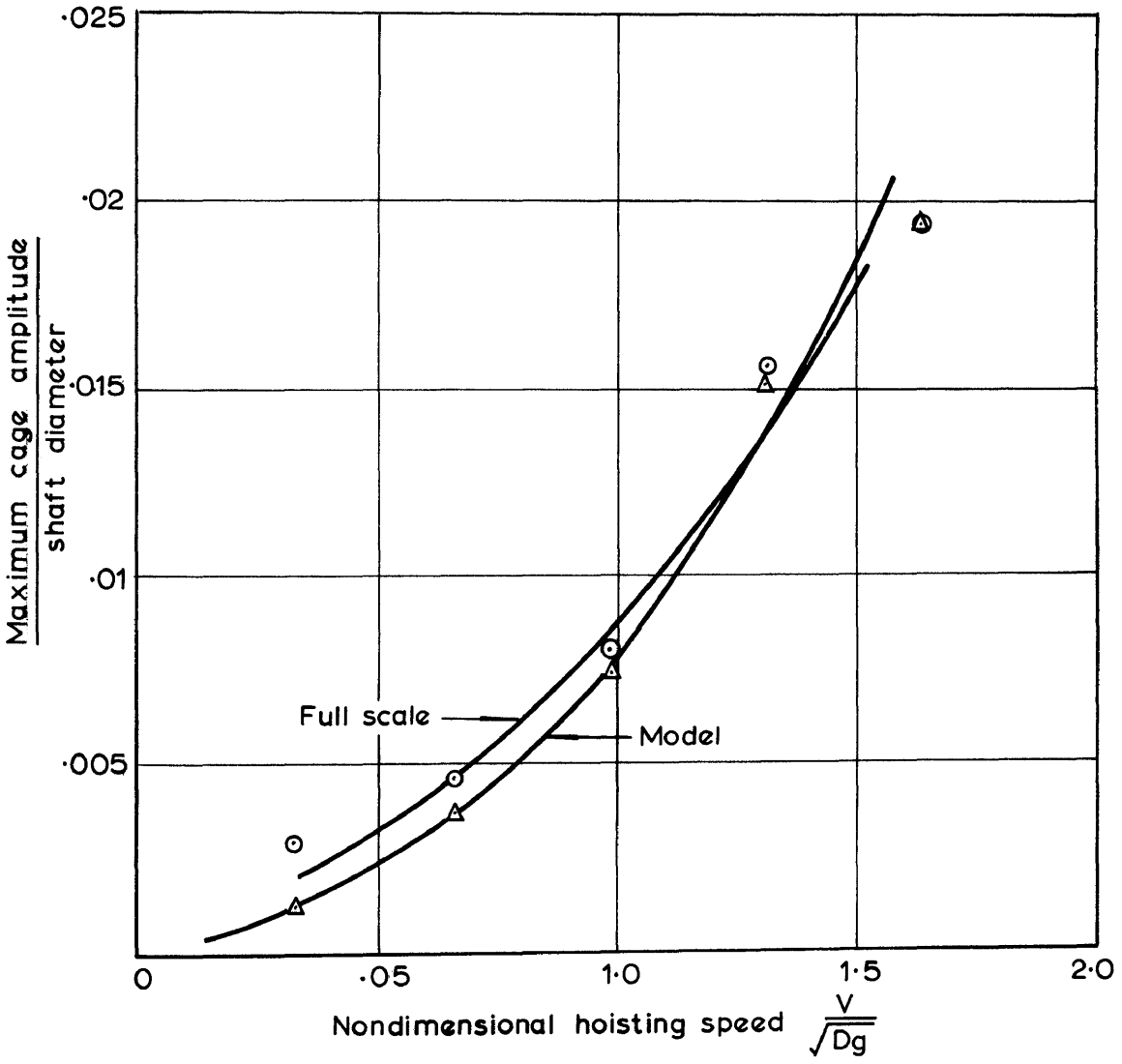

FIGURE 43(b)

Relationship between cage deflection and hoisting speed.
North - South deflection. Downward hoisting

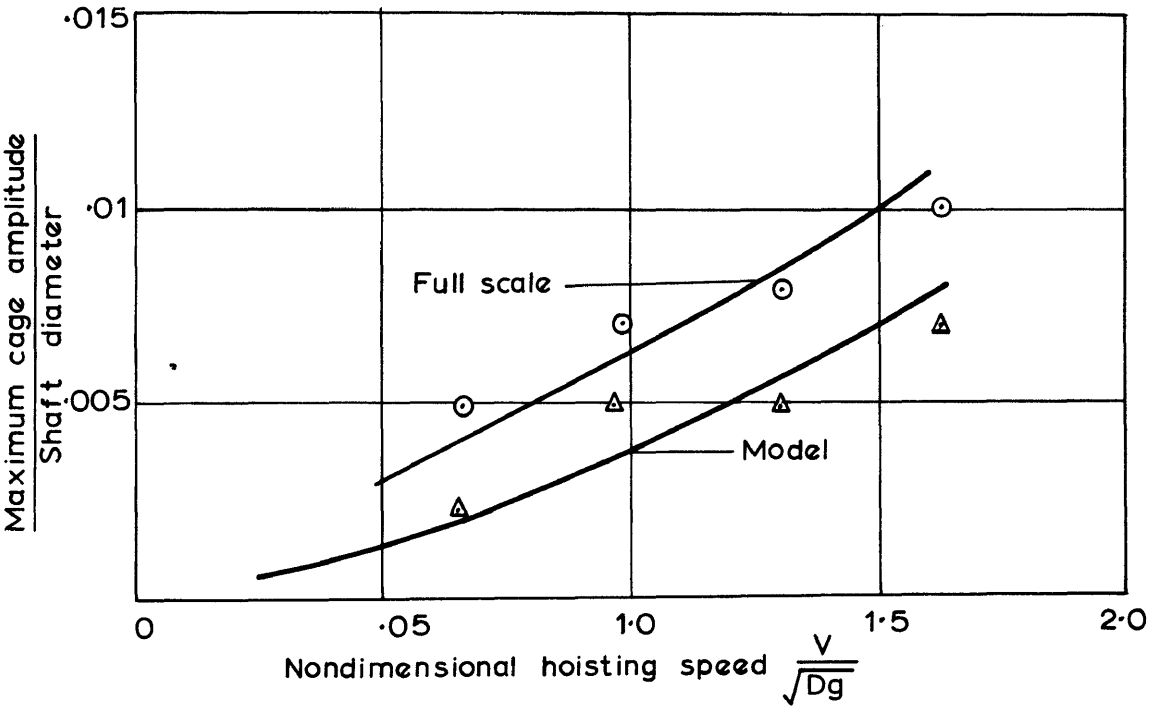

FIGURE 43(c)

Relationship between cage deflection and hoisting speed.
East - West deflection. Upward hoisting

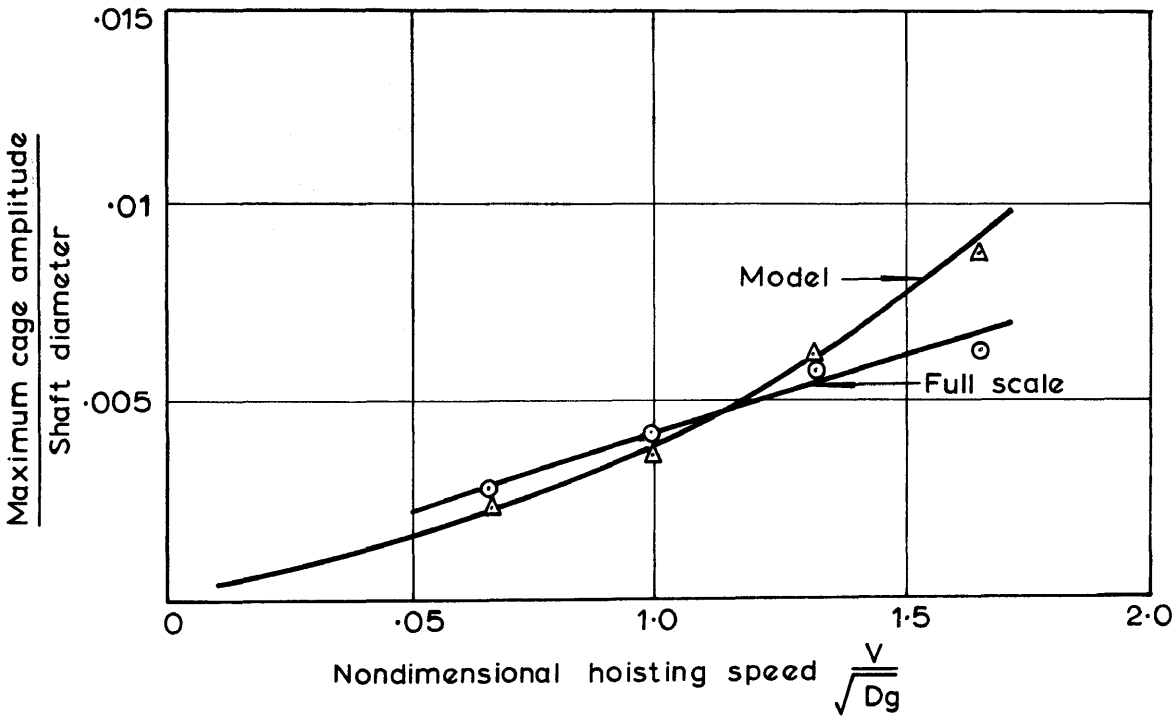

FIGURE 43(d)

Relationship between cage deflection and hoisting speed.
East - West deflection. Downward hoisting

explained above this is attributed to the arbitrary nature of aerodynamic forces and to Coriolis force effects. It is perhaps significant that for the east-west movement the fullscale amplitude tends to vary linearly with the hoisting speed whereas the model amplitudes still show a tendency to vary approximately with the square of the hoisting speed. This is regarded as an indication that the Coriolis force was prevalent in the fullscale installation and that aerodynamic forces were responsible for model deflection (The Coriolis force is directly proportional to hoisting speed and aerodynamic forces vary with the square of the hoisting speed).

4.3.2.4 Conclusions. It may be concluded that the static correlation tests described in section 4.3.1 indicate that, as far as rope tensile, inertial and damping forces are concerned, a model can be used to simulate correctly the behaviour of a fullscale rope-guide installation.

Taking the results of the hoisting tests described in section 4.3.2 into consideration all indications are that, as far as aerodynamic force effects are concerned, a model will simulate the fullscale prototype correctly under hoisting conditions, provided that great care is taken in assuring that model conveyances are aerodynamically similar to their fullscale counterparts. Coriolis force effects, however, are not represented to scale in a model and due allowance must be made for the Coriolis force deflection.

4.4 Supplementary tests.

4.4.1 Object and scope. Due to the fact that some uncertainty still existed as to the degree of accuracy with which aerodynamic forces were simulated in the model, it was decided to conduct a series of supplementary tests. The object of these tests was to investigate more closely the degree of correlation that existed between the model and its fullscale prototype as far as aerodynamic effects on the conveyance were concerned.

While performing hoisting tests in the fullscale mineshaft an unexpected and rather puzzling fact about the dynamic behaviour of the cage was noted, namely that the protective roof of the cage had a very marked effect on the deflection of the cage in the north-south direction. It was realised that this effect, which was clearly of an aerodynamic nature, provided a good subject on which to base a correlation test. It was decided to record carefully the behaviour of the fullscale cage with and without its protective roof, and then to establish whether the model cage behaved likewise under these conditions.

Another series of correlation tests, in which use was made of the aerodynamic effects caused by tilting the cage, was also envisaged. Comparative model and fullscale tests were to be carried out with the cages tilted at various angles of inclination ranging from approximately -20 minutes to +20 minutes.

Thirdly, it was decided to provide the fullscale cage with a large deflector plate which, during hoisting, could create an aerodynamic side force of such a considerable magnitude as to have a masking effect on all other aerodynamic side forces acting on the cage. By installing an accurately scaled-down deflector plate on the model cage it would then be possible to compare the behaviour of the model with the fullscale cage at various angles of incidence of the deflector plates.

For these supplementary tests it was decided only to consider cage movement in the north-south direction since all aerodynamic effects were more marked in this direction. Furthermore, since tests were to be carried out on the protective roof on top of the cage, and also since it was more convenient to mount a deflector plate on top than at the bottom of a cage, it was decided to consider only runs in the upward direction.

4.4.2 Experimental procedure. The procedure adopted to obtain recordings of cage motion in all the supplementary tests was the same as for previous hoisting tests.

To incline the fullscale cage, a block and tackle was rigged up between two adjoining suspension chains as indicated in Figure 22. By pulling the two chains inward towards each other, the cage could readily be tilted to angles of up to 20 minutes, which were measured by means of an inclinometer situated inside the cage. The model cage was tilted by means of turnbuckles in the suspension chains and the angle of inclination was in this case measured by the optical method described in section 4.3.2.2.

The fullscale deflector plate, constructed of masonite sheets and wood, measured 8 feet by 10 feet and was mounted on the cage in the manner indicated in Figure 44. The angle of incidence of the plate was measured with an inclinometer. The model deflector plate was constructed accurately to scale out of wood and paper and could be set at desired angles of incidence by means of a graduated angular scale.

4.4.3 Results and discussion.

4.4.3.1 Tests with protective cage roof.

Recordings of cage motion in the north-south direction with the protective roof installed on the cage had already been obtained in the tests described in section 4.3.2. On repeating these measurements they were found to agree. Their average traces representing model and fullscale cage movements are given in Figure 45. The results of measurements on the model and fullscale cages without roofs are also shown in Figure 45. It can be seen that the presence of a roof on both the model and the fullscale cage affected the flow pattern of the air around the cages in such a way that the aerodynamic forces pushed the cages southwards. On removing the roof, the aerodynamic forces on both the model and fullscale cages were reversed and the cages were now displaced northwards. Figure 45 shows that, as far as the aerodynamic effect of the protective roof was concerned, the model correlated extremely well with the fullscale prototype.

4.4.3.2 Tests on inclined cage.

Figures 46(b) to 46(f) show traces of the displacement obtained with the cages

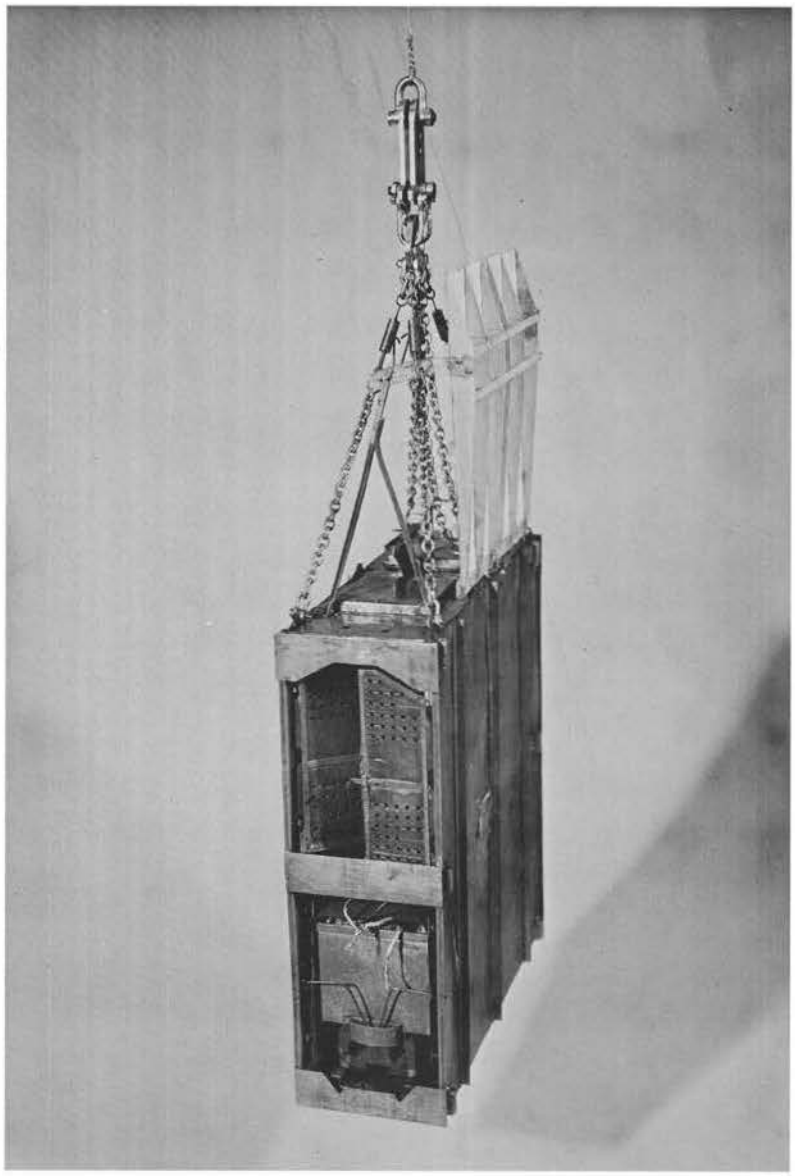

FIGURE 44

Model conveyance with deflector plate

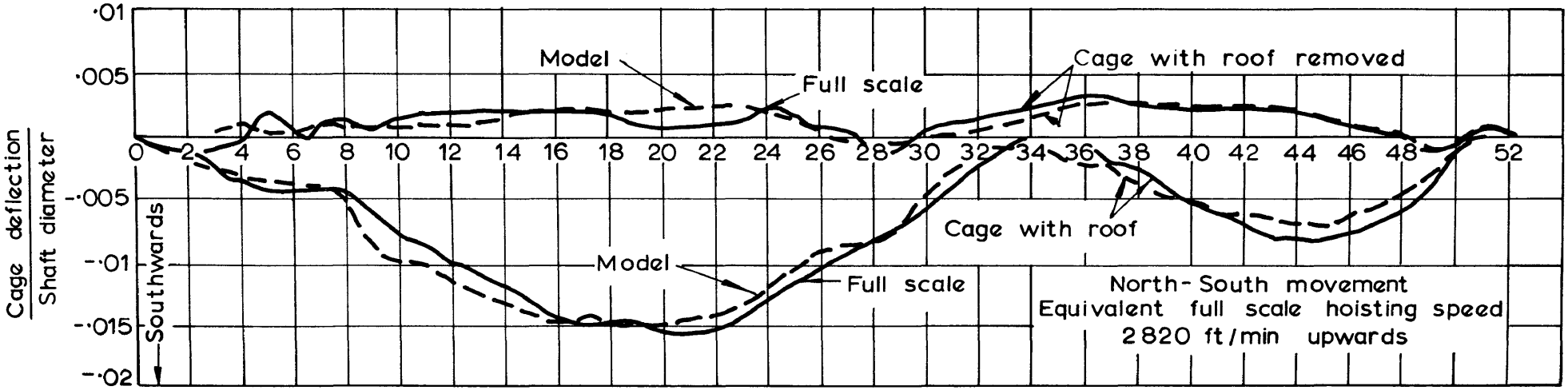

FIGURE 45

Effect of protective roof on model and full-scale cage deflection

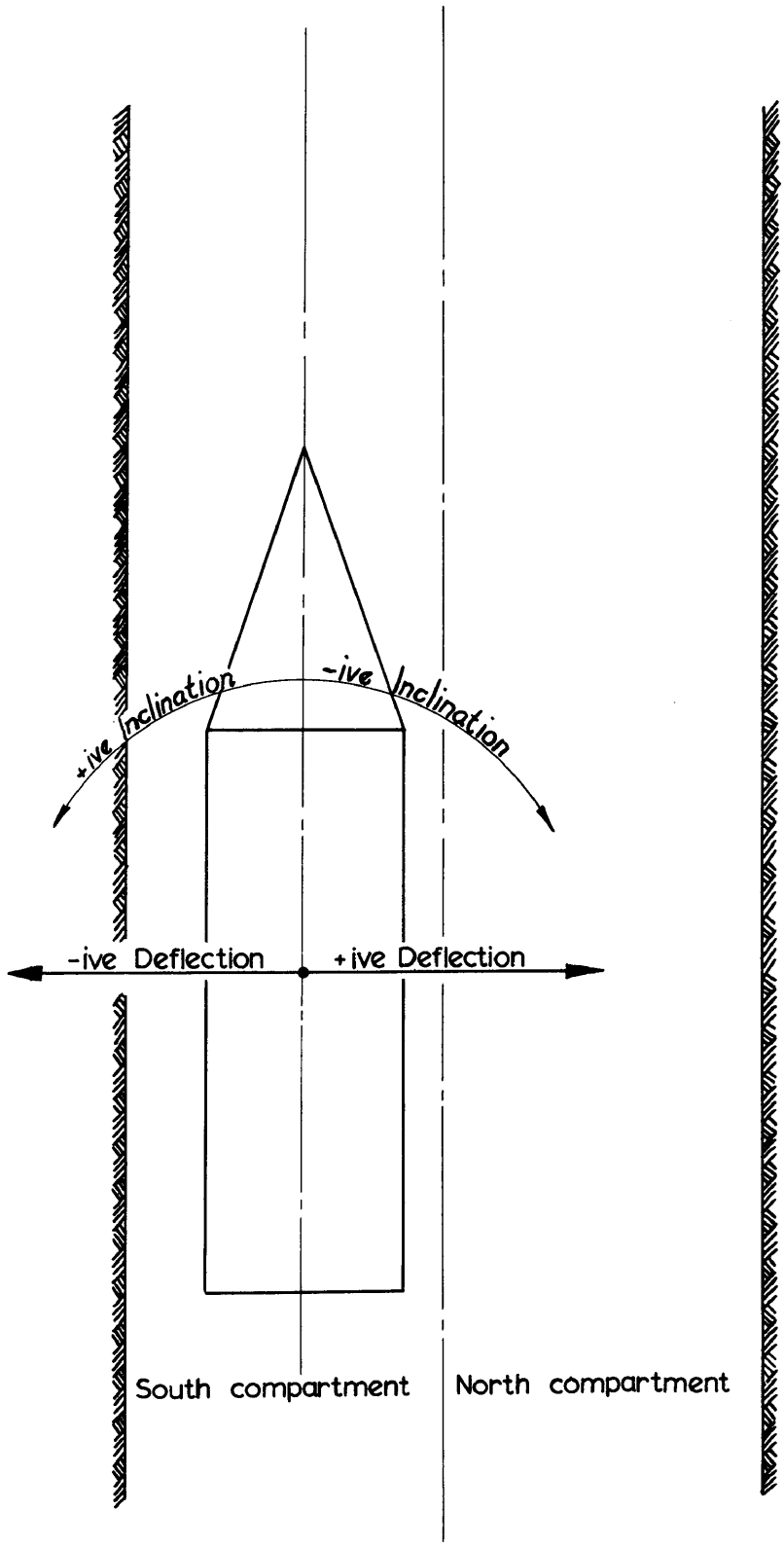

FIGURE 46(a)

Notation used for tests on model and full-scale cage deflections at various cage inclinations

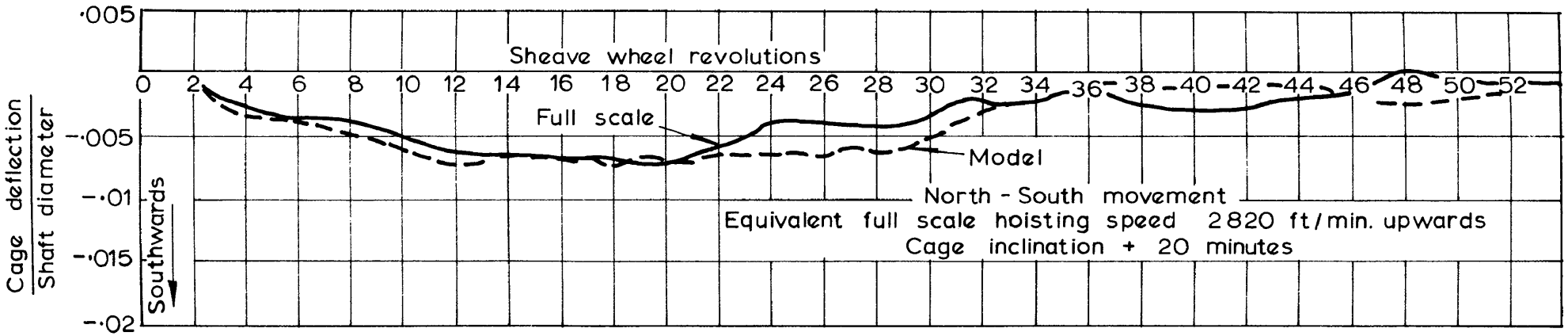

FIGURE 46(b)

Effect of cage inclinations on model and full-scale cage deflection

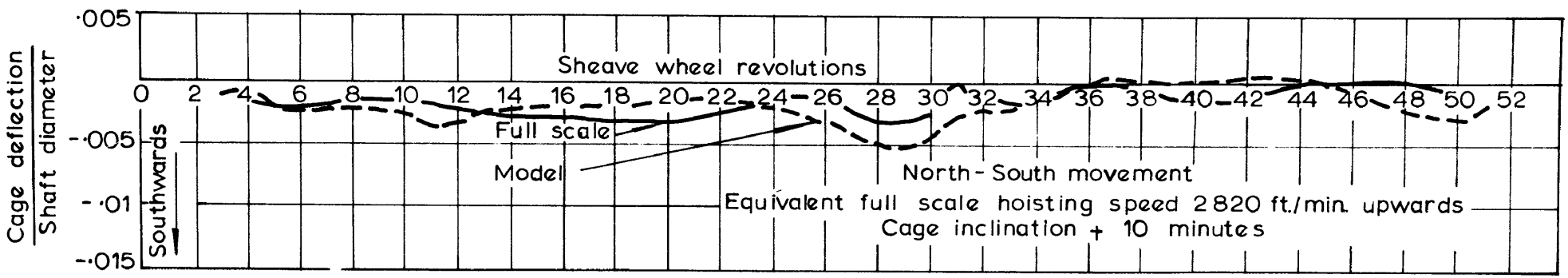

FIGURE 46(c)

Effect of cage inclinations on model and full-scale cage deflection

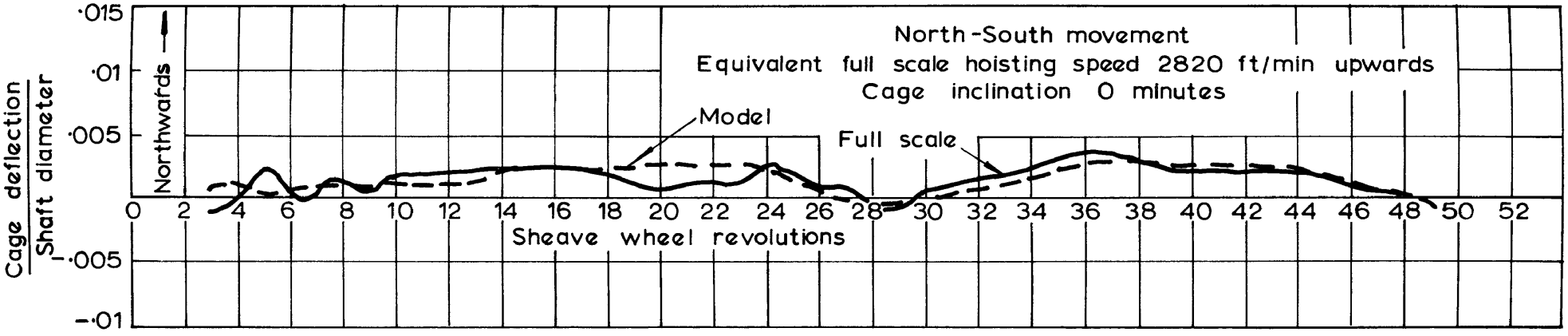

FIGURE 46(d)

Effect of cage inclinations on model and full-scale cage deflection

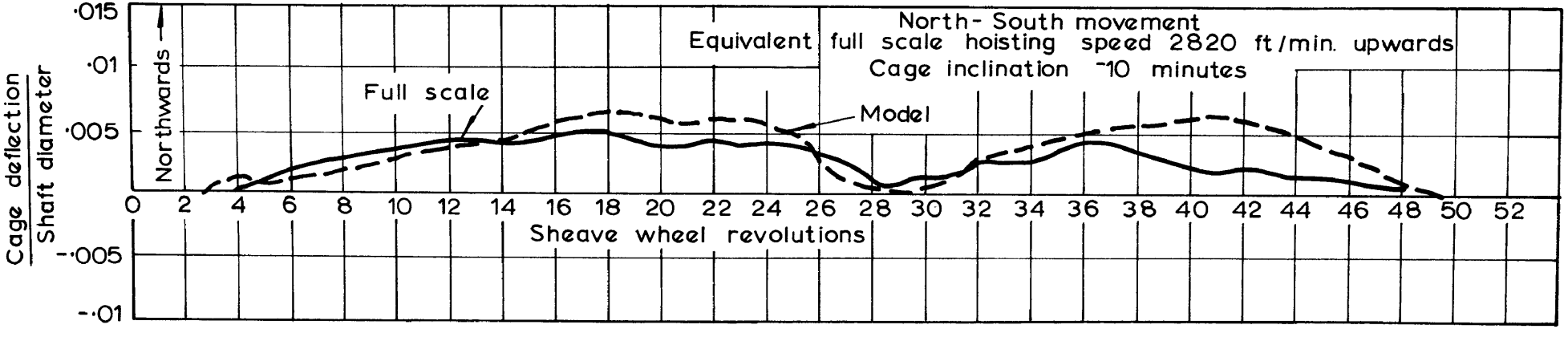

FIGURE 46(e)

Effect of cage inclinations on model and full-scale cage deflection

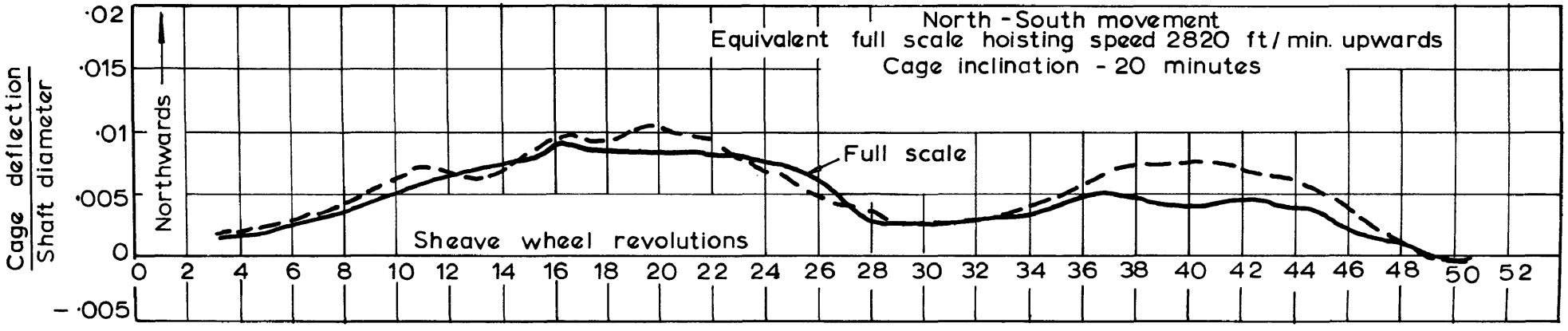

FIGURE 46(f)

Effect of cage inclinations on model and full-scale cage deflection

tilted at various angles of inclination. The notation pertaining to these graphs is given in Figure 46(a). These results were obtained with the protective roofs removed from the cages and show that model and fullscale behaviour had been similar for all angles of cage inclination. Except for the traces in Figure 46(e), the model cage deflection seldom deviated more than 0.6 inches from the fullscale cage deflection.

4.4.3.3 Tests with deflector plate. Preliminary tests on the model cage indicated that the aerodynamic force generated by installing a deflector plate was by no means as large as was expected. Due to the limited space available in the shaft it was only possible to mount the deflector plate on top of the cage. In this attitude the deflector plate did not act as an aerofoil as was originally intended but rather as a scoop which deflected the air in a southward direction towards the shaft wall. With reference to Figure 47(a), the deflector plate, when inclined at an angle of 12^{o} incidence, had a negligible influence on the movement of the cage. When the plate was adjusted to zero angle of incidence, air was deflected southwards, thus causing an aerodynamic force acting in the northward direction. The magnitude of the cage deflection obtained when hoisting at full speed was not much larger than that previously obtained with the inclined cage.

This rather defeated the purpose of the deflector plate which was intended to create large aerodynamic forces masking out all other aerodynamic effects. Figures 47(b) to 47(e) give the results of the correlation tests with the deflector plate while Figure 47(a) shows the notation necessary to interpret the results. Again it will be observed that the model followed the same general pattern of behaviour as its fullscale counterpart, although with the deflector plate set to an angle of zero incidence the model cage tended to swing back more rapidly from its peak deflection than did the fullscale cage. It was also noticed that the fullscale deflector plate showed a tendency to deform under aerodynamic load and during hoisting vibration and buffeting was evident. It is thought that the discrepancies between the shape

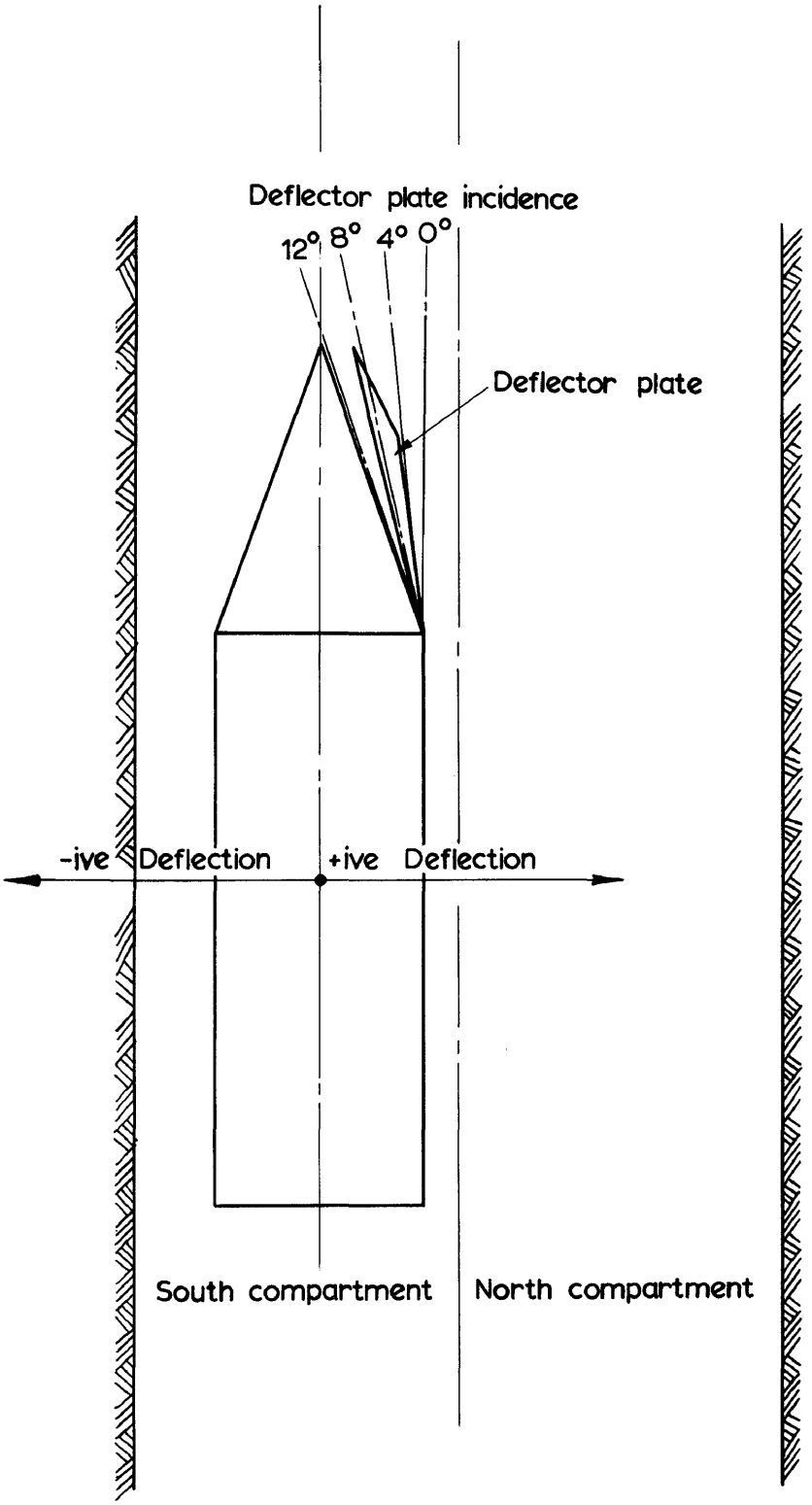

FIGURE 47(a)

Notation for tests on model and full-scale cage deflections at various deflector plate incidences

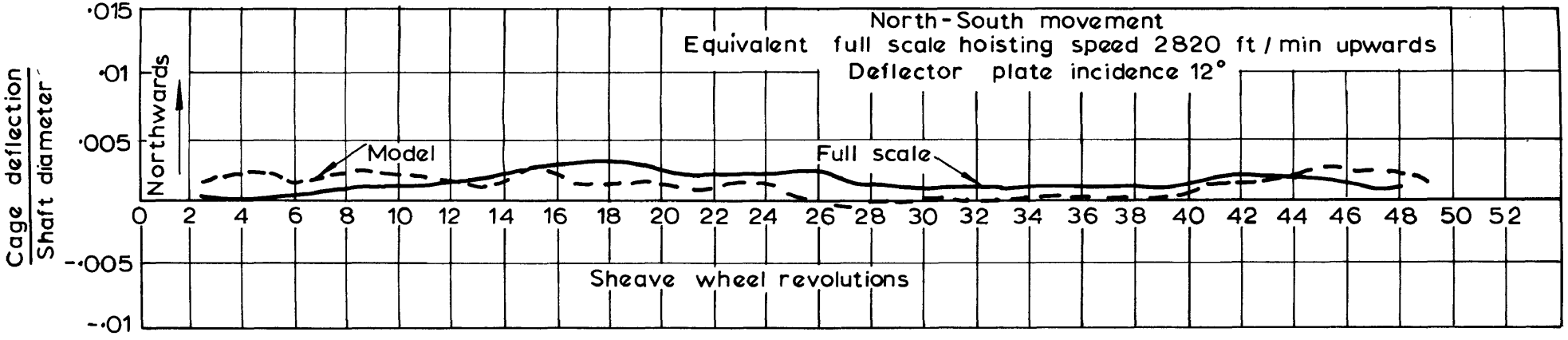

FIGURE 47(b)

Effect of deflector plate incidence on model and full-scale deflection

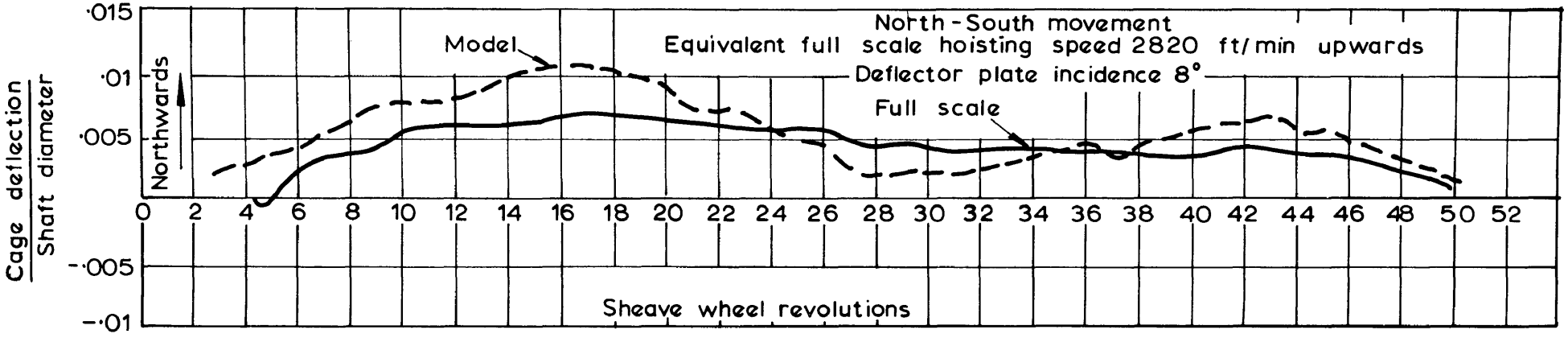

FIGURE 47(c)

Effect of deflector plate incidence on model and full-scale deflection

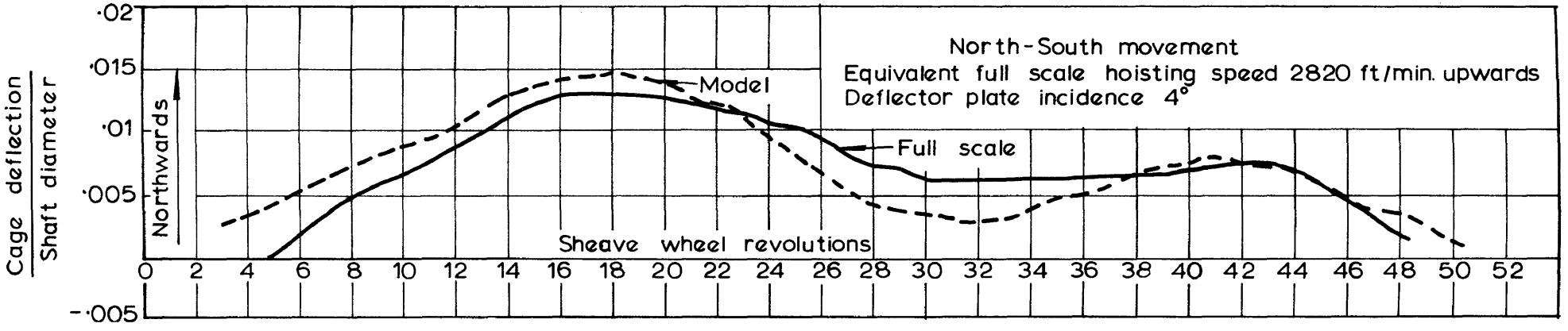

FIGURE 47(d)

Effect of deflector plate incidence on model and full-scale deflection

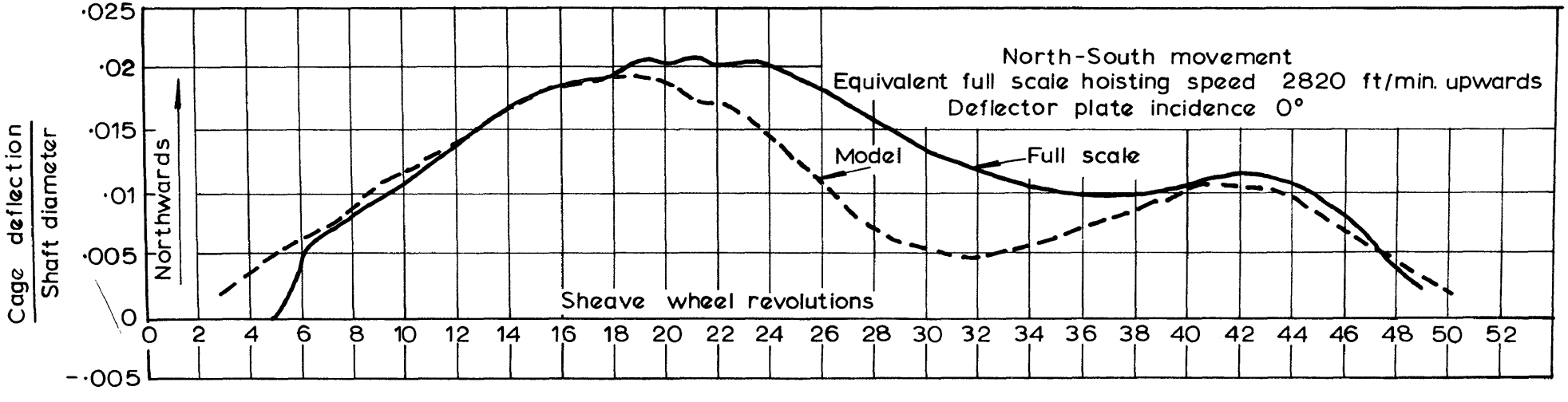

FIGURE 47(e)

Effect of deflector plate incidence on model and full-scale deflection

of the model and fullscale traces are due to deformation of the deflector plate.

4.4.4 Conclusions. It is thought that the results of the correlation tests on the effects of the protective roof and the inclined cage indicate that aerodynamic forces were correctly simulated in the model. The tests on the effect of the protective roof (refer to Figure 45) is regarded as significant in illustrating the degree of similarity attained in the operation of the model and its fullscale prototype. These particular tests were done with great care as far as the model operation was concerned. Model hoisting runs were only done when all natural oscillations in the model rig were reduced to negligible proportions and results from hoisting runs which were done under doubtful conditions of stability were rejected. The degree of simulation depicted by Figure 45 is regarded as typical of what may be obtained with apparatus which is in good order. It is felt that the more limited correlation indicated by some of the other hoisting tests may be attributed chiefly to defects in the apparatus and to unfavourable testing conditions, and not to some basic dynamic dissimilarities between the model and its fullscale prototype.

4.5 Discussion on the accuracy of model correlation attained.

4.5.1 General. The experience gained with the Durban Roodepoort Deep correlation tests has revealed many defects in the type of equipment and the testing techniques employed. Some inherent limitations associated with dynamic scale models of rope-guide systems have also come to light. This section will be devoted to a discussion on the effects which these factors had on the accuracy of the Durban Roodepoort Deep correlation test results.

4.5.2 Defects in equipment. During the design of the Vertical Mineshaft Windtunnel it was realised that the supporting structure for the model shaft had to be as rigid as possible. A pit of sufficient depth to accommodate the entire model shaft

..... 140

would have been ideal but the cost of sinking and lining a pit of some 160 feet deep proved to be prohibitive and it was therefore necessary to use an eighty-feet high steel tower in conjunction with an eighty-feet deep pit. All efforts were made to render the structure as rigid as possible but this tower still proved to be unsatisfactory. The model installation was very susceptible to oscillations caused by wind and movements of personnel stationed on the tower platform. For example it was noticed that when the model cage was hanging stationary at the lower stopping position in the model snaft ready to commence an upward run, slight wind gusts caused cage oscillations of 2 millimeters or more. While engaged on a test programme it was frequently necessary to suspend tests until better wind conditions prevailed. During day time the heat of the sun caused distortion of the model shaft, thus upsetting the various calibrations necessary for analysing the results. Most of the hoisting tests had therefore to be performed at night when conditions were most favourable. It is to be expected that these rather harassing working conditions adversely affected the accuracy of model test results.

Some sources of error in recordings of conveyance motion may also be traced to the electronic recording equipment. Figures 48 and 49 show calibration curves for the fullscale and model induction coils. These curves indicate that, for lateral movement of the coil in a direction perpendicular to the coil legs, an apparent cage deflection parallel to the legs will be registered by the recording system. This is because the magnetic lines of force between the legs are not straight and do not form a uniform parallel field but are curved in the proximity of the legs with the result that the indicator wire, although having a relative displacement perpendicular to the coil legs still cut some of the magnetic lines of force.

In Figure 48 and 49 areas in which the magnetic fields are reasonably uniform, are indicated. An attempt was made in both the model and fullscale tests to ensure that the indicator cables would only operate in these areas. However, this condition could not

..... 141

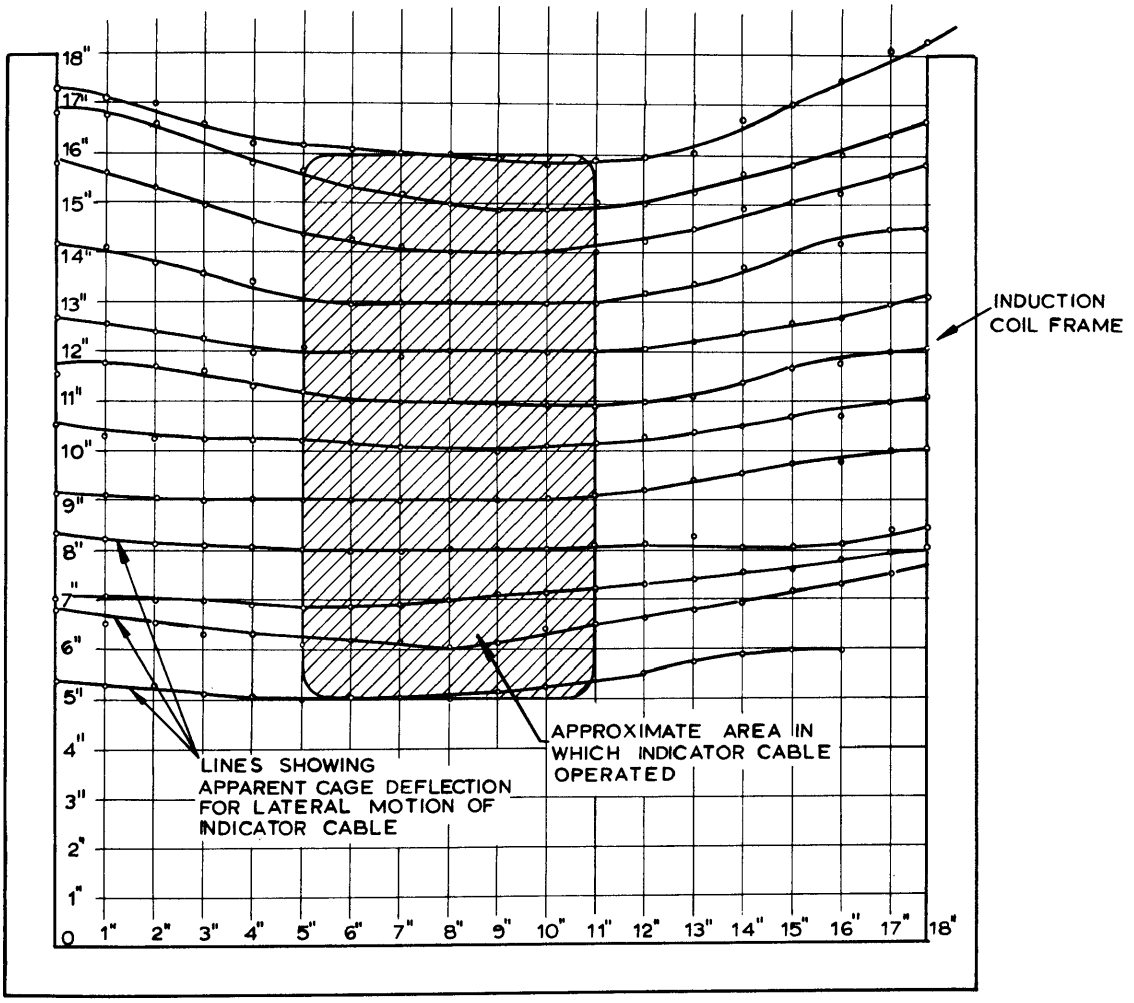

FIGURE 48

Calibration curves for full-scale induction coil

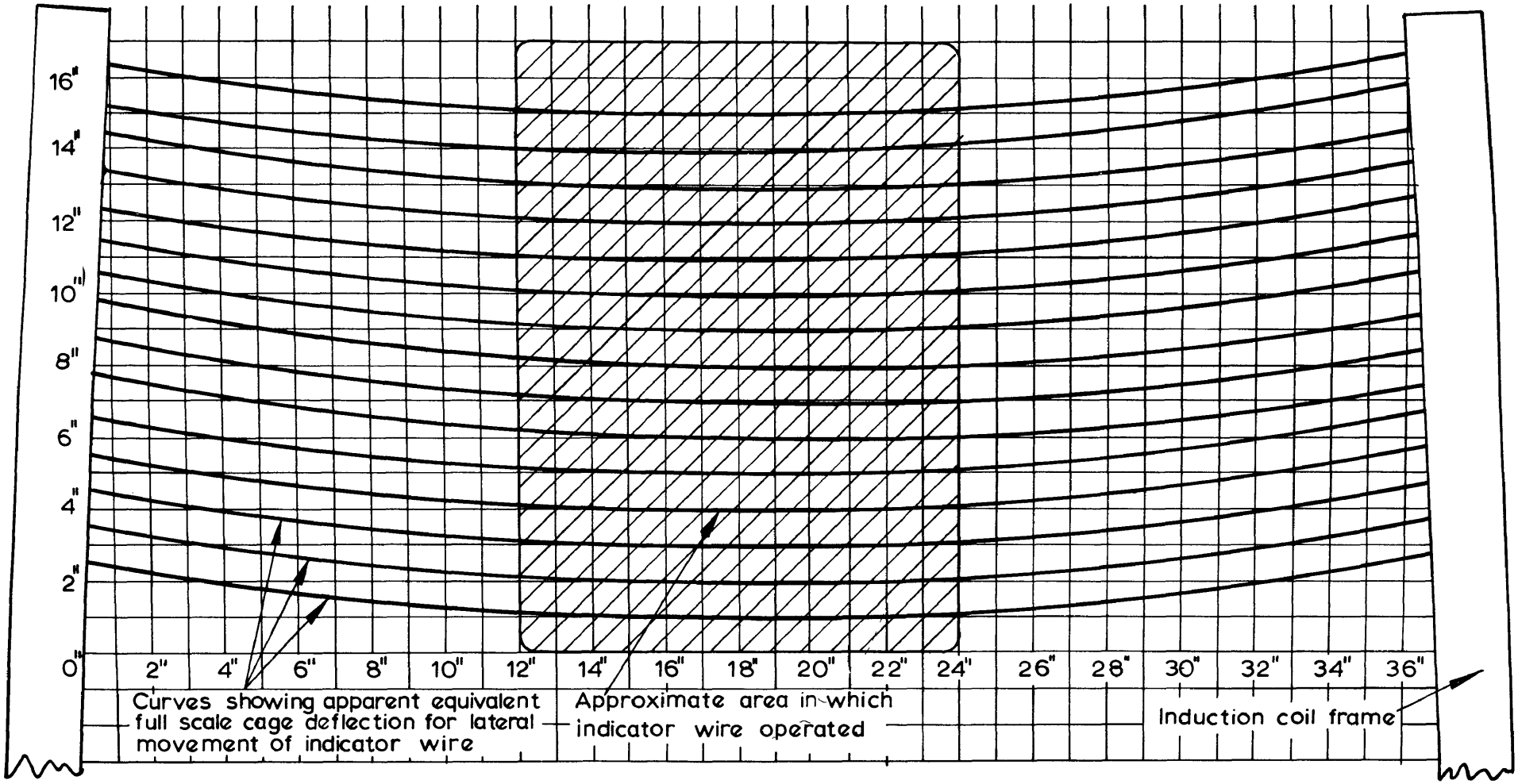

FIGURE 49

Calibration curves for model induction coil

always be strictly observed so that errors appeared in some recordings of the cage motion. Although normally small, these errors could, in some cases, have amounted to $\frac{1}{2}$ inch equivalent fullscale cage deflection.

During laboratory tests on the equipment for recording model cage movement, all indications were that the system operated perfectly and that, despite the small scale, greater accuracy would be achieved than in fullscale recordings. At that stage it was expected that the metal duct, representing the model mineshaft, would have some effect on the calibration of cage movement, but it was thought that such effects would be constant along the lengtn of the model shaft.

Only when commencing hoisting tests was it discovered that joints and irregularities in the metal duct had a marked effect on the recording system. This problem could have been solved very satisfactorily, by using some non-magnetic material for the model shaft ducting. Because of the urgency of the project, such a major change in the model installation was not justified. However, it was found that reasonably accurate recordings of the cage motion could be obtained by carefully calibrating the interference effects and then analysing the results so as to separate these effects from the normal traces of cage movement. This procedure complicated the analysis of experimental data considerably, and most probably some errors were introduced during this analysis.

It is felt that discrepancies in the model and fullscale results may be attributed chiefly to experimental errors due to the above-mentioned causes, and not so much to basic non-similarities between the model and its fullscale counterpart. It must be pointed out that none of the defects encountered were of an unsurmountable nature and it may be confidently assumed that with improved equipment all these problems will be satisfactorily solved. Such improved equipment which is regarded as suitable for dynamic scale model testing of rope-guide systems is discussed in Chapter 6.

4.5.3 Coriolis force, Barometric and Reynolds Number effects. While performing the Durban Roodepoort Deep correlation tests some basic causes for dissimilarity between model and fullscale rope-guide systems came to light.

The Coriolis force effect has already been discussed in section 4.3.2.3. The Coriolis force, caused by the rotation of the earth, acts in the east-west direction on a moving conveyance and it is not possible to simulate this force to scale in a model. At any particular hoisting speed it is possible to compensate for the Coriolis force in the model by means of an artibicially created aerodynamic side force. However, the accurate prediction of aerodynamic side forces is difficult (refer to Chapter 5) and this was not attempted in the Durban Roodepoort Deep model.

Another dissimilarity of a fundamental nature, encountered in models of rope-guide systems, is associated with the variation of air density in deep shafts. Owing to barometric compression the air density increases with the depth of a fullscale shaft, while in a scale model this effect is practically negligible. For model studies on very deep shafts this barometric effect will be quite noticeable but in the 3000 feet Durban Roodepoort Deep shaft this effect was not significant.

While considering theoretical aspects of dynamic scale model rope-guide testing, it was shown that similarity could only be attained when aerodynamic viscous forces were insignificant. Preliminary measurements of total aerodynamic force acting on a travelling conveyance indicated that viscous forces were negligible compared with the large drag forces, rope tension forces, etc. (refer to Chapter 5). Furthermore if aerodynamic viscous force effects (Reynolds number effects) were present in the Durban Roodepoort Deep model, all results would have been influenced consistantly by such a dissimilarity. The very good correlation obtained in some of the tests indicates that any significant Reynolds number effects were extremely unlikely. However, the rate of ventilation air flow in the Durban Roodepoort Deep Circular shaft was very

low and did therefore not in this respect represent a typical mineshaft installation. After completion of the correlation tests some uncertainty still prevailed about the significance of the Reynolds number effect associated with models of rope-guide installations. Chapter 5 is devoted to further studies in this field.

4.5.4 Confidence limits. Since for both the model and fullscale tests a number of runs were made from which an average was calculated, it is necessary to obtain some idea as to the degree of certainty that may be attached to the average results. This may be done by means of statistical analysis which defines a confidence limit on both sides of an average value, such that it is 95% certain that the true average value lies within these limits. The confidence limit of the arithmetic mean of a series of n measurements, t_1, t_2 ..... t_n, the arithmetic mean of which is

$$m = \sum_{i=1}^{n} \frac{t_i}{n}$$ is expressed by

$$\mu = \frac{1.96\,\sigma}{\sqrt{n}}$$

where σ is the standard deviation and is defined as

$$\sigma = \frac{\sqrt{\sum_{i=1}^{n} (m - t_i)^2}}{\sqrt{n - 1}}$$

Standard deviations and confidence limits were calculated for some of the tests, and Figures 50(a) and 50(b) show typical model and fullscale traces together with their confidence limits. In these graphs the arithmetical mean traces are shown, the model and fullscale results having been obtained respectively from 10 and 6 individual measurements.

The confidence belts indicate that there is a 95% certainty that the true arithmetic averages will lie somewhere in these areas. The maximum model and fullscale values for μ proved to be respectively 0.22 inches and 0.30 inches, which indicate that the confidence limits for the model and fullscale tests were very much the same.

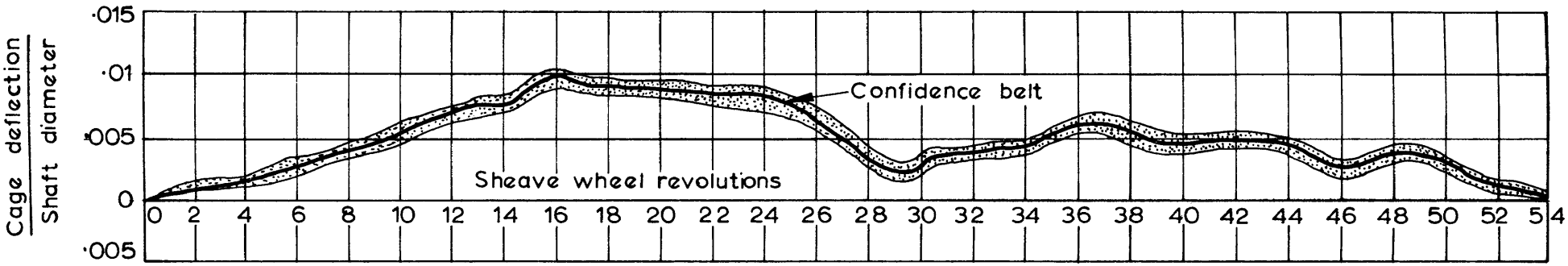

FIGURE 50(a)

Confidence limits for typical full-scale cage deflection trace

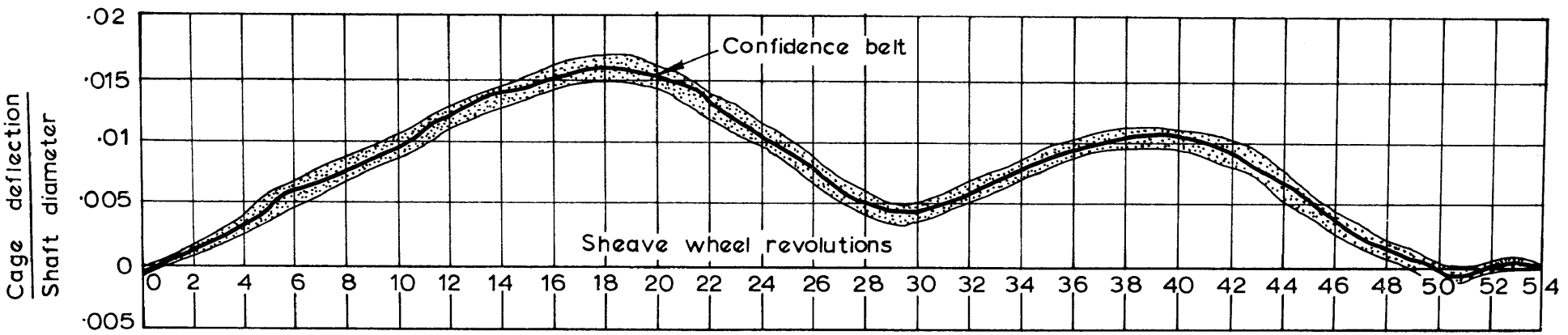

FIGURE 50(b)

Confidence limits for typical model cage deflection trace

This analysis further shows that by doing some ten repetitive tests on a model for a certain set of conditions, the average behaviour of the model can be determined within the close limits of approximately 0.2 inches fullscale.

It is of interest to deduce by statistical means what the probable absolute maximum deflection of the model and the fullscale conveyances would be, given their mean maximum deflections. If, for instance, a model is known to be truly similar to the fullscale installation it represents, the mean trace of any lateral movement of a model conveyance may be assumed to represent, within certain limits, the average movement of the equivalent fullscale conveyance. However, in the design of rope-guide mineshaft installations, it is necessary to obtain an estimate of the absolute maximum cage deflection which might occur, and not merely the mean maximum deflection obtained by doing a number of tests. Use may be made of the formula

$$\mu' = 1.96\sigma$$

where μ' now signifies the maximum probable deviation from the mean deflection value, with a certainty of 95% that this deviation will not be more than μ'.

The value of μ' for both model and fullscale tests proved to be 0.7 inches fullscale, so that this value should be added to the maximum mean cage deflection to obtain, with a certainty of 95%, the absolute maximum cage deflection which might occur in any individual hoisting run.

The above statistical analyses were based on 10 individual model measurements and 6 individual fullscale measurements. By increasing the number of measurements, confidence limits may of course be reduced. However, such statistical analyses only determine the degree of confidence that may be attached to test results from a given model installation. If such a model is not truly similar to its fullscale prototype owing to inaccurate manufacture or for some other reason model tests performed to very narrow confidence

limits is not of any particular value.

The degree of accuracy with which the behaviour of a fullscale rope-guide installation could be predicted, using a dynamic scale model, will depend on the various factors discussed in this section. The author feels confident that, by making due allowance for the fundamental dissimilarities peculiar to rope-guide models and by employing improved apparatus and techniques it will be possible to predict the behaviour of any rope-guide installation satisfactorily. It is thought that, for normal mineshaft installations, it will be possible to predict lateral deflections of conveyances accurately to within $\frac{1}{2}$ inch or even less. The improved apparatus and experimental techniques required for such future investigations is discussed in Chapter 6.

5. AERODYNAMIC SCALE EFFECTS IN MODEL MINESHAFT INSTALLATIONS.

5.1 General

In the theoretical treatment of dynamic similarity between model and fullscale mineshaft installations (refer to section 2) the Reynolds number effect (i.e. aerodynamic viscous force effects) was assumed to be negligible. Without this assumption it was found to be impossible to design a dynamic scale model of a mineshaft installation. It is well established that for turbulent flow past bluff bodies viscous forces are indeed negligibly small. (Reference 6). However, in all available literature on this subject only the aerodynamic drag forces (i.e. forces in the direction of fluid flow) are regarded as important. When studying aerodynamic effects on bluff bodies such as railway trains, road vehicles and rail-guided mineshaft conveyances, only the drag forces, (i.e. the forces in the direction of motion) are regarded to be of any significance. Aerodynamic forces on such bodies acting in a direction perpendicular to the direction of motion are usually very small compared with gravity forces and the high drag forces acting on them. To the best of the authors knowledge no experimental investigations have as yet been carried out on such lateral aerodynamic forces acting on bluff bodies in an air stream. In general such forces perpendicular to the direction

of motion are only considered to be significant for surfaces with streamline cross-sections such as aircraft wings and for flat or curved plates of thin section.

In the case of bluff mineshaft conveyance, guided by ropes, it is found that the lateral aerodynamic forces, although perhaps small compared with the weight of conveyances and the drag forces acting on them, are nevertheless of extreme importance. The experimental investigations indicated that a very small sustained side force on a travelling conveyance causes a considerable lateral deflection. Some doubt now arises as to whether viscous force effects (i.e. the Reynolds number effect) are still insignificant when considering this small lateral force only instead of the large total aerodynamic force acting on a bluff conveyance. The good correlation obtained in the previous investigations may not be regarded as sufficient proof that such a Reynolds number effect is not encountered for lateral forces under all rope-guide operating conditions. In all these investigations the flow-rate of ventilation air in the shaft was very low and the absence of any Reynolds number effects under these circumstances does not preclude possible scale effects in cases where higher flow rates are encountered.

A programme of static aerodynamic tests on a typical conveyance of the type used in the previous correlation tests was devised in order to investigate this Reynolds number problem thoroughly.

5.2 Reynolds number effects referred to total aerodynamic force.*

5.2.1. Object of test.

The object of this test was to establish whether the general rule, stating that viscous forces are insignificant compared with total aerodynamic forces acting on a bluff body, was also applicable to a typical mineshaft conveyance situated in a circular shaft. Following customary procedure[6] it was necessary to investigate total aerodynamic force coefficients over a large range of Reynolds numbers. Any variations in the magnitude of such force coefficients indicate the relative importance of viscous forces.

5.2.2 Experimental equipment and procedure.

A typical model conveyance, of light weight balsa wood construction, mounted on a drag balance sting inside a one foot diameter steel duct, was used for this investigation. The model conveyance, depicted in Figure 51 was of a box-type construction mounted in a bridle and measured 3 inches by 4 inches by 11 inches long. Air flow was obtained with a centrifugal blower connected to the downstream

..... 151

---

* Although included under the separate heading of Aerodynamic scale effects, these Reynolds number tests were completed before commencing experimental work on the model of the proposed shaft for the Buffelsfontein G.M. Co. At this early stage of the investigation it was not realised that only the lateral component of the total aerodynamic force was important and results from these tests were regarded as sufficient proof that viscous force effects were insignificant.

The investigator would have been seriously at fault if these Reynolds number tests had not been carried out at this early stage of the investigations. Although it is an established fact that viscous forces are insignificant for bluff bodies in a free air stream it was still necessary to investigate possible viscous effects due to air flow along the shaft wall.

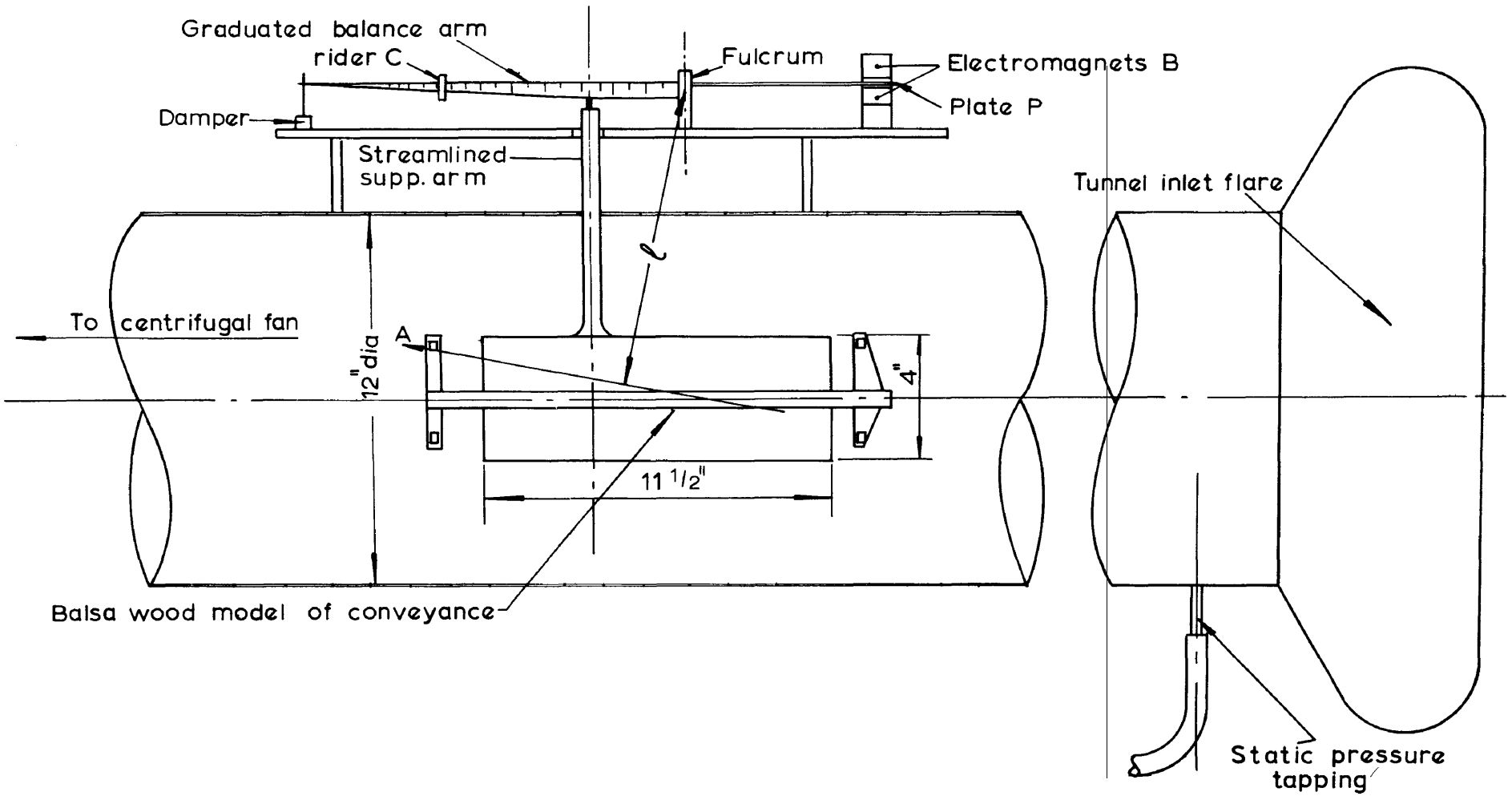

FIGURE 51

Layout of apparatus for Reynolds number tests

end of the 17 foot long duct and a flared inlet to the duct effected smooth air entry. In the case of a conveyance travelling in a mineshaft, the relative flow of air over the conveyance is due to both the velocity of the conveyance as well as to the speed of the air itself flowing in the shaft. In order to investigate aerodynamic force effects on the conveyance, it was thought sufficient to carry out measurements on a stationary model conveyance over which air flows. (Refer to section 5.4.4.). The drag balance, mounted on top of the steel duct as depicted in Figures 51 and 52 had a zero point indicating device in the form of a small plate P situated in the gap between two electromagnets B. The coils of the electromagnets were incorporated in opposite arms of a Wheatstone bridge. The bridge could be balanced for a given position of plate P and any movement of P away from this zero position was then indicated on a sensitive galvanometer. The moment due to the aerodynamic force acting on the cage was indicated accurately by the position of the rider C which could be adjusted on the graduated balance arm so as to obtain the zero position on the galvanometer.

The air flow in the duct was regulated by adjusting the blower speed while simultaneously manipulating a damper situated in the diffuser of the blower. The air velocity in the duct was determined from a calibration of true dynamic head against static head drop through the flared inlet of the duct.

These tests were conducted most conveniently by adjusting the rider C on the balance arm to some predetermined value and then regulating the air flow in the duct so as to balance the aerodynamic drag-moment against the moment of the rider weight.

The sensitivity of the manometer used to measure the static drop over the duct inlet did not allow the accurate measurement of air velocities less than approximately 3 feet per second while the maximum air speed attainable in the duct was 50 feet per second.

5.2.3 Results. For the purpose of these tests the Reynolds number N_R is defined as

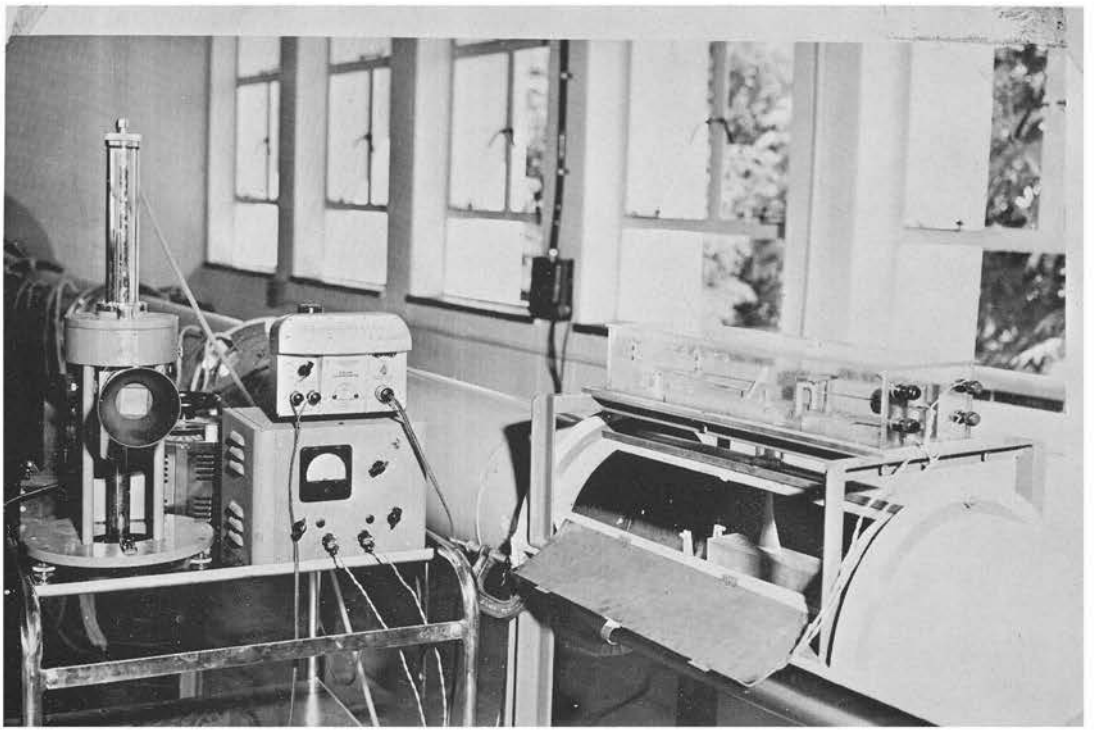

FIGURE 52

An aerodynamic scale model conveyance in a duct

$$N_R = \frac{v_{av} D \rho}{\mu} \text{ *}$$

where v_{av} = average air velocity in the unobstructed duct in feet seconds^{-1}.

D = 1 foot (diameter of shaft).

ρ = air density in slugs feet^{-3}.

μ = air viscosity in slugs feet^{-2} seconds^{-1}.

Since the ambient temperature and relative humidity of the atmosphere remained more or less constant while conducting these tests, it was assumed that

ρ = 0.002 slugs feet^{-3}

μ = 3.77 x 10^{-7} slugs feet^{-2} seconds^{-1}

Hence $N_R = \frac{v_{av}}{1.885} \times 10^4$

Since a single component drag balance was used it was not possible to measure the actual total aerodynamic force A acting on the model conveyance, but only the aerodynamic moment Al (refer to Figure 51). However, for the purpose of investigating the Reynolds number effect, it was thought sufficient to consider only the coefficient of aerodynamic moment defined as

..... 155

---

* In all subsequent work on Reynolds number effects use is made of the duct Reynolds number in which the typical linear dimension is represented by the duct diameter. In section 5.4.4 it is concluded that any possible Reynolds number effects on lateral forces acting on a bluff body in a duct are associated with air flow along the duct walls rather than viscous force effects over the body itself. It is therefore logical to define the Reynolds number in terms of the duct diameter rather than in terms of some linear dimension associated with the bluff body.

$$C_M = \frac{A\ l}{\frac{1}{2}\rho\ v_{av}^{\ 2}\ D^3}$$

where A = total aerodynamic force in pounds.

l = moment arm of the total aerodynamic force around the drag balance fulcrum in feet.

D = 1 foot (diameter of shaft).

Assuming again an air density of ρ = 0.002 slugs feet^{-3}

$$C_M = \frac{A\ l}{0.001\ v_{av}^{\ 2}}$$ where A l is the measured moment of the rider C around the drag balance fulcrum in pounds feet.

Results obtained from measurements are given in Table 4 and a graph showing the relationship between the Reynolds number N_R and the coefficient of aerodynamic drag moment C_M is given in Figure 53. This graph indicates that C_M remained constant for Reynolds numbers ranging from 1.5 x 10^4 to 2.7 x 10^5. Apart from experimental scatter, especially in the low Reynolds number region where the sensitivity of the manometer was insufficient, no marked change in C_M is apparent at low Reynolds numbers. With this apparatus it was of course impossible to attain the high Reynolds numbers normally occurring in fullscale shafts (values as high as 9 x 10^6 are often encountered). However, with bluff bodies it is well known that viscous force scale effects mostly become apparent in the lower Reynolds number range[6] and that aerodynamic force coefficients tend to constant values with increasing values of the Reynolds number. It is therefore reasonable to assume that with no viscous force scale effects exhibited in the Reynolds number region ranging from 1.5 x 10^4 to 2.7 x 10^5, such scale effects would also be absent at higher Reynolds numbers.

It may therefore be concluded that if the Reynolds number in a model shaft is reduced to values as low as 1.5 x 10^4 the coefficient of total aerodynamic force for the type of conveyance used in this investigation will remain unchanged. For such a body the Reynolds

TABLE 4

Measurements of aerodynamic drag force coefficients at various Reynolds numbers on a model conveyance of bluff shape in a circular duct.

Al = aerodynamic moment about balance fulcrum in pounds feet.

v_{av} = average air velocity in duct measured by means of a calibrated inlet flare.

$N_R = \frac{v_{av}}{1.885} \times 10^4$ (Duct Reynolds number)

$C_M = \frac{Al}{0.001\ v_{av}^2}$ (Aerodynamic moment coefficient)

v_{av}	Al	N_R	C_M
2.90	.00084	15,400	.1000
4.35	.00168	23,090	.0890
4.81	.00252	25,500	.0190
5.62	.00334	29,800	.1060
6.15	.00421	32,600	.1110
3.55	.00108	18,825	.0866
4.81	.00242	25,500	.1050
6.15	.00362	32,600	.0958
6.80	.00483	36,100	.1043
7.54	.00594	40,000	.1043
4.35	.00194	23,090	.1027
6.15	.00388	32,600	.1027
7.54	.00584	40,000	.1027
8.71	.00777	46,220	.1022
9.73	.00960	51,600	.1010
5.23	.00268	27,685	.0980
7.25	.00535	38,470	.1020
8.71	.00804	46,220	.1055
10.26	.01070	54,450	.1020
11.40	.01330	60,500	.1023

TABLE 4 (Continued)

v_{av}	Al	N_R	C_M
6.65	.00451	35,300	.1022
9.51	.00904	50,500	.1000
11.30	.01345	60,000	.1048
13.12	.01808	69,700	.1048
14.93	.02240	79,300	.1050
12.97	.01761	68,600	.1048
20.56	.04400	108,850	.1048
29.00	.08800	154,000	.1048
34.80	.13200	184,600	.1090
41.30	.17600	219,000	.1035
46.50	.22000	246,600	.1130
50.50	.36190	268,000	.1050
19.50	.03870	103,500	.1020
28.62	.08595	152,000	.1048
41.00	.17210	217,800	.1020
50.65	.25795	268,600	.1008
58.95	.34500	312,100	.0999
14.50	.02200	76,900	.1049
16.41	.02860	87,200	.1059
17.89	.03515	94,800	.1092
22.00	.05100	116,800	.1051
23.48	.05725	124,700	.1040
25.39	.06600	134,800	.1030
27.60	.07705	146,300	.1014
29.80	.09460	158,000	.1062
31.10	.1010	165,000	.1042
32.43	.1100	172,300	.1048
32.95	.1152	174,800	.1067
34.00	.1189	180,400	.1030
34.50	.1233	183,000	.1038
34.93	.1277	185,500	.1045
36.14	.1365	191,400	.1050

TABLE 4 (Continued)

v_{av}	Al	N_R	C_M
37.25	.1410	197,700	.1022
37.85	.1451	201,000	.1016
38.05	.1497	205,000	.1002
39.20	.1541	208,000	.1005
39.72	.1585	210,800	.1007
40.30	.1630	214,000	.1007
40.90	.1672	217,000	.1000
41.50	.1775	220,000	.1000
42.20	.1805	224,000	.1015
42.78	.1848	227,000	.1018
43.10	.1895	229,000	.1020
44.10	.1939	234,000	.1000
44.70	.1982	237,000	.0995
44.95	.2020	238,700	.1000
45.50	.2070	241,600	.1000
45.80	.2117	243,000	.1008
46.30	.2160	245,800	.1008
47.25	.2246	250,600	.1007
47.65	.2291	252,500	.1016
48.10	.2336	255,300	.1005
48.75	.2378	258,500	.1001
49.05	.2422	260,000	.1003
49.40	.2465	262,000	.1006

..... 159

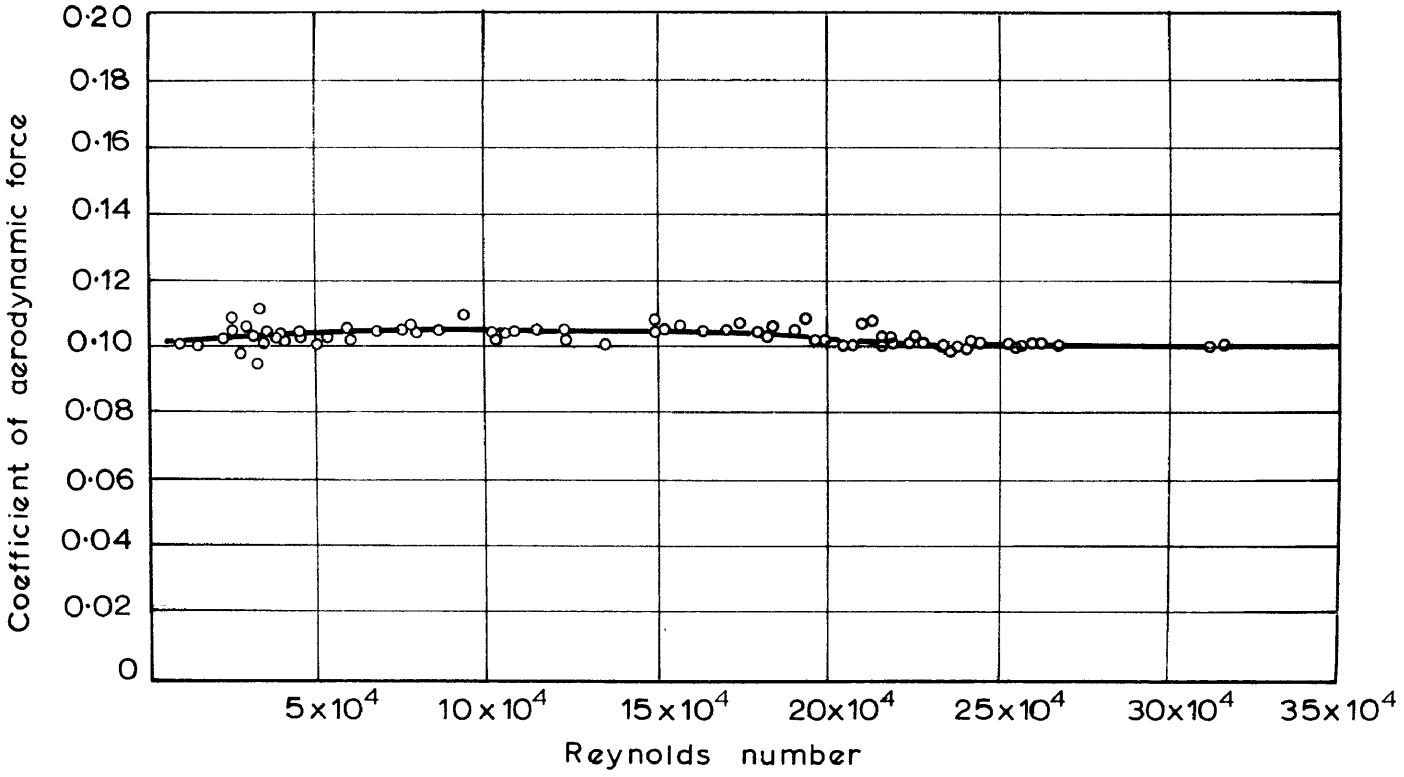

FIGURE 53

Relationship between co-efficient of aerodynamic force and the shaft Reynolds number

number effect may be safely neglected as far as the total aerodynamic force, acting on this body, is concerned.

5.3 Reynolds number effects referred to lateral aerodynamic force.

5.3.1 Object and scope of investigations. The object of this test was to investigate whether any aerodynamic scale effect would become apparent when considering only the relatively small aerodynamic side force acting on a typical bluff mineshaft conveyance situated in a circular shaft. Again it was necessary to investigate any possible variation in lateral aerodynamic force coefficients over a large range of Reynolds numbers.

5.3.2 Apparatus. Figures 54 and 55 depict the apparatus used for this test. Since it was considered desirable to conduct force measurements on a model conveyance situated in a duct with fully developed turbulent air flow, a 60 foot long portion of the original 10-inch diameter Durban Roodepoort Deep shaft model was mounted horizontally in the laboratory. The duct inlet was provided with a wooden inlet flare of a shape known to provide smooth air entry, as well as a honey comb grid and static holes connected to a piezometric ring. Figure 56 depicts this inlet arrangement and also gives the dimensions of the inlet flare profile. A wooden box measuring $7\frac{1}{2}$ inches long, $6\frac{1}{2}$ inches wide and $2\frac{1}{2}$ inches high represented the bluff mineshaft conveyance and was mounted in the lower half of the duct, 45 feet from the inlet, as indicated in Figure 54. A 10 H.P. centrifugal blower was used to draw air through the duct and the flow rate was regulated by means of a butterfly and bypass valve arrangement.

A removable 4 inch diameter standard orifice plate, situated 6 feet from the duct exit, was used to measure low flow rates. Most of the investigations were conducted at high flow rates and lateral force coefficients were referred to the dynamic pressure $\frac{1}{2}\rho v_{av}^2$ where v_{av} was the average air velocity in the duct. Since it was not possible to measure the small lateral aerodynamic forces acting on the model conveyance to a high degree of accuracy, it was considered sufficient to calibrate the duct dynamic head $\frac{1}{2}\rho v_{av}^2$

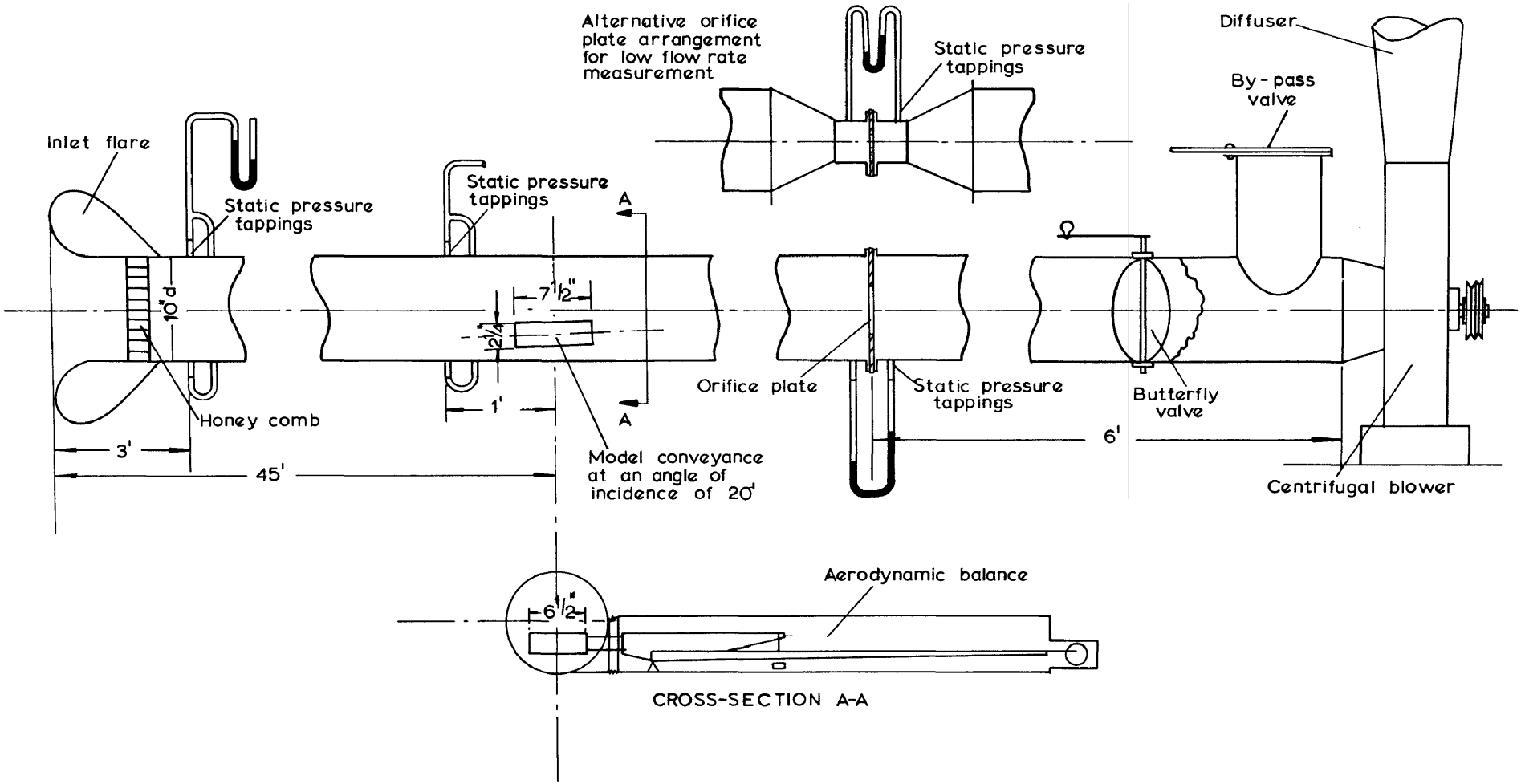

FIGURE 54

General layout of horizontal mineshaft model

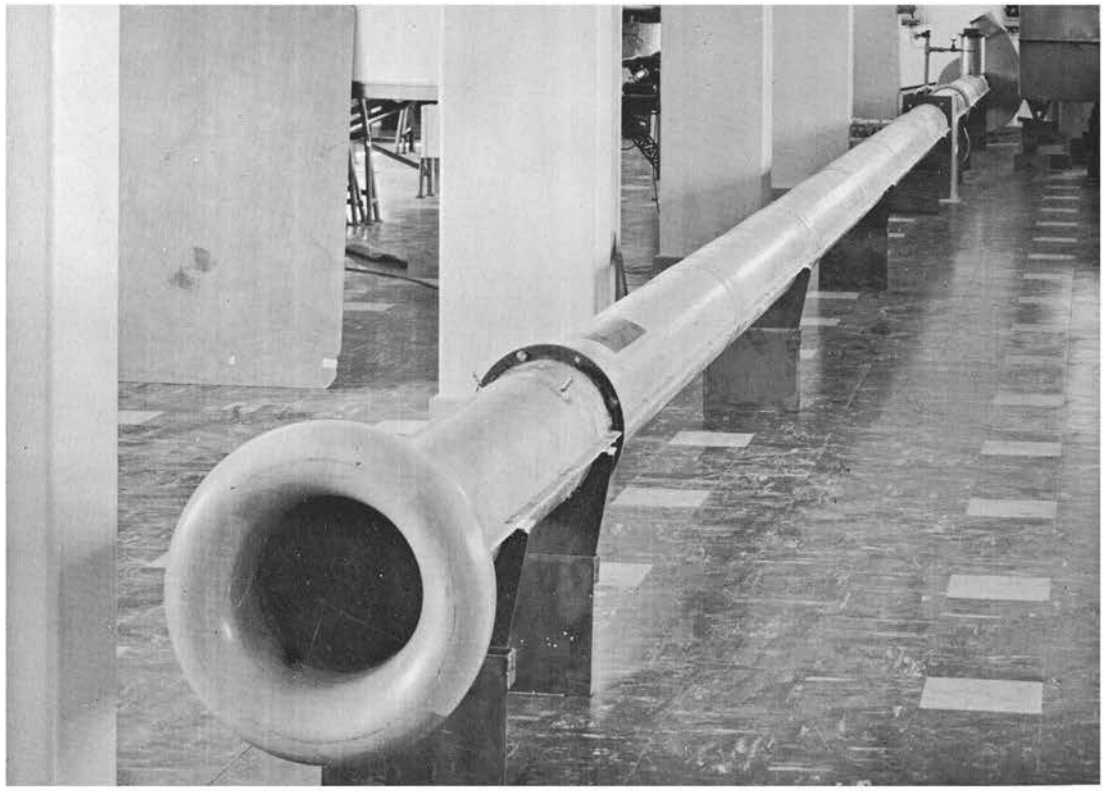

FIGURE 55

A horizontal mineshaft model

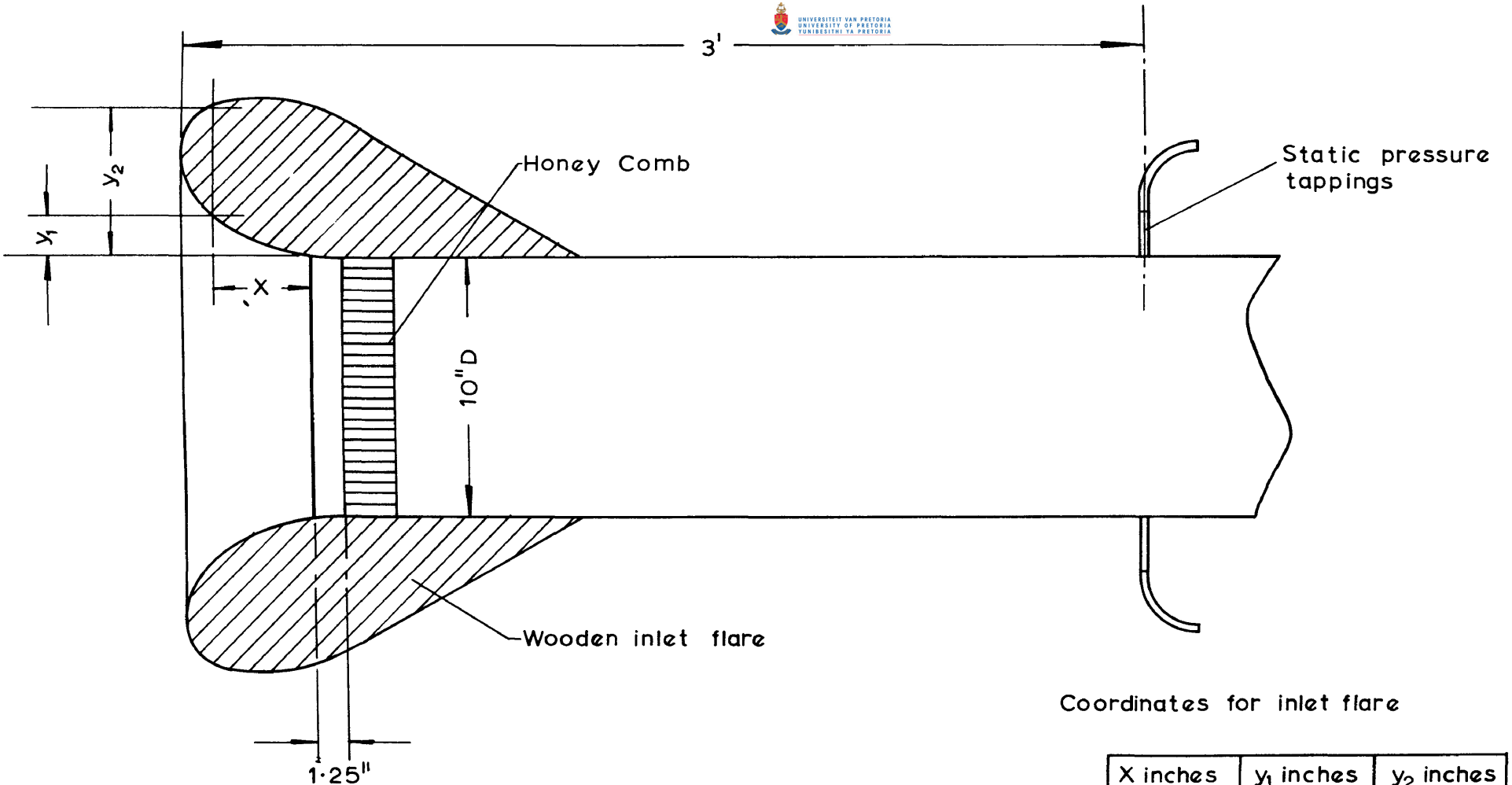

FIGURE 56

Duct inlet mouthpiece used for flow measurement

Coordinates for inlet flare

X inches	y_1 inches	y_2 inches
0·446	0·0141	4·13
0·892	0·028	4·22
1·338	0·089	4·32
1·784	0·167	4·40
2·230	0·285	4·44
2·676	0·446	4·46
3·122	0·685	4·41
3·568	0·970	4·23
4·014	1·410	3·88
4·460	2·700	2·70

against the static pressure drop measured over the duct inlet. For the purpose of calibration three diametrical pitot traverses, spaced 120° apart in one plane through the duct, were made for a number of flow rates. Since the centrifugal blower did not maintain an absolutely constant flow rate during the calibration process, it was necessary to measure the static pressure drop over the inlet for every single pitot measurement and to convert the observed pitot readings to conform to some standard static head drop over the inlet. Average duct air velocities were obtained from graphic integration and Figure 57 shows a graph of duct dynamic head, based on the average duct airspeed, against the static head drop over the duct inlet.

In order to measure the very small lateral aerodynamic forces acting on the model conveyance, it was necessary to develop the sensitive aerodynamic balance detailed in Figure 58. The model conveyance was fixed to the main balance beam A by means of four metal rods; as shown in Figure 54 the model was adjusted at an angle of incidence of 20 foot in order to obtain a lateral aerodynamic force of a magnitude which may be conveniently determined. The balance beam A was pivoted on a crossed steel spring fulcrum and was provided with an oil damper as well as a scale pan for loading. Since it was regarded essential to maintain the model in a fixed position relative to the duct wall, it was necessary to have an accurate null-point indicator on the balance. This was achieved with the long lightwood arm B terminating in the pointer C which was situated in front of a strong light source. A magnified shadow image of pointer C projected on to a screen, facilitated the accurate zero adjustment of the balance. Since fluctuating loads on the model cage were anticipated, a further oil damper was coupled to the long pointer arm. In order to avoid the leakage of air into the duct, the whole balance was mounted inside an airtight perspex box connected to the duct by means of polythene bellows. The latter served to isolate the balance from vibrations occurring in the duct during operation of the blower.

5.3.3 Experimental procedure and results. In order to perform the Reynolds number tests it was only necessary to

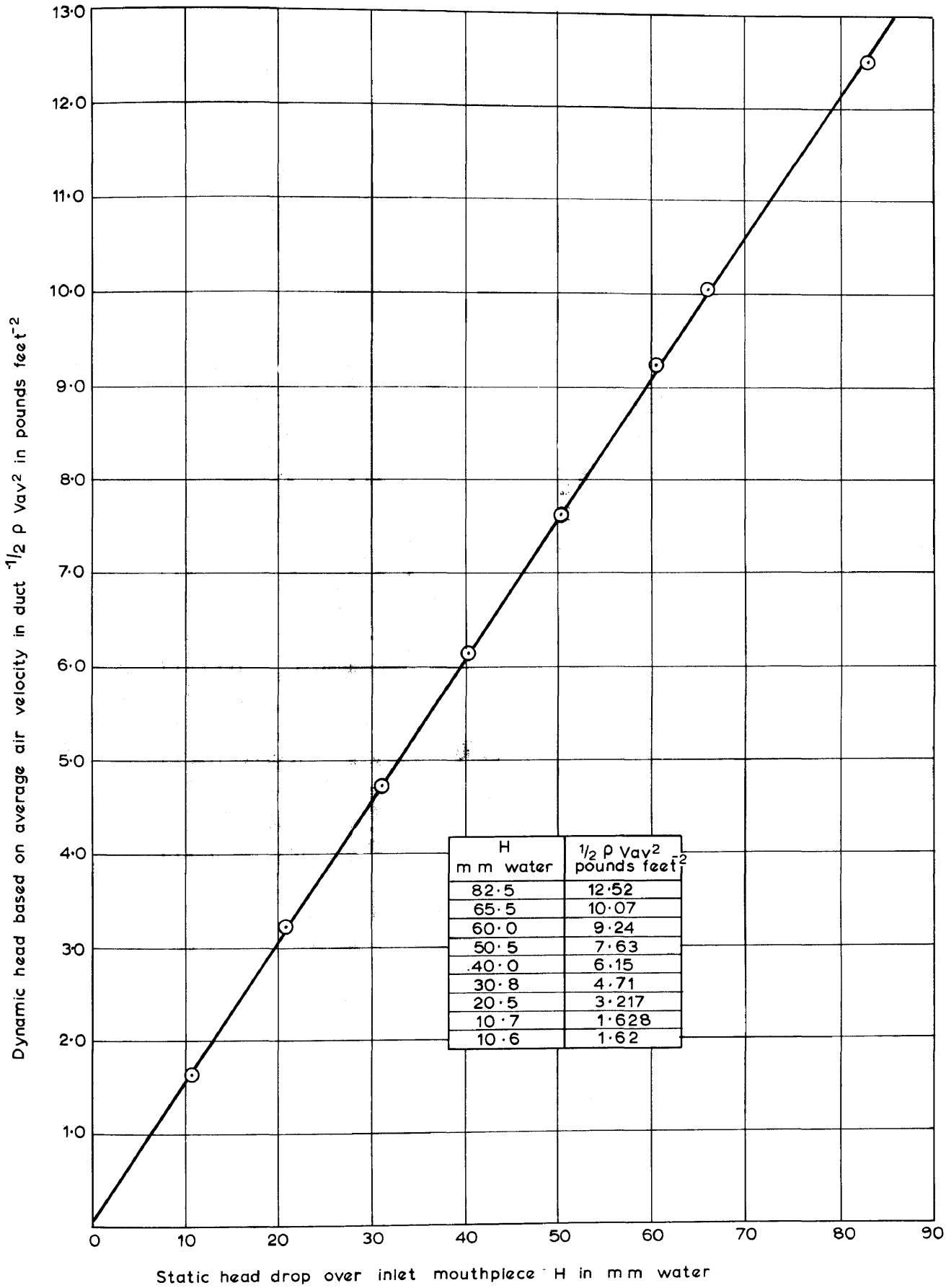

H m m water	½ ρ Vav² pounds feet⁻²
82·5	12·52
65·5	10·07
60·0	9·24
50·5	7·63
40·0	6·15
30·8	4·71
20·5	3·217
10·7	1·628
10·6	1·62

FIGURE 57

Flow calibration for duct inlet mouthpiece

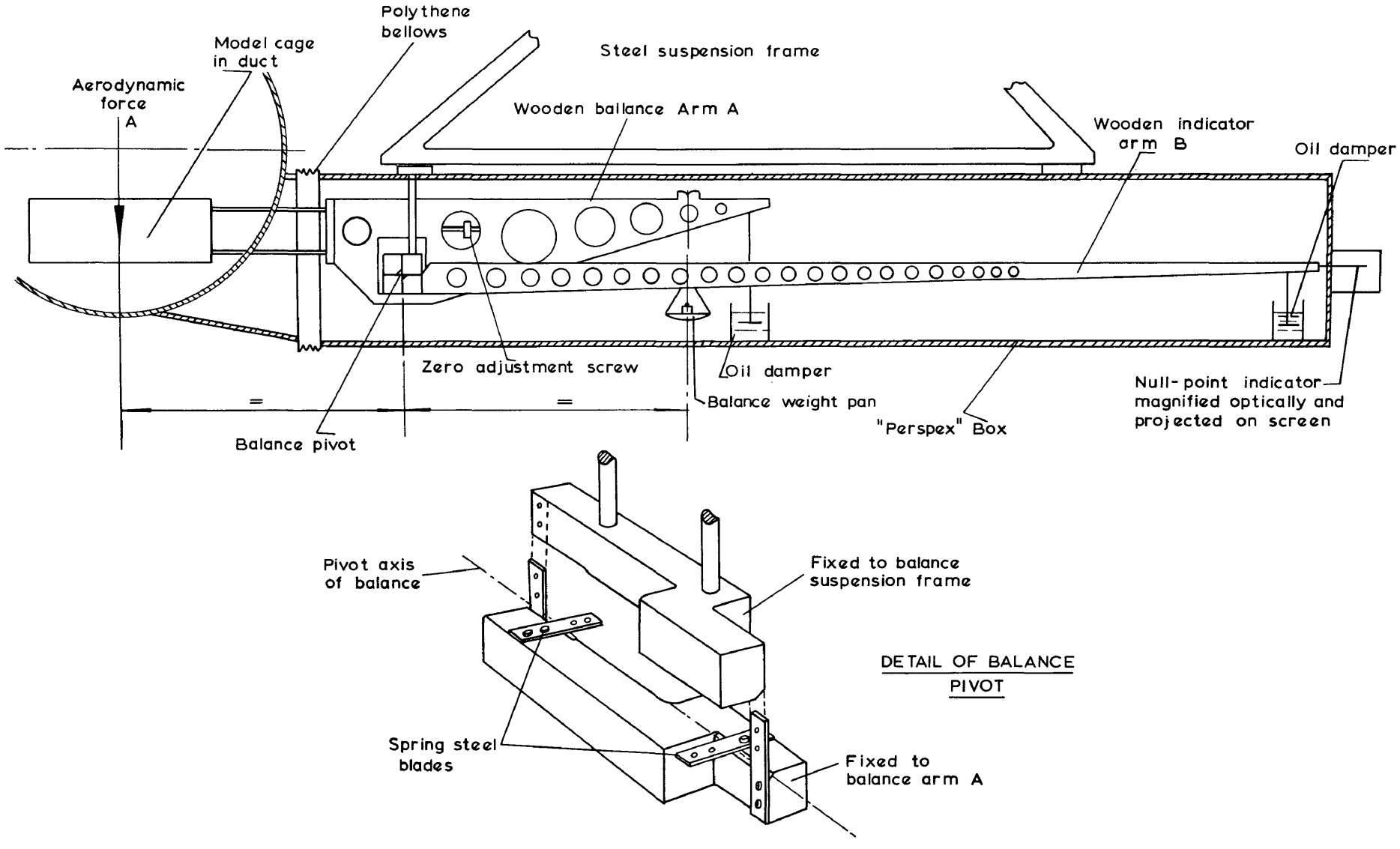

FIGURE 58

General layout of aerodynamic balance

measure the aerodynamic side forces acting on the model conveyance at various values of the duct dynamic head $\frac{1}{2}\rho v_{av}^2$. Before each force measurement the balance was brought to its null position by adjusting the zero-adjustment screw D (refer to Figure 58) with no air flowing in the duct. The balance scale pan was then loaded to balance some predetermined aerodynamic side force S. The blower was then brought into operation and the balance was brought into equilibrium by regulating the air flow in the duct with the butterfly and bypass valves. Coarse adjustments were made with the butterfly valve while accurate balancing was achieved by manipulating the bypass valve. Once equilibrium was attained, the inlet static pressure drop was read off from a Betz type manometer.

For these experiments it was assumed that the lateral aerodynamic force S acted in the centre of the conveyance which was mounted symmetrically about the vertical longitudinal plane through the centre of the duct.

If S = aerodynamic side force in pounds

v_{av} = average air velocity in duct feet second^{-1}

D = diameter of duct in feet

the aerodynamic side force coefficient is defined as

$$C_S = \frac{S}{\frac{1}{2}\rho v_{av}^2 D^2}$$

$$= \frac{S}{0.695\ \frac{1}{2}\rho v_{av}^2} \quad \text{for } D = \frac{10}{12} \text{ feet}$$

In this definition D^2 is used in preference to some typical area associated with the conveyance itself. Provided that the size and geometry of the conveyance relative to the duct is not changed during any particular test the choice of a typical area is immaterial.

The aerodynamic side force is given by

$$S = a \frac{W}{453.6}$$

where a is the balance factor and W is the weight in grams added to the balance pan.

$$\text{Hence } C_S = 0.003175\, a \frac{W}{\frac{1}{2}\rho v_{av}^2}$$

The constant correction factor for this balance was found to be a = 1.08.

$$\text{Hence } C_S = 0.003428 \frac{W}{\frac{1}{2}\rho v_{av}^2}$$

The Reynolds number was referred to the duct diameter D and the average air velocity in the unobstructed duct:

$$N_R = \frac{\rho D v_{av}}{\mu}$$

Any small variations in the air density ρ and the viscosity of the air μ were ignored and it was assumed that

$$\rho = 0.002 \text{ slugs feet}^{-3}$$

$$\mu = 3.8 \times 10^{-7} \text{ slugs feet}^{-1} \text{ seconds}^{-1}$$

For $D = \frac{10}{12}$ feet

$$N_R = 0.4385\, v_{av} \times 10^4$$

v_{av} was determined from knowledge of the dynamic head $\frac{1}{2}\rho v_{av}^2$.

As may be expected, flow conditions around the bluff conveyance were rather unstable and at high flow rates it was found necessary to take a number of readings of the static pressure drop over the duct inlet for a given balance Load. An average value for $\frac{1}{2}\rho v_{av}^2$ was then determined. The results of this test are

given in Table 5. The relationship between the duct Reynolds number N_R and the aerodynamic side force coefficient C_S is given in Figure 59. These results have been obtained with repeated tests and care was taken to obtain a sufficient number of readings to give an acceptable average in cases where instability was evident.

5.3.4 Discussion and conclusion. The graph in Figure 59 illustrates very clearly a sharp decrease in the coefficient of aerodynamic side force below a Reynolds number of $N_R = 12 \times 10^4$. It must therefore be concluded that an aerodynamic viscous force scale effect becomes apparent below this threshold Reynolds number of approximately 12×10^4. This rather unexpected result gave reason for concern since even the highest model Reynolds numbers normally attained in the Durban Roodepoort Deep correlation tests only amounted to approximately 1×10^4. According to the graph in Figure 59 the aerodynamic side force coefficient will be reduced by approximately one half when reducing the Reynolds number from a value encountered in a fullscale mineshaft to a value required for the model.

All possible sources of error were carefully checked. The balance was checked for any non-linearity by calibrating weights in the scale pan against weights placed on the centre line of the model conveyance. Possible aerodynamic effects due to the flow around the butterfly valve were investigated by making pitot traverses at the location of the model conveyance. The butterfly valve was removed and the flow rate was regulated using a valve on the outlet side of the centrifugal blower. However, the Reynolds number effect on the aerodynamic force coefficient was still evident. No errors could be detected in the apparatus and evidence of a threshold Reynolds number value below which viscous aerodynamic forces become important, was regarded as conclusive.

Results obtained during the extensive correlation tests carried out on a similar conveyance configuration did not indicate a marked reduction in lateral aerodynamic force coefficients (refer to Chapter 4). It therefore became apparent that some

TABLE 5

Measurement of aerodynamic side force coefficients at various Reynolds numbers on a model conveyance of bluff shape in a circular duct.

W = balance scale pan weight in grams

H = static pressure drop over duct inlet in mm water

$\frac{1}{2}\rho v_{av}^2$ = duct dynamic pressure based on average duct air speed v_{av} in pounds feet^{-2}, obtained from calibration curve in Figure 57

$C_S = 0.003428 \frac{W}{\frac{1}{2}\rho v_{av}^2}$ (Coefficient of aerodynamic side force)

$N_R = \frac{\rho D v_{av}}{\mu}$ (Duct Reynolds number)

$D = \frac{10}{12}$ feet (Diameter of duct)

$\rho = 0.002$ slugs feet^{-3} (Air density assumed constant)

$\mu = 3.8 \times 10^{-7}$ slugs feet^{-1} seconds^{-1} (Air viscosity assumed constant)

v_{av} = average air velocity in duct

hence $N_R = 0.439\ v_{av} \times 10^4$

W	H	$\frac{1}{2}\rho v_{av}^2$	v_{av}	C_S	$N_R \times 10^{-4}$
0.3	0.63	0.09	9.53	0.0114	4.18
0.5	0.1	0.15	12.31	0.0114	5.40
1.0	1.64	0.24	15.57	0.0142	6.83
2.0	2.77	0.41	20.35	0.0166	8.92
3.0	3.93	0.58	24.21	0.0176	10.62
4.0	4.93	0.73	27.16	0.0187	11.91
5.0	6.13	0.918	30.45	0.0186	13.35
7.0	8.45	1.275	35.89	0.0187	15.74

TABLE 5 (Continued)

W	H	$\frac{1}{2}\rho v_{av}^2$	v_{av}	C_S	$N_R \times 10^{-4}$
8.0	9.51	1.44	38.15	0.0189	16.73
10.0	11.45	1.74	41.93	0.0196	18.39
15.0	17.07	2.65	51.74	0.0193	22.69
20.0	22.65	3.51	59.55	0.0194	26.11
25.083	28.05	4.3	65.90	0.0199	28.90
30.083	33.41	5.125	71.95	0.0200	31.55
35.083	38.75	5.97	77.65	0.0200	34.05
40.083	45.0	6.9	83.49	0.0198	36.61
45.083	51.2	7.65	87.90	0.0201	38.54
50.083	56.2	8.62	93.31	0.0198	40.92
50.083	59.0	9.07	95.72	0.0188	41.97
45.083	53.3	8.16	90.78	0.0189	39.81
40.083	47.1	7.21	85.34	0.0193	37.42
35.166	41.0	6.31	79.84	0.0190	35.01
30.083	34.55	5.29	73.10	0.0194	32.05
25.166	29.1	4.46	67.12	0.0192	29.43
20.083	23.4	3.62	60.48	0.0189	26.52
0.3	0.7	0.1	10.05	0.0102	4.407
0.5	1.01	0.15	12.31	0.0114	5.398
1.0	1.72	0.26	16.21	0.0131	7.108
3.0	4.08	0.61	24.82	0.0168	10.884
5.0	6.38	0.955	31.06	0.0179	13.62
8.0	9.83	1.485	38.73	0.0184	16.98
10.0	11.8	1.80	42.63	0.0189	18.69
15.083	17.73	2.755	52.76	0.0187	23.14
20.083	23.45	3.63	60.56	0.0189	26.56
25.166	28.92	4.43	66.9	0.0194	29.34
30.083	34.3	5.26	72.89	0.0195	31.96
35.166	39.32	6.05	78.18	0.0198	34.28
40.083	45.4	6.96	83.82	0.0197	36.76
45.166	50.85	7.77	88.58	0.0198	38.84
50.083	57.7	8.87	94.66	0.0193	41.51

TABLE 5 (Continued)

W	H	$\frac{1}{2}\rho V_{av}^2$	V_{av}	C_S	$N_R \times 10^{-4}$
5.083	6.3	0.95	30.98	0.0182	13.58
10.00	12.0	1.83	42.99	0.0186	18.85
20.083	23.0	3.57	60.65	0.0192	26.33
30.083	34.3	5.26	72.89	0.0195	31.96
40.083	45.4	6.96	83.82	0.0197	36.76
45.083	54.00	8.27	91.4	0.0186	40.08
40.083	48.5	7.41	86.52	0.0184	37.94
30.083	34.3	5.26	72.89	0.0195	31.96
20.083	23.0	3.57	60.05	0.0192	26.33
10.00	11.75	1.76	42.17	0.0194	18.49
5.083	6.4	0.96	31.14	0.0178	13.65

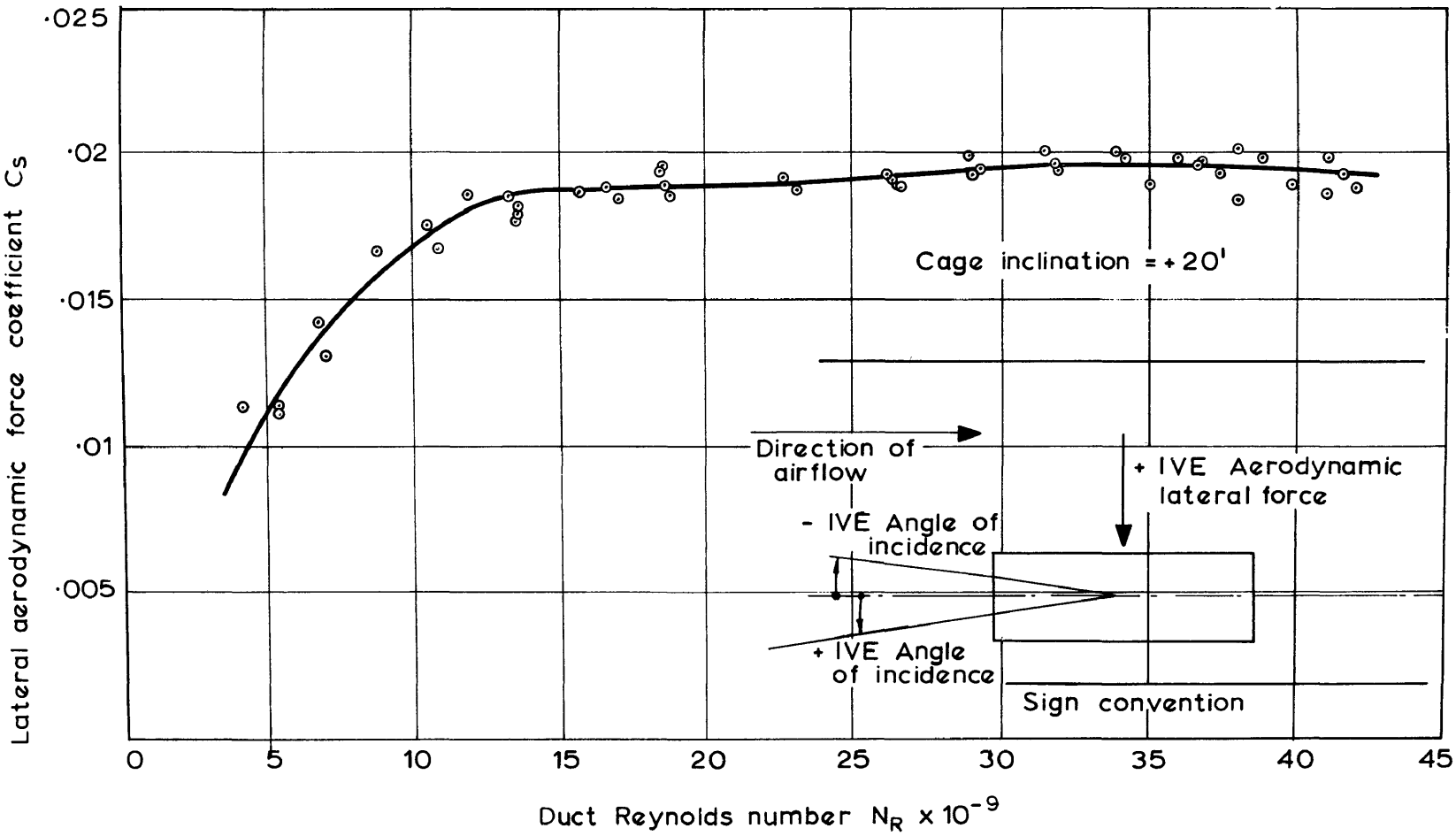

FIGURE 59

Variation of lateral aerodynamic force co-efficient with duct Reynolds number

dissimilarity existed between air flow conditions in the Reynolds number test installation and those in the Durban Roodepoort Deep correlation test installation. Further investigations into the general mechanics of air flow as applied to ducts and bluff bodies became necessary.

5.4 Investigations into the mechanics of air flow around a bluff body in a duct.

5.4.1 General considerations. In the correlation tests done on the vertical dynamic mineshaft model as well as in tests done on a stationary model conveyance in a horizontal duct it became apparent that slight changes in the angle of incidence of the conveyance had a marked effect on the magnitude of lateral aerodynamic forces. Even though great care was taken with the construction and installation of dynamic models, the possibility of some slight error in the suspension of the model conveyance could not be ruled out completely. It was feared that the Reynolds number scale effect described in section 5.3 might have been present in the vertical mineshaft model but that some geometrical error in the conveyance itself compensated for such aerodynamic scale effects. For example, it was thought possible that, by some coincidence, the conveyance was suspended out of plumb to such an extent that the aerodynamic side force was increased sufficiently to compensate exactly for the decrease in the lateral force coefficient due to the scale effect. However, the possibility that such a geometric error concealed the Reynolds number effect in the dynamic model mineshaft was completely disproved by the results obtained from the correlation tests on cages at various angles of incidences, as the following argument will show.

Figures 46(b), 46(c), 46(d), 46(e) and 46(f) show the results of these correlation tests described in section 4.4. It will be noticed that, allowing for reasonable experimental error, a very satisfactory degree of correlation was indicated between the full-scale installation and its model for various cage inclinations over a total range of 40 minutes.

Figure 60 show graphs of aerodynamic force coefficients against duct Reynolds numbers at various angles of incidence of the cage according to the experimental results from section 5.3. The curves for cage angles of incidences of 50, 40, 30 and 20 minutes were determined experimentally. Curves for zero and very small angles of incidence could not be determined satisfactorily but were interpolated.

If such Reynolds number force coefficient curves which exhibit a decreasing force coefficient below a threshold Reynolds number of 12 x 10^4, did in fact apply to the correlation tests described in section 4.4, it means that the dynamic scale model would have operated at a Reynolds number of approximately 3 x 10^4, where a range of C_S values of a much reduced magnitude would have applied. (Indicated by the dotted line AA in Figure 60). The fullscale prototype, on the other hand, would have operated in a high Reynolds number range where constant aerodynamic force coefficients of a much higher magnitude were applicable. The good correlation between the behaviour of the model and fullscale conveyances, indicated in Figures 46(b), 46(c), 46(d), 46(e) and 46(f), could not possibly have been attained if such aerodynamic force coefficients of reduced magnitude were applicable to the model. The reduced C_S values would have resulted in a reduced range of lateral deflections in the case of the model tests. It would still have been possible to attain correlation, due to the maladjustment of one particular cage inclination but certainly not for inclinations ranging from -20 to + 20 minutes. must therefore be concluded that aerodynamic force coefficients were the same for both the model and the fullscale prototype and that for the particular correlation tests on the Durban Roodepoort Deep Installation no scale effect was present.

Since a scale effect did occur in the tests on a stationary conveyance but not in the dynamic scale model it is clear that the explanation for this apparent paradox must lie in the fact that experimental conditions were different for the two cases. The only difference between the two cases was that in the vertical dynamic scale model the conveyance travelled along the shaft through

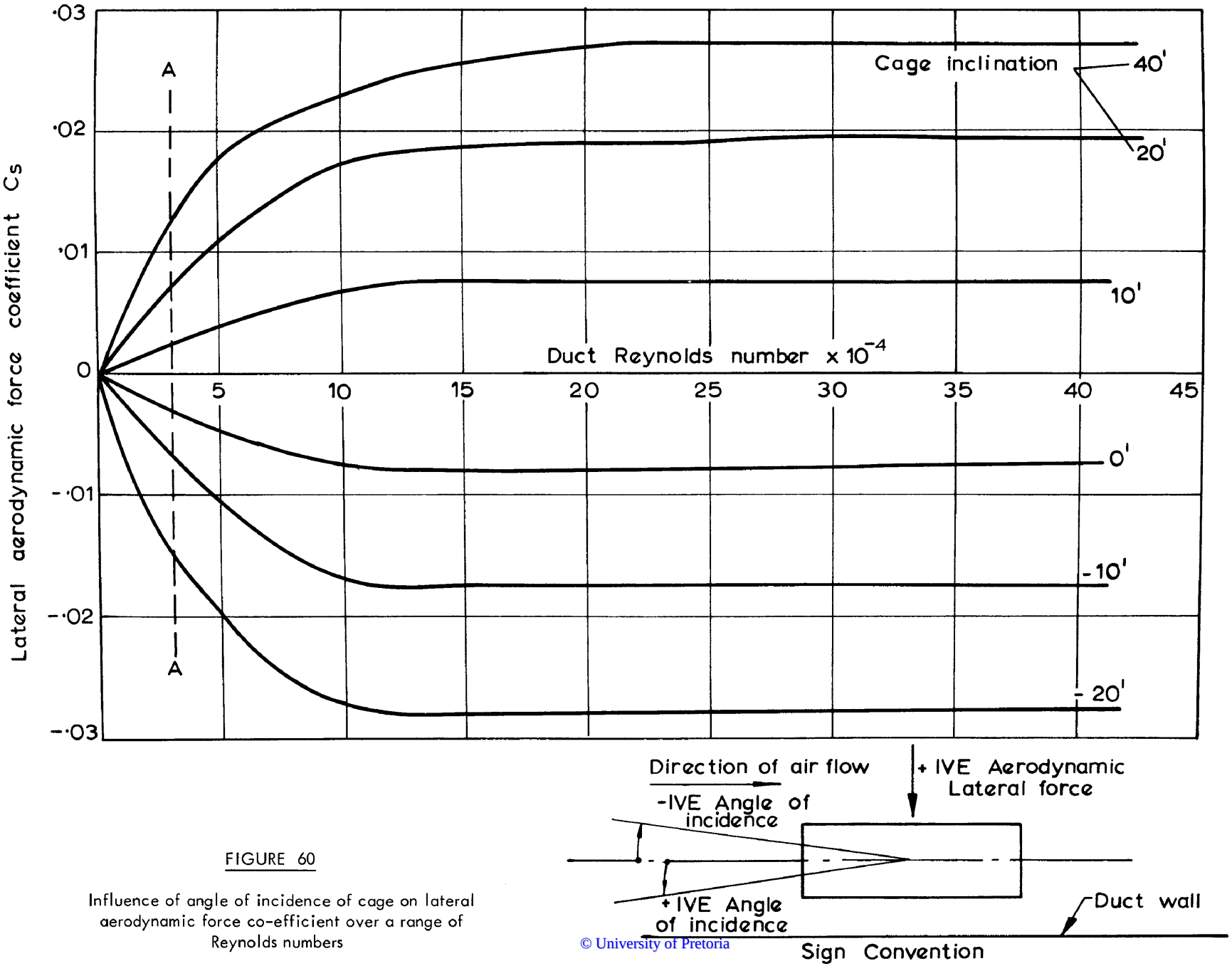

FIGURE 60

Influence of angle of incidence of cage on lateral aerodynamic force co-efficient over a range of Reynolds numbers

relatively stationary air, while in the Reynolds number test rig the conveyance remained stationary in the duct through which air flowed at a relatively high speed.

It now becomes clear that the nature of the air flow over the cage is vastly different in these two experimental cases, as illustrated diagrammatically in Figures 61(a) and 61(b). In the case of a stationary conveyance in a duct in which air flows the air velocity profile upstream of the conveyance assumes a typical parabolic shape exhibited when fully developed turbulent flow occurs in a long duct[7]. When the conveyance is travelling through the duct in which the air is more or less stationary, the air velocity distribution relative to the conveyance is perfectly flat. What is even more important is the fact that in the case of a stationary cage there is a high relative speed between the air and the duct wall, while in the case of a moving conveyance the air remains more or less stationary, relative to the duct wall (assuming that a negligibly small rate of ventilation air flow occurs in the duct).

It is true that during its passage through the duct the conveyance displaces the stationary air and a small flow of air is caused, relative to the duct wall in the immediate vicinity of the conveyance. It is clear, however, that this velocity will be small, relative to the velocity of the conveyance.

It is well established that for air flow through ducts, velocity profile shapes as well as coefficients of resistence to flow are markedly influenced by the magnitude of the Reynolds number[7]. Such Reynolds number effects arise from the fact that viscous forces influence the mechanics of air flow over the duct wall. It is now reasonable to expect that the coefficients of aerodynamic forces acting on a body situated in an air stream flowing in a duct, will also be affected by the Reynolds number, since viscous force effects prevalent at the duct wall, will also influence the flow pattern around the body. On the other hand, when a body moves through a duct with relatively stationary air, very

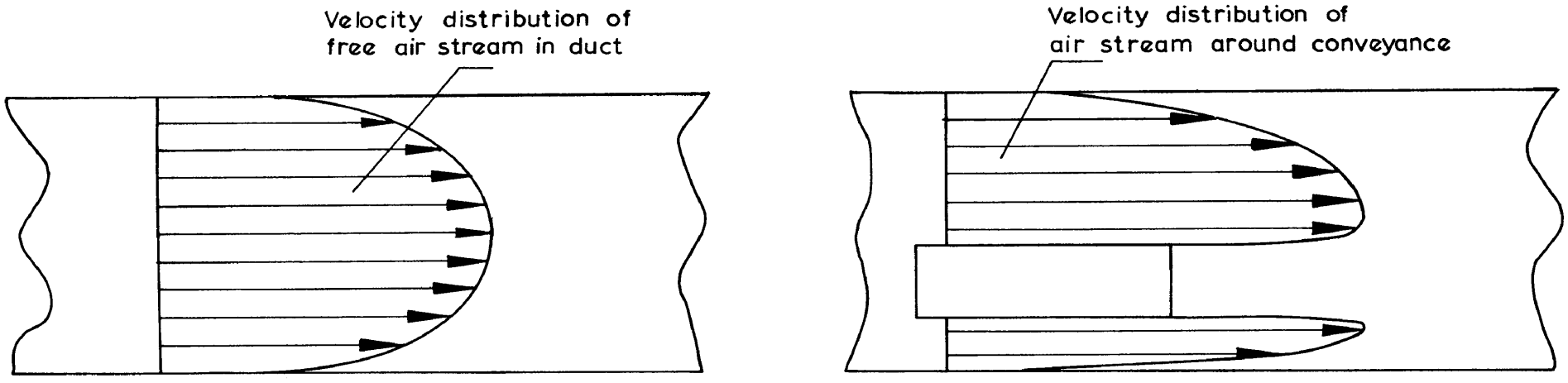

FIGURE 61(a)

Velocity distribution of air flow in a duct containing a stationary conveyance

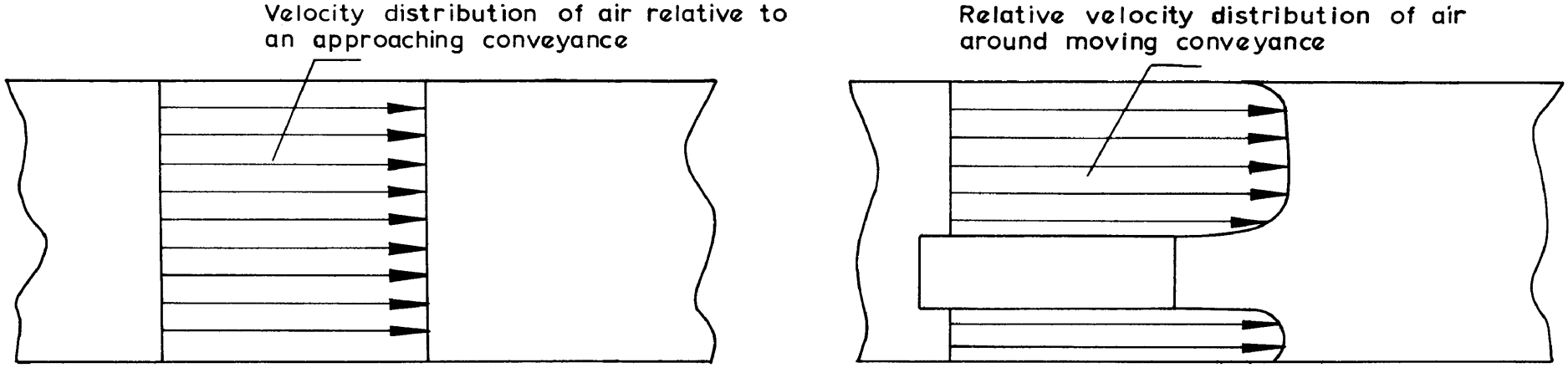

FIGURE 61(b)

Distribution of air velocity relative to a conveyance travelling in a duct in which the air is stationary

little air flow occurs relative to the duct wall and it is therefore reasonable to expect no noticeable Reynolds number effects caused by the wall. It is true that, in the case of a streamlined body moving through a duct, Reynolds number effects may still be exhibited by the relative flow of air over the body itself. However, if this body has a bluff shape, it is clear that no Reynolds number effects may be expected from this quarter. It is felt that these scale effects on the lateral force coefficient of the model conveyance should be attributed solely to a duct wall Reynolds number effect and not to Reynolds number effects associated with the bluff conveyance itself.

In order to obtain a clear picture of the mechanism of flow in a duct containing a bluff body, a series of experimental studies were made, as described in the subsequent sections. These experimental studies also served to substantiate the above theory regarding the true nature of the Reynolds number effect.

The horizontal mineshaft model described in section 5.3 and depicted in Figure 54 was used for all these investigations.

5.4.2 Static pressure distribution measurements on a model conveyance. Since the resultant aerodynamic force acting on a body is caused by a certain distribution of static pressure over the body, it was of interest to determine this static pressure distribution over a typical conveyance situated in a shaft through which air flowed. Such a model conveyance was mounted rigidly in the horizontal mineshaft model, described in section 5.3. This model was constructed from wood with brass strips, containing nine 1 mm diameter static pressure holes, glued centrally to both upper and lower faces, as depicted in Figure 62. The model conveyance was adjusted at an angle of incidence of 50 minutes in order to obtain relatively large static pressure readings. Four static pressure tappings, forming a piezometric ring, were installed about twelve inches upstream of the model conveyance and allowed the measurement of the static pressure in the unobstructed duct.

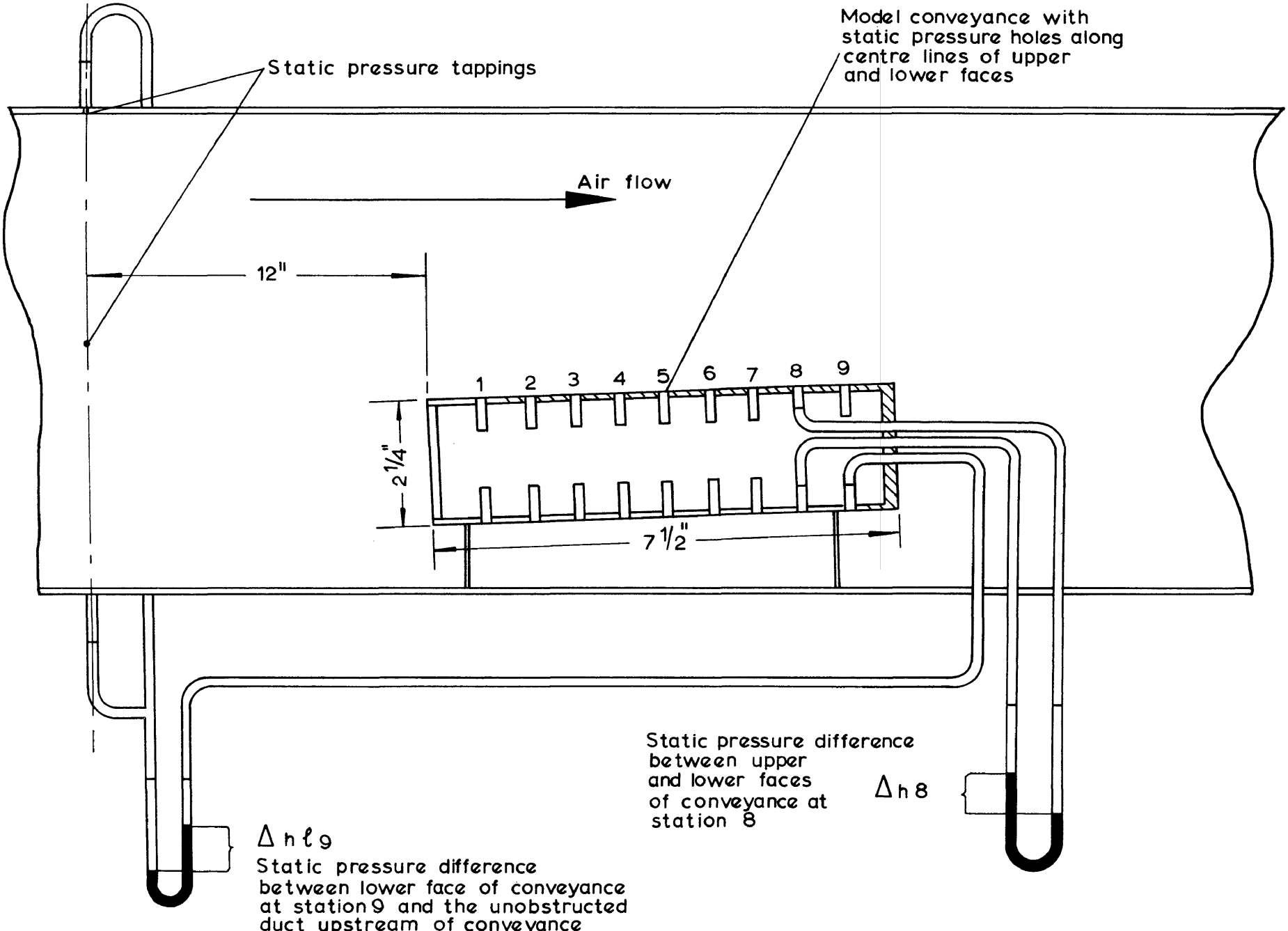

FIGURE 62

Installation of model conveyance for measurement of static pressure distributions

On passing the conveyance the air was accelerated, thus causing a drop in static pressure. This drop in static pressure below that existing in the unobstructed duct was measured for each of the eighteen static pressure holes on the model conveyance, as indicated in Figure 62. The results of these measurements, carried out at two different flow rates, are given in Table 6. The flow rate was determined by measuring the static head drop H over the duct inlet and determining $\frac{1}{2}\rho v_{av}^2$ from the calibration curve given in Figure 57. For the upper face of the conveyance Δh_u represents the static pressure drop relative to the static pressure prevailing in the unobstructed duct. Similarly Δh_l represents the pressure drop observed for the lower face of the model conveyance. All pressure drops are given in pounds feet^{-2} and are represented non-dimensionally by $\frac{\Delta h}{\frac{1}{2}\rho v_{av}^2}$. The measurements made are given in Table 6 and the results are represented graphically in Figure 63. At the static hole station 4 static pressure measurements were unsteady, indicating vortex formation and measurements at this station was therefore ignored.

Comparing the suction pressure distribution on the upper face and on the lower face at any particular Reynolds number, it will be noticed that the distributions are slightly unsymmetrical and that the greater suction pressure prevailing over the lower face of the conveyance will cause a resultant aerodynamic force towards the duct wall in a downwards direction. It is clear that at angles of incidence smaller than 50 minutes the pressure distributions over the two faces of the conveyance will be even more symmetrical and aerodynamic side forces will be caused by relatively small static pressure differences between the two walls of the conveyance. It therefore becomes clear that only a slight change in the geometry of the flow pattern around the bluff conveyance may have a marked influence on the magnitude of the aerodynamic side force. It is a well known occurrence in the mechanics of fluid flow that flow patterns change when the magnitude of the Reynolds number changes. Especially where flow occurs along a duct wall the Reynolds number may be expected to have a marked effect on the flow pattern around

TABLE 6

Measurement of static pressure distribution over model conveyance

Static pressure drop over duct inlet H = 68 mm water.

Dynamic head of airstream in unobstructed duct based on average air speed $\frac{1}{2}\rho v_{av}^2$ = 10.42 pounds feet^{-2}.

Duct Reynolds number N_R = 45 x 10^4.

Δh_u and Δh_l are static pressure drops relative to static pressure in unobstructed duct respectively for the upper and lower faces of the conveyance in pounds feet^{-2}.

Air density ρ = 0.002 slugs feet^{-3} (assumed constant).

Static hole Station	Δh_u	$\frac{\Delta h_u}{\frac{1}{2}\rho v_{av}^2}$	Δh_l	$\frac{\Delta h_l}{\frac{1}{2}\rho v_{av}^2}$
1	4.955	0.475	28.525	2.736
2	5.270	0.505	29.371	2.819
3	4.955	2.250	23.243	2.229
4	-	-	-	-
5	12.25	1.175	12.889	1.236
6	9.3	0.892	11.833	1.135
7	8.46	0.811	10.987	1.054
8	8.46	0.811	10.776	1.033
9	10.14	0.974	10.776	1.033

Static pressure drop over duct inlet H = 31 mm water.

Dynamic head of airstream in unobstructed duct based on average air speed $\frac{1}{2} \rho v_{av}^2 = 4.74$ pounds feet^{-2}.

Duct Reynolds number $N_R = 30 \times 10^4$.

$\rho = 0.002$ slugs feet^{-3} (air density assumed constant)

TABLE 6 (Continued)

Static hole Station	Δh_u	$\frac{\Delta h_u}{\frac{1}{2}\rho v_{av}^2}$	h_l	$\frac{\Delta h_l}{\frac{1}{2}\rho v_{av}^2}$
1	10.353	2.183	12.687	2.675
2	11.199	2.362	13.101	2.764
3	10.565	2.229	10.565	2.229
4	-	-	-	-
5	5.493	1.157	5.705	1.204
6	4.226	0.892	5.283	1.116
7	4.226	0.892	5.283	1.116
8	4.226	0.892	5.071	1.069
9	4.226	0.892	5.071	1.069

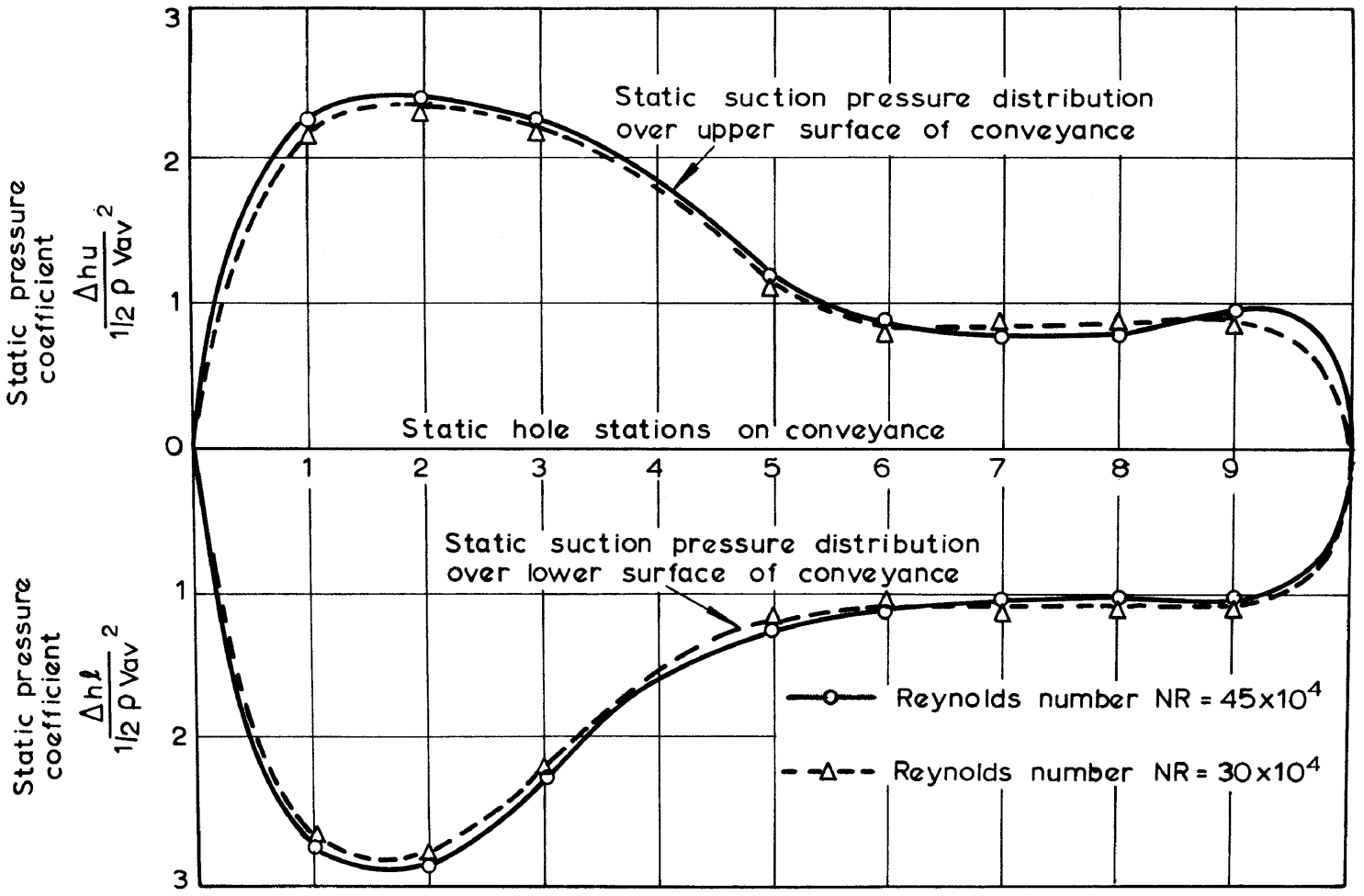

FIGURE 63

Distribution of static pressure over model conveyance

a body placed inside such a duct. It is therefore reasonable to attribute the decrease in the coefficient of lateral aerodynamic force, noticed at low Reynolds numbers, to such a change in the flow pattern around the model conveyance.

5.4.3 Reynolds number effects on coefficients of pressure differences acting on conveyance walls. In section 5.4.2 it was indicated that the lateral aerodynamic force acting on a conveyance is due to the fact that static pressure differences occur between two lateral walls of the conveyance. It was decided that it would be of interest to investigate the effect which the magnitude of the Reynolds number would have on this pressure difference. For such an investigation it was decided to measure the actual static pressure difference occurring between the two surfaces of the conveyance at each of the nine static hole stations depicted in Figure 62, and to repeat such measurements at various rates of flow in the duct.

Let Δh_1, Δh_2, Δh_3, etc., represent the static pressure difference between the upper and lower face of the model conveyance in mm water as indicated in Figure 62. These static pressure differences were again determined in the form $\frac{\Delta h}{\frac{1}{2}\rho v_{av}^2}$ where the dynamic head $\frac{1}{2}\rho v_{av}^2$ was determined from the calibration curve (Figure 57) from knowledge of the static head drop H over the duct inlet.

These static pressure measurements were repeated at various flow rates and the Reynolds numbers were determined as before from $N_R = \frac{\rho D v_{av}}{\mu}$. Constant values were assumed for the density ρ and viscosity μ since any slight variation in these quantities were not regarded as significant.

Table 7 gives the results of these measurements and the variation of the pressure coefficients $\frac{\Delta h_1}{\frac{1}{2}\rho v_{av}^2}$, $\frac{\Delta h_2}{\frac{1}{2}\rho v_{av}^2}$, etc., with the

..... 186

TABLE 7

Differential pressure distribution measurements

Δh_1, Δh_2, etc. are the static pressure differences measured in pounds feet^{-2} over two faces of the model conveyance at the nine static hole stations depicted in Figure 62.

H = static head drop over the inlet of the duct in mm water.
$\frac{1}{2}\rho v_{av}^2$ = duct dynamic head obtained from calibration curve in Figure 57.

$N_R = \frac{\rho D v_{av}}{\mu}$ (the duct Reynolds number)

ρ = 0.002 slugs feet^{-3} (the density of air assumed to remain constant).

μ = 3.8×10^{-7} slugs feet^{-1} seconds^{-1} (the viscosity of air assumed to remain constant).

D = $\frac{10}{12}$ feet (the duct diameter).

v_{av} = average air velocity in the duct.

Hence

$N_R = 0.439\ v_{av} \times 10^4$

H mm water	Δh_1	$\frac{1}{2}\rho v_{av}^2$ pounds feet^{-2}	$\frac{\Delta h_1}{\frac{1}{2} v_{av}^2}$	$N_R \times 10^{-4}$
68.1	4.966	10.45	0.475	45.0
61.8	4.501	9.5	0.474	43.0
53.3	3.824	8.17	0.468	40.0
41.9	3.022	6.45	0.468	35.0
36.5	2.611	5.62	0.464	33.0
28.85	2.039	4.425	0.461	29.5

TABLE 7 (Continued)

H mm water	Δh_1	$\frac{1}{2}\rho v_{av}^2$ pounds feet^{-2}	$\frac{\Delta h_1}{\frac{1}{2}\rho v_{av}^2}$	$N_R \times 10^{-4}$
19.5	1.395	3.025	0.461	24.0
10.1	0.676	1.525	0.443	17.0
4.6	0.275	0.7	0.392	11.5
2.05	0.116	0.32	0.363	7.5
0.09	- 0.002	0.13	-0.163	1.5

H mm water	Δh_2	$\frac{1}{2}\rho v_{av}^2$ pounds feet^{-2}	$\frac{\Delta h_2}{\frac{1}{2}\rho v_{av}^2}$	$N_R vx 10^{-4}$
66.2	3.528	10.17	0.347	44.5
57.7	3.127	8.87	0.353	41.5
49.3	2.662	7.525	0.354	38.5
34.4	1.859	5.275	0.352	32.0
22.3	1.162	3.46	0.336	26.0
15.4	0.824	2.7	0.331	21.5
8.3	0.423	1.25	0.338	15.5
3.35	0.148	0.51	0.290	9.5
1.25	0.048	0.175	0.272	6.0
0.5	0.021	0.075	0.282	4.0

H mm water	Δh_3	$\frac{1}{2}\rho v_{av}^2$ pounds feet^{-2}	$\frac{\Delta h_3}{\frac{1}{2}\rho v_{av}^2}$	$N_R \times 10^{-4}$
67.1	-1.183	10.3	-0.115	44.5
59.0	-0.951	9.075	-0.105	42.0
51.9	-0.866	7.925	-0.109	41.5
40.5	-0.655	6.23	-0.105	35.0
31.7	-0.507	4.85	-0.105	31.0
23.4	-0.338	3.625	-0.093	26.5

TABLE 7 (Continued)

H mm water	Δh_3	$\frac{1}{2}\rho v_{av}^2$ pounds feet^{-2}	$\frac{\Delta h_3}{\frac{1}{2}\rho v_{av}^2}$	$N_R \times 10^{-4}$
14.85	-0.190	2.3	-0.083	19.5
9.00	-0.095	1.36	-0.070	16.0
4.9	-0.063	0.73	-0.087	12.0
2.05	-0.032	0.32	-0.099	7.5

H mm water	Δh_5	$\frac{1}{2}\rho v_{av}^2$ pounds feet^{-2}	$\frac{\Delta h_5}{\frac{1}{2}\rho v_{av}^2}$	$N_R \times 10^{-4}$
68.4	-0.993	10.49	-0.095	45.0
60.5	-0.824	9.3	-0.089	42.5
51.8	-0.676	7.93	-0.085	39.5
40.9	-0.465	6.3	-0.084	35.0
34.8	-0.401	5.36	-0.075	32.0
19.15	-0.232	2.99	-0.078	24.0
9.9	-0.106	1.5	-0.070	17.0
4.5	-0.053	0.67	-0.079	11.5
2.0	0.036	0.3	-0.120	8.0

H mm water	Δh_6	$\frac{1}{2}\rho v_{av}^2$ pounds feet^{-2}	$\frac{\Delta h_6}{\frac{1}{2}\rho v_{av}^2}$	$N_R \times 10^{-4}$
69.5	1.120	10.65	0.105	45.5
62.0	1.067	9.54	0.112	43.0
53.4	0.951	8.175	0.116	40.0
42.5	0.760	6.53	0.116	36.0
36.0	0.655	5.525	0.119	33.5
19.3	0.328	3.0	0.109	24.0
10.15	0.169	1.55	0.109	17.0
4.75	0.074	0.72	0.103	11.5
2.2	0.037	0.325	0.114	8.0

TABLE 7 (Continued)

H mm water	Δh_7	$\frac{1}{2}\rho v_{av}^2$ pounds feet^{-2}	$\frac{\Delta h_7}{\frac{1}{2}\rho v_{av}^2}$	$N_R \times 10^{-4}$
66.4	1.986	10.2	0.195	44.5
58.6	1.754	9.375	0.187	42.0
49.7	1.500	7.58	0.198	38.5
40.3	1.226	6.2	0.198	35.0
34.3	1.046	5.26	0.199	31.0
19.2	0.613	3.0	0.204	24.0
9.9	0.296	1.5	0.197	17.5
4.3	0.127	0.65	0.195	11.5
2.15	0.085	0.32	0.264	8.0
1.93	0.063	0.28	0.226	7.5

H mm water	Δh_8	$\frac{1}{2}\rho v_{av}^2$ pounds feet^{-2}	$\frac{\Delta h_8}{\frac{1}{2}\rho v_{av}^2}$	$N_R \times 10^{-4}$
68.3	2.155	10.48	0.206	45.0
60.9	1.944	9.37	0.207	42.5
52.7	1.648	8.07	0.204	40.0
41.7	1.321	6.42	0.206	35.5
35.5	1.109	5.45	0.203	32.5
19.4	0.613	3.2	0.191	24.0
10.2	0.313	1.55	0.201	17.5
4.7	0.137	0.7	0.196	11.5
2.15	0.063	0.33	0.195	8.0

TABLE 7 (Continued)

H mm water	Δh_9	$\frac{1}{2}\rho v_{av}^2$ pounds feet^{-2}	$\frac{\Delta h_9}{\frac{1}{2}\rho v_{av}^2}$	$N_R \times 10^{-4}$
65.6	1.479	10.08	0.147	44.0
57.9	1.321	8.9	0.148	41.5
49.8	1.141	7.6	0.150	38.5
40.4	0.930	6.22	0.150	35.0
33.8	0.782	5.18	0.151	32.0
18.5	0.444	2.89	0.154	23.5
9.7	0.232	1.48	0.158	16.5
4.3	0.101	0.64	0.157	11.5
1.89	0.063	0.28	0.230	5.0

duct Reynolds number N_R is shown graphically in Figure 64. In these measurements a positive sign is attributed to differential pressures which cause a downward force on the conveyance in the direction of the duct wall near the conveyance.

The graphs in Figure 64 indicate that the nett result of the differential pressures acting on the conveyance would be to force the conveyance in a downward direction towards the duct wall nearest to it. Furthermore these graphs indicate conclusively that at low Reynolds numbers a change occurs in the magnitude of the differential pressure coefficients. The coefficients $\frac{\Delta h_6}{\frac{1}{2}\rho v_{av}^2}$, $\frac{\Delta h_7}{\frac{1}{2}\rho v_{av}^2}$ and $\frac{\Delta h_9}{\frac{1}{2}\rho v_{av}^2}$ increase slightly at very low Reynolds numbers. In general, however, a decided decrease in the magnitude of differential pressure coefficients is indicated at a Reynolds number of approximately 10×10^4 which substantiates the results obtained from the aerodynamic force measurements described in section 5.3.

It is felt that this change in differential pressure coefficients at very low Reynolds numbers can only be attributed to the fact that at these low Reynolds numbers a change in the flow pattern occurs around the model conveyance. It is also felt that this change in flow pattern is due to viscous force effects which become apparent at the duct wall at these very low Reynolds numbers. To substantiate these surmises it becomes necessary to study the nature of the boundary layer flow occurring along such a duct wall.

5.4.4 A study of the boundary layer flow in a duct containing a bluff body.

5.4.4.1 Boundary layer theory as applied to turbulent flow in ducts. Extensive theoretical and experimental work has been done by various investigators on the subject of turbulent flow through pipes[7]. Such studies were mainly concerned with the frictional resistance which must be overcome when a fluid

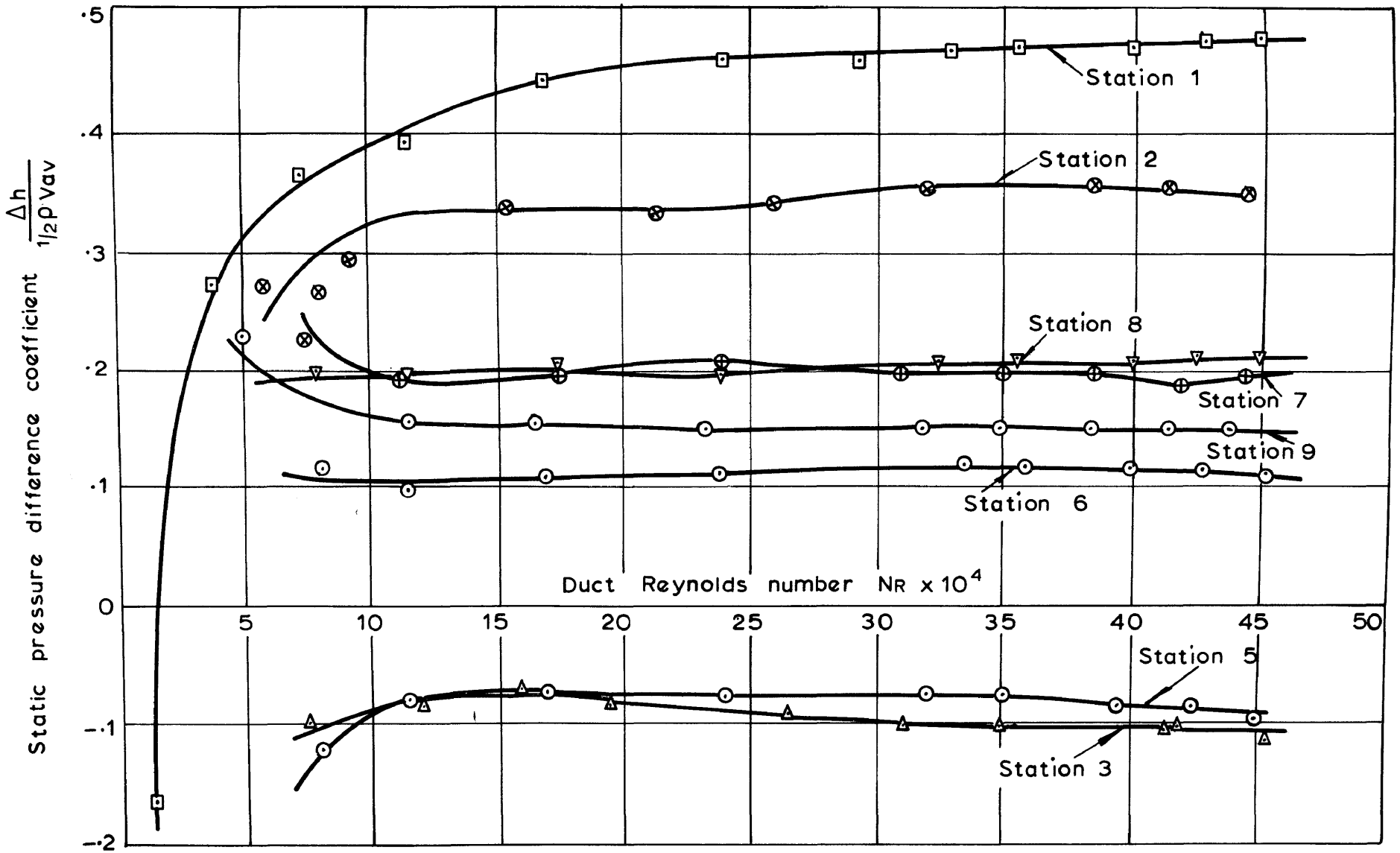

FIGURE 64

Variation of differential pressure co-efficients with duct Reynolds number

is allowed to flow in circular pipes and ducts. However, such studies have an important bearing on the behaviour of flow around a bluff body in a duct. Some of the results of these studies will now be considered.

When a fluid is flowing through a circular duct it was found that near the entrance the velocity distribution is practically uniform over the whole cross-section of the duct. As the flow progresses along the duct, a boundary layer of progressively increasing thickness is generated and, for the flow conditions under consideration, this boundary layer will invariably be turbulent. Inside the boundary layer the axial fluid velocity decreases sharply towards the duct wall but remains uniform in the central portion of the duct corss-section where the flow is still laminar. After an inlet length of somewhere between 25 and 40 duct diameters the thickness of the boundary layer has grown to such an extent that turbulent flow prevails throughout the cross-section of the duct. The flow is now fully developed and stabilised and the velocity profile of the flow will remain unchanged further downstream.

It was found that for smooth ducts the velocity profile, exhibited by fully developed turbulent flow in the duct, depended on the magnitude of the duct Reynolds number

$N_R = \frac{\rho D v_{av}}{\mu}$. Figure 65 depicts the shapes of such velocity profiles at various Reynolds numbers. In this diagram the velocity distribution is given non-dimensionally by dividing the fluid velocity v, existing at a radius r in the duct by the maximum or peak velocity V attained in the duct. It will be noticed that an increase in the Reynolds number has the tendency of flattening the velocity profile. It may be expected that the velocity profile, existing between a bluff body inside the duct and the duct wall, will be affected in a similar way. Such small changes in velocity profile, brought about by a change in Reynolds number, indicate a change in flow pattern which will affect the lateral aerodynamic force acting on the bluff body.

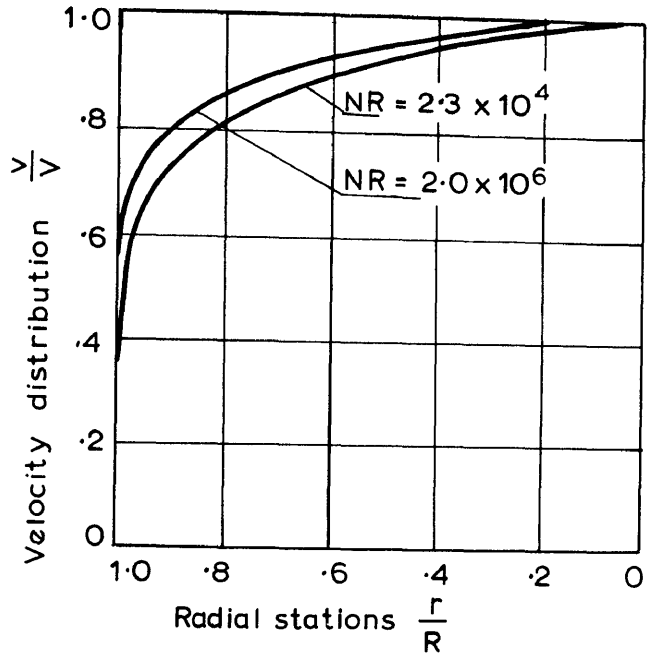

FIGURE 65

Velocity distribution for flow in a smooth duct at different Reynolds numbers

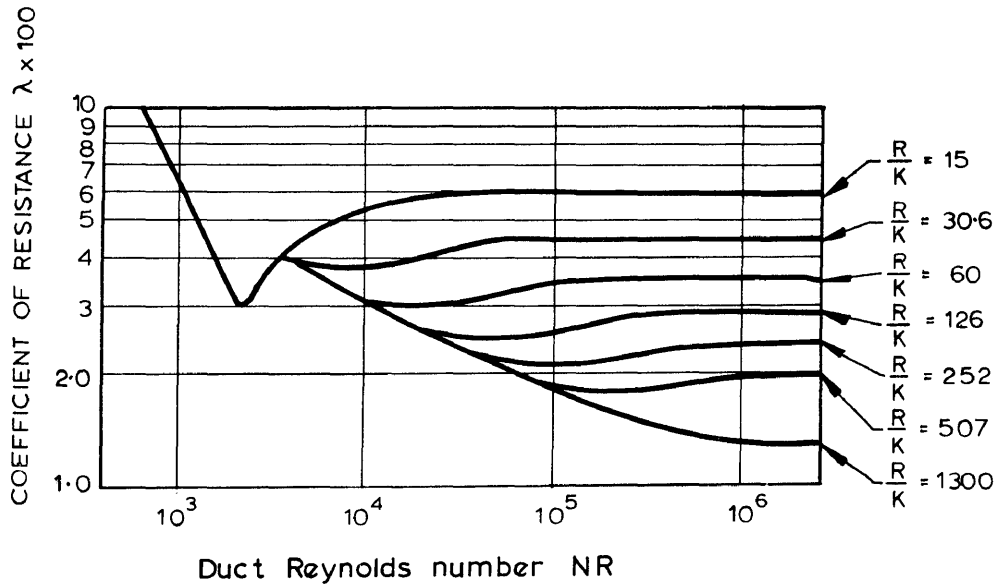

FIGURE 66

Effect of duct wall roughness and duct Reynolds number on the flow resistance co-efficient

The effect which various degrees of duct wall roughness has on the coefficient of frictional resistance will now be considered. Figure 66 indicates the relationships existing between the resistance coefficient λ and the duct Reynolds number with duct having various degrees of sand roughening on the walls. λ is defined by the relationship:

$$\text{static pressure drop per unit length (in pounds feet}^{-3}) = \frac{}{D}\ \frac{1}{2}\ v_{av}^{2}$$

The roughness of the duct wall is given by the factor $\frac{R}{k}$ where R is the radius of the duct and k is the average height of a protrusion.

Figure 66 shows that for a smooth duct the value of λ continually changes with a change in Reynolds number. For ducts which are artificially roughened with sand λ remains constant in the higher Reynolds number range and only starts changing below a certain threshold Reynolds number, the value of which depends on the degree of duct wall roughness. In these regions where λ varies with the Reynolds number, viscous forces are of sufficient magnitude to have an effect on the flow along the walls. In these regions the velocity profile and flow pattern will change with the Reynolds number. However, in those higher Reynolds number regions where λ is independent of the Reynolds number, viscous forces along the duct wall are negligibly small compared with pressure forces arising from the flow of air over the rough particles projecting from the duct wall. In these regions the velocity profile and flow pattern will remain unchanged when the Reynolds number changes.

These Reynolds number effects observed in roughened ducts may conveniently be used to substantiate the previous conclusion that the scale effect on the lateral force coefficient of a bluff conveyance is due solely to wall Reynolds number effects and not to Reynolds number effects associated with the bluff conveyance itself. If such bluff model conveyance is placed in a roughened duct, it is to be expected that the coefficient of lateral aerodynamic force will remain constant in the same Reynolds number range in which λ remains constant. If this is indeed the case, it will provide

adequate proof that only duct wall Reynolds number effects are significant. It is important, however, that the degree of roughness on the duct wall is sufficient to ensure that no duct wall scale effects will become apparent at a duct Reynolds number of approximately 10^5 which appeared to be the threshold Reynolds number for the model conveyance as determined in section 5.3. Such tests using ducts with roughened walls are described in the following section.

5.4.4.2 Experiments with a roughened duct.

For these tests the same apparatus described in section 5.3 was used. Using plastic granules which could be made to adhere to the inner surface of the duct with laquer, the duct was roughened for some fourteen feet upstream of the model conveyance, this roughening extending to about one foot downstream of the conveyance. A roughness factor $\frac{R}{k}$ of between 40 and 50 was attained. With this roughness very little duct wall scale effect should be apparent at the critical Reynolds number range just below 10^5 (refer to Figure 66).

Following the same procedure as that described in section 5.3, values for the lateral aerodynamic force coefficient C_S were determined for various Reynolds number values. The results are given in Table 8.

In order to establish whether the length of roughening on the duct had any significant influence as far as Reynolds number effects are concerned, the above test was repeated with a duct roughened only in the immediate vicinity of the conveyance. This roughening extended some fifteen inches upstream and downdstream of the conveyance. The experimental results are given in Table 9.

Using a duct which had roughening extending some fourteen feet upstream and two feet downstream of the conveyance, the roughening directly opposite the model conveyance was removed. Thus a smooth duct wall surface was provided in the form of an annulus roughly of the same length as the conveyance and directly opposite the side surfaces of the conveyance. Aerodynamic force coefficients and Reynolds number measurements for this arrangement is given in Table 10.

TABLE 8

Measurement of Aerodynamic force coefficients at various Reynolds numbers on a model conveyance in a duct with 14 feet roughening

For nomenclature see Table 5

W gm	H mm water	$\frac{1}{2}\rho v_{av}^2$ pounds feet^{-2}	v_{av} feet seconds^{-1}	C_S	$N_R \times 10^{-4}$
-0.2	0.81	0.12	11.01	-0.0057	4.83
-0.5	1.8	0.27	16.51	-0.0063	7.24
-0.1	3.7	0.55	23.57	-0.0062	10.34
-3.0	10.05	1.52	39.18	-0.0068	17.18
-5.0	15.15	2.33	48.52	-0.0074	21.28
-8.0	22.4	3.47	59.2	-0.0079	25.96
-0.5	1.88	0.28	16.81	-0.0061	7.37
-1.0	3.85	0.57	23.99	-0.0057	10.52
-5.0	17.85	2.577	51.02	-0.0067	22.37
-8.0	26.8	4.12	64.52	-0.0067	28.29
-0.2	0.93	0.13	10.54	-0.0062	4.62
-0.5	1.98	0.29	17.12	-0.0059	7.51
-1.0	3.27	0.49	22.25	-0.007	9.76
-3.0	12.5	1.91	43.92	-0.0054	19.26
-5.0	18.2	2.82	53.36	-0.0061	23.4
-8.0	30.5	4.67	68.68	-0.0059	30.12
-5.0	16.9	2.62	51.44	-0.0065	22.56

TABLE 9

Measurement of Aerodynamic force coefficients at various Reynolds numbers on a model conveyance in a duct with roughening only in vicinity of conveyance.

Nomenclature same as in Table 5

W gm	H mm water	$\frac{1}{2}\rho v_{av}^2$ pounds feet^{-2}	v_{av} feet seconds^{-1}	C_S	N_R x 10^{-4}
-0.2	0.49	0.07	8.409	-0.0098	3.69
-0.2	0.44	0.06	7.786	-0.0114	3.41
-0.3	0.72	0.105	10.31	-0.0098	4.52
-0.5	1.18	0.17	13.11	-0.0101	5.75
-1.0	2.35	0.35	18.8	-0.0098	8.24
-2.0	4.73	0.71	26.78	-0.0097	11.74
-4.0	9.1	1.37	37.2	-0.010	16.31
-5.0	11.2	1.71	41.55	-0.010	18.22
-7.0	15.0	2.32	48.4	-0.0103	21.22

TABLE 10

Measurement of Aerodynamic force coefficients at various Reynolds numbers on a model conveyance in a roughened duct with the roughening removed in the immediate vicinity of the model conveyance.

Nomenclature same as in Table 5

W gm	H mm water	$\frac{1}{2}\rho v_{av}^2$ pounds feet^{-2}	v_{av} feet seconds^{-1}	C_S	$N_R \times 10^{-4}$
5.0	7.8	1.18	34.53	0.0145	15.14
6.0	8.8	1.33	36.65	0.0155	16.07
10.0	15.4	2.38	48.03	0.0144	21.5
20.0	30.4	4.65	68.53	0.0147	30.05
0.3	0.66	0.09	9.54	0.0114	4.18
5.0	7.8	1.18	34.53	0.0145	15.14
6.0	8.8	1.33	36.65	0.0155	16.07
10.0	15.4	2.38	49.03	0.0144	21.5
20.0	30.4	4.65	68.53	0.0147	30.05
0.3	0.66	0.09	9.54	0.0114	4.18
0.5	1.0	0.15	12.31	0.0114	5.4
1.0	2.1	0.31	17.69	0.0111	7.76
0.2	0.49	0.07	8.409	0.0098	3.69
0.3	0.65	0.09	9.54	0.0114	4.18
0.5	1.1	0.16	12.72	0.0107	5.58
1.0	2.1	0.31	17.69	0.0111	7.76
3.0	4.8	0.72	8.53	0.0143	3.74
5.0	7.9	1.19	34.67	0.0144	15.20
10.0	15.05	2.32	48.4	0.0148	21.22
15.0	22.6	3.5	59.45	0.0147	26.29
20.0	31.5	4.82	69.77	0.0142	30.59
25.0	39.9	6.14	78.75	0.0140	34.53

The results of the above three tests are presented graphically in Figure 67.

It is clear that roughening on the duct wall had a very marked effect on the flow around the model, since it caused a complete reversal of the lateral aerodynamic force which became negative. Furthermore, the flow in the duct became rather unsteady and force readings were made with difficulty. However, the graphs in Figure 67 indicate that no Reynolds number effect was apparent for a duct with 14 feet of roughening upstream of the conveyance or when the roughening was confined only to the immediate vicinity of the conveyance. On removing the roughening directly opposite the conveyance, the lateral force on the conveyance again became positive (i.e. in the direction of the duct wall nearest to the conveyance). Furthermore, the appropriate graph in Figure 67 indicate that a decrease in C_S again occurred at low Reynolds numbers, indicating the return of the scale effect. It must therefore be concluded that the Reynolds number effect encountered with bluff bodies in ducts ispurely a scale effect associated with the duct wall. When the duct wall is roughened sufficiently so that viscous force effects along the duct wall become negligibly small, the Reynolds number effect on the coefficient of lateral forces acting on the bluff body disappears. However, when the duct wall is smooth directly opposite the body, the Reynolds number effect again become apparent, even though the duct walls are rough upstream and downstream of the body. This indicates that viscous forces along the duct wall immediately opposite the conveyance again became significant.

In order to illustrate that viscous forces acting along the walls of the conveyance are insignificant and that no Reynolds number effect may be expected from this quarter, the parallel sides of the conveyance were roughened in a manner similar to the roughening on the duct walls. The results of force measurements are given in Table 11, and Figure 68 shows the relationship between C_S and N_R. The angle of incidence of the conveyance was increased slightly in order to obtain larger values for C_S. It is clear that even

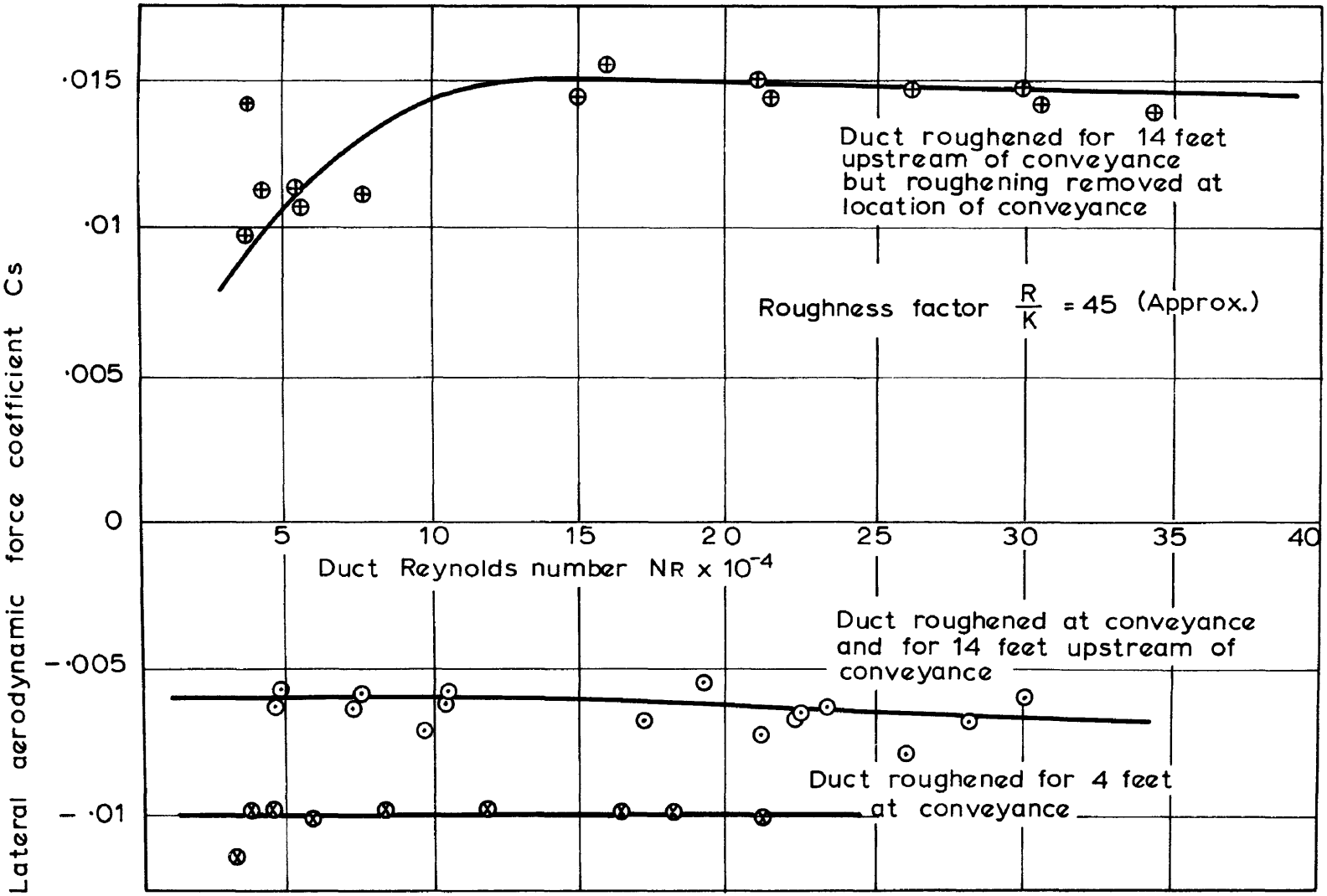

FIGURE 67

The relationship between lateral aerodynamic force co-efficient and duct Reynolds number as affected by roughening of the duct wall

TABLE 11

Measurements of Aerodynamic force coefficients at various Reynolds numbers on a model conveyance with roughened side walls.

Nomenclature same as in Table 5

w gm	H mm water	$\frac{1}{2}\rho v_{av}^2$ pounds feet^{-2}	v_{av} feet seconds^{-1}	C_S	N_R x 10^{-4}
0.3	0.29	0.04	6.36	0.026	2.79
0.5	0.4	0.06	7.89	0.029	3.41
1.0	0.71	0.1	10.05	0.034	4.41
5.08	2.71	0.4	20.10	0.044	8.81
10.08	5.0	0.75	27.52	0.046	12.07
15.16	7.2	1.08	33.04	0.048	14.49
20.16	9.55	1.44	38.15	0.048	16.73
25.16	11.8	1.8	42.63	0.048	18.69
30.08	14.13	2.2	47.14	0.047	20.67
35.16	16.4	2.54	50.66	0.048	22.21
40.16	19.0	2.96	54.68	0.047	23.98
45.24	21.15	3.28	57.56	0.047	25.24
50.08	23.75	3.67	60.89	0.047	26.70

..... 203

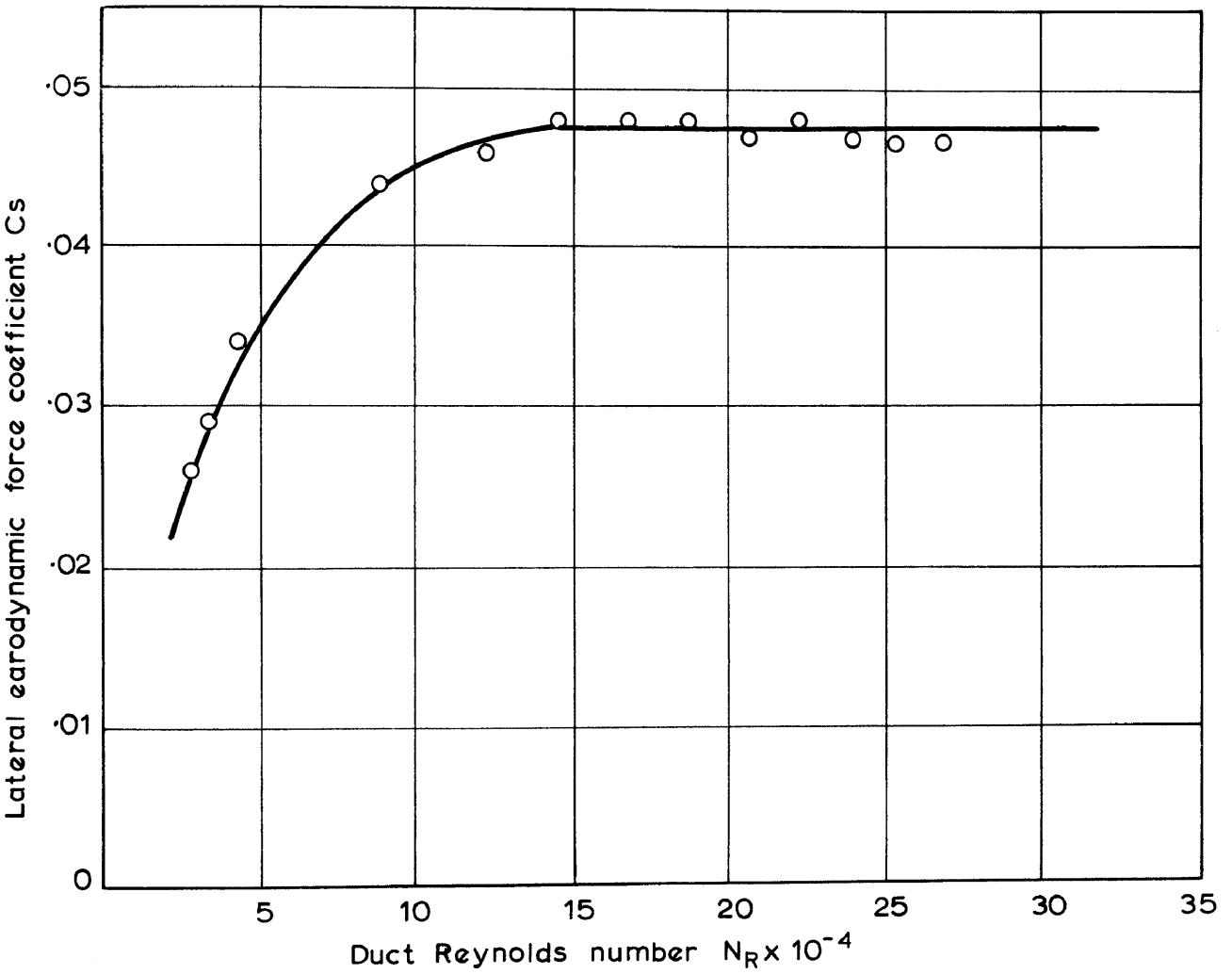

FIGURE 68

Variation of aerodynamic force co-efficient with Reynolds number when side walls of conveyance is roughened

though viscous forces acting along the conveyance walls should have been quite insignificant compared with pressure forces acting on the conveyance, a very definite scale effect is still revealed by the graph in Figure 68 which again points to the fact that this Reynolds number effect is purely associated with the flow along the duct wall directly opposite the conveyance.

The fact that roughening on the walls of the duct has the effect of preventing the Reynolds number effect on the coefficients of lateral aerodynamic forces acting on model conveyances, is purely of academic interest. Such roughening can not effectively be applied in practice to overcome the scale effect difficulty when operating a dynamic scale model mineshaft installation at very low Reynolds numbers. The above tests even indicated a complete reversal of the direction in which the lateral aerodynamic force acts.

5.4.5 The effect of increasing the shaft diameter.

It is of interest to determine to what extent the Reynolds number effect is influenced by the diameter of the duct in which a given model conveyance is installed. In order to carry out such an investigation, the model conveyance, complete with the balance to which it was attached, was installed in the 24 inch octagonal working section of a small wind tunnel as depicted in Figure 69. The model conveyance was again installed at an angle of incidence of approximately 50 minutes so as to cause a downward aerodynamic force on the conveyance. Measurements of lateral aerodynamic force and average free stream air velocities were again obtained and the results are given in Table 12. The average free stream air velocity v_{av} was obtained directly from the calibration of the wind tunnel. The equivalent diameter D of the octagonal wind tunnel section was assumed to be 2 feet and the Reynolds number was again based on the average free stream velocity and this equivalent diameter D. For this test the lateral aerodynamic force coefficient C_S was defined as

$$C_S = \frac{S}{\frac{1}{2}\rho v_{av}^2 B}$$

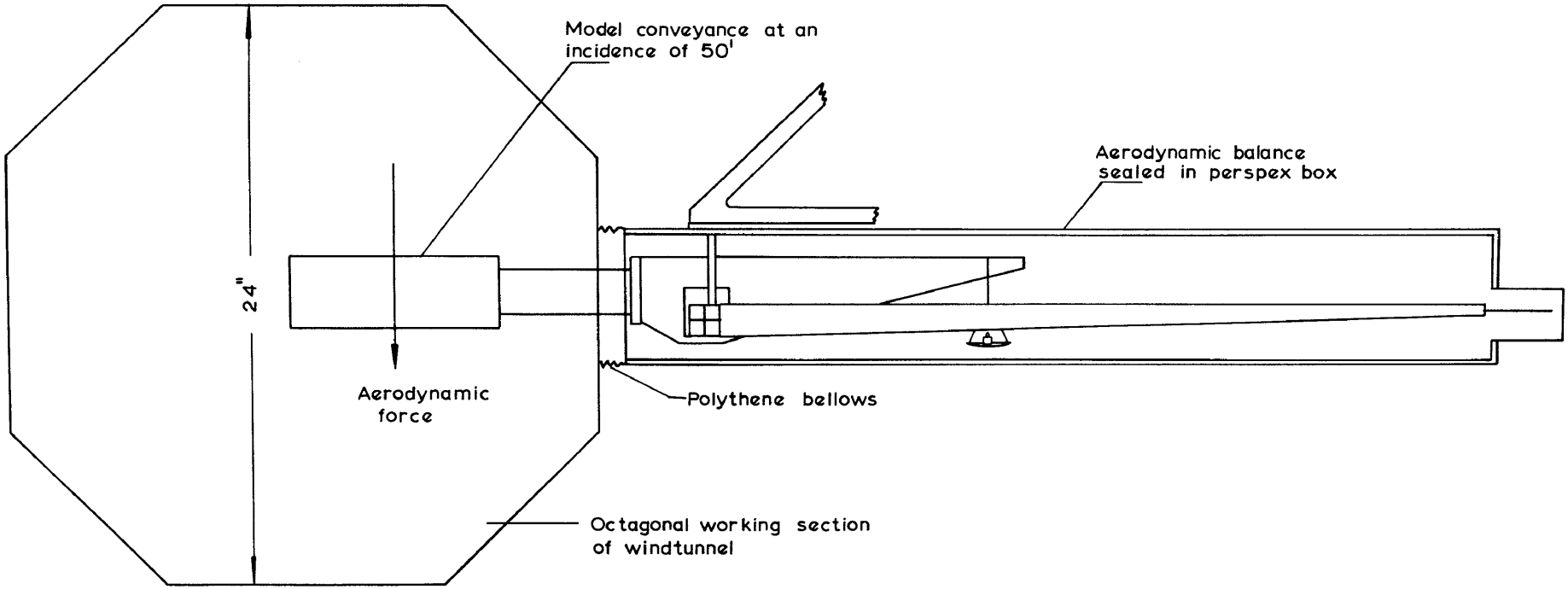

FIGURE 69

Model conveyance mounted in the octagonal working section of a windtunnel

TABLE 12

Measurements of Aerodynamic force coefficients at various Reynolds numbers on a model conveyance installed in a 24 inch octagonal wind tunnel.

W = scale pan weight in grams.

v_{av} = average air velocity in the unobstructed working section of the wind tunnel in feet seconds^{-1}.

$S = a\,W$ = aerodynamic side force in pounds.

a = calibration and conversion factor = 0.00154.

$\frac{1}{2}\rho v_{av}^2$ = dynamic head of free airstream in the wind tunnel working section.

$C_S = \dfrac{S}{\frac{1}{2}\rho v_{av}^2 B}$ = lateral aerodynamic force coefficient.

B = area of lower face of conveyance = 0.336 feet^2

$N_R = \dfrac{\rho D v_{av}}{\mu}$ = Reynolds number.

D = distance measured between parallel sides of wind tunnel = 2 feet.

ρ = 0.002 slugs feet^{-3} (assumed constant).

μ = 3.8 x 10^{-7} slugs feet^{-1} seconds^{-1} (assumed constant)

W gm	v_{av} feet seconds^{-1}	S pounds	$\frac{1}{2}\rho v_{av}^2$ pounds feet^{-2}	C_S	N_R x 10^{-4}
0.1	4.15	0.0002	0.017	0.0351	4.37
0.3	6.18	0.0005	0.038	0.0391	6.50
0.5	7.45	0.0008	0.056	0.0426	7.84
0.8	9.33	0.0012	0.087	0.0411	9.78
1.0	10.26	0.0015	0.105	0.0426	10.8
2.0	13.1	0.0031	0.173	0.0534	13.8

TABLE 12 (Continued)

W gm	v_{av} feet seconds^{-1}	S pounds	$\frac{1}{2}\rho v_{av}^2$ pounds feet^{-2}	C_S	$N_R \times 10^{-4}$
3.0	16.8	0.0046	0.282	0.0486	17.7
5.1	21.8	0.0079	0.475	0.0495	23.0
8.1	26.2	0.0120	0.686	0.0521	27.57
10.1	29.1	0.0156	0.847	0.0549	30.65
13.2	33.0	0.0203	1.089	0.0555	34.7
15.2	35.8	0.0234	1.282	0.0544	37.7
18.3	39.0	0.0282	1.521	0.0552	41.1
20.1	40.9	0.0310	1.673	0.0552	45.1
23.2	42.6	0.0357	1.815	0.0586	44.9
25.2	45.0	0.0388	2.025	0.0571	47.4
30.1	49.6	0.0464	2.460	0.0562	52.2
35.2	54.1	0.0542	2.927	0.0552	56.9
40.2	57.4	0.0619	3.295	0.0560	60.4
45.3	61.1	0.0698	3.733	0.0557	64.3
50.2	65.4	0.0773	4.277	0.0538	68.9
2.0	12.9	0.0031	0.166	0.0555	13.6
5.1	21.0	0.0079	0.441	0.0534	22.1
23.2	43.5	0.0357	1.892	0.0562	45.8
25.2	45.6	0.0388	0.079	0.0556	48.0
1.0	10.1	0.0015	0.102	0.0439	10.63
2.0	13.0	0.0031	0.169	0.0547	13.7
3.1	16.0	0.0046	0.256	0.0536	16.8
4.1	18.5	0.0063	0.322	0.0582	19.5
5.1	20.7	0.0079	0.429	0.0549	21.8

where

B = lower face area of model conveyance in feet^2.

S = lateral aerodynamic force in pounds.

The relationship between N_R and C_S, obtained from this investigation, is given in Figure 70 which shows that a threshold Reynolds number having an approximate value of 15×10^4 is still present. This is to be expected, since viscous force effects are still present along the tunnel walls, even if the size of the model conveyance is much reduced relative to the cross-section of the duct or tunnel. However, on reducing the ratio of conveyance cross-sectional area to duct cross-sectional area, the blockage effect of the conveyance in the duct is reduced and the acceleration of the air stream between the conveyance and the duct wall will therefore be less. Since it was found that scale effects are due to the action of viscous forces between the conveyance and the duct wall, it is clear that the local air velocity in this region is most important. A Reynolds number based on this local velocity rather than on the average velocity in the unobstructed duct would have been more significant. The threshold Reynolds number indicated in Figure 70 is slightly higher than that obtained for the conveyance in a 10 inch diameter duct. This is most probably due to the fact that the local acceleration of the air between the conveyance and tunnel walls was less in the relatively large tunnel working section.

All previous investigations on Reynolds number effects were conducted with geometrically identical installations. For comparative tests it was therefore immaterial on which linear dimension and on which air velocity the Reynolds number or the aerodynamic force coefficient was based. However, when different geometrical installations are compared, the exact linear dimension and air velocity selected in order to define the Reynolds number become important and it is felt that the duct diameter and the local air speed between the conveyance and the duct wall are the two significant quantities which will adequately define the Reynolds number. Unfortunately, from the experimental point of view, it becomes impractical to attempt

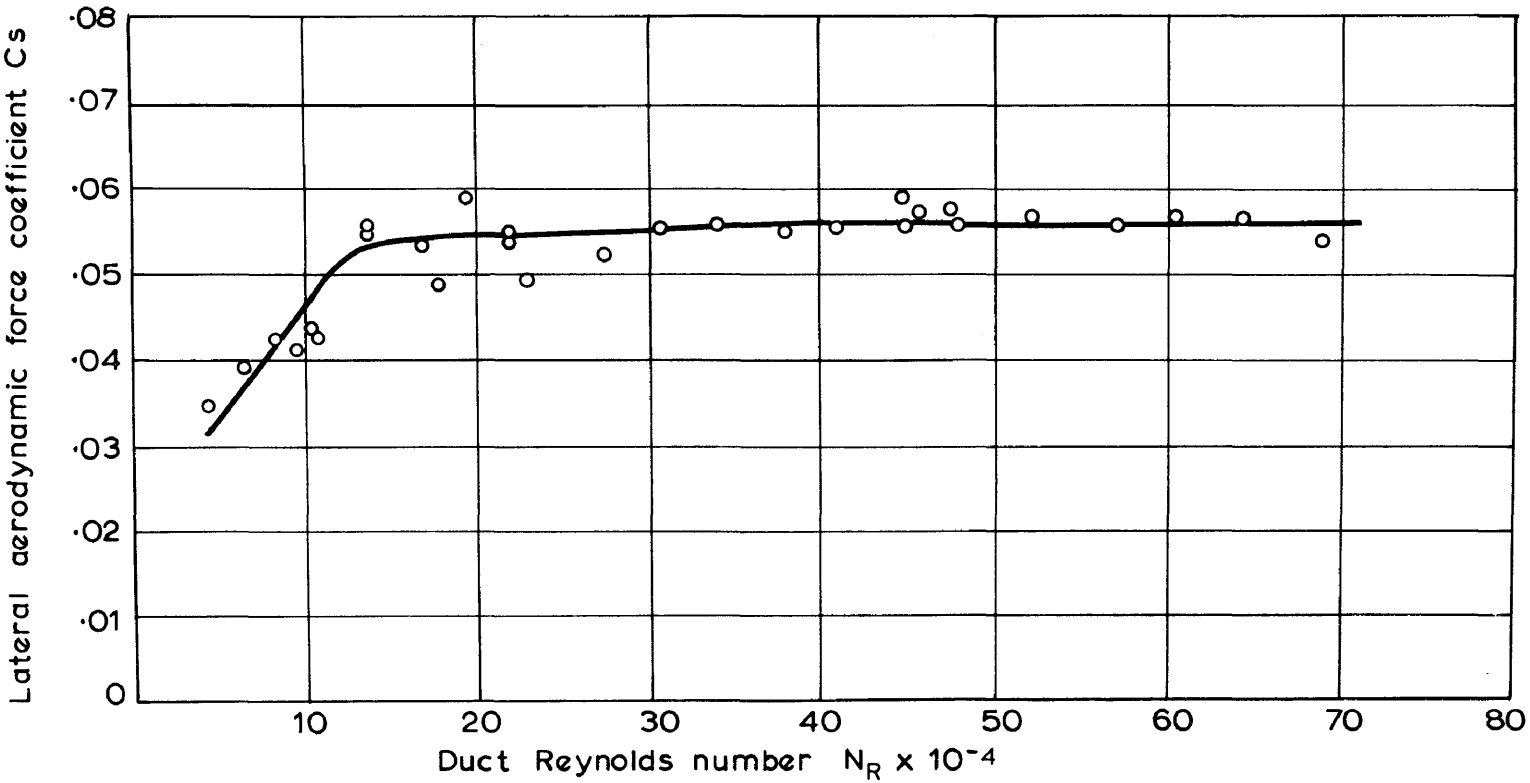

FIGURE 70

Relationship between aerodynamic force co-efficient and duct Reynolds number for a model conveyance in a 24 inch octagonal windtunnel

measuring the average air velocity between the side face of a conveyance and the duct wall. When changing the geometry of the installation the flow pattern between the conveyance and duct wall may change in any unpredictable fashion and it therefore also becomes impractical to measure the air velocity at some fixed point between the conveyance and duct wall.

5.4.6 The importance of the aerodynamic shape of a conveyance. In section 5.4.5 it was indicated that an increase in the streamwise cross-sectional area of the conveyance, relative to the duct cross-sectional area (i.e. increasing the duct blockage effect) had the effect of speeding up the air between the conveyance and duct walls. Such an increase in local velocity between the conveyance and duct walls may also be effected by changing the aerodynamic shape of the conveyance, as for example, adding the roof used in the correlation tests to the model conveyance. (Illustrated in Figure 23). As described in section 4.4, this roof deflected air towards the wall because of the venturi effect which caused a reduced pressure between the conveyance and the wall. This increase of air velocity in the region between the conveyance and the wall was considerable since a very marked deflection of the conveyance was indicated during hoisting tests.

Such a roof was added to the model conveyance in the horizontal duct and the normal test procedure for establishing the relationship between C_S and N_R was again followed. However, for this conveyance configurations the value of C_S at low Reynolds numbers only showed a gradual decrease in magnitude and it was rather difficult to establish a definite value for a threshold Reynolds number. Table 13 shows the results of these measurements in the Reynolds number range below $N_R = 10^5$ and curve 1 in Figure 71 illustrates the gradual decrease in C_S. In order to attempt a more accurate determination of the very low air speeds, a 2.75 inch diameter orifice plate was installed some 15 feet downstream of the conveyance in a contraction (refer to Figure 54).

Following the procedure set out in Reference 8, the low flow rates were determined using the orifice plate formula

..... 211

TABLE 13

Measurements of Aerodynamic force coefficients at various Reynolds numbers on a model conveyance with a roof.

Nomenclature same as in Table 5.

W gm	H mm water	$\frac{1}{2}\rho v_{av}^2$ pounds feet^{12}	C_S	N_R x 10^{-4}
11	3.2	0.475	0.0792	9.6
10	3.0	0.45	0.0762	9.3
9	2.8	0.42	0.0735	9.0
8	2.4	0.36	0.0762	8.2
7	2.15	0.32	0.075	7.7
6	1.86	0.275	0.0748	7.1
5	1.63	0.24	0.0714	6.6
4.	1.33	0.19	0.0722	5.8
3	1.06	0.16	0.0643	5.3
2	0.75	0.115	0.0596	4.2
1	0.4	0.06	0.0572	3.4
9	2.65	0.39	0.0791	8.8
8	2.45	0.36	0.0762	8.3
4	1.4	0.21	0.0653	6.1
5	1.7	0.25	0.0686	6.7
6	1.9	0.28	0.0735	7.2
7	2.2	0.325	0.0738	7.9
8	2.45	0.36	0.0762	8.3
10	3.05	0.46	0.0745	9.5
20	5.5	0.82	0.0836	12.9

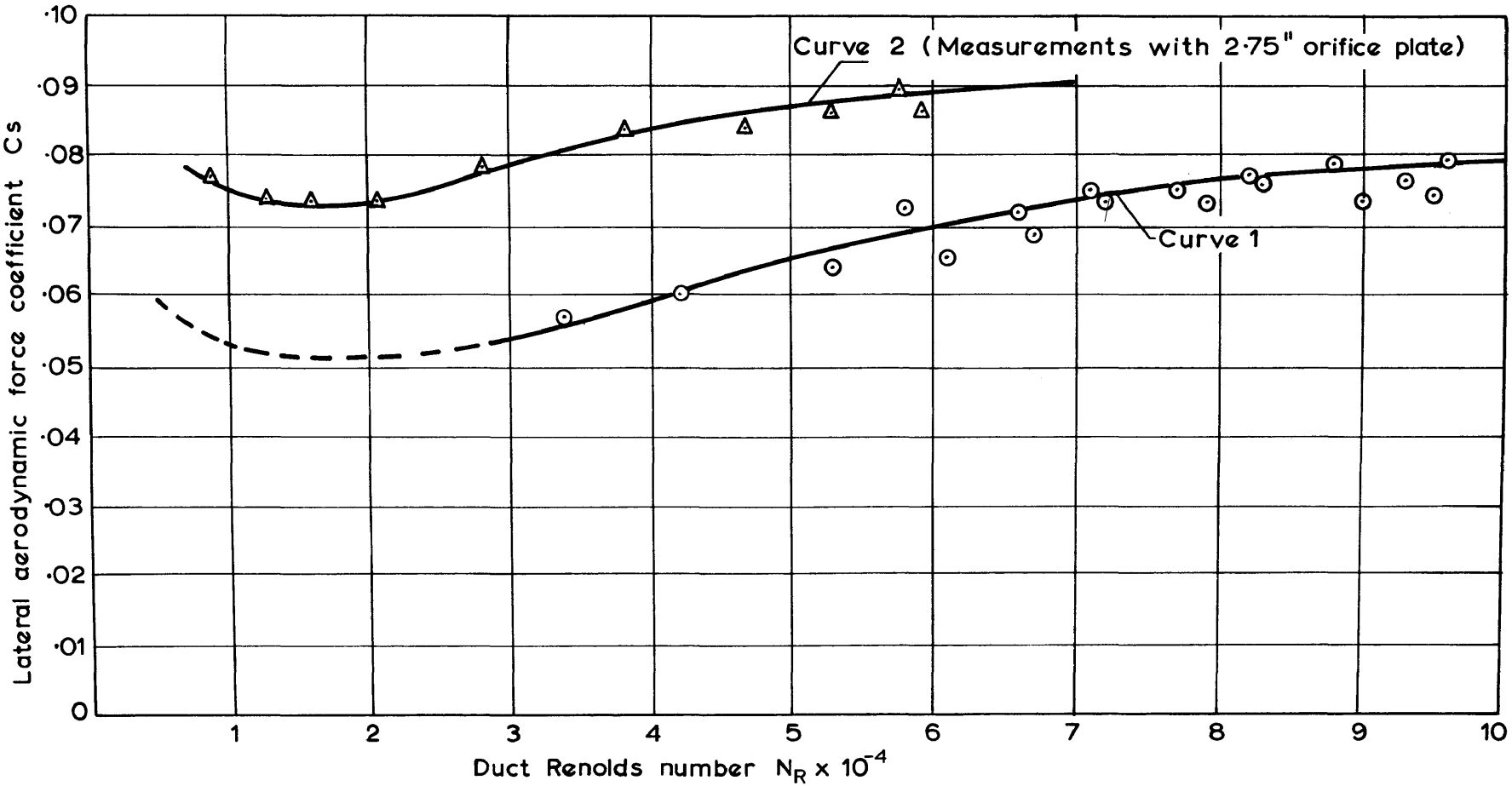

FIGURE 71

Variation of lateral aerodynamic force co-efficient in a low Reynolds number range for a conveyance with a roof

$Q^1 = 7859\ Czd^2E\sqrt{\frac{h}{25.4}}\sqrt{\frac{P_1}{T}}$ cubic feet per hour of standard air.

where

d = 2.75 inches (diameter of orifice)

C = 0.606 (coefficient of discharge of orifice)

z = 1.0 (general correction factor)

$E = \frac{1}{\sqrt{1-m^2}} = 1.136$ (velocity of approach factor)

$m = \frac{d^2}{D_t} = 0.472$ (D_t is diameter of throat of contraction)

P_1 = 12.58 pounds inches^{-2} (absolute air pressure on high pressure side of orifice plate)

h = differential pressure over orifice plate in mm water.

T = 534 ^{o}F absolute (absolute temperature of air)

Assuming an air density of ρ = 0.002 slugs feet^{-3}, it follows that

$Q^2 = 0.1635\ h$

or

$\rho Q^2 = 0.000327\ h$

where Q is the actual rate of flow in cubic feet per second.

In these tests C_S was determined directly from knowledge of the flow rate Q.

$$C_S = \frac{S}{\frac{1}{2}\rho v_{av}^2 D^2} = \frac{0.857S}{\rho Q^2}$$

The Reynolds number was determined from

$$N_R = \frac{1.527\rho Q}{\mu}$$

The results of measurements at these low flow rates are given in Table 14 and curve 2 in Figure 71 shows the variation of C_S with N_R. The vertical displacement of curve 2 relative to curve 1 is

TABLE 14

Measurement of Aerodynamic force coefficients at various Reynolds numbers on a model conveyance with a roof, using a 2.75 inch diameter orifice plate.

h = static head drop over orifice in mm water.

Q = rate of air flow in duct in feet^3 seconds^{-1}.

ρQ^2 = 0.000327 h in slugs feet^3 seconds^{-2}.

W = balance scale pan weight in grams.

S = $\frac{a\ W}{453.6}$ pounds (aerodynamic side force on conveyance).

a = 1 (balance factor).

C_S = $\frac{0.857\ S}{\rho\ Q^2}$ (coefficient of aerodynamic side force).

ρ = 0.002 slugs feet^{-3} (air density assumed constant).

μ = 3.8 x 10^{-7} slugs feet^{-1} seconds^{-1} (air viscosity assumed constant).

h	ρQ^2	Q	W	S	C_S	N_R x 10^{-4}
334.0	0.1092	7.35	5.0	0.0110	0.0864	5.9
268.0	0.0876	6.56	4.0	0.0088	0.0863	5.27
206.0	0.0673	5.79	3.0	0.0066	0.0842	4.66
139.0	0.0454	4.77	2.0	0.0044	0.0832	3.83
74.0	0.0242	3.48	1.0	0.00221	0.0780	2.8
39.5	0.0129	2.54	0.5	0.00110	0.0733	2.04
23.5	0.0077	1.96	0.3	0.00066	0.0737	1.58
15.7	0.0051	1.60	0.2	0.00044	0.0736	1.29
7.5	0.0025	1.11	0.1	0.00022	0.0771	0.89

attributed to the fact that the angle of incidence of the conveyance was not identical for the two tests. However, to study the scale effect at low values for N_R curve 2 may be displaced downwards so as to coincide with curve 1.

It is clear that even at a very low Reynolds number of $N_R = 2 \times 10^4$ no marked drop in C_S is indicated and below this Reynolds number C_S appears to increase again. No definite threshold Reynolds number is indicated and C_S decreases slightly over a wide range of Reynolds numbers. This different behaviour of a conveyance with a roof is again attributed to the fact that the local Reynolds number, based on the locally accelerated air velocity between the conveyance and the duct wall, was considerably increased. It is clear that the nature of the flow around this conveyance and the nature of the viscous force effects which appear at low velocities differ considerably from the conveyance without a roof.

In tests of this nature where studies are made of bluff obstructions which may cause various flow effects in ducts, the significant Reynolds number should always be that based on the local velocity between the obstruction and the duct wall, since it is here where Reynolds number effects become apparent. However, as pointed out in section 5.4.5, the experimental difficulties experienced in establishing a representative local air velocity between the conveyance and the duct wall again apply. There also appears to be no satisfactory way of making an estimate of the expected local velocity between the conveyance and the duct wall.

It must be concluded that each individual conveyance shape or conveyance mineshaft configuration should be treated on its own merits. As long as the geometry of such a conveyance or installation remains unchanged the Reynolds number may be conveniently based on the average air velocity in the unobstructed duct and on the duct diameter. The aerodynamic forces acting on such a conveyance may then also be expressed non-dimensionally by simply defining force coefficients in terms of the average duct air velocity and the duct diameter as was done in most of the investigations

described in previous sections. It will then be possible to establish a threshold Reynolds number for each individual conveyance shape or conveyance duct configuration, such a threshold Reynolds number only applying for that particular geometric configuration.

A great variety of conveyance shapes and conveyance installations are encountered in general mining practice. It was thought that no further significant facts, concerning the general subject of aerodynamic scale effect in mineshafts, could be brought to light by investigating Reynolds number effects on any further conveyance shapes and configurations.

5.4.7 General conclusions. It is felt that the work described in this section 5.4 adequately illustrates the nature of the mechanics of air flow around a bluff body in a duct. Aerodynamic force measurements as well as static pressure measurements on a model conveyance clearly indicate a Reynolds number effect which causes a decrease in the coefficient of the aerodynamic side force acting on a conveyance. Above a certain threshold Reynolds number the aerodynamic side force coefficient remains reasonably constant up to the maximum duct Reynolds number of $N_R = 7 \times 10^5$ which could be reached in any of the tests made. It is assumed that the aerodynamic force coefficient will remain constant for the higher Reynolds numbers which apply for fullscale mineshaft installations.

It was also established that the above threshold Reynolds number, when defined in terms of the duct diameter and the average velocity of air in the unobstructed duct, was dependant on the aerodynamic shape of the conveyance and on the relative size and position of the conveyance in the duct.

From investigations into the nature of the boundary layer flow it became clear that the observed scale effect on the aerodynamic force coefficient at low Reynolds numbers must be attributed solely to a duct wall effect and not to flow effects over the conveyance walls. Because of this fact no noticeable Reynolds

number effects should be present when a conveyance travels through a shaft in which the air is stationary or moving at very low speeds which implies very slight movement of air relative to shaft walls.

It now becomes clear that when a model conveyance travels in a shaft in which ventilation air also flows (as is the case in most mine-shaft installations) Reynolds number effects may be encountered, depending on the actual magnitude of the flow rate in the duct. The speed of the conveyance itself will have no bearing on the Reynolds number effect. When the flow rate in a model mineshaft is very small (as was the case in the Durban Roodepoort Deep dynamic scale model) the Reynolds number effect may be negligibly small. On the other hand if the duct Reynolds number (based on the speed of the air flowing in the duct) equals or exceeds the threshold Reynolds number for that particular conveyance instal-lation, scale effect will again not be evident in the operation of the model. On exceeding this threshold Reynolds number the coefficient of lateral force acting on the conveyance will remain constant and will also be approximately equal to the force coefficient that will apply in a fullscale prototype installation. However, it is clear that for a certain range of duct Reynolds numbers, there will be the danger of appreciable scale effect which may effect the results obtained from dynamic scale model testing.

Unfortunately it was not possible to determine, by means of experiments, the magnitudes of error arising from the Reynolds number effect. With the apparatus at the disposal of the investigators it was not possible to determine lateral aerodynamic force coefficients while a model conveyance was travelling in a shaft. However, in order to make an estimate of the degree of error which might be expected in any given model installation, the following procedure is suggested:

Let the model conveyance travel at a velocity u through the shaft, and let v_{av} be the average velocity of the air flow in the shaft.

Let C_{Sv} be the coefficient of lateral aerodynamic force applying to a conveyance which is situated stationary in a duct through

which the air flows at a velocity of v_{av}. Let C_{Su} be the coefficient of lateral aerodynamic force applying when the conveyance is moving at a speed of u through a shaft in which the air is stationary. Let C_S be the lateral aerodynamic force coefficient when both the conveyance and the air in the shaft is moving, thus causing an air velocity of $u + v_{av}$ relative to the conveyance.

The relationship

$$C_S \tfrac{1}{2}\rho (u + v_{av})^2 = \tfrac{1}{2}\rho (\sqrt{C_{Su}}\ u + \sqrt{C_{Sv}}\ v_{av})^2$$

is now assumed.

Since C_{Su} is applicable to the case when a conveyance is travelling in a shaft in which the air is stationary, the distribution of the air velocity relative to the conveyance will be perfectly flat. Such a flow condition over a model conveyance may be simulated by installing a number of gauze screens upstream of the model conveyance, installed inside a long duct in which air is allowed to flow. Such screens will have the tendency of flattening the velocity profile and by measuring the aerodynamic force on the conveyance, it will then be possible to obtain the normal C_{Su} Reynolds number graph applicable to such a flat velocity distribution. C_{Su} may naturally be expected to decrease in value below a certain threshold Reynolds number, as illustrated in Figure 72. However, the constant value of C_{Su} obtained at high Reynolds numbers, should correspond approximately to the required value for the model conveyance travelling in a shaft with stationary air.

On removing the gauze screens the velocity profile just upstream of the model conveyance will again assume the normal parabolic shape associated with fully developed turbulent flow in circular ducts. In general it will be found that for a parabolic velocity distribution the value of the lateral aerodynamic force coefficient will be consistently less than in the case of a uniform velocity distribution, as illustrated in Figure 72 (refer to section 5.5). Furthermore, if a dynamic scale model installation is operated at a point A (refer to Figure 72) where the duct Reynolds number

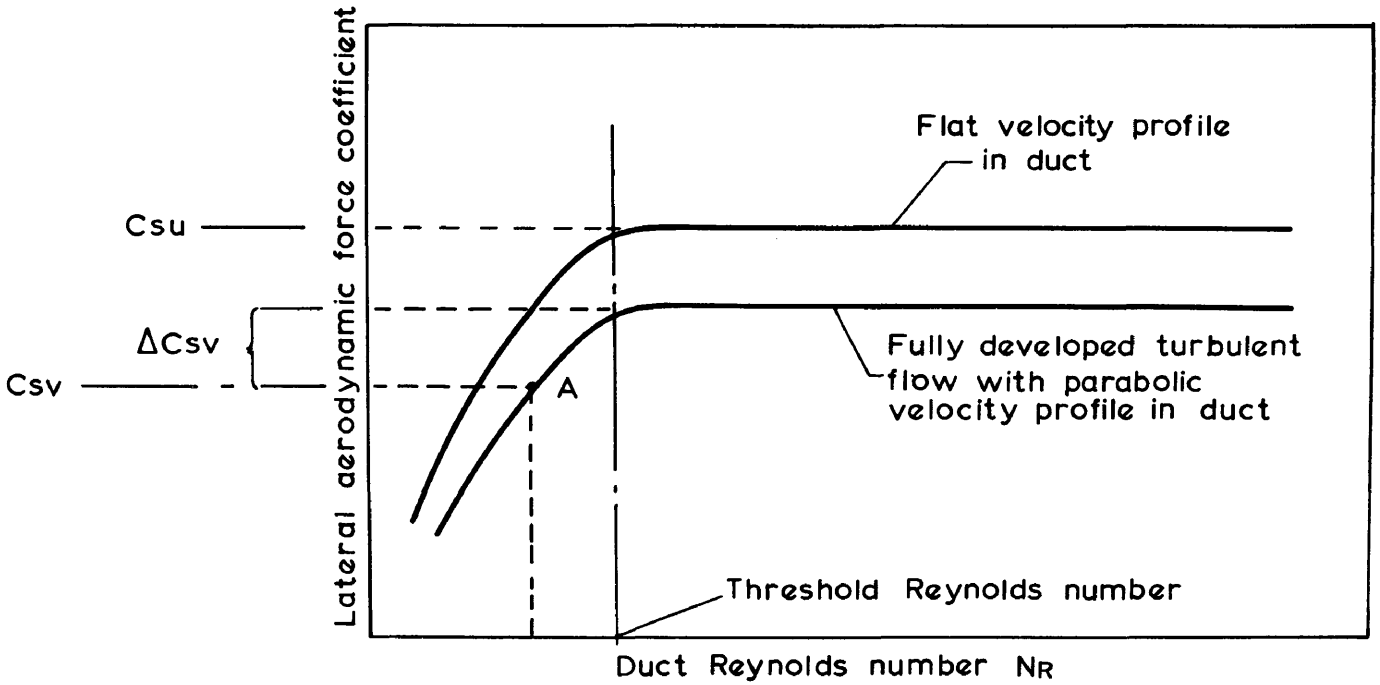

FIGURE 72

N_R is less than the threshold value, C_{Sv} will be reduced by a decrement $\triangle C_{Sv}$ below the value of the aerodynamic force coefficient to be expected for the fullscale prototype. Using the above formula, the error $\triangle C_S$, to be expected in the actual aerodynamic force coefficient C_S for the model installation, may be expressed by

$$\triangle C_S = \frac{1}{(u+v_{av})^2} \left\{ 2\sqrt{C_{Su}}\, u\, v_{av} \left(\sqrt{C_{Sv} + \triangle C_{Sv}} - \sqrt{C_{Sv}} \right) + \triangle C_{Sv}\, v_{av}^2 \right\}$$

The percentage error to be expected in the actual lateral aerodynamic force coefficient acting in the dynamic scale model may then be expressed by

$$\text{percentage error} = \frac{\triangle C_S}{C_S + \triangle C_S} \times 100$$

Experience with dynamic scale models of rope-guide installations has shown that lateral deflections of conveyances were approximately proportional to the lateral aerodynamic forces acting on them. Hence the expected error in measurements of lateral conveyance displacements, attributed to the duct Reynolds number effect, may also be expressed by

$$\frac{\triangle C_S}{C_S + \triangle C_S} \times 100.$$

Generally, in most of the experimental work done on model rope-guide installations an accuracy of 5% in all measured results were regarded as satisfactory. Hence, if a scale effect error of 5% or less is indicated for any particular model installation operating at a given duct Reynolds number, this Reynolds number may be regarded as safe.

In order to give an example, the estimated percentage error due to the duct Reynolds number effect will now be determined for the model used in the Durban Roodepoort Deep mineshaft correlation tests.

In this model a ventilation air velocity of $v_{av} = 0.93$ feet seconds^{-1}

..... 221

was used at a maximum hoisting speed of u = 9.54 feet seconds^{-1}. Figure 74 shows the variation of lateral aerodynamic force coefficients with Reynolds number for both a flat velocity profile and a profile for typical fully developed turbulent pipe flow. These curves were obtained for a conveyance adjusted at a rather large angle of incidence of approximately 30 minutes. The indicated force coefficients

$$C_{Su} = 0.024 \text{ (for the flat velocity profile)}$$

and $C_{Sv} = 0.0205$ (for the parabolic profile)

will be larger than those encountered during most of the correlation tests.

The lower curve in Figure 74 indicates a decrease $\triangle C_{Sv} = 0.0105$ (approximately) when operating at the usual duct Reynolds number of approximately 3×10^4. Substituting these values for C_{Su}, C_{Sv}, and $\triangle C_{Sv}$ in the above formulae, it follows that $C_S = 0.0237$ and $\triangle C_S = 0.00091$, indicating a duct Reynolds number effect error of 3.7%. It is clear that an error of this magnitude would not have been at all noticeable in the recording of lateral conveyance displacements during the correlation tests on the Durban Roodepoort Deep guide rope installation.

5.5 A study of the significance of velocity profile shapes for air flow in dynamic scale model mineshafts.

5.5.1 Purpose of study. The purpose of this study was to establish to what extent the exact shape of the velocity profile of air flow in a duct effected the lateral aerodynamic forces acting on a bluff body.

In general the internal surfaces of mineshafts are reasonably smooth and for such surfaces the velocity profile of fully developed turbulent flow in the shaft is dependent on the Reynolds number[7]. In a dynamic scale model of such a mineshaft the flow will occur at a very much reduced duct Reynolds number and the velocity distribution will consequently have a more pronounced parabolic

shape (refer to Figure 65). For ducts with a reasonably high wall roughness it is possible to obtain a flatter velocity profile by decreasing the wall roughness[7]. However, in the case of a scale model mineshaft which already has a smooth internal surface it will not be possible to improve the velocity profile shape which will then not be simulated geometrically to scale in the model. It therefore became necessary to study the possible effect which this dissimilarity may have on the behaviour of a dynamic scale model.

5.5.2 Experimental procedure. Using the usual apparatus described in section 5.3 the coefficients of aerodynamic side force acting on the model conveyance were determined for different velocity profiles. The velocity profiles were changed by changing the length of the duct upstream of the model conveyance. At a distance less than about twenty diameters from the duct inlet the flow is not yet fully developed, with the result that the central portion of the velocity profile in the duct still has a flat shape. Thus changing the length of duct upstream of the conveyance provided a convenient method for changing the velocity profile shape.

Velocity profile shapes were determined by removing the conveyance from the duct and then carrying out careful pitot tube traverses at the location of the model conveyance. The duct static pressure, required in order to determine the dynamic head during the pitot traverse, was obtained from four static hole tappings in the duct at the location of the model conveyance.

5.5.3 Results and conclusion. The velocity distribution profiles for two different duct lengths, namely 6 feet and 45 feet, are shown in Figure 73. The velocity distribution for each profile is plotted as a fraction of its peak value so that comparison of the two profiles may be facilitated.

Figure 74 illustrates the variation of the aerodynamic force coefficients with duct Reynolds number obtained for the flat and the

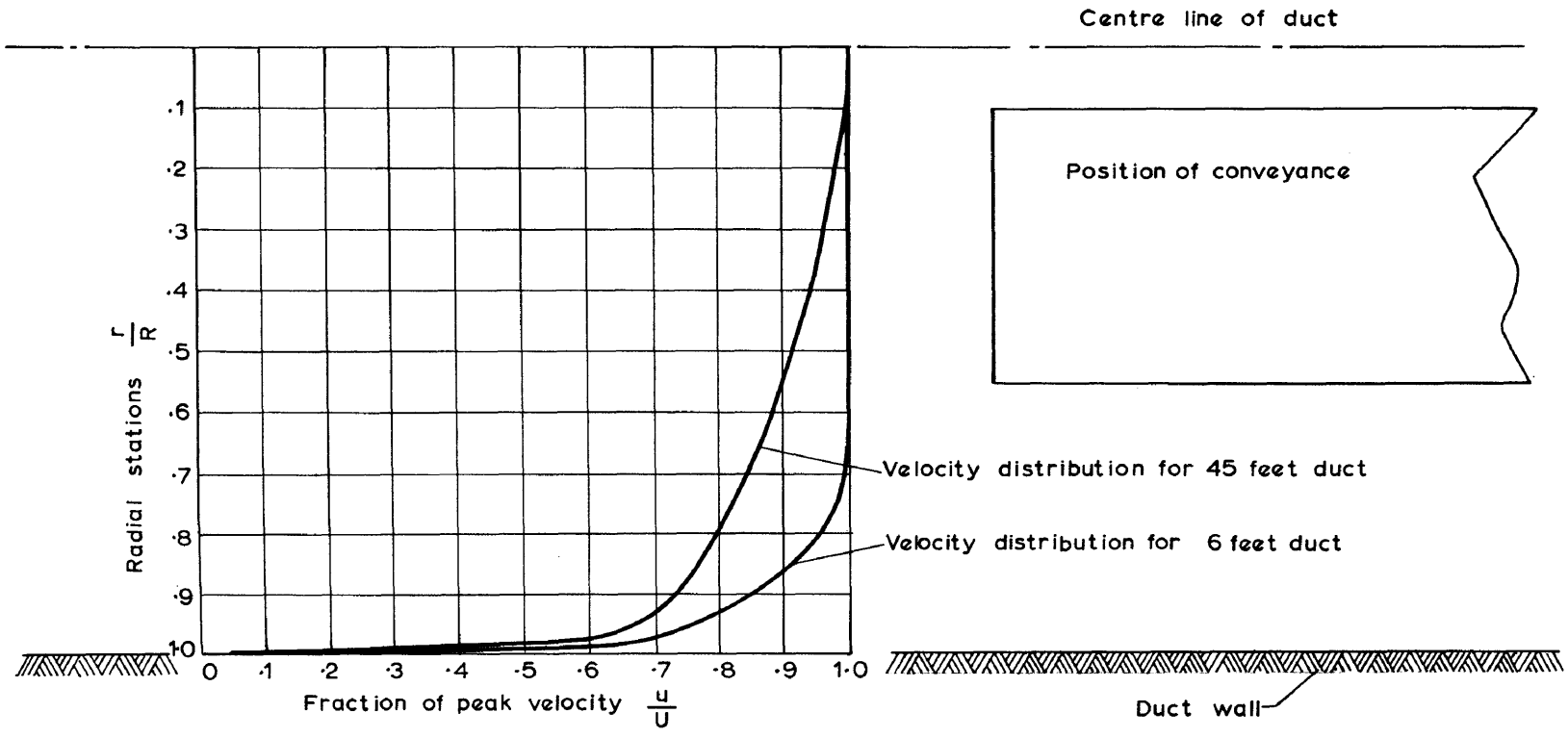

FIGURE 73

Velocity distributions in ducts with 6 feet and 45 feet upstream lengths

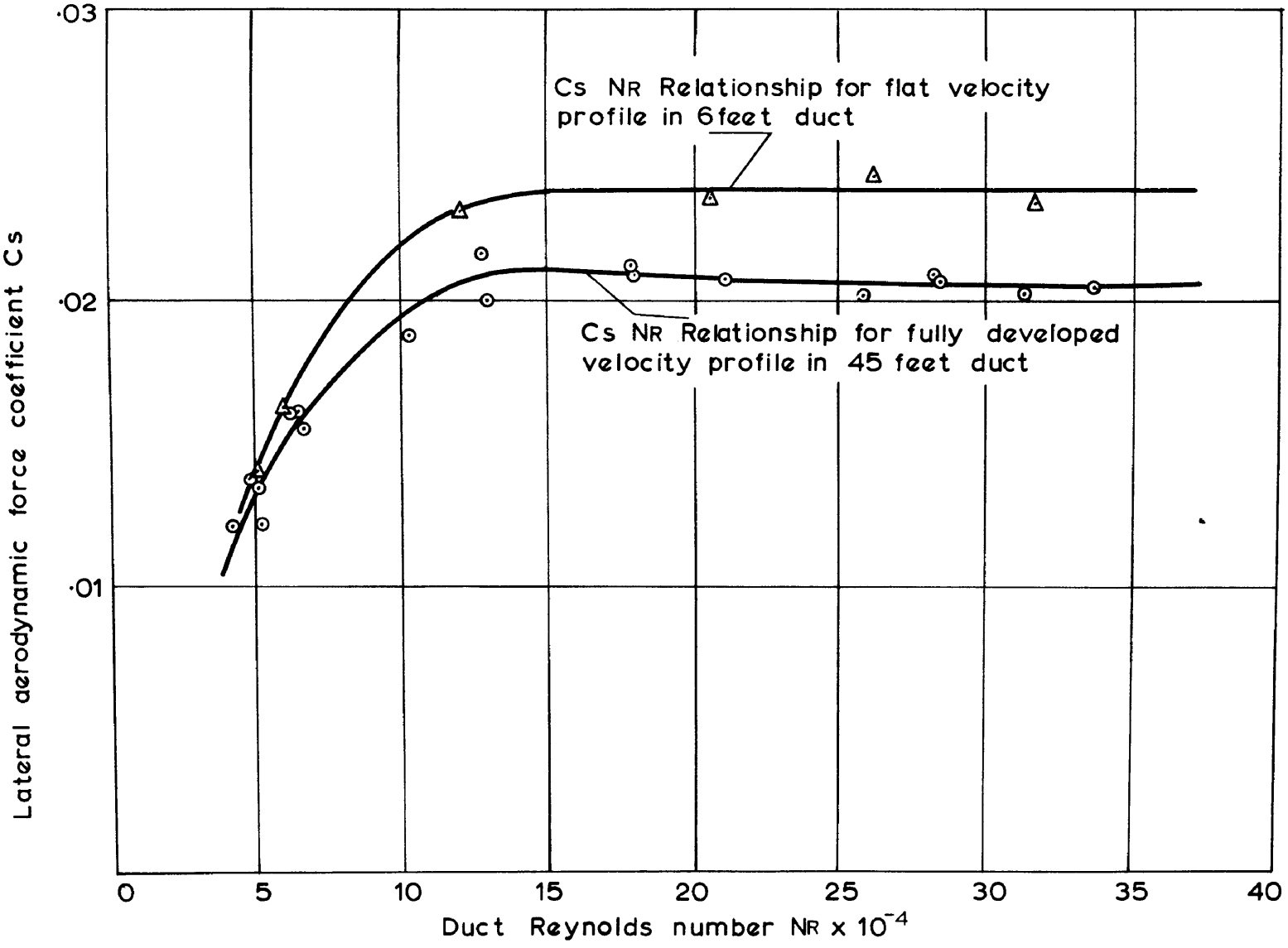

FIGURE 74

The effect of velocity profile shape on the aerodynamic force coefficient over a range of Reynolds numbers

curved air velocity distributions. These curves show clearly that the coefficient of the lateral aerodynamic force acting on a conveyance is increased when the velocity profile becomes flatter. This result was expected since in the case of a flat velocity profile the increase in air velocity between the conveyance and duct wall will be greater than for a velocity profile in which the velocity progressively diminishes towards the duct wall.

Furthermore, the graphs in Figure 74 show that a change in the velocity profile shape in no way alters the Reynolds number effect discussed in sections 5.3 and 5.4. The threshold Reynolds number below which the coefficient of lateral aerodynamic force rapidly decreases occurs at more or less the same value for both of the two velocity profiles.

The two velocity profiles used in this test differed widely from each other. In practice the velocity distribution in a fullscale mineshaft and in its dynamic scale model will both be typical fully developed turbulent flow velocity distributions. Referring to Figure 65 the velocity distribution for a Reynolds number of 2.0×10^6 is representative of fullscale mineshaft ventilation air flow. In a 1/20 scale model the velocity distribution will change approximately to the profile drawn for a Reynolds number of 2.3×10^4. Such dissimilarities in the velocity profiles of model mineshafts and their fullscale prototypes should not seriously affect the magnitude of the coefficients of lateral aerodynamic forces acting on the models. However, before performing any tests on a particular mineshaft model, it will be necessary to compare the velocity distributions in the fullscale and model mineshafts in order to establish whether the dissimilarity is not excessive.

6. THE APPLICATION OF DYNAMIC SCALE MODEL TESTING TO ROPE-GUIDE MINESHAFT INSTALLATIONS.

6.1 General.

The theoretical and experimental work described in the preceding chapters have shown that scale model investigations of rope-guide

mineshaft installation problems are feasible. However, as experience was gained with such model investigations, may defects in the model installations, equipment and testing procedures came to light. Owing to the time and expense involved, the rectification of many of these defects could not be considered. However, it is felt that most of the major difficulties encountered could be entirely obviated in any future work on rope-guide model installations. This chapter deals with recommendations for improved models, ancillary equipment and testing procedures.

Two types of models may be employed in the investigation of rope-guide mineshaft installation problems. Firstly, a stationary aerodynamic scale model of conveyance in a model shaft may be used for investigating aerodynamic forces and flow patterns occurring in an installation. Secondly, a fully dynamic scale model of a rope-guide installation may be used to investigate the dynamic behaviour of the system of conveyances, guide ropes, hoist ropes and ventilation air flow. These two types of models will now be considered separately.

6.2 Stationary aerodynamic scale models.

6.2.1 The significance of stationary aerodynamic models.

In a stationary aerodynamic scale model the lateral movement of a conveyance in a mineshaft and the dynamic effect of guide and hoist ropes are ignored. The stationary model conveyance, situated in a model shaft through which air is allowed to flow, merely allows the measurement of lateral aerodynamic forces and the study of flow patterns in the shaft.

A stationary aerodynamic mineshaft model is essential for the investigation of the nature of any Reynolds number effects which may be present in such a model installation. As pointed out in Chapter 5, no fully dynamic model tests should be attempted until the value of a shaft Reynolds number above which no serious scale effects are prevelant, has been established. Such Reynolds number tests can only be carried out satisfactorily with a stationary aerodynamic mineshaft model. Facilities for such aero-

dynamic model testing should therefore be regarded as essential ancillary equipment for any fully dynamic model rope-guide test rig.

Apart from its use in preliminary Reynolds number tests, a stationary aerodynamic model installation may also be of considerable value in solving certain aerodynamic problems concerned with the design of rope-guide conveyances and mineshafts. For example the design of the outer shape of a rope-guided conveyance could be readily achieved with stationary aerodynamic tests. In Chapter 4 it has been established that the major cause for lateral conveyance deflections is lateral aerodynamic forces. In order to eliminate such lateral forces, it is merely necessary to suitably modify the outer aerodynamic shape of the conveyance and such modifications may be studied conveniently with a stationary aerodynamic model of the conveyance.

As pointed out in Chapter 5, it is not possible to obtain a true representation of the air flow around a model conveyance which does not move relative to the model mineshaft walls. Profiles of air velocities relative to a moving conveyance in a shaft may be approximated by installing gauze screens upstream of the stationary model conveyance but velocity gradients on the shaft wall can never be correctly simulated. With these limitations in mind it is clear that tests on stationary aerodynamic models should only be regarded as supplementary to true dynamic scale model testing.

6.2.2 Suggested horizontal mineshaft wind tunnel.

Figure 75 depicts the general lay-out of a small wind tunnel which will be suitable for tests on stationary aerodynamic models of rope-guided conveyances. A 2 foot diameter duct with an inlet flare some 40 feet upstream of the test section and a centrifugal blower approximately 15 feet downstream of the test section should give satisfactory flow conditions. A honeycomb should be installed in the inlet and facilities for installing 4 to 5 gauze screens should be provided. Control of the rate of air flow could best be effected by means of a butterfly valve installed in a diffuser on the blower outlet. Flow measurement should be effected by

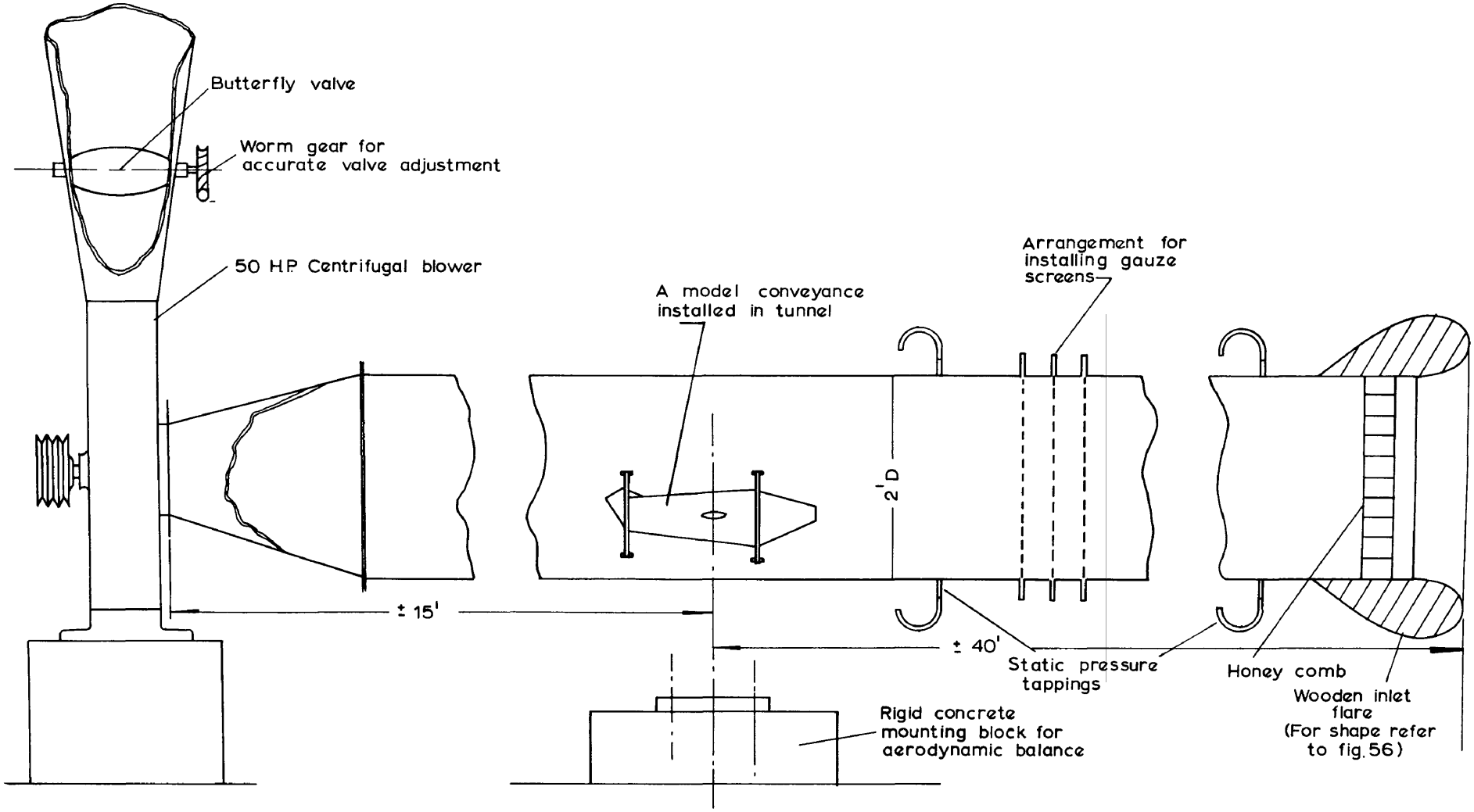

FIGURE 75

Schematic layout for a horizontal mineshaft windtunnel

suitably calibrating the static pressure drop over the inlet flare against the rate of flow in the tunnel[9]. The profile of a suitable inlet flare is given in Figure 56.

Although satisfactory results were obtained with the mechanical balance for measuring lateral aerodynamic forces as described in Chapter 5 (refer to Figure 58), it is thought that a compact strain-gauge balance as depicted schematically in Figure 76, will be more convenient. Such a strain-gauge balance should be rigidly mounted on its own foundation and should be isolated from the duct to prevent vibrations from influencing strain-gauge readings. An inherent disadvantage of this type of strain-gauge balance as opposed to the null-point balance described in Chapter 5, is the absence of any mechanical damping arrangement. During operation it is possible to encounter troublesome resonant oscillations in certain airspeed ranges. Such resonant oscillations can only be obviated by changing some component masses in the balance or by changing the stiffness of some of the elastic hinges. The deflection of this type of balance presents another disadvantage.

6.3 Complete dynamic rope-guide models.

6.3.1 The significance of dynamic scale models.

In complicated rope-guide installation problems where both the dynamics of the ropes and aerodynamic forces on conveyances play a part, only a complete dynamic scale model can be used effectively to obtain a solution. As indicated in section 6.2 it will always be necessary to establish the extent of Reynolds number effects in any particular mineshaft model before results from a fully dynamic test may be interpreted with confidence. When such Reynolds number effects are present, this does not entirely preclude any dynamic testing. When the model is operated below its threshold Reynolds number (refer to Chapter 5) useful qualitative results may nevertheless be obtained and, with careful circumspection, quantitative predictions regarding the behaviour of the system may be made.

6.3.2 Suggested vertical mineshaft wind tunnel.

The vertical mineshaft wind tunnel, described in Chapter 4, proved

..... 230

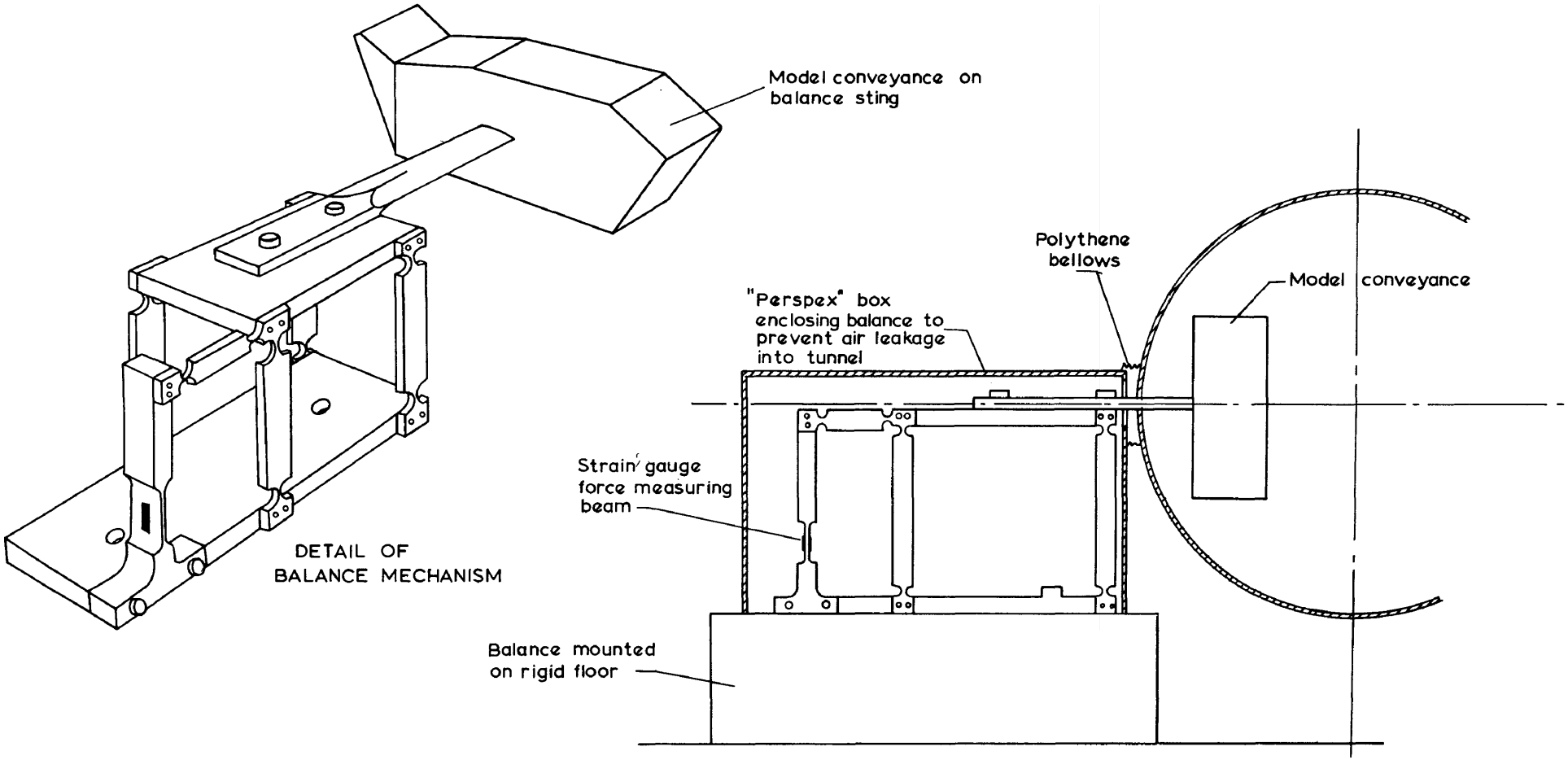

FIGURE 76

Aerodynamic strain gauge balance

adequate for the successful conduction of the correlation tests on the Durban Roodepoort Deep rope-guide model. However, during the course of these tests, many inherent defects of this apparatus came to light and experience gained with these investigations now enables the author to put forward suggestions for a much improved apparatus.

The main source of errors in all previous investigations may be attributed to the non-rigidity of the steel tower used to support the mineshaft model. Experience has shown that any swaying or vibrations in the support of the model may completely spoil test results. In order to obtain a rigid model support the obvious solution is to install the model in a pit similar to the 80 feet concrete lined pit described in Chapter 3. Figure 77 gives the general lay-out of such a vertical mineshaft wind tunnel with facilities for varying the air density. However, the costs involved in the sinking and lining of a suitable pit which will accommodate all types of mineshaft models are rather prohibitive. It is now suggested that use should be made of one of the disused mineshafts which are available in the Witwatersrand Area. In such a shaft the length of the model will present no problem and models of 10,000 feet rope-guide installations, now under consideration by some of the mining authorities, could be readily accommodated in a 500 feet deep test shaft.

Figure 78 depicts the general lay-out of such a 500 feet deep shaft which will be suitable to accommodate models of very great length. It will be necessary to install a platform which could be hoisted to any arbitrary level along the 500 feet working depth in order to enable the installation of model shafts. It is suggested that this working platform be steadied by three guide ropes, each tensioned by means of a 10 ton tensioning weight. This working platform should be equipped with steadying beams which may be pressed against the shaft wall to prevent the platform from swaying while suspended at any particular level in the shaft. A second platform which can be installed on fixed brackets, spaced at some 10 feet intervals along the 500 feet shaft length, will be useful

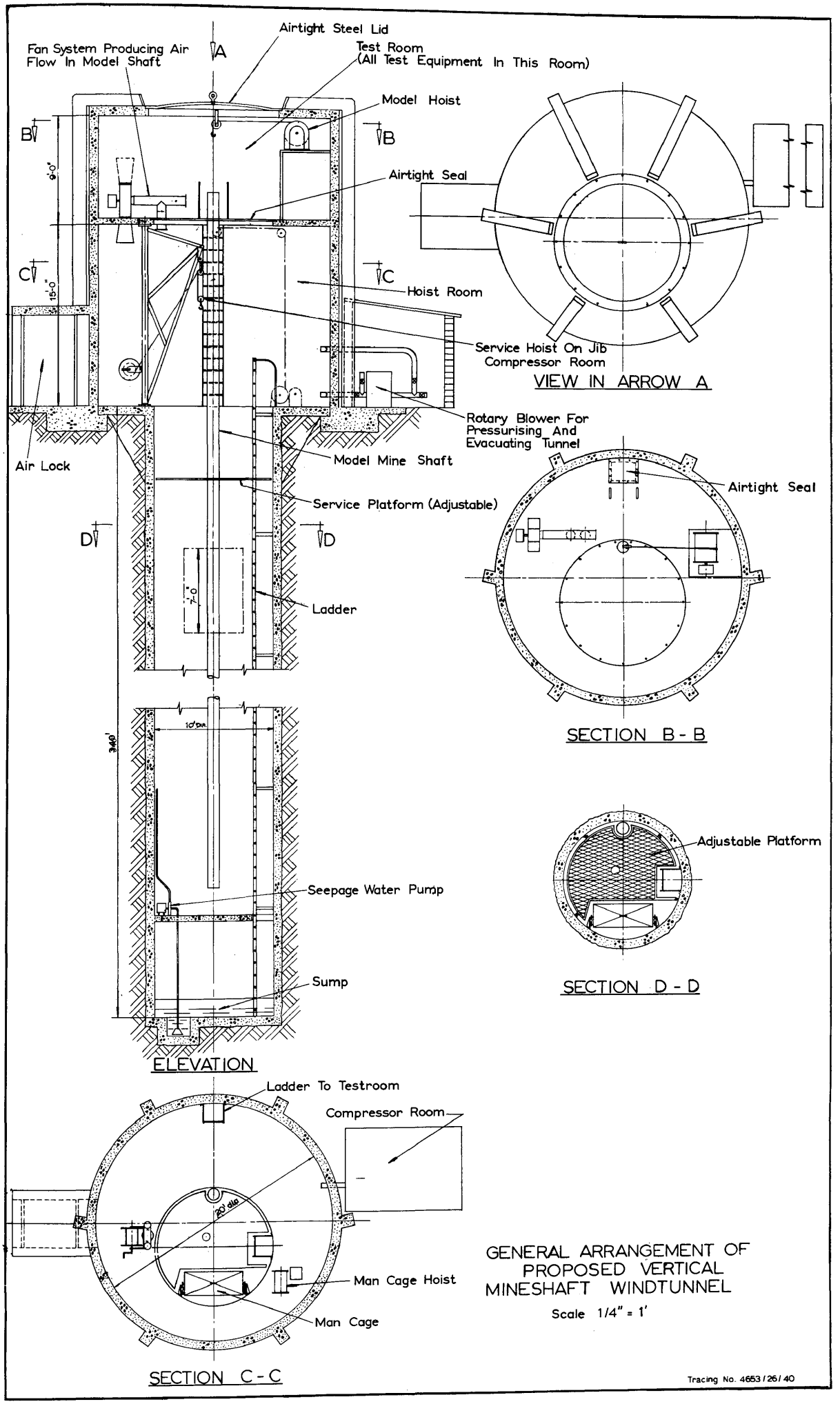

FIGURE 77

General arrangement of a proposed vertical mineshaft windtunnel

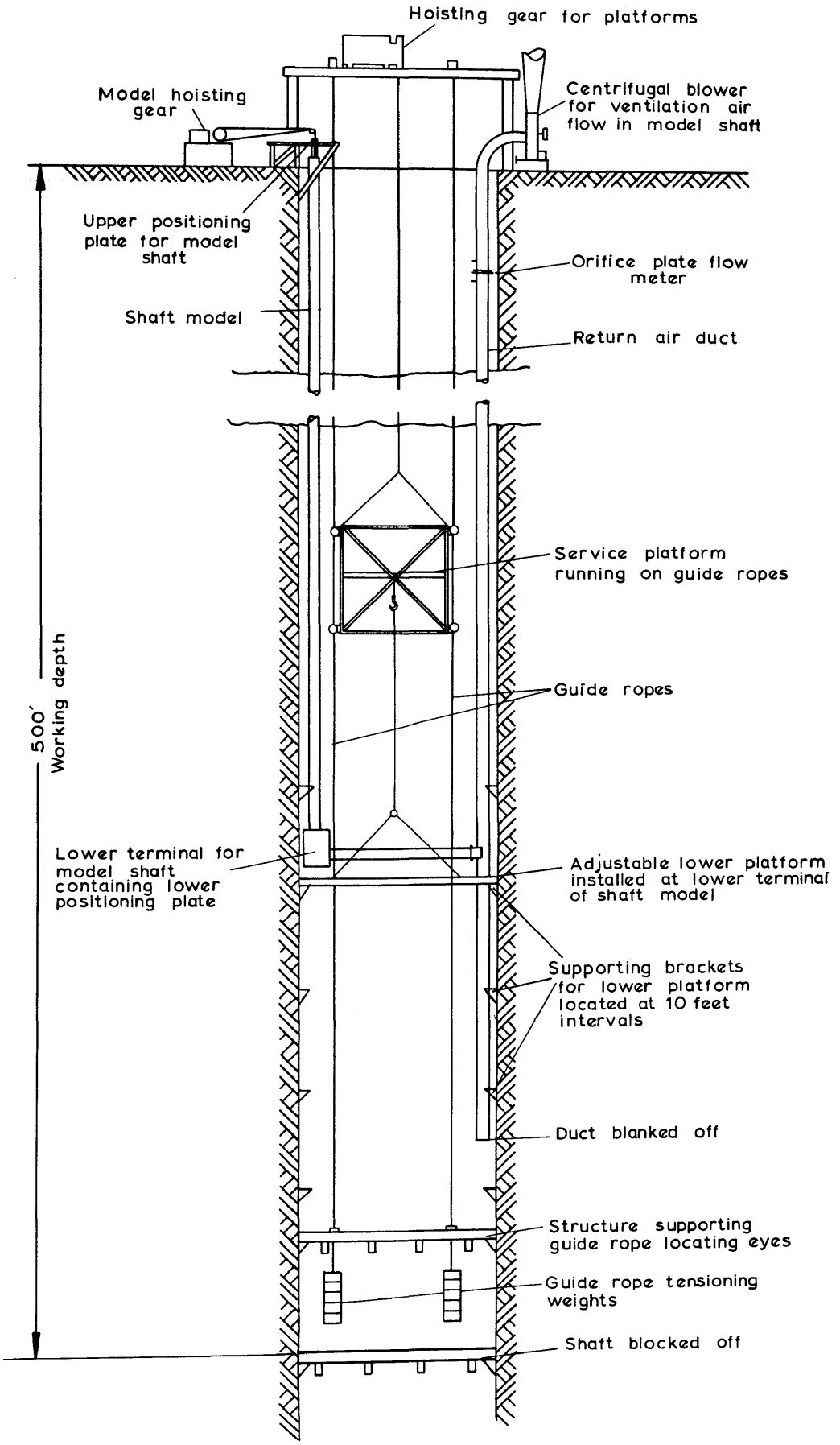

FIGURE 78

Proposed layout for a vertical mineshaft windtunnel using

at the lower extremity of any particular model shaft.

Permanent mounting brackets should be fixed along the shaft wall to support mineshaft models of any length and diameter (refer to section 6.3.3). The model winding gear, control and recording equipment and all other instrumentation should be accommodated on ground level at the upper extremity of the mineshaft model.

6.3.3 Model shaft ducting. The electro-magnetic recording of lateral conveyance deflection, described in Chapter 4, is regarded as the most satisfactory method. However, as pointed out in Chapter 4, the model shaft ducting, when constructed from a magnetic material, causes very troublesome interference effects in the recording system. It is suggested that ducting for model shafts be constructed from aluminium sheeting which will have the added advantage of providing light duct sections which may be easily handled and installed. Brass bolts and nuts should be used in the entire structure of the model shaft and its supports.

The duct should be constructed in some ten or twelve feet lengths and each section should consist of two halves which will facilitate the installation of internal shaft structures and ropes in the model. The general mode of construction and installation of these duct sections is illustrated in Figure 79. Figure 80 depicts an adjustable mounting bracket suitable for fixing the duct sections to the shaft wall. Portion A of this bracket should be fixed permanently to the shaft wall and will be suitable for all models. Portion B of each bracket must be manufactured for each particular model diameter. These brackets should also be manufactured from aluminium sheeting to prevent any possible interference on electromagnetic recording systems in the model shaft.

The exact alignment of the model shaft sections is extremely important. This can be effected conveniently by aligning section B of each bracket by means of a line and plumb-bob. After all these brackets have been installed and aligned, the duct section may then be installed without further alignment.

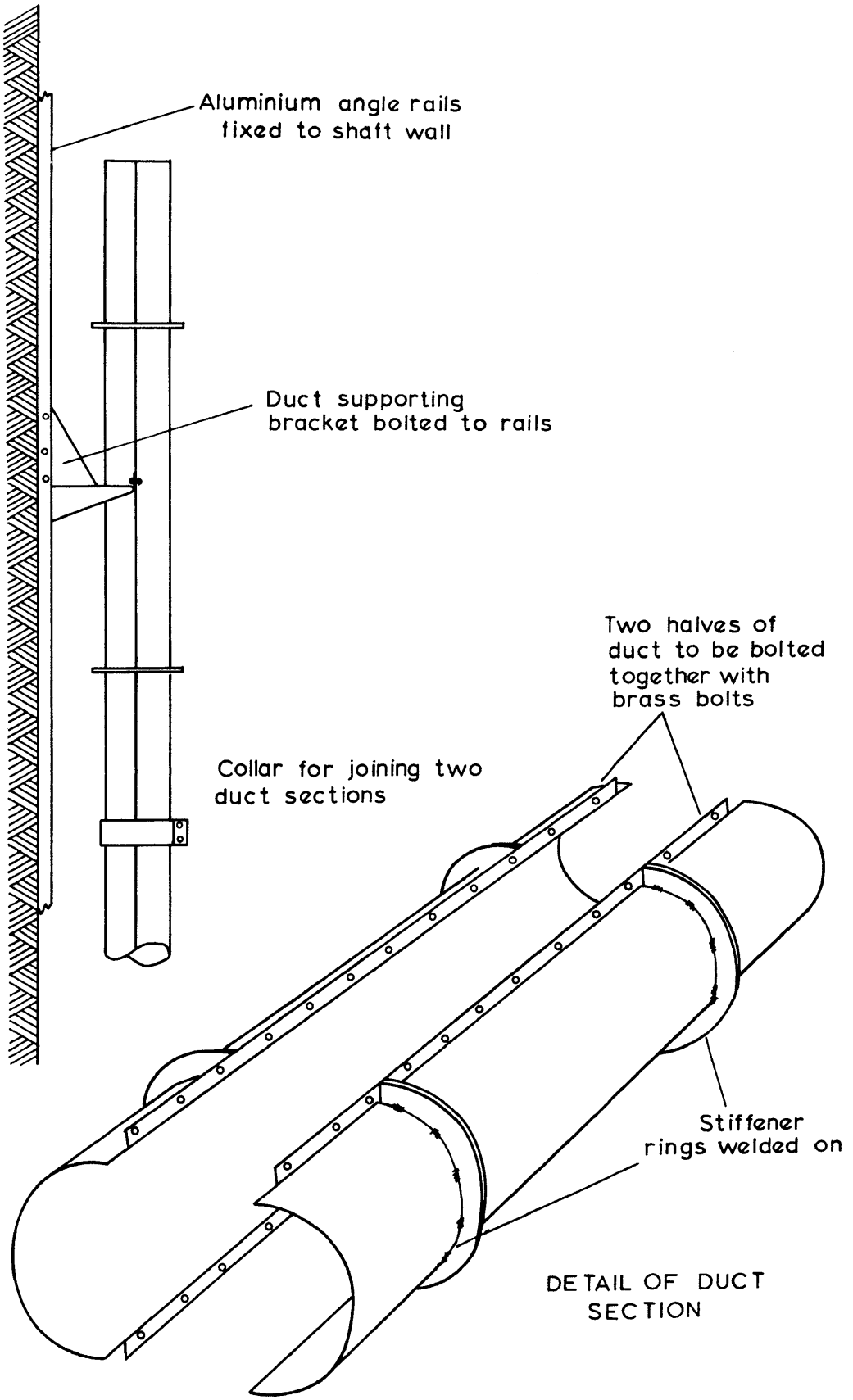

FIGURE 79

Proposed method of constructing aluminium model shaft sections

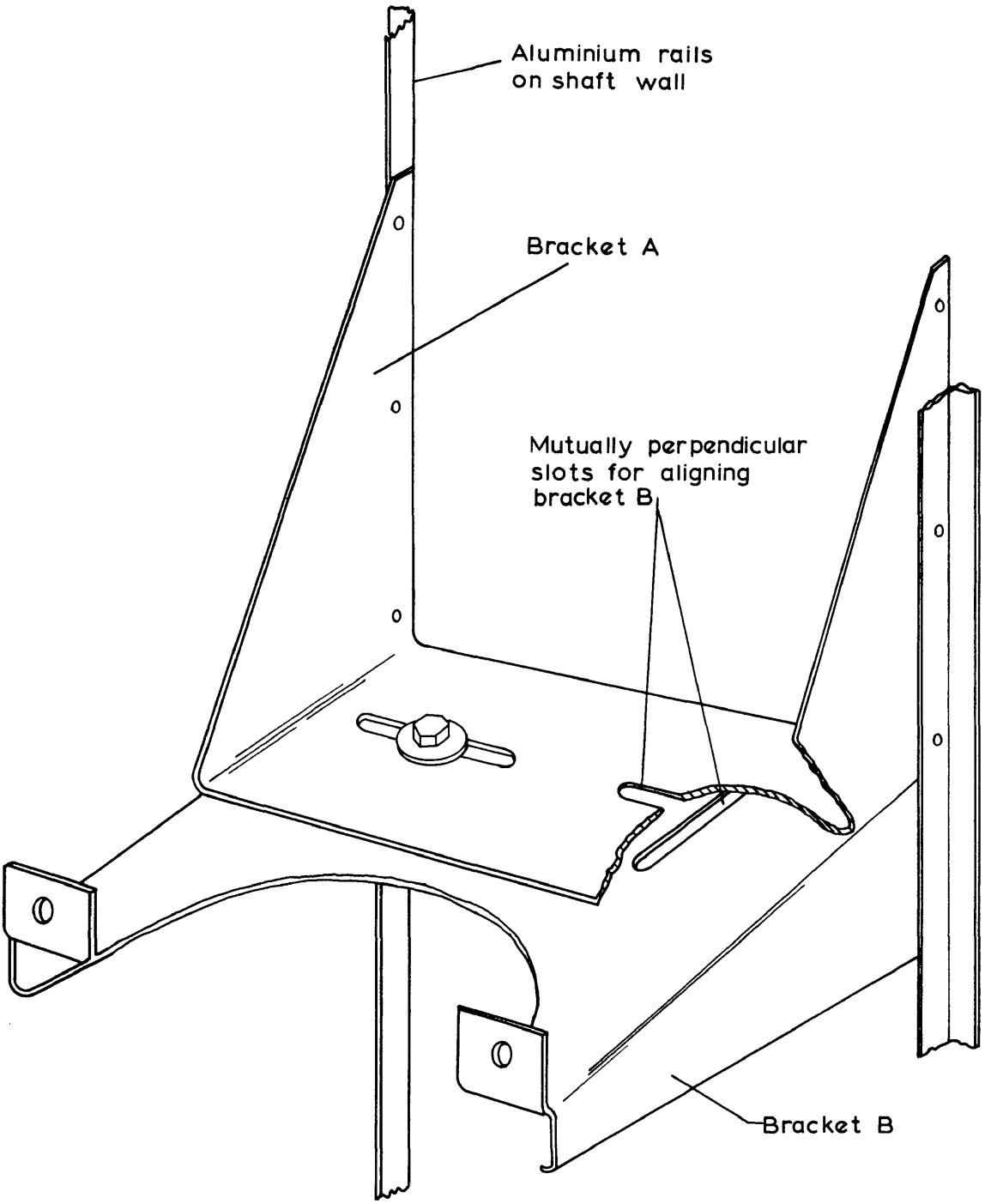

FIGURE 80

Proposed aluminium brackets for supporting model mine shaft

6.3.4 Model guide and hoist ropes. The guide ropes are the most important components in a model rope-guide mineshaft installation. If model guide ropes are not dynamically representative of its fullscale prototype, the behaviour of the model is found to be inaccurate.

Model guide ropes are only tensioned to a few pounds at the most and this tensioning will never be sufficient to remove coils in a rope. It will therefore always be necessary to straighten out guide ropes before use. The ropes used in the Durban Roodepoort Deep correlation model were straightened out by tensioning each rope with some 100 pounds and then twisting the rope in a direction opposite to the natural coils occurring in the rope.

Figure 81 illustrates another method which, when carefully applied, should ensure absolutely straight guide ropes. In this suggested method the guide rope unwinds from a drum through a high frequency electric induction heating coil while being tensioned to some 300 pounds by means of a tensioning weight. A simple pendulum and clockwork mechanism, indicated in Figure 81, may be used to ensure that the rope unwinds and passes through the heating coil at a suitable rate. When suitably adjusted, the wire rope will be heated locally to its annealing temperature and the tensioning weight will ensure that the rope is straightened out properly. This equipment for straightening ropes should be installed in the vertical mineshaft wind tunnel adjacent to the actual model shaft in which the guide rope is to be installed. The guide rope can then unwind from its drum down into the shaft of the vertical mineshaft wind tunnel and may be suspended in its position in the model installation immediately after it has been straightened.

It is recommended that the linear scale factor for any model should always be deduced from knowledge of the weight of the most suitable guide ropes available. This will ensure that the model is dynamically to scale as far as the guide ropes are concerned. A considerable range of small wire rope sizes are available and wire rope manufacturers can manufacture ropes approximately to some predetermined weight per foot.

..... 238

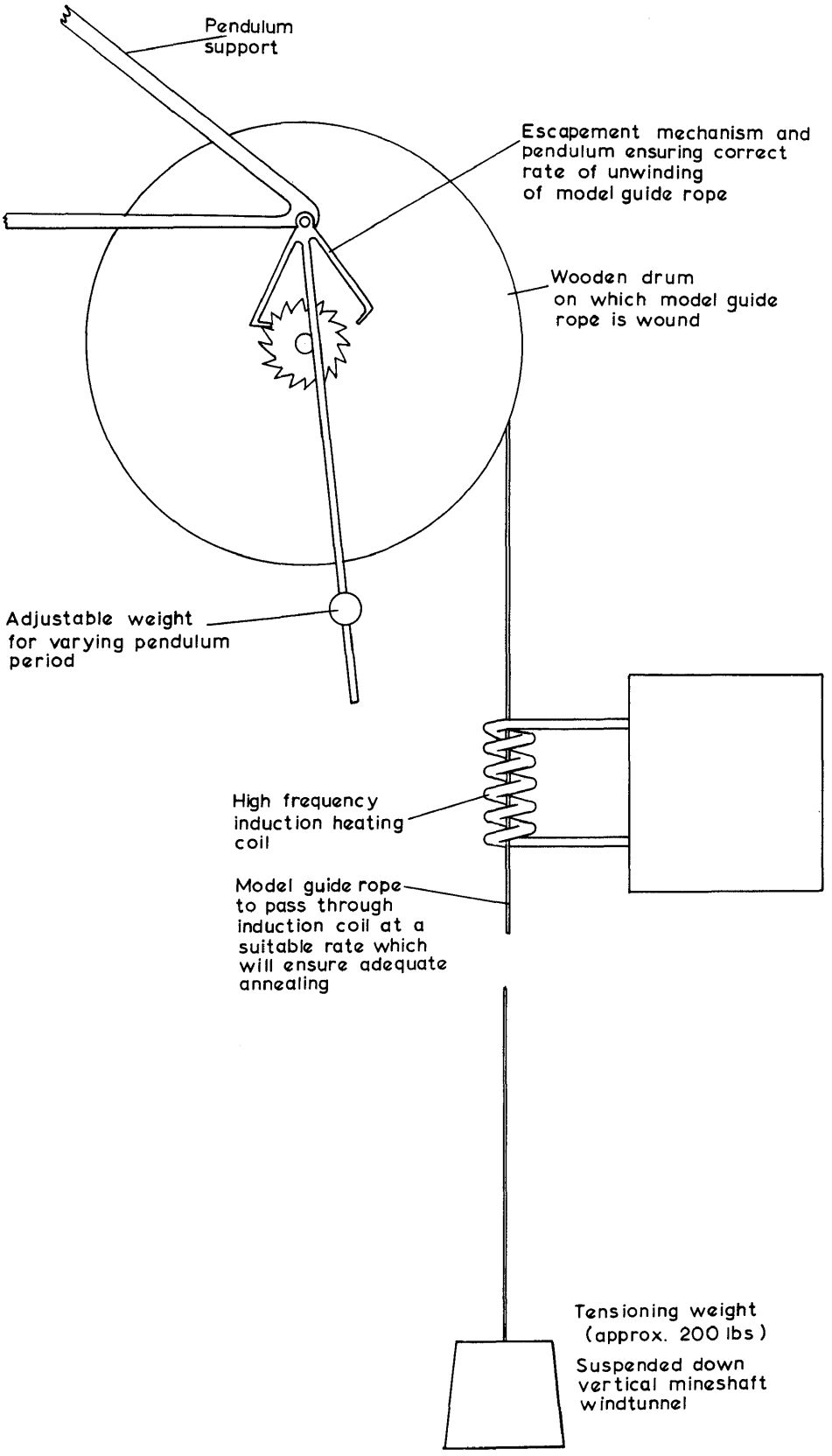

FIGURE 81

Apparatus for straightening out model guide ropes by annealing

Model guide ropes may also be constructed from copper or brass wire. Excellent results were obtained with the copper wire guide ropes used in the Durban Roodepoort Deep correlation model. Copper ropes are more flexible than steel ropes and may also be straightened out more readily.

The exact simulation of hoist ropes are generally not so critical, since the total weight of hoist ropes in a shaft is usually very much less than the total weight of guide ropes. It will usually be possible to select a suitable hoist rope to fit any set of guide ropes.

Since hoist ropes always pass over pulleys and over the winding drum they should always be constructed from steel wire to avoid breakage and wear. It will also be necessary to attach hoist ropes to conveyances by means of anti-spin bearings. Most full-scale hoist ropes are of the "non-spin" type in which the torque, tending to rotate the conveyance, is reduced to a minimum.

When mounting model guide ropes and hoist ropes inside a model shaft, the exact positioning of these ropes is very important. It is recommended that positioning plates, illustrated in Figure 82 should be used at the top and the bottom of a model rope-guide installation. These positioning plates may then also be conveniently employed for locating the indicator cables used for recording lateral movements of conveyances as described in Chapter 4.

6.3.5 Model conveyances. In all previous investigations dynamic scale models of rope-guide conveyances were constructed from brass or steel sheet. With this construction the mass distribution in the model and its moment of inertia could be simulated exactly. However, such models are costly and are difficult to construct accurately. It is thought that models could be constructed much more conveniently from some machinable material such as perspex. Figure 83 illustrates the suggested method of construction of such a perspex model. The walls of the

..... 240

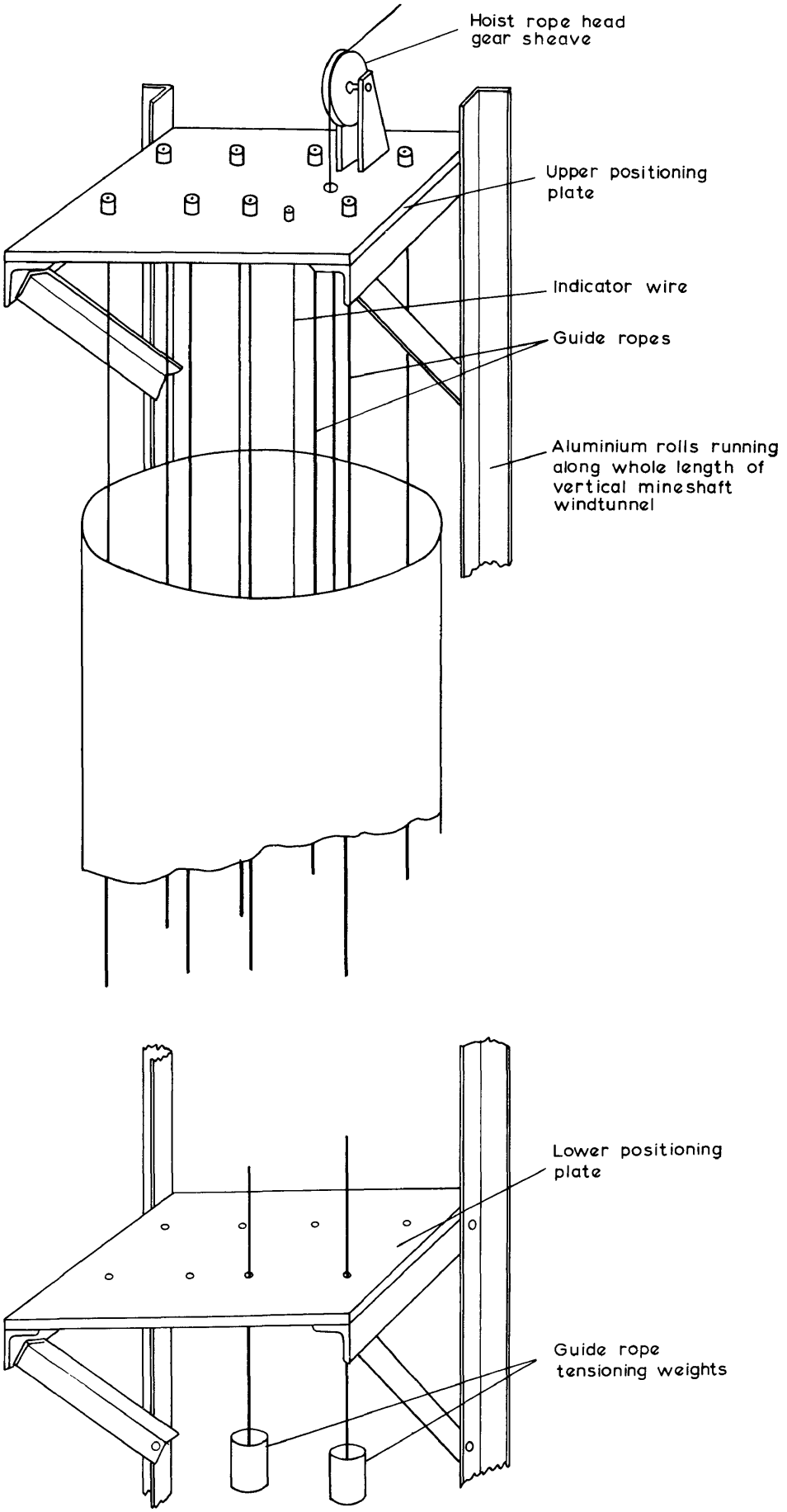

FIGURE 82

The upper and lower terminals of a model rope-guide installation

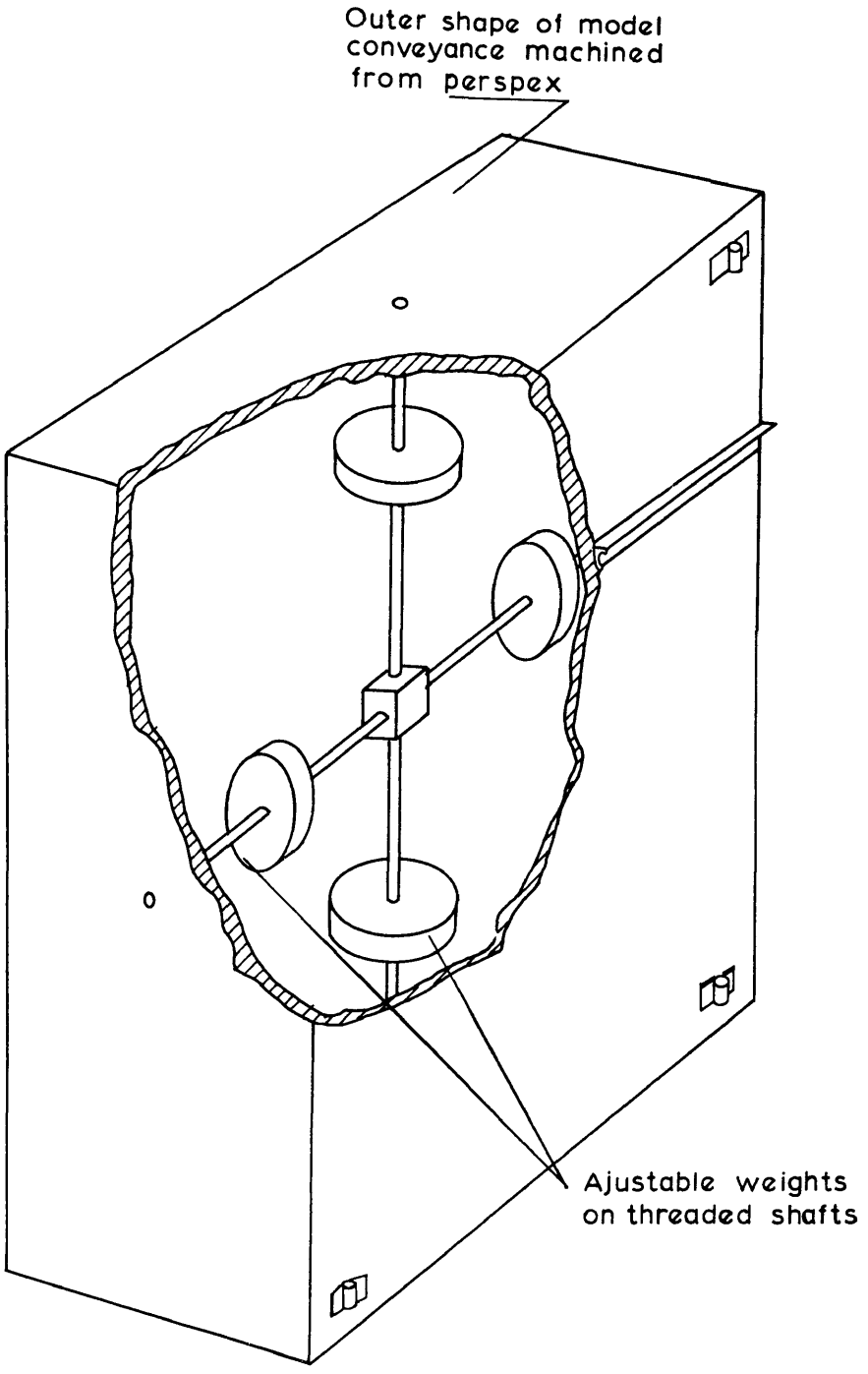

FIGURE 83

Model conveyance with adjustable moment of inertia weights

model should be constructed from thick perspex sheets and the outer surfaces of the model conveyance may then be accurately machined to its correct shape. Fittings on the outer surfaces, such as angle stiffeners, brackets etc. may then be glued in position. In such a model the guide rope sliding bearings may be spaced and aligned with great accuracy and should ensure that the model conveyance is suspended correctly.

As described in Chapter 4, it was found that normal rope-guide conveyances show little or no tendency to pitch or yaw and only execute lateral translatory movements during hoisting. Under these circumstances the exact position of the centre of gravity and the magnitudes of the moments of inertia of the conveyance do not affect its dynamic behaviour. In such models it will therefore not be necessary to simulate moments of inertias correctly to scale. It will merely be necessary to represent the overall mass of the conveyance correctly and in a perspex model this may be achieved by placing lead or sand loads inside the model. If it is desired to obtain the correct moments of inertias and centre of gravity position in a model, this may be readily achieved by six masses which are adjustable along the three axes of the model. This system is illustrated in Figure 83.

6.3.6 Control of air flow.

In the vertical mineshaft wind tunnel described in Chapter 4, air flow was induced in a model mineshaft by either sucking air from or blowing air into the sealed pit. When using an abandoned mineshaft as a vertical mineshaft wind tunnel, this method will most probably not be plausible. It is suggested that a permanent air duct of some 18 inches diameter should be installed in the shaft along the full working depth of 500 feet. Facilities for tapping off air at regular invervals along this duct should be provided. The lower extremity of a model mineshaft of any length may then be connected to this return air duct in a manner illustrated in Figure 84. Measurement of the rate of air flow could be obtained by installing an orifice or venturi flow meter in the return air duct. Upward or downward ventilation air flow in the

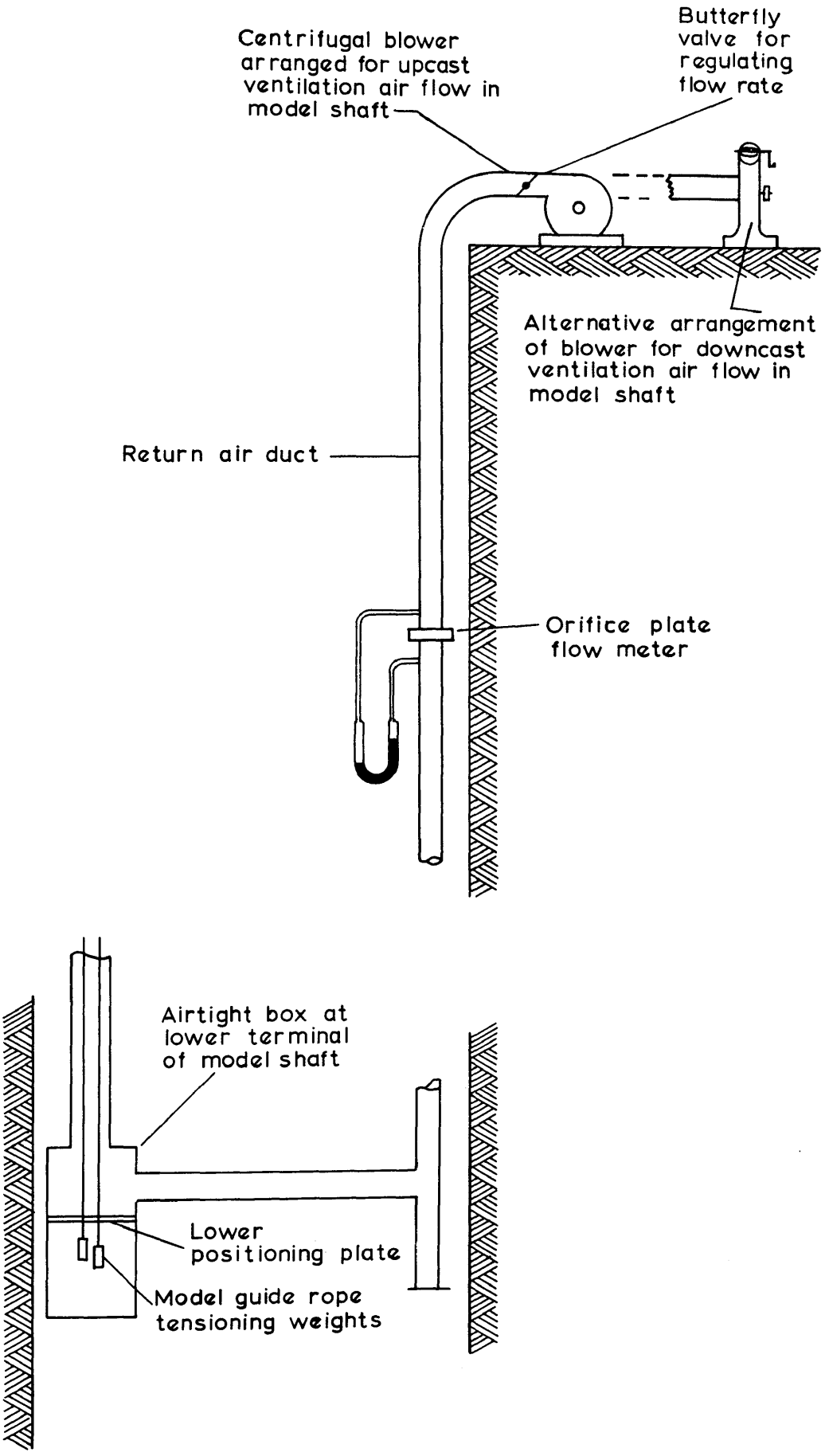

FIGURE 84

The air flow system of the proposed vertical mineshaft wind tunnel

model shaft could be obtained by respectively connnecting the outlet or inlet of the centrifugal blower to the return air duct.

6.3.7 General instrumentation and model hoisting gear. The electro-magnetic induction method used for obtaining recordings of lateral conveyance movement as described in Chapter 4 is regarded as satisfactory, provided that the induction coils are never allowed to come in close proximity to any magnetic material. It is also recommended that the model hoisting gear and the system used for simulating hoisting cycles, as described in Chapter 4, should be applied.

6.4 Development of a general design code for rope-guide installations.

6.4.1 General. Facilities for aerodynamic scale model testing of conveyances and for fully dynamic model testing of rope-guide installations will probably be utilised most frequently for investigating problems peculiar to particular mine-shaft installations. However, while carrying out such investigations, advantage should be taken of the opportunity of comparing the dynamic behaviour of various installations for the purpose of ultimately developing a general design code which may be used in future for designing fullscale rope-guide installations. For this purpose some additional measurements on fullscale rope-guide installations may also be useful.

In developing such a design code it will be necessary to assess all the important parameters which influence the design of a rope-guide installation, and to establish the relationship between such parameters, preferably in a non-dimensional form. The following preliminary survey of rope-guide installation parameters and the possible non-dimensional grouping of these parameters, may serve as a guide for future investigations which may lead to the ultimate formulation of a satisfactory general design code for rope-guide installations.

..... 245

6.4.2 Disturbing forces acting on rope-guide conveyances.

Only two significant types of disturbing forces acting on rope-guided conveyances are envisaged, namely steady lateral aerodynamic or Coriolis forces and impulsive lateral forces. The latter may be caused aerodynamically when conveyances pass each other or when a conveyance passes a station cutting from which air is flowing into the shaft. Alternatively some accidental collision between two conveyances or between a conveyance and some protrudence in the shaft may impart a lateral impulsive force to a moving conveyance.

Experience with dynamic scale models of rope-guide installations have shown that the accurate assessment of the magnitude of lateral steady and impulsive forces acting on a moving conveyance is a difficult matter. It was for this very reason that it became necessary to study lateral aerodynamic forces on conveyances in a horizontal mineshaft wind tunnel in which a stationary conveyance was installed. It is now suggested that it should not be attempted to include lateral aerodynamic force effects in those investigations in which fully dynamic rope-guide models are used to determine the relationship between the various shaft parameters. Such lateral aerodynamic force effects should be simulated by some artificial means which will enable the accurate assessment of the magnitude of these forces. For example, a steady lateral aerodynamic force may be readily simulated by the reaction on the conveyance of a small lateral air jet, fed from a miniature high pressure air vessel installed in the conveyance and forming part of the model load. A lateral impulsive force may be imparted to a moving conveyance by means of a cam projecting into the shaft and fixed to a pendulum. When the moving conveyance strikes the cam the maximum swing of the pendulum will provide an accurate measure of the magnitude of the impulse imparted to the conveyance.

By thus simulating lateral steady and impulsive forces and accurately establishing their magnitudes, it will be possible to make a thorough study of the relationships existing between such forces and the various other rope-guide installation parameters such as lateral conveyance deflections, guide rope weights,

..... 246

guide rope tensioning weights etc.

6.4.3 Various mineshaft parameters and their non-dimensional grouping. The following are regarded as the most important mineshaft parameters to be considered when designing the installation of a rope-guide system:

M	mass of conveyance in slugs
m_r	mass of guide ropes in slugs feet^{-1}
m_h	mass of hoist rope
F	lateral impulsive force in slugs feet seconds^{-1}
Y_{Fmax}	maximum lateral deflection of conveyance in feet, due to impulsive force F
A	lateral steady force in pounds
Y_{Amax}	maximum lateral deflection of conveyance in feet, due to a steady force A
T_b	tension force in pounds on the lower extremity of one guide rope
n	number of guide ropes per conveyance
H	length of guide ropes between the upper and lower points of attachment
D	shaft diameter in feet
u	hoisting speed in feet seconds^{-1}
t	time interval in seconds for a guide rope wave to travel a distance H
d	logarithmic decrement of lateral conveyance oscillations due to internal rope friction and aerodynamic damping
ρ	density of the air in the mineshaft in slugs feet^{-3}
g	acceleration due to gravity in feet seconds^{-2}.

In reference 2 mathematical analyses of lateral conveyance motion are presented for a conveyance with four guide ropes suspended in

..... 247

a shaft and subjected to steady as well as impulsive lateral forces. This analysis gives the following approximate expressions which illustrate the effect of shaft parameters on the lateral displacements of a conveyance due to steady and impulsive lateral forces.

For an impulsive force:

$$\sqrt{\frac{Mg\,m_r\,Y_{Fmax}}{0.391\,F}} = \sqrt{\frac{4\,T_b}{Mg} + 1.15} - \sqrt{\frac{4\,T_b}{Mg}}$$

For a steady force:

$$\frac{2\,m_r\,g\,Y_{Amax}}{A} = \left(\sqrt{\frac{T_b}{m_r g\,H} + 1} - \sqrt{\frac{T_b}{m_r g\,H}}\right)^2$$

Although these expressions are applicable to a conveyance which is not travelling up or down a shaft but is suspended at a particular level in the shaft these equations nevertheless suggest the most significant grouping of the shaft parameters. Thus when carrying out tests on the effect of impulsive forces on a conveyance the significant groups of parameters may be regarded as

$$\sqrt{\frac{Mg\,m_r\,Y_{Fmax}}{F}} \quad \text{and} \quad \frac{nT_b}{Mg}$$

When steady forces are considered, the significant parameter groups should be

$$\frac{m_r\,g\,Y_{Amax}}{A} \quad \text{and} \quad \frac{nT_b}{m_r g\,H}$$

These theoretically derived non-dimensional groups of variables indicate that the effect of impulsive forces is independent of the shaft depth, while steady forces cause a greater deflection in deep shafts than in shallow ones. These theoretical predictions may be readily substantiated by model tests and further non-dimensional groups of parameters may be added to the above. For example, the effect of hoisting speed may be represented by introducing the ratio $\frac{u\,t}{H}$.

This ratio of hoisting speed u to the average speed of wave

..... 248

propagation $\frac{H}{t}$ in the ropes will most probably have a significant effect on the lateral displacement of a conveyance. Test results may be conveniently presented by plotting a family of curves of say $\frac{nT_b}{Mg}$ against $\sqrt{\frac{M g m_r}{F}}\, Y_{Fmax}$ for various values of $\frac{ut}{H}$.

The theoretical analysis indicates that the effect of the hoist rope weight m_h should not be significant. However, a factor $\frac{m_h}{m_r}$ should be introduced in the experimental analysis and the effect of varying this ratio should be studied.

The shaft diameter D and the air density ρ will have a significant effect on any aerodynamic force effects on conveyances. However, if all lateral force effects are simulated artificially as recommended in section 6.4.2, D and ρ should have no further effect on the dynamic behaviour of the rope-guide system.

The effect of the logarithmic decrement d may also be investigated conveniently by model tests. The lateral swaying of conveyances may possibly be reduced by absorbing the wave energy in guide ropes near their upper and lower extremities, using hydraulic or friction dampers. Model tests will indicate to what extent the magnitude of the logarithmic decrement will influence the lateral deflection of conveyances.

6.4.4 The aerodynamic design of conveyances. In section 6.42 it was suggested that in order to develop a design code incorporating all mineshaft parameters the lateral forces acting on a conveyance should be simulated and that in such model tests all aerodynamic lateral force effects should be zero. This procedure is desirable in order to obtain reliable experimental data where the dynamic behaviour of the guide ropes and hoist ropes are concerned. However, aerodynamic lateral forces are usually the most important disturbing forces acting on rope-guided conveyances. In developing a general design code for rope-guide installations it will be necessary to give special attention to the aerodynamic design of conveyances.

Fortunately experimental work concerning aerodynamic shapes of conveyances will be much less involved than the experimental investigations concerned with rope-guide systems as a whole. Such aerodynamic investigations may be readily carried out in a horizontal mineshaft wind tunnel as described in section 6.2.

In general the aerodynamic design of a conveyance will be aimed at obtaining zero lateral aerodynamic forces on such a conveyance. Relatively simple tests will be required to obtain a design code giving the required basic shapes of various standard types of conveyances. In certain cases it may be required to obtain certain predetermined lateral aerodynamic forces on conveyance installations. For example, in the case when it is required to counteract the Coriolis force by means of a lateral aerodynamic force. Again the experimental development of standard devices, such as deflector plates, which may be attached to conveyances to produce desired lateral aerodynamic force effects, will be relatively simple.

7. THE DESIGN OF FULLSCALE ROPE-GUIDE SYSTEMS.

7.1 General.

The establishment of a design code for the development of rope-guide mineshaft installations does not fall within the scope of this report. Nevertheless, while carrying out the various investigations, some important aspects of rope-guide design have come to light. These aspects may be of assistence to engineers engaged upon the design of rope-guide installations and this information is therefore presented.

7.2 Aerodynamic design of conveyances.

The chief concern of the designer of a rope-guide system will probably be to reduce the lateral swaying of conveyances to a minimum. The results of various model investigations have clearly indicated that lateral deflection of conveyances are cause mainly by the action of lateral aerodynamic forces on these conveyances. The aerodynamic shape of a conveyance should therefore be designed in such a manner that no lateral aerodynamic forces are present for both upward and downward hoisting. The

..... 250

aerodynamic effect of the flat roof or plate, placed some distance above the conveyance, as described in Chapter 4, suggests a convenient method for controlling lateral aerodynamic forces (refer to Figure 23). During the correlation tests described in Chapter 4 it was noticed that such a plate has the tendency of forcing the conveyance towards the shaft wall nearest to the conveyance. If a conveyance has the tendency to swing away from a shaft wall, such a flat plate may be used to cancel out this tendency. The height of the plate above the conveyance and the area of the plate may be varied until the resulting aerodynamic force is zero.

A variety of deflector plates or vanes, attached to a conveyance, may be used for cancelling out lateral aerodynamic forces. Figure 85 depicts a few schemes which may be used to adjust lateral aerodynamic forces. For upward hoisting deflector vanes or plates should be installed on top of the conveyance and for downward travel lateral movement may be controlled by plates or vanes situated below the conveyance. When such a conveyance is travelling in any particular direction any vanes or plates situated in the turbulent region on the downstream side of the conveyance will cause little or no lateral forces on the conveyance.

In addition to such external devices which must be fitted to conveyances, a conveyance may simply be tilted slightly, relative to the guide rope, until no lateral aerodynamic effects are apparent. In Chapter 4 it was shown that a conveyance could be readily made to deviate either towards a shaft wall or away from it by adjusting the angle of suspension of the conveyance by only a few minutes. It must, however, be pointed out that conveyances should never be tilted within their guide ropes which will result in severe wear on the guide rope sliding bearings. Guide rope sliding bearings should be adjusted to allow for the tilt of the conveyance.

Unfortunately it is not possible to predict the aerodynamic effects of deflector plates, vanes, etc. by theoretical calculations. However, these devices may be readily tested with the use of simple stationary aerodynamic models, as described in Chapter 6. Alternatively aerodynamic tests may be carried out in the full-scale mineshaft after the conveyances have been installed. For

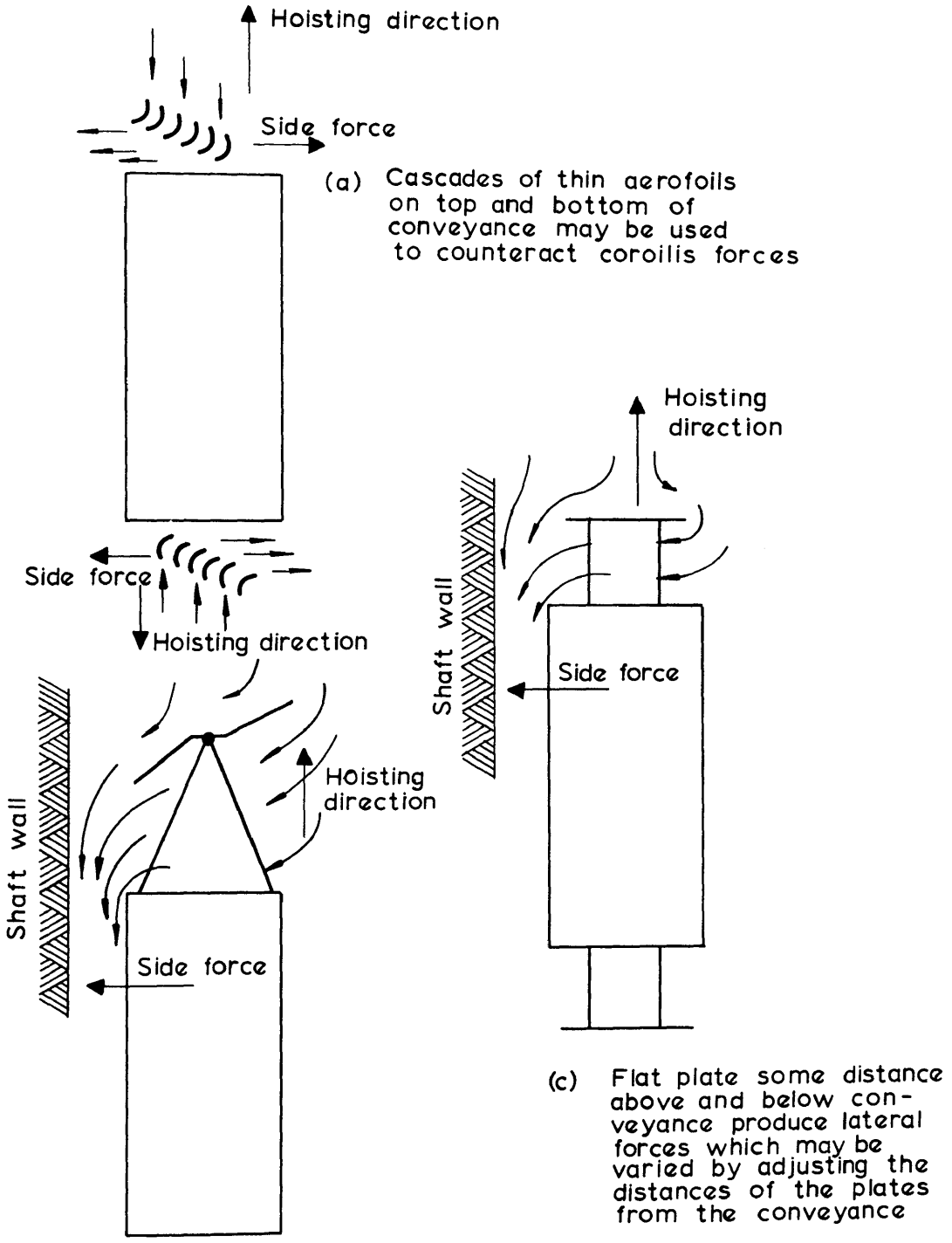

FIGURE 85

Devices for producing lateral aerodynamic forces on conveyances

example, a set of deflector vanes may be fitted to a conveyance and adjustments may then be made to these vanes during hoisting. Using a reference cable suspended down the shaft in a manner described in Chapter 4, it will be possible to determine the exact setting of the vanes so as to ensure zero lateral deflection of the conveyance. For such tests it should not be necessary to use an electro-magnetic induction system to obtain graphical traces of the lateral movement of the conveyance. If it is practical for an observer to travel on the conveyance during hoisting tests, it is possible to obtain a fairly accurate impression of lateral conveyance movement by using a ruler to measure displacements relative to the reference cable.

7.3 Aerodynamic interference between conveyances.

When two or more conveyances pass each other at speed in a shaft in which ventilation air flows, it is clear that these conveyances will cause a momentary blockage of the shaft. It is possible that rather large impulsive aerodynamic side forces may be caused to act on conveyances under such circumstances, and this has caused some concern to the designers of rope-guide installations. This effect has been investigated for the case of three conveyances passing each other simultaneously[10 and 11]. No unusual lateral deflections could be observed when these conveyances passed each other. The traces of lateral conveyance movement obtained in the Durban Roodepoort Deep correlation tests, also showed no additional deflection at the level where the conveyances passed each other. It is clear that in these installations the deflections due to the impulsive aerodynamic forces have been so small that they were completely masked by other aerodynamic effects. It appears that the rope-guide system resists impulsive forces of considerable magnitude, but gives way readily to any sustained lateral force.

It is possible that dangerous conditions may arise in a multi-conveyance shaft where clearances of only a few inches are provided between conveyances. Such conditions can only be studied satisfactorily with a dynamic scale model. However, in conventional rope-guide systems where a clearance of between one and two feet is allowed, the interference effect between conveyances passing each

..... 253

other will be negligible.

A far more serious aerodynamic interference effect is observed when two conveyances travel in the same direction, the one some distance ahead of the other. Under such circumstances the one conveyance is continuously moving in the turbulent wake of the conveyance travelling ahead of it and is subjected to buffeting and lateral disturbing forces[10]. Such conditions should always be avoided. In the case of a multi-conveyance shaft where it is unavoidable for two conveyances to travel in the same direction, such conveyances should be hoisted in compartments as far removed from each other as possible. Even then it will be advisable to carry out dynamic model tests to ascertain the magnitude of aerodynamic disturbing effects.

7.4 Effects of station cuttings.

At various levels in a mine shaft station cuttings often occur. Any air drawn from or blown into the shaft at these points may have a slight effect on the lateral movement of rope-guided conveyances, but such effects will also be of an impulsive nature and may usually be neglected. In Reference 11 a model test is described in which a rope-guide installation shaft, having a ventilation air flow rate of 600,000 cubic feet per minute, was simulated. On increasing the air draw-off through a station cutting from zero to 40% of the flow rate in the shaft, an increase in fullscale conveyance deflection of only half an inch could be noticed. In this case the conveyance passed the station cutting at a hoisting speed of 3,000 feet per minute.

7.5 The tensioning of guide ropes.

It is common practice in rope-guide mineshaft engineering to stagger the tensioning weights on guide ropes. It is argued that such unequal tensioning will prevent any resonant swaying of conveyances during hoisting. Theoretical analysis of rope-guided conveyance behaviour[2] clearly show that on imparting an impulsive force a conveyance will undergo a certain lateral displacement and will then remain in that position, while the energy required to produce this deflection will travel along the guide ropes in

..... 254

the form of a wave. The conveyance will only start swinging back when the guide rope waves, after being reflected from their extremeties, again return to the conveyance. When the guide ropes are not tensioned equally, the waves in the guide ropes will not travel at equal speeds. Reflected waves will therefore not return to the conveyance simultaneously and the conveyance will tend to twist about its vertical axis. It is thought that no advantage is gained by staggering guide rope tensioning weights. The resulting yawing motion of the conveyance might even prove to be troublesome in certain cases. In Reference 9 comparative tests on uniform and staggered guide rope tensioning weights indicated no marked difference between maximum conveyance deflections.

On increasing the tensioning weights on guide ropes, it appears that the maximum conveyance deflection reduces asymptotically towards some minimum value. In Reference 10 a test is described in which the effect of various guide rope tensioning weights on conveyance deflection is studied for a particular mineshaft installation. The results are presented graphically in Figure 86. Guide rope tensioning weights are rendered non-dimensional by dividing by the weight of the conveyance. A conveyance deflection is given as a fraction of the shaft diameter. From this diagram it appears that for this particular installation not much advantage is gained in increasing the magnitude of the sum of the rope-guide tensioning weights to beyond four times the conveyance weight.

7.6 Theoretical prediction of conveyance deflection and the influence of various parameters.

Even when rope-guided conveyances have been aerodynamically designed in such a way that no lateral aerodynamic forces will be present during hoisting, the designer of a rope-guide installation will nevertheless want to set certain criteria for the safe operation of the system. It will be necessary for the designer to estimate maximum lateral steady and impulsive forces which may be exerted on conveyances due to unforseen circumstances. Estimates of such forces may be based on past experience or may be established from tests on model or fullscale installations.

..... 255

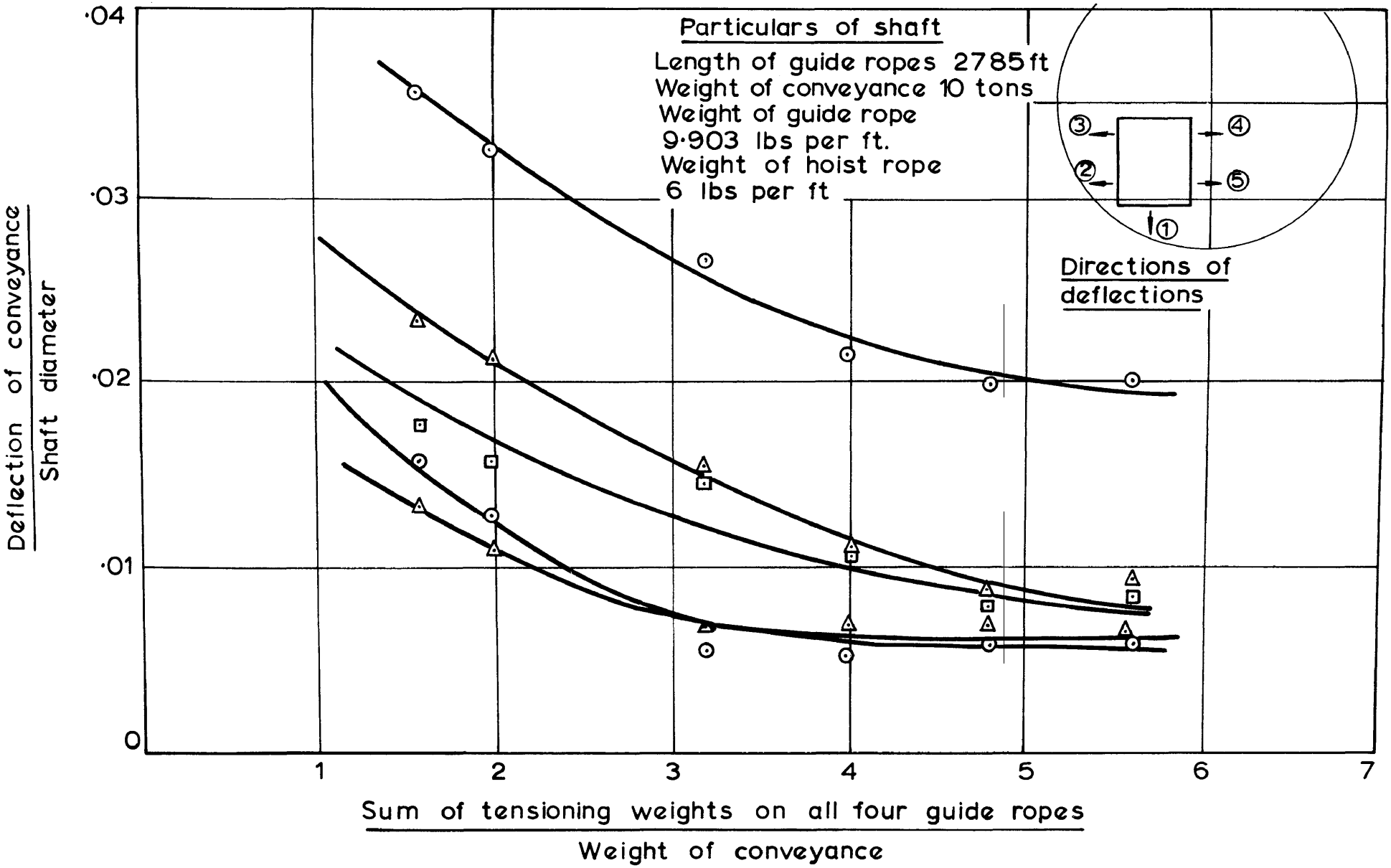

FIGURE 86

The effect of guide-rope tensioning weight on the deflection of a conveyance

Once having established the maximum values of lateral impulsive and steady forces which must be tolerated in a rope-guide installation, it will be necessary to know what maximum lateral displacement of conveyances may be expected. It will also be desirable to know to what extent such lateral deflections due to lateral impulsive and steady forces will be influenced by the various shaft parameters.

In Reference 2 approximate relationships between the various mineshaft parameters have been established theoretically for a conveyance which is suspended at some fixed level in the shaft. Figure 87(a) and 87(b) present these theoretical relationships graphically for the case of a conveyance with four guide ropes. The nomenclature applicable to these graphs is as follows:

M = mass of conveyance in slugs

m_r = mass of a guide rope in slugs feet^{-1}

Y_{Fmax} = maximum lateral deflection of conveyance in feet, due to an impulsive force F

F = lateral impulsive force in slugs feet seconds^{-1}

T_b = sum of tensioning forces on the lower extremities of guide ropes in pounds

Y_{Amax} = maximum lateral deflection of conveyance in feet, due to a steady lateral force A

A = steady lateral force on conveyance in pounds

H = length of guide ropes measured between upper and lower fastening points in feet

g = acceleration due to gravity in feet seconds^{-2}.

According to these theoretically derived relationships, it appears that the effects of impulsive forces will be equally severe in deep and shallow shafts with the same rope tensions and rope masses. Steady forces, however, will have a more pronounced effect in deep shafts than in shallow shafts. The effects of the weights of hoist ropes have been assumed to be insignificant and have been ignored in this theoretical analysis.

..... 257

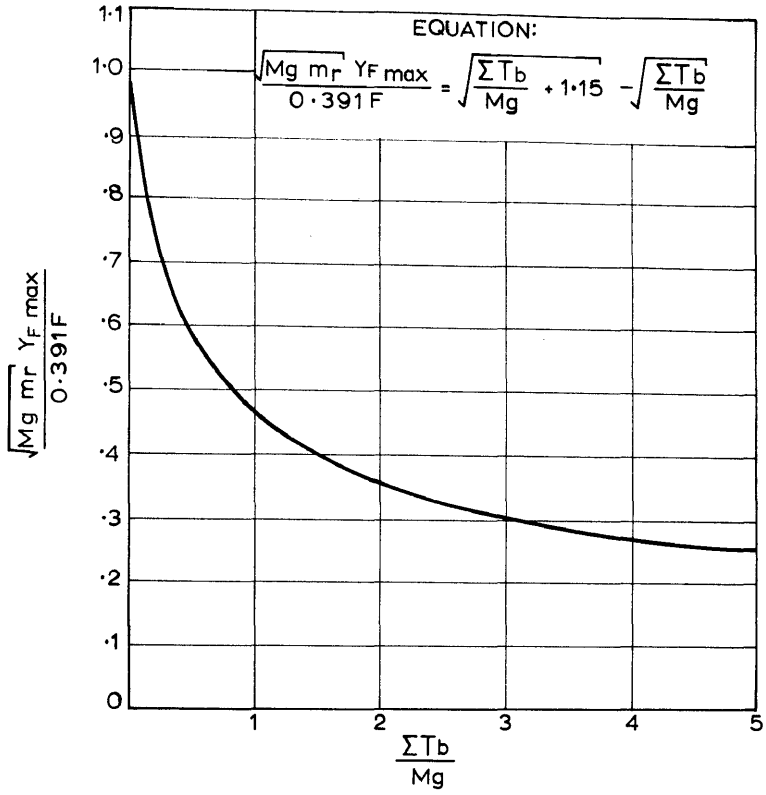

(a) A lateral impulsive force F acting on a conveyance

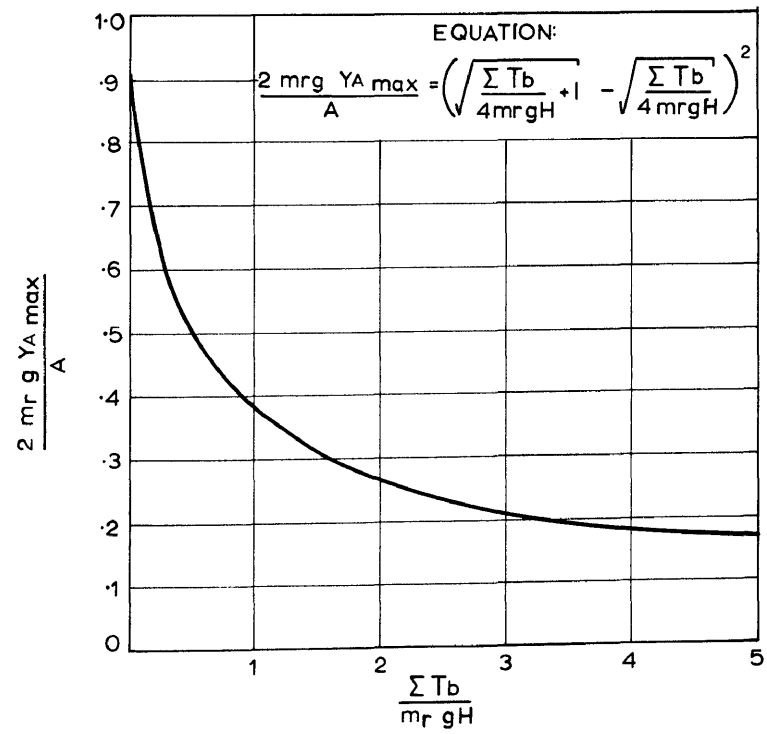

(b) A lateral steady force A acting on a conveyance

FIGURE 87

Approximate lateral displacements of a stationary conveyance due to impulsive and steady forces, given in terms of the shaft parameters M, m_r and ΣTb

Although the theoretical curves in Figure 87 apply to a stationary conveyance in a shaft, they represent conditions at that particular level in the shaft where lateral deflections will be a maximum. During hoisting operations it may be assumed that values of Y_{Fmax} and Y_{Amax} as determined by these curves will not be exceeded. These curves may therefore be used as a guide when establishing the various shaft parameters for design purposes.

7.7 The Coriolis force effect.

In Cahpter 4 it was shown that owing to the rotation of the earth a travelling conveyance is subjected to a Coriolis force of magnitude $2M\Omega v$ pounds where M, Ω and v are respectively the conveyance mass in slugs, the rotational speed of the earth in radians seconds^{-1} and the hoisting speed of the conveyance in feet seconds^{-1}.

Taking Ω = 0.0000727 radians seconds^{-1}
Coriolis force = 0.0001454 Mv pounds.

For a conveyance travelling upwards, the Coriolis force causes a westward deflection and for a conveyance travelling downwards, the Coriolis force causes an eastward deflection.

In rope-guide installations where very high hoisting speeds are employed, the Coriolis force may not be neglected. For example, a conveyance of 800 slugs mass travelling at 4,000 feet per minute will be subjected to a lateral force of 7.75 pounds. In very deep shafts where such high hoisting velocities will be very desirable, a lateral force of 7.75 pounds may cause a considerable deflection.

Coriolis force deflection may be conveniently counteracted by using some device such as deflector vanes, which will create an aerodynamic side force of equal magnitude acting in a direction opposite to the Coriolis force. Figure 85(a) depicts a system of deflector vanes which will be suitable for counteracting Coriolis forces for both upward and downward hoisting. Un-

..... 259

fortunately the Coriolis force can not be couteracted by means of fixed deflector vanes at all hoisting speeds since the Coriolis force is linearly proportional to hoisting speed, whereas aerodynamic forces are proportional to the square of the hoisting speed. Furthermore it will be necessary to consider possible variations in the rate of ventilation air flow when deflector vanes are used to generate lateral aerodynamic forces. However, in most cases it will be possible to compensate aerodynamically for Coriolis effects at the normal hoisting speed at which any particular installation is operated.

8. CONCLUSION.

It is considered that the investigations aimed at establishing the degree of dynamic similarity existing between a dynamic scale model rope-guide installation and its fullscale prototype have adequately illustrated the feasibility of dynamic scale model testing of rope-guide systems. These investigations as well as the various model studies on Reynolds number effects in mineshafts equipped with rope-guides have also indicated the necessary conditions for the satisfactory execution of dynamic scale model tests.

The stationary and hoisting correlation tests dealt with in Chapter 4 have shown that although elastic bending forces in ropes, damping forces due to internal rope friction and aerodynamic viscous forces have not been simulated to scale, the dynamic behaviour of the model and its fullscale prototype was nevertheless similar.

During the investigations on fullscale and dynamic scale models of rope-guide installations it became apparent that only two significant types of lateral disturbing forces act on rope-guided conveyances, namely aerodynamic forces and the Coriolis force. This latter force can never be simulated to scale in a dynamic model rope-guide system but fortunately the magnitude of this disturbing force can be determined accurately and it will always be possible to simulate this force with an artificially generated aerodynamic lateral force or by some other means. Aerodynamic lateral forces on rope-guided conveyances are of a more complex nature but it was found that by

..... 260

studying these force effects with careful circumspection it should be possible to simulate aerodynamic force effects satisfactorily for most types of rope-guide mineshaft installations.

Extensive tests on the mechanics of air flow around a bluff body situated stationary in a duct have indicated that aerodynamic viscous force scale effects will become apparent below a certain threshold Reynolds number. It was found that these scale effects were associated with viscous aerodynamic force effects due to the flow of air relative to the duct walls. It became apparent that in mineshafts where the velocity of ventilation air is very low compared with the hoisting velocity of conveyances the Reynolds number scale effect on lateral forces may be insignificant. On the other hand high flow rates of ventilation air in a model shaft may bring about a noticeable Reynolds number effect when the magnitude of the shaft Reynolds number (i.e. the Reynolds number based on the ventilation air velocity) is less than a certain critical or threshold value which can be determined experimentally. In order to ensure the correct simulation of all aerodynamic lateral forces in such a scale model shaft it will be necessary to maintain a shaft Reynolds number equal to or higher than the threshold Reynolds number applicable to such a model shaft. In certain instances it may be found that, in order to maintain such a relatively large Reynolds number in a model, the scale model may become too large to be practical. However, particular attention should be given to the probable percentage error which will be introduced when a Reynolds number lower than the threshold Reynolds number is employed in a dynamic scale model. Errors due to Reynolds number effects may be small enough not to detract from the value of model experiments and usually allowances may readily be made for such errors.

The experience gained during the various correlation tests and investigations into aerodynamic phenomena in rope-guide installations made it possible to present data necessary for future dynamic scale model investigations required for the development of efficient and safe rope-guide mineshaft installations.

..... 261

9. GENERAL NOMENCLATURE.

The following list indicates the significance of all symbols used throughout this thesis:

A — total aerodynamic force acting on a model conveyance (in pounds). Alternatively a steady lateral force acting on a conveyance (in pounds).

B — lower face area of a model conveyance (in $feet^2$).

b — vertical distance between upper and lower points of contact between guide ropes and conveyance (in feet).

b_h — vertical distance between the point of contact of the hoist rope and the centre of gravity of the conveyance (in feet).

b_u — vertical distance between the upper points of contract of the guide ropes and the centre of gravity of the conveyance (in feet).

C — coefficient of discharge for an orifice plate flow meter.

C_L — aerodynamic couple coefficient acting in the pitching plane, defined as

$$C_L = \frac{L}{\frac{1}{2}\rho(w+v)^2 b^3}$$

C_M — coefficient of the total aerodynamic force moment defined as

$$C_M = \frac{Al}{\frac{1}{2}\rho v_{av}^2 D^3}$$

C_R — aerodynamic drag force coefficient defined as

$$C_R = \frac{R}{\frac{1}{2}\rho(w+v)^2 b^2}$$

..... 262

C_S lateral aerodynamic force coefficient defined as

$$C_S = \frac{S}{\frac{1}{2}\rho (w+v)^2 b^2}$$ or alternatively as

$$C_S = \frac{S}{\frac{1}{2}\rho (w+v)^2 D^2}$$

or alternatively as

$$C_S = \frac{S}{\frac{1}{2}\rho v_{av}^2 D^2}$$

$\triangle C_S$ error induced in C_S due to Reynolds number effect.

C_{Su} coefficient of lateral aerodynamic force applicable to a conveyance which is moving at a speed u through a shaft in which the air is stationary.

C_{Sv} coefficient of lateral aerodynamic force applicable to a conveyance which is situated stationary in a duct through which air flows at a velocity of v_{av}.

$\triangle C_{Sv}$ decrement in C_{Sv} due to Reynolds number effect.

c perpendicular distance between the line of action of the impulse P and the pivot point of the impulse pendulum used during tests.

c^1 distance between the point of percussion and the pivot point of the impulse pendulum used during tests.

D diameter of shaft (in feet).

d logarithmic decrement of damping of lateral conveyance oscillations. Alternatively the orifice diameter of an orifice plate flow meter (in inches).

..... 263

E — Youngs modulus for steel used in the wire ropes (in pounds feet^{-2}). Alternatively the velocity of approach factor for an orifice plate flow meter, defined as $E = \frac{1}{1-m^2}$ where $m = \frac{d^2}{D_t}$ and D_t is the throat diameter of the flow meter contraction in inches.

e — Strain in a rope due to bending.

F — lateral impulsive force on a conveyance (in slugs feet seconds^{-1}).

g — acceleration due to gravity (feet seconds^{-2})

H — length of guide ropes between upper and lower attachment points, i.e. the effective depth of the shaft (in feet). Alternatively the static pressure drop over the flared inlet of the horizontal mineshaft wind tunnel (in mm water).

h — distance of the centre of gravity from the pivot point of the impulse pendulum used during tests (in feet). Alternatively the differential pressure over the orifice plate in an orifice plate flow meter (in mm water).

$\triangle h_l$ — static pressure drop between the lower face of a model conveyance and the unobstructed duct upstream of the conveyance (in pounds feet^{-2}).

$\triangle h_u$ — static pressure drop between the upper face of a model conveyance and the unobstructed duct upstream of the conveyance (in pounds feet^{-2}).

..... 264

$\Delta h_1, \Delta h_2$ etc. static pressure differences between the upper and lower faces of a model conveyance (in pounds feet^{-2}).

I moment of inertia of conveyance in the pitching plane (in slugs feet^2). Alternatively the sectional moment of area of a rope (in feet^4).

k radius of gyration about the pivot point of the impulse pendulum used during tests (in feet).

L steady aerodynamic couple acting on a conveyance in the pitching plane (in pounds feet).

l moment arm of total aerodynamic force A around the drag balance fulcrum (in feet).

M mass of conveyance (in slugs).

M_p mass of pendulum used to impart impulses to a conveyance during tests (in slugs).

m mass of a rope (in slugs feet^{-1}). Alternatively the ratio $\frac{d^2}{D_t}$ where d is the orifice diameter and D_t is the diameter of the throat of contraction of an orifice plate flow meter,

or

m arithmetic mean of n measurements t_1, t_2 ..... t_n

m_h mass of a hoist rope (in slugs feet^{-1}).

m_r mass of a guide rope (in slugs feet^{-1}).

N_R duct Reynolds number defined as

$$N_R = \frac{v_{av} D \rho}{\mu}$$

..... 265

n frequency of pendulum (in cycles per second). Alternatively the number of guide ropes per conveyance.

P impulse imparted to the conveyance during tests (in pounds seconds or slugs feet seconds^{-1}).

P_1 absolute air pressure on the high pressure side of the orifice plate of an orifice plate flow meter.

Q actual flow rate in a duct (in cubic feet per second).

Q^1 equivalent flow rate of standard air in a duct (in cubic feet per hour).

R steady aerodynamic drag force acting on a conveyance in the vertical direction (in pounds).

R/k roughness factor of a duct wall where R and k are respectively the duct radius and the average height of a protrusion on the duct wall.

S steady aerodynamic side force acting on a conveyance in the lateral direction (in pounds).

s non-dimensional time lapse defined as $s = t\sqrt{\frac{g}{D}}$. Alternatively the displacement of the imaginary pin joint in a guide rope above or below the guide blocks on a conveyance, caused by the elasticity of the rope.

T tension in a rope (in pounds). Alternatively the absolute air temperature (in ^{o}F).

T_b tension force on the lower extremity of one guide rope (in pounds).

t some time lapse (in seconds). Alternatively the time interval for a guide rope wave to travel a distance of H feet (in seconds).

U peak air velocity existing in a circular duct (in feet seconds^{-1}).

u velocity of conveyance in a shaft in which the air is stationary.

..... 266

v hoisting velocity of conveyance (in feet seconds^{-1})

v_{av} average air velocity in an unobstructed portion of a circular duct (in feet seconds^{-1}).

W weight in the pan of the aerodynamic balance, required to balance the aerodynamic side force S (in grams).

w velocity of ventilation air in the shaft (in feet seconds^{-1}).

X horizontal co-ordinate of the centre of gravity of a conveyance (in feet).

x horizontal co-ordinate of some point in a guide or hoist rope (in feet).

Y vertical co-ordinate of the centre of gravity of a conveyance (in feet).

Y_{Amax} maximum lateral deflection of conveyance in feet, due to a steady force A.

Y_{Fmax} maximum lateral deflection of a conveyance in feet, due to an impulsive force F.

y vertical co-ordinate of some point in a guide or hoist rope (in feet).

z linear scale factor defined as some linear fullscale dimension divided by the corresponding linear model dimension. Alternatively the correction factor for an orifice plate flow meter

η friction coefficient of conveyance guide blocks on guide ropes. Alternatively a confidence limit.

..... 267

θ angle of pitch of conveyance (in radians).

θ_1 initial angle of elevation of impulse pendulum before release, measured from its position of rest (in degrees).

θ_2 angle of rebound of impulse pendulum after impact, measured from its position of rest.

$\dot{\theta}_1$ angular velocity of impulse pendulum just before impact (in radians per second).

$\dot{\theta}_2$ angular velocity of rebound of impulse pendulum just after impact (in radians per second).

λ flow resistence coefficient in duct defined as

$$\lambda = \frac{\text{(static pressure drop per unit duct length) x D}}{\frac{1}{2}\rho v_{av}^2}$$

μ viscosity of air (in slugs feet^{-1} seconds^{-1}).

μ^1 maximum probable deviation from a mean experimental measurement.

ρ density of air (in slugs feet^{-3}).

σ density of some typical material from which a rope-guide installation is constructed (e.g. the density of steel in slugs feet^{-3}). Alternatively a statistical standard deviation.

Ω rotational speed of the earth (= 0.0000727 radians seconds^{-1}).

Suffixes:

h refers to hoist rope.

l refers to the portion of a guide rope below a conveyance.

..... 268

m refers to the model.

p refers to the fullscale prototype.

r = 1, 2, 3, ... n refers to n guide ropes.

s refers to the point of contact of a rope with the conveyance.

u refers to the portion of a guide rope above a conveyance.

..... 269

10. REFERENCES

1. GRAY, E.W. The use of rope-guides in deep shafts. The South African Mechanical Engineer. Volume 11 Number 4, November 1961.

2. VAN DER LINGEN, T.W. Dynamic behaviour of rope-guided conveyances with reference to scale model testing. The South African Mechanical Engineer. Volume 11 Number 5, December 1961.

3. DUCAN, W.J. Physical Similarity and Dimensional Analysis, Edward Arnold and Co., London, 1955.

4. FOCKEN, C.M. Dimensional Methods and their Applications, Edward Arnold and Co., London, 1953.

5. BINDER, R.C. Fluid Mechanics, Constable and Co., London.

6. HOERNER, S. Aerodynamic Drag. Published by the author, 1951.

7. SCHLICHTING, H. Boundary Layer Theory. Translated by Dr. J. Kesting, London. Pergamon Press Ltd. 1955.

8. British Standard Code for Flow Measurement. B.S. 1042: 1943.

9. KEMP, J.F. and CHASTEAU, V.A.L. Flow calibration of a duct with flared inlet. N.Mech.Eng.R.I. Special Report Ref. No. ME/LL/4 N.145 1959.

10. Model Tests to Determine the Dynamic Behaviour of Rope-Guided Conveyances in a Proposed Installation in No. 1 Subvertical Shaft of the Buffelsfontein G.M. Co. Ltd. CSIR Contract Report No. n.274.

11. Further model tests to determine the dynamic behaviour of rope-guided conveyances in a proposed installation in No. 2 subvertical shaft of the Buffelsfontein G.M. Co. Ltd. CSIR Contract Report No. N.351.

..... 270

ACKNOWLEDGEMENT.

The author is deeply indebted to a number of his colleagues without whose assistance the execution of this work would not have been possible. In particular, the author whishes to express his gratitude to:

Dr. H.G. Denkhaus, the director of the National Mechanical Engineering Research Institute, whose assistance and encouragement is highly appreciated.

Dr. J.F. Kemp, now professor of the Mechanical Engineering Department of Stellenbosch University, who, as head of the Aeromechanics Department, gave invaluable assistance and guidance in this project.

Mr. T.W. van der Lingen who worked jointly with the author on this project during its initial stages and who carried out extensive theoretical studies to which frequent refference has been made in this work.

Mr. L.M. Strydom who showed great initiative and resourcefulness in the development of electronic instrumentation used during the various investigations and whose unfailing enthusiasm and perseverence during the difficult stages of the investigation proved to be invaluable.

Mr. J. van Graan who constructed intricate scale models and who was responsible for the operation and maintainance of the vertical mineshaft models.

Mr. E.O.G. Wilhelm and Mr. B. van Wamelen who gave valuable assistance during the various model and fullscale investigations.

The author is also deeply indebted to the Transvaal an Orange Free State Chamber of Mines who sponsored a considerable portion of the work included in this report and who have given kind permission for its publication.